ABSTRACT

HELLER, MICHAEL LEONARD. Polymer Grafted Nonwoven Membranes for Bioseparations. (Under the direction of Dr. Ruben G. Carbonell).

Polybutylene terephthalate (PBT) nonwovens can be readily grafted with glycidyl methacrylate (GMA) via UV induced radical polymerization to create uniform and conformal polymer brush networks around each fiber that can be chemically modified to function as anion or cation exchangers. As ion exchangers these systems are capable of achieving equilibrium protein binding capacities hundreds of times what is possible from monolayer adsorption on the membranes. Capacities, as high as, 1000 mg of protein per gram of material were observed for the ion exchange capture of bovine serum albumin (BSA) and human immunoglobulin G (hIgG) for these systems. However, diffusion limitations in the grafted layer result in very long time scales to reach these large binding capacities. The rates of protein adsorption were determined to be a function of the thickness of the grafted layer. A high surface area islands-in-the-sea (I/S) PBT nonwoven (specific surface area = 2.5 m^2/g) was investigated for polyGMA grafting and protein capture. Compared to commercially available PBT nonwovens (specific surface area = 0.9 m^2/g) it was determined that polyGMA grafting was capable of being distributed in thinner layers at a given degree of grafting. This resulted in a significantly higher instantaneous amount of protein bound and a faster observed rate of adsorption. The comparatively faster rates of protein adsorption are due to the thinner grafting layers of the I/S nonwovens.

To overcome issues with polyGMA grafting by UV-light, PBT nonwovens were successfully grafted with polyGMA using a heat. When functionalized as ion exchangers, protein binding capacities, as high as, 200 mg/g were achieved for PBT nonwovens grafted

using this thermal initiated grafting method. Compared to UV grafted polyGMA PBT nonwovens, the rates of protein adsorption are several times faster for the heat grafted PBT nonwoven. However, ion exchange polyGMA UV grafted PBT nonwovens are capable of binding between 5 and 7 times more protein for similar degrees of grafting. It was determined that the molar binding capacity of the heat grafted nonwovens significantly decreased as the molecular weight of the target increased. The heat grafted polyGMA layer is highly cross-linked and denser than the UV grafted polyGMA layer resulting in size exclusion effects for protein capture. On the other hand, the UV grafted polyGMA layer is a network of brushes that can accommodate a large amount of protein but also suffers from diffusion limitations in the graft layer.

PolyGMA grafted PBT nonwovens functionalized as ion exchangers were evaluated for their performance under flow conditions. It was determined that the UV grafted polyGMA brushes swell and shrink as the ionic strength of the solution changes. At low ionic strength the grafted layers swell significantly, reducing the membrane permeability and increasing the pressure drop of the nonwoven. At high ionic strength the flow permeability increases and the pressure drop is greatly reduced. Ion exchange membranes grafted using heat do not exhibit this behavior and have better flow properties than ion exchange membranes grafted with UV-light. The cation exchange polyGMA PBT nonwovens grafted using UV- light and heat exhibited dynamic binding capacities of 16 mg/ml and 20 mg/ml respectively at residence times from 1-5 minutes. The dynamic binding capacity is significantly lower than the equilibrium or static binding capacity of the membranes due to pore blockage occurring when the membranes are packed into the column for dynamic studies. The use of rigid PET nonwoven spacers increased the effective porosity of the

columns, resulting in an increase in dynamic binding capacity for IgG of 24 mg/ml for the UV-light grafted materials and 35 mg/ml for the heat grafted materials.

Polymer Grafted Nonwoven Membranes for Bioseparations

by
Michael Leonard Heller

A dissertation submitted to the Graduate Faculty of
North Carolina State University
in partial fulfillment of the
requirements for the Degree of
Doctor of Philosophy

Chemical Engineering

Raleigh, North Carolina
2015

APPROVED BY:

_____	_____
Dr. Ruben G. Carbonell Committee Chair	Dr. Behnam Pourdeyhimi
_____	_____
Dr. Patrick Gurgel	Dr. Gary Gilleskie

_____
Dr. Michael Flickinger

BIOGRAPHY

Michael Heller was born in Cleveland, Ohio to his parents Colleen and Leonard Heller. He lived in North East Ohio for 18 years until he moved to Columbus, Ohio to attend the Ohio State University. He completed his Bachelors of Science in Chemical Engineering in 2010 receiving *magna cum laude* honors. He began his graduate studies in the Department of Chemical and Biomolecular Engineering at North Carolina State University in the fall of 2010. He enjoyed his graduate program under the advisement of Dr. Ruben Carbonell. After completion of his graduate studies in the fall of 2015, Michael will move to Northern California to become an entrepreneur starting a company specializing in cannabis extraction technologies.

ACKNOWLEDGEMENTS

I would like to express my gratitude to my adviser Dr. Ruben G. Carbonell. His wealth of knowledge and guidance allowed me to reach higher levels of achievement in my research career than I would have been capable of otherwise. Additionally, his leadership drove me to become an independent thinker while fostering my creativity. I have learned many life lessons working under his guidance that will benefit me as I apply them throughout my life.

I am extremely grateful for having Dr. Patrick V. Gurgel as a mentor throughout my graduate career at NC State. He was always willing to give his advice and guidance about my research. However, I valued his advice on life substantially more than anything related to my research experience. He was always willing to offer me his advice even when it was something that I may not have wanted to hear. Thank you for taking the time to organize all of our group activities and engaging everyone in the lab with often heated discussions, your presence brought a sense of community to our research group. I do not know if I would have been able to finish without his support, I consider him a true friend and hope that we keep in touch.

I would like to thank the bioseparations group for their support and encouragement over my research career. In particular I would like to thank Dr. Haiyan Liu and Dr. Yong Zheng for teaching me the fundamentals of my project. I would like to thank Dr. Amith Naik for being one of the nicest people I have met in the research community and his advice on many of my projects; I hope that he reaches the level of success that his career deserves. I would like to thank Dr. Nafisa Islam for sharing a lab bench with me and putting up with my mess as well as dealing with being the only female in the group for many years. I would like

to thank Dr. Tuhidul Islam for taking over many of the responsibilities of my project; I know the work is in good hands. I would like to thank William “Billy” Kish for going through all the growing pains of graduate school with me. He is one of the most genuine and caring people that I have ever met; finish strong my friend.

I would like to thank Dr. Benham Pourdeyhimi for providing his support and expertise in the area of nonwoven membranes, in addition to providing many of the base materials for my project. I would also like to thank Dr. Orlando Rojas, Chuck Mooney, Birgit Andersen, Lisa Lentz, Jeff Kraus for their technical support.

I would like to thank my undergraduate researchers, Robert Wimbish, Luke Dickinson, Kellie Esinhart, Ridge Butler, Andrew Daniel, Chase Stamey, and Jessica Stryjewksi. They were all great to work with and taught me a great deal. I hope that each one has success as they move forward into their careers.

I would like to thank my core group of friends, Garrett Wheaton, Daniel Morales, Jeff Zurawski and Collin Eaker. We all started at NC State together and I have some of the best memories of my life from hanging out with you guys. I don’t think the graduate school has ever seen a group of guys like us and I doubt they ever will, good luck finishing your PhDs I am excited to see where we are all at over the next couple of years. Finally I would like to thank Emily Clement you gave me the confidence, support and encouragement to finish up my degree and to pursue my dreams, thank you for that.

TABLE OF CONTENTS

LIST OF TABLES

LIST OF FIGURES

Chapter 1

Introduction

1.1 Overview of bioseparations and downstream processing

Biopharmaceuticals are medicines derived from biological sources such as plants, animals or microbial systems. They include vaccines, blood or blood components, hormones, enzymes, gene therapies, fusion proteins and recombinant proteins to name a few [1]. The biopharmaceutical industry is a $140 billion market (2013) with monoclonal antibodies (mAbs) representing 6 of the top 10 products accounting for $63 billion [1]. There are currently 246 approved biopharmaceutical drugs in the United States and the European Union. This is expected to significantly increase with the introduction of biosimilars as 17 of the 20 top selling drugs patents will expire within the next 5 years [1]. From a manufacturing perspective biopharmaceuticals resulted in the production of 26.4 metric tons of pure protein in 2010. The production of mAbs alone is expected to reach 13.4 metric tons by 2016 [1]. The majority of these drugs are expressed in microbial systems such as *E.Coli* or mammalian cell cultures such as Chinese hamster ovary (CHO) cultures. A few drugs such as influenza vaccines and recombinant glucocerebrosidase are expressed in insect cells and plants respectively; however these types of expression systems are not as common. All expression systems are complex and contain many potentially harmful components including host cell proteins, DNA, RNA, endtoxins, pyrogens, improperly folded proteins, and protein aggregates that must be removed before they can be introduced into the body [2]. This makes downstream purification indispensible to the manufacturing of biopharmaceuticals.

Continuous improvement in upstream processing has resulted in dramatic increases in cell culture titers and the overall production of biotherapeutics [3]. Product recovery is not a trivial task often requiring several unit operations to achieve necessary purities for health and safety standards, in some cases this can account for as much as 80% of the operational costs for manufacturing [4]. The increased production and the required high purity of these biotherapeutics have resulted in a tremendous burden in downstream processing. This bottleneck is driving the development of high-throughput processes, improved unit operations, and the pursuit of continuous processing [3]. Aqueous two-phase extraction, precipitation and crystallization are known protein/biotherapuetic bulk purification processes based on protein phase separations [5-9]. However, these processes rarely meet the needed purity requirements for biotherapeutics. Solid phase adsorptive platforms such as packed bed chromatography are capable achieving high purities and are the standard in the biopharmaceutical industry.

Packed bed chromatography is ubiquitous in the purification of therapeutic proteins, due to its high binding capacity, high resolution ability and the mature understanding of the process [10]. The high protein binding capacity and separation ability of commercial chromatography resins stems from their large porosities and high specific surface areas, with an internal pore structure whose surface can be modified to have ion exchange, affinity or hydrophobic interaction functionality. However, packed bed chromatography suffers from large pressure drops, low throughput, complex scale-up, high buffer consumption, high material cost and time consuming process validation [11,12]. Additionally, the relatively small pores of the resin are ineffective at capturing large biomolecules due to size exclusion. To prevent column fouling clarified feed streams are required in traditional packed bed

chromatography. Therefore, filtration and/or centrifugation are necessary unit operations for cell cultures and fermentation broths prior to purification.

A significant amount of work is being done to improve the performance of fixed bed chromatography regarding capacity and purity. The use of polymer grafted networks in the pores of chromatography resins have shown to increase binding capacity by creating a three dimensional binding environment [3]. Novel chromatography resins with optimal pore sizes, ligand densities and the use of dextran surface extenders have resulted in dynamic binding capacities as high as 200 mg/ml for ion exchange capture of mAbs and antibody variants [13]. To improve the selectivity of resins, novel ligands are currently being investigated. Novel multimodal ligands are designed using multiple adsorption mechanisms to improve selectivity and reduce the number of downstream processing steps. They very often have a hydrophobic component and a charged component. Multimodal ligands have been used for the capture of antibodies, viruses, nucleic acids, antibody dimers and human growth factor [14-16]. Hydrophobic charge induction chromatography (HCIC) is a commercial multimodal support that has been used as an alternative to Protein A chromatography for the capture of antibodies. The HCIC ligands combine thiophilic, hydrophobic and electrostatic interactions for easy pH based elution that can eliminate the need for buffer exchange, these ligands have found some application as a post Protein A polishing step [17]. Peptide ligands are currently being designed to replace biologically derived ligands such as Protein A that is expensive and unstable under certain processing conditions. These ligands aim to mimic the binding regions that are present in traditional large molecule affinity ligands. Combinatorial libraries and phage display techniques are capable of screening millions of peptide sequences for specificity against a target protein significantly reducing the time to discover new peptide

ligands [18,19]. Protein A is still the preferred ligand for the purification of mAbs due to its excellent selectivity and binding affinity [3]. However, it suffers from pH instability that can cause denaturing and leaching from the column. Alkali resistant Protein A has been developed using genetic engineering to improve the stability of the column during separations [20]. In some instances mobile phase additives such as arginine, urea, ethylene glycol have been used for packed bed chromatography to enhance separation ability, increase product quality or improve protein stability however, this is not a very common practice [3].

In an effort to increase the throughput of downstream processes, monoliths and membranes are being investigated as potential replacements for packed bed chromatography. The large interconnected pore structures of monoliths and membranes allow for convective flow dominated mass transfer compared to resins where mass transfer is dominated by intra-particle diffusion. Additionally, the open pore structure significantly reduces the pressure drop compared to packed bed chromatography. Monolith columns are characterized as porous rod structures consisting of mesopores and macropores. An SEM micrograph image of a polymeric monolith is presented in Fig. 1.1 [21].

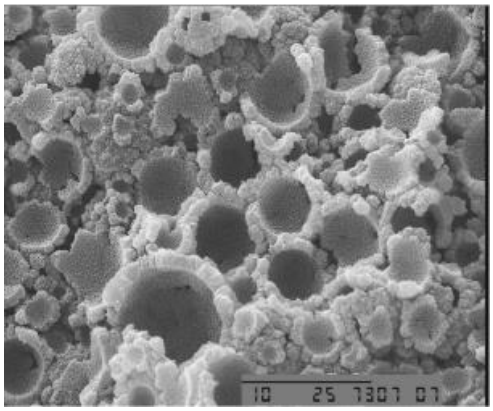

Fig. 1.1 SEM image of a polymeric monolith with visible macropores and mesopores [21].

In Fig. 1.1 the macropores and a mesopores of a polymeric monolith column are readily visible [21]. Monolith columns have been synthesized out of a wide range of polymers including polymethacrylate, polyacrylamide, polystyrene, agarose and cellulose, as well as, from inorganic materials such as silica [21,22]. Polymer based monoliths are made by radical polymerization of monomers in the presence of porogens that induce phase separation to create the pores of the monolith [23]. Silica based monoliths are created using the two step sol-gel process that uses two solvent exchanges to create various macropore and mesopore architectures [22]. Monoliths have the benefit of being manufactured in any shape or dimension including columns, disks or radial flow devices [24-26]. In bioseparations they have primarily been used for the capture of large biomolecules such as plasmid DNA and viruses [27,28]. This chromatographic stationary phase has not found wide acceptance in protein purification because of lower binding capacities compared to resins due to a limited surface area per volume [29]. Additionally, creating large monoliths with homogenous properties suitable for chromatography is difficult, restricting these relatively expensive stationary phases to smaller volume processes [29]. Membranes have many of the same advantages of monoliths regarding convective dominated mass transport and low-pressure operations. A comparison of the types of mass transport between chromatographic resins and membranes is presented in Fig. 1.2 [30].

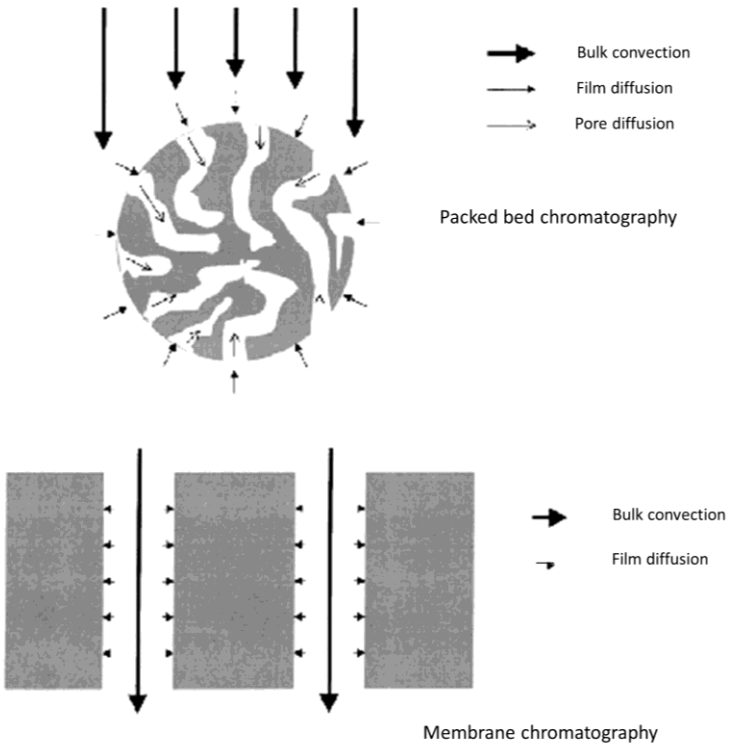

Fig. 1.2 A comparison of the types of mass transport in chromatography resins and membranes [30].

Membranes tend to be less expensive to manufacture than resins and monoliths potentially making them a disposable stationary phase for chromatography. Membranes also have the potential to process crude feed streams when their pores are adequately large which is not possible with resins or monoliths [3]. The main limitation of membranes is the low biomolecule binding capacity associated with their inherent low specific surface area. Methods to increase biomolecule adsorption capacity of membranes and their applications in bioseparations are the focus of this dissertation and will be discussed in more detail in future sections.

1.2 Membrane chromatography

Traditional packed bed chromatography suffers from diffusional mass transfer limitations within the resin and high pressure-drops across the column. The micro porous structure of membranes has the potential to overcome these issues. The mass transfer limitations of packed bed chromatography arise from intra-particle diffusion of molecules in the inner pores of resins before they reach their binding sites; this is visually represented in Fig. 1.2. High pressure-drops arise from the low hydraulic permeability associated from a column packed with small beads or resins (50-90 μm), in addition to any fouling that occurs from the accumulation of colloidal matter and debris [30-34]. The large interconnected pores (200 nm - 20 μm) of membranes permit high rates of volumetric throughput without substantial pressure drops when compared to packed beds [30-34]. Additionally, binding typically occurs on the surface of the membrane eliminating any diffusional resistance that is commonly associated with gel or bead based chromatography. The convective flow dominated binding kinetics of adsorptive membranes results in protein being bound in one tenth the time required for packed bed chromatography [35-37]. The enhanced flow properties and fast binding kinetics permit membranes to be operated at high superficial velocities resulting in shorter residence times that could improve the productivity of a separation process. Adsorptive membranes also have the potential to reduce the amount of mobile phase consumed during processing [30]. In packed bed chromatography the slow diffusion of bound proteins during elution results in large recovery volumes. Membranes have demonstrated that they can rapidly concentrate proteins during elution with a 10+ fold concentration factor, comparatively reducing the recovery volume while recovering between 85-100% of the bound proteins [31]. Another issue with packed bed chromatography is the

need for an efficiently packed column to achieve a high resolution separation which can be difficult to achieve. In a poorly packed column channeling can occur resulting in an underutilization of the bed [30]. Membranes do not require column packing to achieve an efficient separation. All of these factors make scale up of packed bed chromatography difficult whereas membrane chromatography has demonstrated to be linearly scalable [36, 38-40].

A membrane support must meet certain requirements to be used in bioseparations. The membrane should have a micro porous structure that permits liquid flow and the free interaction between target molecules and binding sites. It must be hydrophilic and neutral to allow permeation of aqueous solutions and prevent biomolecules from binding nonspecifically to the surface. There must be functional groups or active sites on the surface that allow the attachment of ligands or surface modification that facilitates selective target adsorption. The support must be chemically stable in all binding, elution, regeneration, and, when applicable, sterilization conditions to prevent degradation of the material. It also must be mechanically stable and incompressible, capable of handling trans-membrane pressures. It is also advantageous if the support is inexpensive to compete with conventional packed bed chromatography or to be used in disposable applications [31]. The ability to functionalize the membrane support can be the limiting factor in a lot of cases. The majority of polymers used to make membranes commercially are hydrophobic and chemically inert. However, there are a handful of membrane supports that can readily be functionalized. Cellulose has found many applications as a support material for affinity membranes [34, 41-43]. It has a high density of hydroxyl groups on the surface that make it both hydrophilic and easy to functionalize. However, cellulose membranes generally have relatively small pores and can

be compressible under flow conditions resulting in high pressure drops [31]. Guo *et al.* have successfully improved the mechanical stability of cellulose affinity membranes by using coarse fibers (1-2 μm) that are cross linked creating a rigid incompressible structure [41]. Another polymer used to make membranes, polysulfone, has good film-forming properties and is biologically resistant. As a membrane it has been functionalized with metal chelating groups and triazine dyes [44-46]. Polyamides such as nylon are capable of making membranes with a narrow poor size distribution that are mechanically rigid and strong. These polymers have terminal amine groups that can be functionalized however the density of these groups is usually low resulting in ligand densities not adequate for protein capture. Additionally, polyamides suffer from nonspecific protein adsorption [47,48]. PVDF is a hydrophobic polymer that offers high mechanical strength and chemical stability when used for making membranes. Strong bases can be used to create active sites for further functionalization [49]. Thermoplastic polymers such as polyolefins and polyesters are used for making inexpensive commercial nonwoven membranes at large production scales. However, these polymers are hydrophobic and chemically inert requiring some form of surface coating for them to be used in bioseparations; this will be discussed in further detail in proceeding sections.

Membranes with functional groups can be modified to have the same adsorptive mechanisms as chromatography resins such as anion exchange, cation exchange, affinity, hydrophobic interaction and reversed phase functionalities. Affinity membranes have been created by the immobilization of immunoaffinity ligands, Protein A or G, low molecular weight ligands, peptides and metal affinity ligands [31]. Antibodies specific to an antigen target have been immobilized on hollow fiber membranes for the industrial scale production

of interferon-α2a, interleukin-2 and interleukin-2 receptor [50,51]. These membranes demonstrate the ability to capture proteins from dilute feed streams with residence times on the order of seconds. Protein A and Protein G have been immobilized on cellulose, nylon and polysulfone membranes in a variety of configurations for the affinity capture of IgG from complex media [52-56]. Low molecular weight pseudo affinity ligands such as Cibacron Blue F3GA dye and L-histidine have been immobilized on variety of membrane supports for the capture of enzymes and antibodies respectively [57-60]. Immobilized metal affinity membranes have also been investigated for their capture of histidine tagged proteins. Iminodiacetic acid-Cu^{2+} has been immobilized onto nylon and polysulfone membranes for the capture of lysozyme, concanavalin A and ovalbumin [44,45,48]. Strong and weak cation exchange membranes have been made by functionalization with sulfonic acid (S) or carboxylic acid groups respectively [39, 61-63]. Strong and weak anion exchange membranes have been made by functionalization with quaternary ammonium (Q) and diethylaminoethyl groups respectively [38,64]. These membranes have demonstrated the selective adsorption of various charged proteins based on the ionic strength and pH of the mobile phase [30]. There are a number of commercially available ion exchange membranes produced by companies like Pall, Sartorius and Millipore. These types of membranes typically find applications in polishing steps and impurity removal during a chromatography process but have not found significant use as a product capture step due to capacity issues [30,31,35]. Hydrophobic interaction membranes and membranes for reverse phase chromatography have previously been reported, however, there are many issues associated with these types of membrane functionalities [30,31]. Hydrophobic interaction membranes do not have the resolution ability that chromatography resins have and irreversible

conformational changes often occur to bound proteins [30,32]. Most synthetic membranes are not compatible with organic solvents used in reverse phase chromatography therefore using membranes for this form of chromatography is very limited [30,31].

Membrane chromatography can be operated in a variety of configurations and flow patterns. The configurations include flat sheets, hollow fibers and radial flow membranes operated either as dead end filtration or as a cross flow filter [30,31]. A visualization of the various membrane configurations and flow patterns is presented in Fig. 1.3 [32].

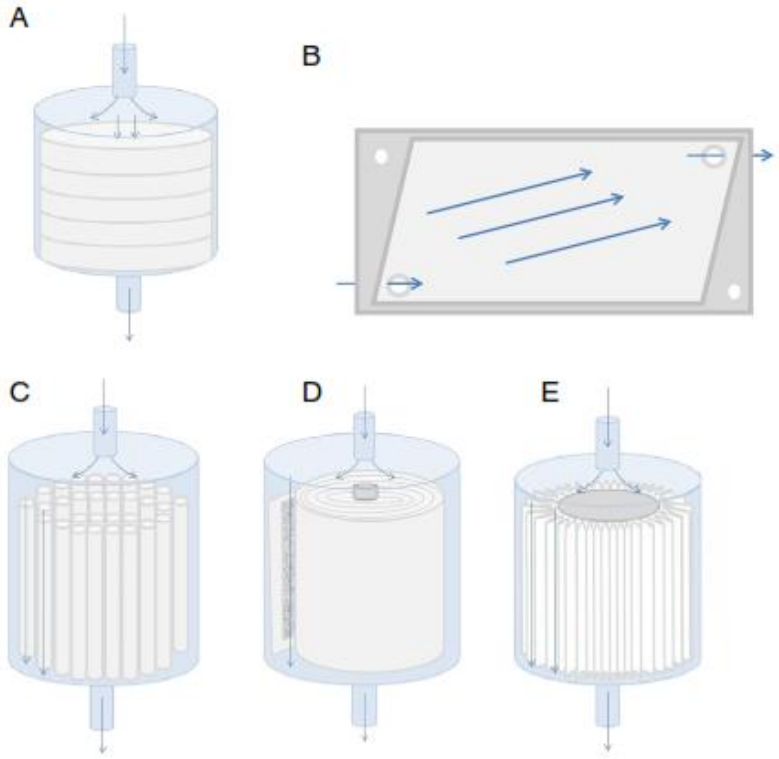

Fig. 1.3 Visual representations of various membrane flow configurations. (A) stacked discs, (B) cross-flow flat sheet, (C) hollow fiber, (D) spiral wound and (E) pleated sheet [32].

Flat sheet tangential flow membranes are similar in design to a plate and frame filter press. This mode of operation is often used in ultrafiltration processes but has found limited use in chromatography due to a limited amount of surface area. Flat sheet membranes are most

often used as stacks of discs where liquid flow is normal to the membrane surface in column format, Fig. 1.3A, for direct comparison to chromatography resins. This is the preferred method for testing adsorptive membranes when pulse injection chromatography is to be performed [30]. Hollow fiber membranes consists of a bundle of several hundred tubes (0.25-2.5 mm in diameter) contained in a shell and tube configuration (Fig. 1.3C). In this configuration liquid flows parallel to the fiber and gradually permeates the pores entering the lumen of the tubes by hydrostatic pressure. Hollow fiber filtration has the benefit of having high surface areas and tangential flow makes them resistant to fouling [30-32]. However, in chromatography operations breakthrough is severely broadened for hollow fiber membranes and the column suffers from poor efficiency [30-32]. Radial flow filtration (Fig. 1.3D) consists of a flat sheet membrane spirally wound around a porous cylindrical core. Flow can be parallel to the sheets and permeate into the core or it can originate from the core and permeate with flow normal to the membranes. Radial flow configurations are best suited for large scale applications and have been used in bind and elute chromatography capture steps. However, flow distribution and module design for this type of filtration is extremely challenging. As the mobile phase permeates the membrane in the radial direction the superficial velocity varies with position making it difficult to predict binding performance of these filters [30]. Additionally, the housing module and core have to designed and manufactured in a way that promotes even flow distribution and prevents bypassing [30-32].

There are several challenges and limitations that need to be considered in membrane chromatography. The most apparent limitation when comparing membrane chromatography to traditional packed bed chromatography is the limited amount of available surface area of the material. A lower specific surface area results in a lower protein binding capacity on a

per volume basis compared to resins [30-34]. For this reason membrane chromatography is best suited for large production volumes with target molecules at low concentrations. An example of this is the commercial production of therapeutic antibodies that use ion exchange membranes for polishing after primary capture to remove host cell proteins, endotoxins, nucleic acids and viruses where the product is passed through column in a flow through mode of operation [32]. For membranes to be used as a primary protein capture step, the binding capacity of the material needs to be increased. This can be done by increasing the surface area of the support or by introducing a three dimensional binding environment inside the pores of the support. High surface area nanofiber cellulose nonwoven membranes have been used for affinity capture of various proteins [65-66]. However the production of these types of supports has only been observed at laboratory scale. There are also physical limitations when increasing a membranes specific surface area before mechanical strength, hydraulic permeability and porosity become compromised. Creating a three dimensional environment inside the pores of cast membranes or around the fibers of nonwoven membranes has been shown to increase the binding capacity of the support while maintaining good flow properties and mechanical strength. Polymer grafting to membrane supports is discussed in more detail in the proceeding sections. Another challenge for membrane chromatography is flow distribution. Membranes generally have a large frontal area making it difficult for a mobile phase to evenly penetrate the membrane [30]. Poor flow distribution within the adsorptive membrane leads to broadened break through curves and a less efficient column. Therefore, a significant amount of work needs to be done on the design of inlet distributors for specific membrane configurations. In addition to even flow distribution, resolution in membrane-based separations depends on a narrow pore size distribution and an

even membrane thickness to prevent broadening and early breakthrough that reduces the overall efficiency of the column [30,33,67,68]. An uneven membrane thickness will result in in preferential flow in the thinner section of the material. A wide pore size distribution will result in preferential flow in larger pores with flow often excluded from smaller pores.

Membranes have the potential to be used in novel applications not well suited for traditional packed bed chromatography including large biomolecule recovery and capture from crude feed streams. Biomolecules with molecular weights >250 kDa are inaccessible to the inner pores of traditional chromatography resins that were designed for smaller targets. For this reason membranes often have higher capacities for large targets compared to resins where binding is limited to the low external surface area of the resin. This is most relevant for the purification of plasmid DNA and viruses. Anion exchange membranes have been used to purify plasmids that are negatively charged on their DNA backbone. Nucleic acids show stronger binding affinity to anion exchangers than proteins, requiring salt concentrations greater than 500 mM NaCl for elution, compared to proteins that can be eluted at salt concentrations below 200 mM NaCl [69]. This makes separation of plasmids from host cell proteins a relatively straight forward process. Regenerated cellulose membranes functionalized with DEAE and 1,4-butandiol diglycidyl ether have successfully been used to capture plasmid DNA from *E.Coli* lysate with capacities of 4 mg/ml and 32.5 mg/ml respectively [70,71]. Similarly, ion exchange membranes have been used for the purification of various viruses and viral vectors. However, ionic strength and pH can have a tremendous effect on the bioactivity of the purified virus and great care must be taken when developing the purification conditions [72,73]. Regenerated cellulose and polyethersulfone membranes functionalized with DEA or quaternary ammonium ligands (membranes made by

Pall [Mustang] and Sartorious [Sartobind]) have been used to purify recombinant Baculovirus, Influenza virus, Modified vaccinia Ankara, Lentiviral vector with recoveries between 70 and 100% [72,74-77]. When the pores of membranes are sufficiently large it becomes possible to capture target biomolecules from crude feed streams such as fermentation broth, mammalian cell cultures, pooled human plasma and un-clarified lysate with cell debris that would foul a packed bed chromatography column. However, this is typically limited to nonwoven membranes that have larger pores than cast membranes. This will be discussed in more detail in the proceeding section.

1.3 Nonwoven Membranes

Nonwoven fabrics are comprised of randomly oriented fibers that form a web. Nonwovens can be made from a wide range of materials using a wide range of techniques. They have found a broad range of applications including clothing, automotive interiors, consumer products, electronics, filtration media, home furnishings, geotextiles, hygiene products, medical supplies, and packaging. Nonwoven membranes are attractive for use as bioseparation filters because they can be highly engineered to exhibit controllable porosities, fiber diameters, and pore sizes with low cost materials using high-rate manufacturing technologies [78].

Nonwovens can be made from a variety of polymers that are derived from natural sources such as cellulose, cotton, silk and wool. However, the majority of commercial nonwovens are made from synthetic thermo plastic polymers such as polyolefins, polyesters, polyamides, polycarbonate, polyvinyl chloride, polyvinyl alcohol, polysulfone, polyurethane, polystyrene, polyacrylates, etc. [79-84]. The nonwoven webs can be formed

through processes such as dry laying, wet laying, and melt or direct spinning (spunbond, meltblown, flashspun, or spunmelt) [78,85-87]. Dry laid nonwoven formation uses staple fibers that are carded into a web that is bonded together using mechanical entanglement (needle punching or stich bonding), thermal bonding, chemical bonding, or hydroentanglement [88]. Wet laying is a similar process to paper making. Fibers are in water slurries that are deposited on a screen followed by similar bonding techniques used to make dry laid nonwovens [88]. Melt/direct spinning processes are capable of making nonwovens from continuous filaments where the fibers are being spun from molten plastics [86]. The continuous nature of these manufacturing techniques results in high rates of production at reduced costs compared to the other techniques. Spunbonding and melt blowing are two commercial production techniques capable of making nonwovens with properties useful for bioseparations. In spunbonding, molten polymer is extruded through a spinneret as filaments that are attenuated by an air stream. The randomly oriented filaments are deposited on a collection belt where they then can undergo some form of bonding to become a nonwoven with mechanical integrity [86]. The fiber diameter of the extruded filament is the major determining factor for the properties of the nonwoven. It influences the overall strength of the material, porosity and surface area to name a few [89]. The spunbonding process is capable of making fibers with diameters between 20- 500 μm although there are some novel methods of making bicomponent fibers that can reach much smaller diameters [86, 90]. Melt blowing is similar to spunbonding but is capable of creating fibers with diameters between 300 nm and 20 μm [91]. The spinneret used for melt blowing contains hundreds of orifices that have jets of hot air that converge at the mouth of the orifice in the direction of extrusion.

The hot air stream used in melt blowing is capable of drawing filaments at finer diameters than is possible in traditional spunbonding [86,91].

The physical and chemical properties of nonwovens are critical for their application in filtration and bioseparations. The chemical properties of nonwovens are dictated by the polymers used to make the nonwoven. Cellulose and cotton based nonwovens have a high density of hydroxyl groups on the fiber surface making them hydrophilic and chemically active for ligand attachment [92,93]. Nylon nonwovens contain terminal amino groups that can covalently attach ligands however the surface density is usually very low limiting their use in bioseparations [94]. However, the majority of polymers used in spunbonding and melt blowing processes are chemically inert and hydrophobic. These types of nonwovens require a post manufacturing surface modification to make them hydrophilic and chemically active for ligand attachment. This is discussed in more detail in the subsequent sections. In general, the polymer used to make nonwovens determines the softness, elasticity, wettability, dyeability and chemical functionality of the bulk material [95]. In bioseparations, the physical characteristics of primary concern for membranes are the specific surface area, porosity and pore size. These properties are dependent on the fiber diameter and spatial variation/orientation of the filaments as well as the basis weight of the nonwoven [86]. The following spunbonding and melt blowing processing parameters can be used to alter these properties: polymer/die temperature, polymer flow rate, air temperature, air velocity and angle, die to collector distance, collector speed, and the die orifice size/spacing [95].

Low specific surface area has been the limiting factor when membranes have been used for protein adsorption, resulting in low binding capacities [96]. In nonwovens it is related to the linear density of the fibers [90]. Fig. 1.4 shows the relationship between the

linear density of a fiber and the resulting specific surface area as well as the specific surface area as a function of PET fiber diameter. The units of linear density are denier, defined as the mass per 9000 meters of filament.

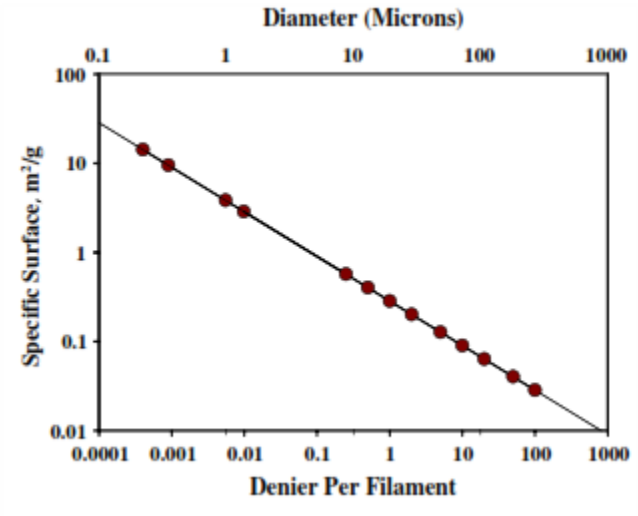

Fig. 1.4 Relationship between the theoretical specific surface area of a nonwoven and the linear density of a nonwoven fiber as well as how the specific surface area is related to the fiber diameter for a PET nonwoven fiber. A Denier is a unit of linear density defined as the mass in grams for 9000 meters of filament [90].

From Fig. 1.4 it is apparent that to increase protein binding capacities by an increase in the surface area of the nonwoven smaller fibers must be used. Melt blown nonwovens have reported diameters as small as 300 nm however the majority of commercially available nonwovens are between 1 and 10 μm [95,97]. There are some nonwoven fabric technologies capable of producing nonwovens with submicron sized fiber diameters that can yield a significant increase in specific surface area. Electrospinning is an emerging technology capable of making nanofiber nonwovens. In electrospinning polymers are dissolved in an appropriate solvent and a high electrical potential is applied between the spinning tip and the collector. As the polymer/solvent system is drawn towards the collector the solvent

evaporates resulting in the formation of very fine polymer fibers, fiber diameters smaller than 100 nm have been reported [98,99]. However, the membranes resulting from this process often exhibit low mechanical integrity requiring a support for reinforcement. They also tend to be highly compressible resulting in high pressure drops and flow issues when used in liquid based filtration. Additionally, electrospinning production is relatively slow and expensive compared to spunbonding and melt blowing [97-99]. A solution to the potential commercial production of high specific surface area nonwovens is the utilization of bicomponent fibers using the spunbonding process for production of nonwoven mats. In this production scheme two polymers can be coextruded from the same spinneret where they combine to become a cohesive fiber [97]. Bicomponent fibers can be extruded in a wide range of conformations including segmented pie, core in sheath, and side by side. These fibers can then be fractured to release many fibers of much smaller diameter, or one of the polymers can be selectively dissolved leaving a much smaller set of fibers in the nonwoven matrix [90,97]. Islands-in-the-Sea (I/S) nonwoven technology is an extension of the core in sheath bicomponent filament process. This type of nonwoven has many permanent polymer cores within the fiber known as "islands" embedded in a removable polymer sheath known as the "sea". Fedorova *et al*. [97] investigated how varying the number of "islands" and the ratio of "islands" to "sea" affects final fiber diameter. In this study I/S nonwovens were made with nylon-6 (islands) and polylactic acid (sea). Nonwovens were synthesized with the number of islands ranging from 36 to 360 and with "islands" to "sea" ratios of 25:75 (w:w) and 75:25 (w:w). Fig. 1.5 displays a schematic of the cross sectional view of two different I/S fibers from the study by Fedorova *et al.*.

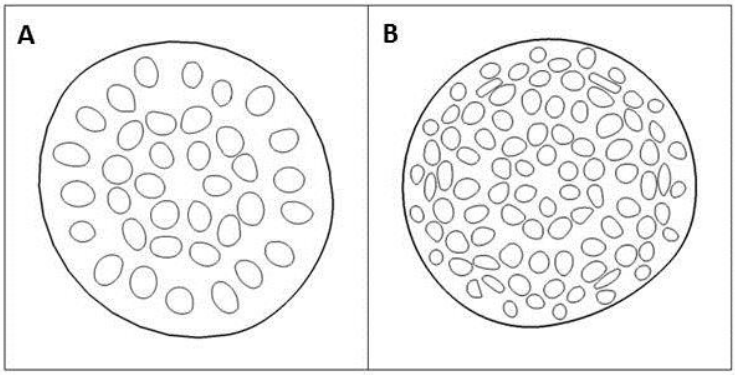

Fig. 1.5 Cross section schematic of I/S fibers with 36 nylon-6 islands in a PLA sea (A) and 108 nylon-6 islands in a PLA sea (B) [97].

Fig. 1.5 offers a visual comparison of two different I/S fibers synthesized with nylon-6 "islands" and polylactic acid (PLA) "sea" at an "island" count of 36 (A) and an "island" count of 108 (B). Polylactic acid (PLA) has a relatively low melting temperature compared to nylon-6 and can easily be decomposed with a hot caustic bath, making it a great candidate for a dissolvable "sea". It was found that fiber diameters as small as 360 nm could be obtained by increasing the island count or by decreasing the polymer ratio of "islands" to "sea" [97]. I/S nonwovens are capable of achieving smaller fiber diameters and therefore higher specific surface areas compared to commercially available nonwovens made by melt blown or spun bond technologies while still conserving high productivity for fiber production [97].

Nonwoven membranes have begun to find applications in bioseparation processes. Nonwoven membranes have pore sizes of several microns compared to traditional cast membranes that have pores sizes between 200 nm and 800 nm [100]. The small pore sizes of cast membranes result in significant membrane fouling when used as filters in cell culture processes. The large pores of nonwoven membranes have been shown to easily pass cells of

several microns without any fouling. Hergistad *et al.* successfully impregnated nonwoven PP with anion exchange chromatography resin [101]. These particle impregnated nonwoven membranes were successful at passing 90% of an *E.Coli* (0.8-2 μm) stream and 96% of a red blood cell (6-8 μm) stream. Additionally, these same materials were capable of capturing BSA at an equilibrium binding capacity of 80 mg/g. Particle impregnated nonwovens have the ability to bind proteins with capacities similar to chromatography resins but with the flow properties of nonwoven membranes. There is potential to use particle impregnated or functionalized nonwovens for product capture directly from fermentation broths, mammalian cell cultures, pooled human plasma, and un-clarified lysate with cell debris; eliminating the need for centrifugation and microfiltration steps typically required prior to packed bed chromatography.

Functionalized nonwovens have found limited applications in protein adsorption. The major body of work for protein capture on nonwovens has been done on electrospun cellulose due to its high specific surface area (10 m^2/g) and functionalization potential [102-104]. Ma *et al*. successfully functionalized electrospun cellulose nanofiber nonwovens with Cibracon Blue F3GA dye and were able to capture BSA and bilibrubin with capacities of 13 mg/g and 4 mg/g respectively [102]. Ma and Ramakrishna were able to immobilize a Protein A/G affinity ligand to electrospun cellulose for the selective capture of IgG from BSA with an equilibrium capacity of 18 mg/g [103]. Zhang *et al*. created anion exchange functionalized cellulose acetate nanofiber nonwovens and were able to capture BSA at a capacity of 40 mg/g [104]. Functionalized nonwovens that rely on surface adsorption have the potential to be used for contaminant removal or bioseparations that have low capacity requirements such as virus or plasmid capture [105]. However, product capture of proteins

typically requires high binding capacities that are difficult to achieve using membrane adsorbers. For this reason a significant amount of research has been done on polymer grafting of surfaces for protein capture. Polymer grafting is capable of creating a three dimensional network that results in protein capture many times what would be allowed by the available surface area of filters. In a study by Zheng *et al*. nonwoven polypropylene was grafted with polyGMA and functionalized to be anion exchange nonwovens capable of reaching protein-binding capacities of 120 mg/g for BSA capture [106]. Similarly, Liu *et al*. grafted polyGMA to nonwoven PBT that were functionalized to be anion exchangers capable of capturing BSA at 800 mg/g [107]. Grafting of polymeric surfaces will be covered in more detail in the proceeding sections.

An attractive feature of using nonwoven membranes in bioseparations is their potential to be disposable due to their low production costs. Bioprocessing based on disposable components has the potential to reduce the time to market, reduce production costs and create an increased flexibility in process development [108]. Disposable equipment eliminates the need for cleaning-in-place, steaming-in-place, sterilization, maintenance, and extensive process validation that is currently required for stainless steel bioprocess equipment. Additionally, disposable membrane chromatography prevents cross contamination for chromatography processes that handle viruses, pathogens or toxins [109]. Disposable anion and cation exchange membranes are currently commercially available, manufactured by companies such as Pall and Sartorius to name a few. They have shown to effectively remove host cell proteins, DNA, leached Protein A and mAb aggregates in polishing steps following primary recovery in the purification of mAb [110]. However, the limited capacity of membranes has prevented their use as a disposable primary capture in

protein purification. It is of interest to design a high capacity grafted nonwoven for the capture of proteins that is cost effective and can be used in a single use disposable chromatography system.

1.4 Polymer Grafting of polymeric surfaces

Polymer grafting has the potential to drastically change the surface properties of polymeric materials by imparting different properties at the interface between the surface and environment that were not present on the native substrate [111-113]. Polymeric materials typically are hydrophobic and chemically inert creating issues when using them as filters in bioseparations. In particular the hydrophobic nature of polymeric filters makes them difficult to pass aqueous solutions through them in addition to suffering from unwanted nonspecific protein adsorption and cell adhesion. However, these issues can be overcome by surface modification [114,115]. Grafting of polymeric surfaces is one of the most widely used techniques for modifying polymeric surfaces because it is easy to control the process and it creates covalent bonds at the surface that are not prone to delamination like other coating techniques [112]. Grafting can be performed by "grafting to" the surface or "grafting from" the surface. In the "grafting to" method highly uniform polymer chains with reactive end groups are covalently attached to the surface, resulting in a surface with attached polymer chains all of the same length and properties. However, achieving a high grafting density at the surface is difficult due to steric effects of already grafted polymers. Additionally, each grafting approach is graft specific and therefore has not observed industrial relevance [113,116]. In the "grafting from" method, polymerization is initiated at the surface and propagates from that surface. In the "grafting from" approach an active site on the surface is

required to initiate polymerization, anchoring the polymer grafts to the surface. Typically, initiators or special treatments are used to create polymerization sites at virtually every point on the exposed surface. For this reason, the "grafting from" method, results in a higher grafting density compared to the "grafting to" method. The polymerization conditions in the "grafting from" method can be manipulated to control the grafted polymer chain length and overall degree of grafting. The "grafting from" is the focus of this work and will be solely discussed from here on.

All "grafting from" techniques of polymeric surfaces require the generation of an active site on what are generally regarded as inert materials. The surfaces of polymeric materials can be modified a number of ways including plasma treatment, ozone treatment, high energy radiation, UV radiation, using redox/ATRP initiators or using free radical initiators [112,113]. Plasma treatment of surfaces has the ability to introduce polar groups such as hydroxyl and amino groups in addition to free radicals depending on whether exposure is done in the presence of oxygen/nitrogen/argon or if it is performed under vacuum [112,113,117]. The activation of a surface using plasma is almost always done in the gas phase. However, after activation, polymerization can be performed in the gas phase or in solution. Exposure of a plasma treated surface to air results in the gradual decay of active groups resulting in a finite shelf life for the material [112, 113]. Plasma treatment for surface grafting is capable of creating highly uniform grafted layers with low degrees of coverage. However, it is a slow and expensive process that is only capable of grafting the immediate surface of exposure finding limited application in the grafting of filters [113, 118]. Ozone treatment is capable of oxidizing polymeric surfaces creating carboxyl, carbonyl, peroxide and hydroperoxide sites capable of initiating polymerization or allowing the adsorption of

other initiators [119,120]. Ozone is typically used to modify surfaces for the adsorption of photoinitiators used in UV irradiated graft polymerization [112,119]. High energy radiation such as x-rays, γ-ray and energy rich particle rays are capable inducing radical polymerization directly on a chemically inert surface without the necessity of an initiator. However, these type of polymerizations are complicated and elaborate, requiring high cost experimental setups with excessively stringent reaction conditions, possible at laboratory scale but are rarely seen industrially [121]. Photosensitive polymer backbones are capable of being polymer grafted directly after exposure to UV-light that creates surface radical sites for initiation. Polyarylsulfone, polystyrene, polyethersulfone are sensitive to light at wavelengths between 200-300 nm and have been known to self-initiate the polymerization of HEMA, GMA and MAA directly to the surface [113,122-124]. There are only a limited number of polymeric surfaces that can be grafted this way and the ones that can are degraded from exposure to UV-light. Redox/ATRP systems are capable of free radical initiation for grafting of polymeric surfaces. Both of these methods use transition metals as catalysts. In redox polymerizations peroxides are decomposed to create free radicals capable of initiating polymerization. ATRP uses alkyl halides to create free radicals on the polymerization surface. ATRP is capable of creating highly uniform grafted layers, however, the reaction conditions are stringent and have only been implemented at laboratory scale [112,113].

One of the most versatile ways to create radical propagation sites for vinyl grafting from polymeric surfaces is using free radical initiators. Certain free radical initiators have the ability to adsorb to polymeric surfaces. When the appropriate energy source is applied free radical initiators decompose creating radical species that are capable of hydrogen abstraction from the polymeric surface they are adsorbed to creating an initiation site for

grafting [121]. Surface grafting using these initiators can be done in solution and is capable of being performed at much larger production scales than the previously discussed grafting techniques [112,113]. The effectiveness of this grafting approach is largely dependent on the surface being grafted, the initiator, the vinyl monomer, and the solvent. It is critical that the initiator be able to adsorb to the surface being grafted by van der Waals forces, physical entrapment, or by covalent attachment to the surface [113]. The solvent chosen for surface grafting with free radical initiators must be able to effectively wet the surface for grafting and solubilize the free radical initiator [113,116,125]. Additionally, as grafting progresses the molecular weight of the grafted polymer chain significantly increases and solubility issues may arise. Therefore, it is advantageous if the grafting polymer is soluble in the solvent preventing any precipitation that might reduce the effectiveness of grafting. Photosensitive and heat labile free radical initiators have previously been used to graft the surfaces of polyolefin and polyester nonwovens. Benzophenone (BP) is a UV induced initiator that has been used to vinyl graft polyethersulfone, polypropylene, polyethylene, polyacrylonitrile, polystyrene, polyurethane, polyethylene terephthalate, polyvinylidene fluoride, nylon and polybutylene terephthalate to name a few . These surfaces were effectively grafted with acrylic acid, methylacrylic acid, hydroxyethyl methacrylate, N,N-dimethylaminoethyl methacrylate, 4-vinylpyridine, 2-aminoethyl methacrylate, N-isopropylacrylamide, 2-acrylamido-2-mthylpropane sulfonic acid, and glycidyl methacrylate (GMA) [113,125-132]. In previous work by the Carbonell research group, BP has been used effectively for grafting on polypropylene (PP) and polybutylene terephthalate (PBT) nonwovens with GMA monomer using UV-light at 365 nm; creating polyGMA brushes with active epoxy functional groups capable of further derivatization [125, 133]. The issue with UV-light polymerization

is that it is limited to the penetration depth of the light source. Therefore, nonwoven samples that are sufficiently thick or have a minimal pore structure for light penetration will result in insufficient graft coverage in the depth of the material due to a lack of UV-light penetration. This is not an issue when thermally labile free radical initiators are used. Thermally induced vinyl polymerization is commonly used industrially to create bulk polymerizations in solution but has found limited application for surface modification of membranes [121]. A few studies have been conducted investigating thermal grafting of vinyl monomers on polyethylene terephthalate (PET) and PP using benzoyl peroxide as a thermal initiator [134-137]. Arslan has successfully grafted polyGMA onto PET and then further functionalized the material for removal of chromium from aqueous solutions [134]. Carroll *et. al*. grafted acrylic acid, 2-(N,N-dimethyl amino)ethyl methacrylate, and poly(ethylene glycol) monomethyl ether monoacrylate to PP to reduce membrane fouling by organic waste [135]. However, no work has been done on the thermal grafting of polyGMA onto PBT nonwovens.

The chosen grafting technique, grafting density, degree of grafting, intrinsic properties and structures of the grafted layer, as well as environmental conditions have dramatic impacts on the properties, performance and intended use of the grafted material. Surface grafting using the free radical UV initiator BP is known to create a brush structure that extends normal to the grafted surface [112,113,138]. At a low grafting density polymers grafted to the surface tend to coil up in what is known as a mushroom conformation [112]. In practice these can be observed by SEM micrograph as isolated bumps that increase the surface roughness of the material. However, as the grafting density increases such that the distance between polymer chains is less than the radius of gyration of these chains the polymer chains are forced to stretch away from the grafted surface, when in the presence of a

"good" solvent [139]. As the grafting density increases the grafted surface transforms from having isolated mushroom grafts into a brush structure, resulting in a substantially smoother surface [112,125]. In practice the grafting density can be controlled by the initiator concentration [112,125,140]. The degree of grafting is controlled by a number of factors including the monomer concentration, initiator concentration, solvent, energy input such as radiation intensity or temperature, and polymerization time [121]. The degree of grafting is proportionally equivalent to the grafted layer thickness and overall volume of the grafted layer. The effective volume of the grafted layer is critical for the design of polymer grafted nonwoven membranes for bioseparations because it determines the overall equilibrium binding capacity of the material. Polymer grafted layers are three dimensional in nature and capable of overcoming surface area limitations typically associated with filtration, by creating a binding volume that can accommodate target molecules [125, 140-143].

The three dimensional structure of polymer brushes are largely dynamic and change due environmental factors. In the presence of a "good" solvent polymer brushes will extend away from the grafted surface. However, in the presence of a "bad" solvent the polymer brushes will collapse onto the grafted surface to minimize free energy [112,113,138]. This is often dependent on the functionality of the polymers grafted to the surface. If the polymers grafted to the surface are hydrophobic in nature, organic solvents are required to observe an extended brush conformation and an aqueous solvent would result in a collapse of the brush network. Conversely, hydrophilic grafted layers will be extended in an aqueous solvent and collapse in an organic solvent. The behavior of polyelectrolyte brushes is of particular interest for their potential use as ion exchange biomolecule capture systems. Polyelectrolyte brushes possess a large charge density that results in an electrostatic repulsion between

neighboring polymer chains in aqueous solvents. This leads to a significant amount of swelling in the grafted layer. The swelling nature of polyelectrolyte brushes can be controlled by the ionic strength and pH of the solvent used. Iwata *et al.* successfully grafted anionic acrylic acid brushes to membranes creating molecular valves that open and close based on changes in pH [144]. Similarly, it has been well documented that increasing ionic strength results in a shrinking of polymer grafted layers with large charge densities [145,146]. Changes in pH can reduce the charge of polyelectrolyte brushes to a net charge of zero that eliminates any electrostatic repulsion resulting in a shrinking of the grafted layer. Similarly, at high salt concentrations counter-ions associate with the charges located on the polyelectrolyte brushes causing Debye screening that also reduces the electrostatic repulsions of the brushes. Dynamic changes in the grafted polymer layer can be minimized via cross linking of the polymer network. Cross linking creates physical constraints that reduce the mobility of grafted polymer chains [112]. Saito *et al.* investigated the flow performance of hollow fibers grafted with polyGMA that were functionalized with phosphoric acid creating anionic brushes [147]. This work determined that hollow fibers grafted with anionic brushes restricted flow through the material due to swelling of the charged brushes. The introduction of a high ionic strength mobile phase resulted in a collapse of these brushes and the flow properties of these filters improved. They further determined that cross linking of the polymer brushes created a grafted layer that did not swell or collapse based on the ionic strength of the environment [147]. Cross linking can be achieved by using a chemical cross linking agent or by using the appropriate grafting technique. Thermally induced grafting has been shown to increase polymer branching and cross linking in the grafted layer based on the polymerization temperature [121,148-150].

In addition to creating a three dimensional network on a grafted surface, polymer grafting can be used to change the functionality of the surface. Surface grafting is capable of introducing functional groups such as amine, imine, carboxylic acid, sulfonic acid, epoxide, and hydroxyl groups to substrates such as polyolefins and polyesters that are non-polar and chemically inert by nature [112]. Grafting of polyGMA has been used extensively to modify the surfaces of PP, PBT and PET filters. GMA monomer has the unique characteristics of having a vinyl group for polymerization and pendant epoxide group that can have ligands covalently attached to the polyGMA graft such as amines, hydroxyls, carboxylic acids, sulfonic acids, thiols, pyridines and peptides [111]. In previous works nonwoven PP and PBT were successfully grafted using UV-light to create a polymer brush network of polyGMA [125,140]. In these studies diethylene glycol was covalently attached to the polyGMA brushes resulting in a hydrophilic surface capable of rejecting any nonspecific protein adsorption. In general nonspecific protein adsorption and cell/platelet adhesion have been known to be reduced by the grafting of hydrophilic polymers to the surface [151-153]. PolyGMA surface grafting has also been shown to selectively adsorb proteins and other targets through functionalization as ion exchangers or polymer layers that contain affinity ligands [125,140, 154-156]. When functionalized as ion exchanger's, polyGMA grafted polyolefin and polyester membranes observe high equilibrium binding capacities for proteins. The achieved protein binding capacities are many times higher than what would normally be capable from the available surface area of the material. This is due to an extended brush conformation that results from the electrostatic repulsion of the ion exchange functionalized brushes that can accommodate a large number of protein molecules. On the other hand, similar membranes grafted with polyGMA that were functionalized with a high

density of affinity ligands had protein binding capacities that were proportional to the available surface area of the grafted material. These affinity ligand functionalized polyGMA grafted layers do not have the benefit of an extended brush conformation due to electrostatic repulsions. Therefore, protein diffusion into a dense grafted layer becomes difficult limiting the majority of protein binding to the surface of the grafted layer.

1.5 Overview of this dissertation

In this study, commercially available PBT nonwovens were evaluated for their use as target biomolecule capture devices. PolyGMA surface grafting was used to create chemical functionality on a material that is inherently hydrophobic and inert. A UV-light based grafting method and heat induced grafting method were evaluated for their ability to effectively graft polyGMA to the surface of the PBT nonwoven. The epoxy pendant groups of the polyGMA graft layer were easily modified with diethylamine, sulfonic acid or phosphoric acid to create ion exchange nonwovens. These materials were tested for their ability to capture proteins as well as separate proteins from complex mixtures. The adsorption kinetics and affinity of protein binding was evaluated and modeled for both grafting techniques. Structural and behavioral differences in the polyGMA grafted layer that arise from the two different grafting techniques were also investigated. The polyGMA grafted PBT nonwovens were also evaluated for their behavior under various flow conditions and were evaluated for their performance as high through put filters for the dynamic capture of target proteins. Also evaluated in this study is the UV-light grafting of novel high surface area islands-in-the-sea PBT nonwovens. These materials were evaluated for their ability to statically capture protein with modeling of their rates of adsorption.

1.6 References

[1] G. Walsh, Biopharmaceutical benchmarks 2014, Nature Biotechnology, 32 (2014) 992-1000.

[2] F. Li, J. Zhou, X. Yang, T. Tressel, B. Lee, Current therapeutic antibody purification production and process optimization, Bioprocessing Journal, (2005) 1-8.

[3] S.M. Cramer, M.A. Holstein, Downstream bioprocessing: recent advances and future promise, Current Opinion in Chemical Engineering, 1 (2011) 27-37.

[4] J. Gonzalez-Valdez, K. Mayolo-Deloisa, M. Gonzalez-Gonzalez, M. Rito-Palomares, Trends in Bioseparations, 13 (2014) 19-27.

[5] J.A. Asenjo, B.A. Andrews, Aqueous two-phase systems for protein separation: A perspective, Journal of Chromatrography A, 49 (2011) 8826-8835.

[6] K. Qu, F.H. Lu, H.J. Zhang, Smart polymer based aqueous two-phase systems applied in bio-molecule separation and purification, Progess in Chemistry, 22 (2010) 125-132.

[7] F. Hilbrig, R. Freitag, Protein purification by affinity precipitation, Journal of Chromatography B, 790 (2003) 79-90.

[8] P.C. McDonald, C. Victa, J.N. Carter-Franklin, R. Fahrner, Selective antibody precipitation using polyelectrolytes: A novel approach to the purification of monoclonal antibodies, Biotechnology and Bioengineering, 102 (2009) 1141-1151.

[9] V. Klyushnichenko, Protein crystallization: From HTA to kilogram-scale, Current Opinion in Drug Discovery and Development, 6 (2003) 848-854.

[10] B. Kelley, Industrializtion of mAb production technology- the bioprocessing industry at a crossroads, mAbs, 1 (2009) 443-452.

[11] T.M. Przybycien, N.S. Pujar, L.M. Steele, Alternative bioseparation operations: life beyond packed-bed chromatography, Current Opinion in Biotechnology, 15 (2004) 469-478.

[12] C. Charcosset, Purification of proteins by membrane chromatography, Journal of Chemical Technology and Biotechnology, 71 (1998) 95-110.

[13] D.S. Hart, C. Harinarayan, G. Malmquist, A. Axen, M. Sharma, R. van Reis, Surface extenders and an optimal pore size promote high dynamic binding capacities of antibodies on cation exchange resins, Journal of Chromatography A, 1216 (2009) 4372-4376.

[14] A. Voitl, T. Muller-Spath, M. Morbidelli, Application of mixed mode resins for the purification of antibodies, Journal of Chromatography A, 1217 (2010) 5753-5760.

[15] M.A. Snyder, Working with powerful and robust mixed-mode resin for protein purification, BioProcess Int. (2011) 50-53.

[16] K.A. Kaleas, C.H. Schmelzer, S.A. Pizarro, Industrial case study: evaluation of mixed-mode resin for selective capture of human growth factor recombinantly expressed in E. coli, Journal of Chromatography A, 1217 (2010) 235-242.

[17] J. Chen, J. Tetrault, A. Ley, Comparision of standard and new generation hydrophobic interaction chromatography resins in the monoclonal antibody purification process, Journal of Chromatography A, 1177 (2008) 272-281.

[18] H. Yang, P. Gurgel, R. Carbonell, Purification of human immunoglobulin G via Fc-specific small peptide ligand affinity chromatography, Journal of Chromatography A, 1216 (2009) 910-918.

[19] R.J. Rickles, M.C. Botfield, A, Weng, J.A. Taylor, O.M. Green, J.S. Brugge, M.J. Zoller, Identification of Src, Fyn, Lyn, PI3K and Abl SH3 domain ligands using phage display libraries, Then Embo Journal, 13 (1994) 5598-5604.

[20] E.X. Perez-Almodovar, G. Carta, IgG adsorption on new protein A adsorbent based on macroporous hydrophilic polymers. I. Adsorption equilibrium and kinetics, Journal of Chromatography A, 1216 (2009) 8339-8347.

[21] E.G. Vlakh, T.B. Tennikova, Preparation of methacrylate monoliths, J. Sep. Sci. 30 (2007) 2801-2813.

[22] F.C. Leinweber, U. Tallarek, Chromatographic performance of monolithic and particulate stationary phases hydrodynamic and adsorption capacity, Journal of Chromatography A, 1006 (2003) 207-228.

[23] E.C. Peters, F. Svec, J.M.J. Frecht, Rigid macroporous polymer monoliths, Advanced Materials, 14 (1999) 1169-1181.

[24] F. Svec, J.M.J. Frecht, Continuous rods of macroporous polymer as high-performance liquid chromatography separation media, Anal. Chem. 64 (1992) 820-822.

[25] S. Xie, R.W. Allington, F. Svec, Rapid reversed-phase separation of proteins and peptides using optimized "molded" monolithic poly(styrene-co-divinylbenzene) columns, Journal of Chromatography A, 865 (1999) 169-174.

[26] A. Podgornik, M Barut, A. Strancar, Construction of large volume monolithic columns, Anal. Chem. 72 (2000) 5693-5699.

[27] D. Josic, A. Strancar, Application of membranes and compact porous units for the separation of biopolymers, Industrial & Engineering Chemsitry Research, 38 (1999) 333-342.

[28] M. Vodopivec, A. Podgornik, M. Berovic, Application of convective interaction media (CIM (R)) disk monolithic columns for fast separation and monitoring of organic acids, J. Chromatogr. Sci. 38 (2000) 489-495.

[29] E.L. Pfaunmiller, M.L. Paulemond, C.M. Dupper, D.S. Hage, Affinity monolith chromatography: A review of principles and recent analytical applications, Anal. Bioanal. Chem. 405 (2013) 2133-2145.

[30] R. Ghosh, Protein separation using membrane chromatography: opportunities and challenges, Journal of Chromatography A, 952 (2002) 13-27.

[31] C. Charcosset, Purification of proteins by membrane chromatography, J. Chem. Technol. Biotechnol. 71 (1998) 95-110.

[32] V. Orr, L. Zhong, M. Moo-Young, C.P. Chou, Recent advances in bioprocessing application of membrane chromatography, Biotechnol. Adv. 4 (2013) 450-465.

[33] D.K. Roper, E. Lightfoot, Separation of biomolecules using adsorptive membranes, J. Chromatogr. A 702 (1995) 357-367.

[34] E. Klein, Affinity membranes: a 10-year review, J. Membr. Sci. 179 (2000) 1-27.

[35] K.G. Briefs, M.R. Kula, Fast protein chromatography on analytical and preparative scale using modified microporous membranes, Chem. Eng. Sci. 47 (1992) 141-149.

[36] W.C. McGregor, D.P. Szesko, R.M. Mandaro, V.R. Rai, High performance isolation of recombinant protein on composite ion exchange media, Bio/Tech. 4 (1986) 526-527.

[37] V. Prpic, R.J. Uhing, T.W. Gettys, Separation and assay of phosphodiesterase isoforms in murine peritoneal macrophages using membrane matrix DEAE chromatography and [^{32}P]cAMP, Anal. Biochem. 208 (1993) 155-160.

[38] D. Lutkemeyer, M. Bretschneider, H. Buntmeyer, J. Lehmann, Membrane chromatography for rapid purification of recombinant antithrombin III and monoclonal antibodies from cell culture supernatant, J. Chromatogr. 639 (1993) 57-66.

[39] W.K. Wang, S.P. Lei, H.G. Monbouquette, W.C. McGregor, Membrane adsorver process development for the isolation of recombinant immunofusion protein, BioPharm. June (1995) 52-59.

[40] S.H. Huang, S. Roy, K.C. Hou, G.T. Tsao, Scaling up of affinity chromatography by radial-flow cartridges, Biotechnol. Progr. 4 (1988) 159-165.

[41] W. Guo, Z. Shang, Y. Yu, L. Zhou, Membrane affinity chromatography of alkaline phosphatase, Journal of Chromatography A, 685 (1994) 344-348.

[42] W.O. Olson, C.K. Colton, M.L. Yarmush, Electrophoretic elution and adsorption: investigation using microporous membrane immunoadsorbents, J. Membr. Sci. 56 (1991) 247-278.

[43] T. Adachi, M. Mogi, M. Harada, K. Kojima, Selective removal of human serum amyloid P component from rat blood by use of an immunoaffinity membrane in an extracorporeal circulation system, J. Chromatogr. B, 682 (1986) 47-54.

[44] K. Rodemann, M. Staude, Synthesis and characterization of affinity membranes made from polysulfone, Journal of Membrane Science, 88 (1994) 271-278.

[45] K. Rodemann, E. Staude, Polysulfone affinity membranes for the treatment of amino acid mixtures, Biotechnol. Bioeng. 46 (1995) 503-509.

[46] W. Guo, Z. Shang, Y. Yu, Y. Guan, L. Zhou, Membrane affinity chromatography used for the separation of trypsin inhibitor, Biomed. Chromatogr. 6 (1992) 95-98.

[47] K. Kugel, A. Moseley, G.B. Harding, E. Klein, Microporous poly(caprolactam) hollow fibers for therapeutic affinity adsorption, Journal of Membrane Science, 74 (1992) 115-129.

[48] T.C. Beeskow, W. Kusharyoto, F.B. Anspach, K.H. Kroner, W.D. Decker, Surface modification of microporous polyamide membranes with hydroxyethyl cellulose and their application as affinity membranes, Journal of Chromatrography, 715 (1995) 49-65.

[49] K. Ritter, Affinity purification of anitbodies from sera using polyvinylidenedifluoride (PVDF) membranes as coupling matrices for antigens present by autoantibodies to trosephosphate isomerase, Journal of Immunological Methods, 137 (1991) 209-215.

[50] M. Nachman, A.R. Azad, P. Bailon, Efficient recovery of recombinant proteins using membrane-based immunoaffinity chromatography (MIC), Biotech. Bioeng. 40 (1992) 564-571.

[51] M. Nachman, Kinetic aspects of membrane-based immunoaffinity chromatography, Journal of Chromatography, 597 (1992) 167-172.

[52] K.C. Hou, C.J. Hou, S. Roy, R. Zaniewski, Immobilization of protein G on nylon membrane for the removal of IgG from human plasma, Polym. Mater. Sci. Eng. 61 (1989) 670-674.

[53] E. Klein, E. Eichhloz, D.H. Yeager, Affinity membranes prepared from hydrophilic coatings on porous polysulfone hollow fibers, J. Membr. Sci. 90 (1994) 69-80.

[54] M. Unarska, P.A. Davies, M.P. Esnouf, B.J. Bellhouse, Comparative study of reaction kinetics in membrane and agarose bead affinity systems, J. Chromatogr. 519 (1990) 53-67.

[55] J.E. Kochan, Y.J. Wu, M.R. Etzel, Purification of bovine immunoglobulin G via protein G affinity membranes, Ind. Eng. Chem. Res. 35 (1996) 1150-1155.

[56] E. Klein, D. Yeager, R. Seshadri, U. Baurmeister, Affinity adsorption devices prepared from microporous poly(amide) hollow fibers and sheet membranes, J. Membr. Sci. 129 (1997) 31-46.

[57] B. Champluvier, M.R. Kula, Dye-ligand membranes as selective adsorbents for rapid purification of enzymes: a case strudy, Biotech. Bioeng. 40 (1992) 33-40.

[58] Y. Li, H.G. Spencer, Dye grafted poly(ethylene imine) coated, formed-in-place class affinity membranes for selective separation of proteins, Polym. Prepr. 33 (1992) 472-473.

[59] S.M. Bueno, K. Haupt, M.A. Vijayalashmi, Separation of immunoglobulin G from human serum by pseudobioaffinity chromatography using immobilized L-histidine in hollow fibre membranes, Journal of Chromatography B, 667 (1995) 57-67.

[60] K. Haupt, S.M. Bueno, M.A. Vijayalakshmi, Interaction of human immunoglobulin G with L-histidine immobilized onto poly(ethylene vinyl alcohol) hollow-fiber membranes, Journal of Chromatography B, 674 (1995) 13-21.

[61] H. Shinano, S. Tsuneda, K. Saito, S. Furasaki, T. Sugo, Ion exchange of lysozyme during the permeation across a microporous sulfopropyl-group-containing hollow fiber, Biotechnol. Prog. 9 (1993) 193-198.

[62] B. Gupta, A. Chapiro, Preparation of ion exchange membranes by grafting acrylic acid into pre-irradiated polymer films. 1. Grafting onto polyethylene, J. Eur. Polym. 25 (1989) 1137.

[63] S.H. Choi, Y. Nho, Radiation-induced graft copolymerization of binary monomer mixture containing acrylonitrile onto polyethylene films, Radiat. Phys. Chem. 58 (200) 157.

[64] K. Kobayashi, S. Tsuneda, K. Saito, H. Yamagishi, S. Furasaki, T. Sugo, Preparation of microfiltration membranes containing anion exchange groups, J. Membr. Sci. 76 (1993) 209-218.

[65] Z.W. Ma, M. Kotaki, S. Ramakrishna, Electrospun cellulose nanofibers as affinity membranes, Journal of Membrane Science, 265 (2005) 115-123.

[66] Z.W. Ma, S. Ramakrishna, Electrospun regenerate cellulose nanofiber affinity membrane functionalized with protein A/G for IgG purification, Journal of Membrane Science, 319 (2008) 23-28.

[67] H.C. Liu, J.R. Fried, Breakthrough of lysozyme through an affinity membrane of cellulose-cibracon blue, J. AICHE, 40 (1994) 40-49.

[68] F.T. Sarfert, M.R. Etzel, Mass transfer limitations in protein separations using ion exchange membranes, J. Chromatogr. A, 764 (1997) 3-20.

[69] L.Y. Zhong, K. Srirangan, K. Scharer, M. Moo-Young, D. Fenner, L. Crossley, Developing an RNase-free bioprocess to produce pharmaceutical-grade plasmig DNA using selective precipitation and membrean chromatography, Sep. Purif. Technol. 83 (2011) 121-129.

[70] L.R. Pereira, D.M. Prazeres, M. Mateus, Hydrophobic interaction membrane chromarography for plasmid DNA purification design and optimization, J. Sep. Sci. 33 (2010) 1175-1184.

[71] P.O. Syren, A. Rozkov, S.R. Schmidt, P. Stromberg, Miligram scale parallel purification of plasmid DNA using anion-exchange membrane capsules and multi-channel peristaltic pump, J. Chromatogr. B. 856 (2007) 68-74.

[72] T.A. Grein, R. Michalsky, M.V. Lopez, P. Czermak, Purification of a recombinant baculovirus Autographa californica M nucleopolyhedrovirus by ion-exchange membrane chromatography, J. Viral Methods (2012).

[73] K. Zimmermann, O. Scheibe, A. Kocourek, J. Muelich, E. Jurkiewicz, A. Pfiefer, Highly efficient concentration of lenti- and retroviral vectore preparations by membrane adsorbers and ultrafiltration, BMC Biotechnol. 11 (2011) 55.

[74] M. Wolff, C. Siewert, S. Lehmann, S.P. Hansen, R. Djurup, R. Faber, Capturing of cell culture-derived modified vaccinia Ankara virus by ion exchange and pseudo affinity membrane adsorbers, Biotechnol. Bioeng. 105 (2009) 761-769.

[75] T. Vicente, C. Peixoto, M.J.T. Carrondo, P.M. Alves, Purification of recombinant baculoviruses for gene therapy using membrane processes, Gene. Ther. 16 (2009) 766-775.

[76] B. Kalbfuss, M. Wolff, L. Geisler, A. Tappe, R. Wickramasinghe, V. Thom, Direct capture of influenza A virus from cell culture supernatant with Sartobind anion-exchange membrane adsorbers, J. Membr. Sci. 299 (2007) 251-260.

[77] R.H. Kutner, S. Puthil, M.P, Marino, J. Reiser, Simplified production and concentration of HIV-1-based lentiviral vectore using HYPERFlask vessels and anion exchange membrane chromatography, BMC Biotechnol. 9 (2009) 10.

[78] I.M. Hutten, Handbook of Nonwoven Filter Media, Butterworth-Heinemann, Oxford, Burlington, MA 2007

[79] H.T. Zhuo, J.L Hu, S.J. Chen, Electrospun polyurethane nanofibres having shape memory effect, Materials Letters, 62 (2008) 2078-2080.

[80] E.S. Abdou, S.S Elkoly, M.Z. Elsabee, E. Mohamed, Improved antimicrobial activity of polypropylene and cotton nonwoven fabrics by surface treatment and modification with chitosan, Journal of Applied Polymer Science, 108 (2008) 2290-2296.

[81] T.H. Cho, M. Tanaka, H. Onishi, Y. Kondo, T. Nakamura, H. Yamazaki, S. Tanase, T. Sakai, Battery performance and thermal stability of polyacrylonitrile nano-fiber-based nonwoven separations for Li-ion battery, Journal of Polymer Science, 181 (2008) 155-160.

[82] C.V. Cretu, C. Cojocaru, C. Preda, M. Macoveanu, Polypropylene thermocalendered nonwoven fabrics used for decontaminating waters polluted with oil products, Industrial Textiles, 59 (2008) 168-174.

[83] A. Patanaik, R.D. Anandjiwala, Water flow through the polypropylene-based geotextiles, Journal of Applied Polymer Science, 108 (2008) 3876-3880.

[84] C. Prahsarn, A. Matsubara, S. Motomura, T. Kikutani, Development of bicomponent spunbond nonwoven webs consisting of ultra-fine splitted fibers, International Polymer Processing, 28 (2008) 178-182.

[85] Z. Lewandowski, A. Ziabicki, L Jarecki, The nonwoven formation in the melt-blown process, Fibres & Textiles in Eastern Europe, 15 (2007) 77-81.

[86] G.S. Bhat, S.R. Malkan, Extruded continuous filament nonwovens: Advances in scientific aspects, Journal of Applies Polymer Science, 83 (2002) 572-585.

[87] Z.M. Huang, Y.Z. Zhang, M. Kotaki , S. Ramakrishna, A review on polymer nanofibers by electrospinning and their applications in nanocomposites, Composites Science and Technology, 63 (2003) 2223-2253.

[88] A. Turbak, Nonwovens: Theory, Process, Performance, and Testing, Tappi Press, Altanta, GA 1993.

[89] K. Singha, S. Maity, M. Singha, P. Paal, D.P. Gon, Effects of fiber diameter distribution of nonwoven fabrics on its properties, International Journal of Textile Science, 1 (2012) 7-14.

[90] A. Durany, N. Anantharamaiah, B. Pourdeyhimi, High surface area nonwovens via fibrillating spunbonded nonwovens comprising Islands-in-the-Sea bicomponent filaments: structure-process-property relationships, J. Mater. Sci. 44 (2009) 4926-5934.

[91] C.J. Ellison, A. Phatak, D.W. Giles, C.W. Macosko, F.S. Bates, Melt blown nanofibers: Fiber diameter distribution and onset of fiber breakup, Polymer, 48 (2007) 3306-3316.

[92] E.M. Teixeira, A.C. Correa, A. Manzoli, F.L. Leite, C.R. Oliveira, L.H.C Mattoso, Cellulose nanofibers from white and naturally colored cotton fibers, Cellulose, 17 (2010) 595-606.

[93] D. Stollner, F. Scheller, A. Warsinke, Activation of cellulose membranes with 1,1'-carbonyldiimidazole or 1-cyano-4-dimethylaminopyridinium tetraflouroborate as a basis for the development of immunosensors, Analytical Biochemistry, 304 (2002) 157-165.

[94] K. Kugel, A. Moseley, G.B. Harding, E. Klein, Microporous poly(caprolactam) hollow fibers for therapeutic affinity adsorption, Journal of Membrane Science, 74 (1992) 115-129.

[95] D. Duran, Investigation of the physical characteristics of polypropylene meltblown nonwovens under varying production parameters, Themoplastic Elastomers, Intech, Rijeka, Croatia 2012.

[96] E. Klein, Affinity membranes: a 10-year review, J. Membr. Sci. 179 (2000) 1-27.

[97] N. Fedorova, B. Pourdeyhimi, High strength nylon micro- and nanofiber based nonwovens via spundbonding, J. Appl. Polym. Sci. 104 (2007) 3434-3442.

[98] D. Li, Y. Xia, Electrospinning of nanofibers: Reinventing the wheel?, Adv. Mater. 16 (2004) 1151-1170.

[99] D. Reneker, I. Chun, Nanometre diameter fibers of polymer, produced by electrospinning, Nanotechnology 7 (1996) 216-223.

[100] H. Liu, Surface modified nonwoven membranes for bioseparations, Raleigh NC USA, North Carolina State Univ., PhD thesis, 2012.

[101] O.M. Herigstad, P.V. Gurgel, R.G. Carbonell, Transport and binding characterization of a novel hybrid particle impregnated membrane material for bioseparations, Biotechnol. Prog. 27 (2011) 129-139.

[102] Z.W. Ma, M. Kotaki, S. Ramakrishna, Electrospun cellulose nanofibers as affinity membranes, Journal of Membrane Science, 265 (2005) 115-123.

[103] Z.W. Ma, S. Ramakrishna, Electrospun regenerate cellulose nanofiber affinity membrane functionalized with protein A/G for IgG purification, Journal of Membrane Science, 319 (2008) 23-28.

[104] L.F. Zhang, T.J. Mankhaus, H. Fong, Fabrication and bioseparation studies of adsorptive membranes/felts made from electrospun cellulose acetate nanofibers, Journal of Membrane Science, 319 (2008) 176-184.

[105] H.L. Knudsen, R.L Fahmer, Y. Xu, L.A. Norling, G.S. Blank, Membrane ion-exchange chromatography for process-scale antibody purification, Journal of Chromatrography A, 907, 145-154.

[106] Y. Zheng, H. Liu, P.V. Gurgel, R.G. Carbonell, Polypropylene nonwoven fabrics with conformal grafting of poly(glycidyl methacrylate) for bioseparations, J. Membr. Sci. 364 (2010) 362-371.

[107] H. Liu, P.V. Gurgel, R.G. Carbonell, Preparation and characterization of anion exchange adsorptive nonwoven membranes with high protein binding capacity, Journal of Membrane Science, 493 (2015) 349-359.

[108] J.L. Novalis, N.J. Titchener,-Hooker, M. Hoare, Economic comparison between conventional and disposables-based technology for the production of biopharmaceuticals, Biotechnology and Bioengineering, 75 (2001) 143-153.

[109] J.X. Zhou, F. Solamo, T. Hong, M. Shearer, T. Tressel, Viral clearance using disposable systems in monoclonal antibody commercial downstream processing, Biotechnology and Bioengineering, 100 (2008) 488-496.

[110] J.X. Zhou, T. Tressel, Basic concepts in Q membrane chromatography for large-scale-antibody production, Biotechnol. Prog. 22 (2006) 341-349.

[111] E. Klein, Affinity membranes: a 10-year review, J. Membr. Sci. 179 (2000) 1-27.

[112] K. Kato, E. Uchida, E. Kang, Y Uyama, Y. Ikada, Polymer surface with graft chains, Progress in Polymer Science 28 (2003) 209-259.

[113] Z. Xu, L Wan, X Huang, Surface engineering of polymer membranes, surface modification by graft polymerization, Springer Berlin Heidelberg, Berlin Germany 2009.

[114] F. Garbassi, M. Morra, E. Occhiello, Contact angle hysteresis in oxygen plasma treated poly(tetrafluoroethylene), Langmuir 5 (1989) 872-876.

[115] C-M. Chan, Polymer surface modification and characterization, Carl Hanser, Munich Germany 1993.

[116] B. Zhao, W. Brittain, Polymer brushes: surface-immobilized macromolecules, Prog. Polym. Sci. 25 (2000) 677-710.

[117] Z. Zhao, J. Li, D. Zhang, C. Chen, Nanofiltration membrane prepared from polyacrylonitrile ultrafiltration membrane by low-temperature plasma: 1. Graft of acrylic acid in gas. Journal of Membrane Science 232 (2004) 1-8.

[118] Y. Lee, J Shim, Preparation of pH/temperature responsive polymer membrane by plasma polymerization and its riboflavin permeation, Polymer 38 (1997) 1227-1232.

[119] M. Walzak, S. Flynn, R. Foerch, J. Hill, E. Karbashewski, A. Lin, M. Srobel, UV and ozone treatment of polypropylene and poly(ethylene terephthalate), J. Adhes. Sci. Technol. 9 (1995) 1229-1248.

[120] P. Gatenholm, T. Ashida, A. Hoffman, Hybrid biomaterials prepared by ozone-induced polymerization. 1. Ozonation of microporous polypropylene, J. Polym. Sci. 35 (1997) 1461-1467.

[121] M. Mishra, Y. Yagci, Handbook of Vinyl Polymers: Radical Polymerization, Process, and Technology, CRC Press, Boca Raton, FL 2008

[122] S. Kuroda, I. Mita, K. Obata, S. Tanaka, Degradation of aromatic polymers: part IV. Effect of temperature and light intensity on the photodegradation of polyethersulfong, Polym. Degr. Stab. 27 (1990) 257.

[123] J. Crivello, G. Belfort, H. Yamagishi, Low fouling ultrafiltration and microfiltration aryl polysulfone, US Patent 5468390.

[124] H. Yamagishi, J. Crivello, G. Belfort, Development of a novel photo-chemical technique for modifying poly(arylsulfone) ultrafiltration membranes, J. Membrane Sci. 105 (1995) 237-247.

[125] Y. Zheng, H. Liu, P. Gurgel, R. Carbonell, Polypropylene nonwoven fabrics with conformal grafting of poly(glycidyl methacrylate) for bioseparations, J. Membr. Sci. 364 (2010) 362-371.

[126] M. Ulbricht, A. Oechel, C. Lehmann, G. Tomaschewski, H. Hicke, Gas phase photoinduced graft polymerization of acrylic acid onto polyacrylonitrile ultrafiltration membranes. J. Appl. Polym. Sci. 55 (1995) 1707-1723.

[127] M. Ulbricht, H. Matuschewski, A. Oechel, H. Hicke, Photo-induced graft polymerization surface modifications for the preparation of hydrophilic and low-protein-adsorbing ultrafiltration membranes, J. Membrane Sci. 115 (1996) 31-47.

[128] M. Ulbricht, M Riedel, U. Marx, Novel photochemical surface functionalization of polysulfone ultrafiltration membranes for covalent immobilization of biomolecules, J. Membr. Sci. 120 (1996) 239-259.

[129] M. Ulbricht, H. Yang, Porous polypropylene membranes with different carboxyl polymer brush layers for reversible protein binding via surface-initiated graft copolymerization, Chem. Mater. 17 (2005) 2622-2631.

[130] B. Yang, W. Yang, Thermo-sensitive switching membranes regulated by pore-covering polymer brushes, J. Membrane Sci. 218 (2003) 247-255.

[131] J. Kim, S. Ha, S. Nam, J. Rhim, K. Baek, Y. Lee, Selective permeation of CO_2 through pore-filled polyacrylonitrile membrane with poly(ethylene glycol), J. Membrane Sci. 186 (2001) 97-107.

[132] M. Hu, Q. Yang, Z. Xu, Enhancing the hydrophilicity of polypropylene microporous membranes by the grafting of 2-hydroxyethyl methacrylate via synergistic effect of photoinitiators, J. Membrane Sci. 285 (2006) 196-205.

[133] H. Liu, Y. Zheng, P. Gurgel, R. Carbonell, Affinity membrane development from PBT nonwoven by photo-induced graft polymerization, hydrophilization and ligand attachment, J. Membr. Sci. 428 (2013) 562-575.

[134] M. Arslan, Preparation and Use of Amine-Functionalized Glycidyl Methacrylate-g-Poly(ethylene terephthalate) Fibers for Removal of Chromium(IV) from Aqueous Solution, Fibers and Polymer, 11 (2010) 325-330.

[135] T. Carroll, N. Booker, J. Meier-Haack, Polyelectrolyte-grafted microfiltration membranes to control fouling by natural organic matter in drinking water, J. Mem. Sci. 203 (2002) 3-13.

[136] S. Abdel-Fattah, S. Shalaby, E. Allam, A. Hebeish, Benzoyl peroxide induced graft polymerization of 2-methyl-5-vinylpyridine onto polyester/wool blend, J. Appl. Polym. Sci. 21 (1977) 3355-3365.

[137] M. Okoniewski, J. Sojka-Ledakowicz, Chemically induced graft copolymerization of acrylic acid on polyester frabrics. I. Kinetic investigation of grafting, J. Appl. Polym. Sci. 35 (1988) 1241-1249.

[138] S. Edmondson, V. Osborne, W. Huck, Polymer brushes via surface-initiated polymerizations, Chem. Soc. Rev. 33 (2004) 14-22.

[139] P. de Gennes, Polymers at an interface: a simplified view, Adv. Colloid Interf. Sci. 27 (1987) 189-209.

[140] H. Liu, Y. Zheng, P. Gurgel, R. Carbonell, Affinity membrane development from PBT nonwoven by photo-induced graft polymerization, hydrophilization and ligand attachment, J. Membr. Sci. 428 (2013) 562-575.

[141] S. Tsuneda, H. Kagawa, K. Saito, T. Sugo, Hydrodynamic evaluation of three-dimensional adsorption of protein to a polymer chain grafted onto a porous substrate, J. Colloid Interface Sci. 176 (1995) 95-100.

[142] B. Bowes, A. Lenhoff, Protein adsorption and transport in dextran-modified ion-exchange media. II. Intraparticle uptake and column breakthrough, J. Chromatogr. A 1218 (2011) 4698-4708.

[143] H. Shinano, S. Tsuneda, K. Saito, S. Furasaki, T. Sugo, Ion exchange of lysozyme during permeation across a microporous sulfopropyl-group-containing hollow fiber, Biotechnol. Prog. 9 (1993) 193-198.

[144] H. Iwata, I. Hirata, Y. Ikada, Atomic force microscopic analysis of a porous membrane with pH sensitive molecular valves. Macromolecules 31 (1998) 3671-3678.

[145] B. Lego, W. Skene, S. Giasson, Swelling study of responsive polyelectrolyte brushes grafted from mica substrates: Effect of pH, salt, grafting density, Macromolecules 58 (2010) 4384-4393.

[146] E. Bittrich, K. Rodenhausen, K. Eichhorn, T. Hofmann, M. Shubert, M. Stamm, P. Uhlmann, Protein adsorption on and swelling of polyelectrolyte brushes: A simultaneous ellipsometry-quartz microbalance study, Biointerphases 5 (2010) 159-167.

[147] K. Saito, T. Kaga, H. Yamagishi, S. Furasaki, T. Sugo, J. Okamoto, Phosphorylated hollow fibers synthesized by radiation grafting and crosslinking, J. Membr. Sci. 43 (1989) 131-141.

[148] H. Allcock, F. Lampe, Contemporary Polymer Chemistry 2nd Edition, Prentice Hall, Englewood, NJ 1990.

[149] G. Odian, Principles of Polymerization 4th Edition, Wiley and Sons, Hoboken, NJ 2004.

[150] C. Wolf, W. Burchard, Branching in free radical polymerization due to chain transfer. Application to poly(vinyl acetate), Macromol. Chem. 177 (1976) 2519-2538.

[151] K. Fukimotoa, H. Inone, Y. Ikada, Protein adsorption and platelet adhesion onto polyurethane grafted with mthoxyl-poly(ethylene glycol) methacylate by plasma technique, J. Biomed. Mater. Res. 27 (1993) 1559-1567.

[152] P. Wang, K. Tan, K. Kang, Surface modification of poly(tetraflourothylene) films via grafting of poly(ethylene glycol) for reduction in protein adsorption, J. Biomater. Sci. Polym. Ed. 11 (2000) 169-186.

[153] J. Lee, B. Jeong, H. Lee, Plasma protein adsorption and platelet adhesion onto comb-like PEO gradient surface, J. Biomed. Mater. Res. 34 (1997) 105-114.

[154] M. Kim, K. Saito, S. Furusakei, T. Sugo, I. Ishigaki, Protein adsorption capacity of porous phenylaniline-containing membrane based on a polyethylene matrix, J. Chromatogr. 586 (1991) 27–33.

[155] M. Kim, K. Saito, S. Furusaki, T. Sato, T. Sugo, I. Ishigaki, Adsorption and elution of bovine bovine gamma-globulin using an affinity membrane containing hydrophobic amino acids, J. Chromatogr. 585 (1991) 45–51.

[156] H. Iwata, K. Saito, S. Furusaki, T. Sugo, J. Okamoto, Adsorption characteristics of an immobilized metal affinity membrane, Biotechnol. Prog. 7 (1991) 412–419.

Chapter 2

Reducing Diffusion Limitations in Ion Exchange Grafted Membranes Using High Surface Area Nonwovens

Abstract

Polybutylene terephthalate (PBT) nonwovens can be readily grafted with glycidyl methacrylate (GMA) via UV induced radical polymerization to create uniform and conformal polymer brush networks around each fiber that can be chemically modified to function as anion or cation exchangers. Protein binding capacities achieved by these grafted materials are many times larger than monolayer coverage around the fibers, but require very long residence times to reach equilibrium due to diffusional limitations within the grafted layers. The rates of adsorption of proteins by ion exchange were measured in an islands-in-the-sea (I/S) PBT nonwoven with average fiber diameter of approximately 1 μm and in a commercially available PBT nonwoven with average fiber diameter of approximately 3 μm. Both nonwovens were grafted successfully with polyGMA and they showed almost identical ion exchange equilibrium protein binding capacities at similar weight % grafting. However, the grafted I/S nonwoven membrane exhibited a substantially higher amount of protein binding at short times and it was able to reach equilibrium in a fraction of the time required by the grafted commercial nonwoven with larger fiber diameters. The faster rate of protein adsorption observed with the I/S PBT nonwoven is the result of the thinner polyGMA graft layer thicknesses around the fibers compared to those in the commercial PBT with the same weight % grafting. The data for the rate of adsorption of protein through the functionalized polyGMA grafted layers was analyzed using a shrinking core model.

Keywords: UV grafting, islands-in-the-sea nonwoven, diffusion limited, ion exchange protein capture, shrinking core

2.1 Introduction

Membrane chromatography offers several potential advantages over traditional packed bed chromatography as a platform for bioseparations. The interconnected pores of membranes permit high rates of volumetric throughput without substantial pressure drops when compared to packed beds [1-5]. Chromatographic resins need to be packed, they are not normally disposable, and as a result they require validated cleaning and regeneration processes for their use [4]. On the other hand, many membranes can be made from polymers using scalable production techniques, enabling their use as stackable, ready-to-use, disposable bioseparation filters [3]. Nonwoven membranes are particularly attractive for these applications since they are highly engineered to exhibit controllable porosities, fiber diameters, and pore sizes with low cost materials using high-rate manufacturing technologies [6]. Protein binding to membranes is largely limited to the surface area created by the pores that are available for both flow and adsorption [1,2,4,5]. This eliminates all diffusional limitations to adsorption, but it also reduces the binding capacity of membranes compared to chromatographic resins. Commercial nonwovens have a fraction of the surface area of chromatographic resins, resulting in low binding capacities for most target protein capture applications [7]. By tethering polymer brushes to the surface of the fibers in a nonwoven membrane, 3-dimensional binding domains can be created that can substantially increase the overall protein binding capacity [2,8-11]. Polymer brush grafting has been known to increase protein adsorption capacity by several times that of monolayer coverage in traditional

chromatography resins, hollow fiber membranes, cast membranes, and nonwoven membranes [2,12-14].

Polymer grafting can change drastically the surface properties of supports. It can help tune the polarity of a surface to reduce or increase biomolecule adsorption and it can be used to introduce functional groups for ligand or spacer arm attachment in the 3-dimensional micro-environment introduced on the supporting interface [2,3, 12-16]. In a previous study conducted by Liu *et al.,* glycidyl methacrylate (GMA) monomer was successfully grafted to a commercially available polybutylene terephthalate (PBT) nonwoven fabric [13]. Uniform and conformal polyGMA grafts were achieved around individual PBT fibers using UV-induced free radical polymerization. The polyGMA was attached directly to the PBT surface via hydrogen abstraction to initiate GMA polymerization using benzophenone (BP) as the initiator [13]. PBT is advantageous to use as a starting material for polyGMA grafting because it does not require the separate surface UV pretreatment necessary for grafting many polyolefins commonly used in the production of nonwoven fabrics [2,12,16]. PBT Nonwoven is inherently hydrophobic in nature leading to a high degree of nonspecific protein adsorption, making the base material itself a poor platform for bioseparations. Direct hydrolysis of polyGMA grafts on PBT using acidic conditions makes the fiber surface completely hydrophilic and substantially decreases nonspecific hydrophobic protein adsorption [13]. Each monomer unit of GMA contains an epoxy end group that can be used to covalently attach ligands via nucleophilic substitution with available amines, thiols, and hydroxyl groups [17,18]. In the study by Liu *et al*., diethylene glycol covalently attached to the polyGMA brushes was also found to substantially eliminate protein adsorption by nonspecific hydrophobic interactions [13].

PolyGMA grafted nonwovens offer a convenient platform for the development of effective ion exchange membranes. Saito et al. [15] successfully grafted polyGMA brushes to polypropylene fabrics and polyethylene hollow fibers. These grafted materials were functionalized with phosphoric acid groups to develop strong cation exchange membranes to capture divalent metal cations. In a study by Zheng *et al*. [12] polyGMA was grafted to polypropylene nonwoven and functionalized with diethyl amine (DEA) to develop a weak anion exchanger. This material achieved equilibrium binding capacities for bovine serum albumin (BSA) of 120 mg/g of membrane. Liu *et al*. [19] investigated the effects of various degrees of polyGMA grafting on nonwoven PBT for the capture of BSA by anion exchange. In that study, polyGMA grafts were converted to weak anion exchangers with DEA and challenged with BSA. It was determined that the overall protein binding capacity increased with the degree of grafting (% weight gain). The largest equilibrium binding capacity of 800 mg/g was observed at a 12% polyGMA weight gain. This investigation also showed that residence times of several hours to a full day were required to reach maximum binding, and that these binding times increased with increased grafting weight % gain. These long residence times preclude the use of these polyGMA grafted nonwoven PBT membranes for the development of high throughput, high capacity protein capture devices for downstream processing. These long residence times resulted from diffusional limitations for protein transport through the grafted polymer layer. It was suspected that the diffusional limitations could be mitigated using nonwoven PBT membranes with smaller fiber diameters, and thus higher specific surface areas, that would result in correspondingly thinner polyGMA grafted layers for a given weight % gain of grafting.

The specific surface area of a nonwoven material (area/mass) is inversely proportional to the average fiber diameter [20]. There are some nonwoven fabric technologies capable of producing nonwovens with submicron sized fiber diameters that can yield a significant increase in specific surface area. Electrospinning is an emerging technology capable of making nanofiber nonwovens. However, the membranes resulting from this process often exhibit low mechanical integrity and high compressibility, and production rates are relatively slow [21- 23]. A solution to the potential commercial production of nanofiber nonwovens is the utilization of bicomponent fibers in the spunbonding process for production of nonwoven mats. In this production scheme two polymers can be coextruded from the same spinneret where they combine to become a cohesive fiber [23]. The fibers can also be extruded in a segmented pie or core in sheath configuration. These fibers can then be fractured to release many fibers of much smaller diameter, or one of the polymers can be selectively dissolved leaving a much smaller set of fibers in the nonwoven matrix [20, 23].

The Islands-in-the-Sea (I/S) nonwoven technology is an extension of the core in sheath bicomponent filament process. This type of nonwoven has many permanent polymer cores within the fiber known as “islands” embedded in a sacrificial polymer sheath known as the “sea”. Fedorova *et al*. [23] investigated how varying the number of “islands” and the ratio of “islands” to “sea” affects final fiber diameter. In this study I/S nonwovens were made with nylon-6 (islands) and polylactic acid (sea). Nonwovens were synthesized with the number of islands ranging from 36 to 360 and with “islands” to “sea” ratios of 25:75 (w:w) and 75:25 (w:w). Fig. 2.1 displays a schematic of the cross sectional view of two different I/S fibers from the study by Fedorova *et al.*.

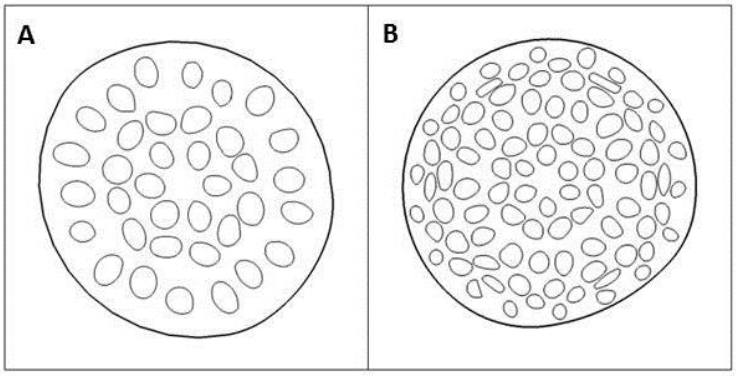

Fig. 2.1 Cross section schematic of I/S fibers with 36 nylon-6 islands in a PLA sea (A) and 108 nylon-6 islands in a PLA sea (B) [23].

Fig. 2.1 offers a visual comparison of two different I/S fibers synthesized with nylon-6 "islands" and polylactic acid (PLA) "sea" at an "island" count of 36 (A) and an "island" count of 108 (B). Polylactic acid (PLA) has a lower melting temperature compared to nylon-6 and can easily be decomposed with a hot caustic bath, making it a great candidate for a dissolvable "sea". It was found that fiber diameters as small as 360 nm could be obtained by increasing the island count or by decreasing the polymer ratio of "islands" to "sea" [23]. I/S nonwovens are capable of achieving smaller fiber diameters and therefore, higher specific surface areas compared to commercially available nonwovens made by melt blown or spunbond technologies while still conserving high productivity of fiber production and dimensional stability [23].

In this paper, we investigate the properties of anion and cation exchange membranes generated by grafting polyGMA layers onto I/S PBT nonwovens with 1 μm average fiber diameters and commercial melt blown PBT nonwoven fabrics with 3 μm fiber diameters.

The grafted nonwovens were functionalized to create both weak anion exchange and strong cation exchange membranes and tested for their ability to capture the target proteins BSA and human immunoglobulin G (hIgG) respectively. The effects of the polyGMA grafting levels on the equilibrium binding capacities for protein adsorption were determined and compared. The rates of protein adsorption were also measured to determine the extent of protein diffusion limitations within the polyGMA grafted layers in these two nonwoven systems and the results were analyzed using a shrinking core diffusion model.

2.2 Experimental

2.2.1 Materials and reagents

Islands-in-the-sea nonwoven PBT fabrics with a 108 island count were produced on the pilot facilities at the Nonwovens Institute (NWI, North Carolina State University, Raleigh, NC). The island count refers to the number of discrete PBT fibers that are liberated once the PLA "sea" has been removed. The I/S nonwoven was manufactured with a basis weight of 100 g/m^2 consisting of 50% PLA as the "sea" polymer and 50% PBT as the "island" polymer, the basis weight after "sea" removal is 50 g/m^2. Macopharma (Tourcoing, France) provided commercially available meltblown PBT nonwovens with a basis weight of 52 g/m^2. Glycidyl methacrylate (GMA) was purchased from Pflatz & Bauer (Waterbury, CT). Inhibitors in GMA were removed through a pre-packed inhibitor removal column to remove hydroquinone and monomethyl ether hydroquinone (Sigma Aldrich, St. Louis, MO). Benzophenone (BP) was purchased from Sigma Aldrich (St. Louis, MO). Sodium hydroxide, 1-butanol, tris base, hydrochloric acid, sodium chloride and sodium acetate trihydrate were purchased from Fisher Scientific (Fairlawn, NJ). Tetrahydrofuran (THF), methanol, sulfuric acid, and acetic acid were purchased from BDH (West Chester, PA). Diethylamine (DEA)

was purchased from Alfa Aesar (Ward Hill, MA). Phosphoric acid (85%) was purchased from Acros Organics (Fairlawn, NJ). Solid phase extraction tubes were purchased from Supelco (Bellefonte, PA). Albumin from bovine serum (BSA) was purchased from Sigma Aldrich (St. Louis, MO). Human immunoglobulin G (hIgG) was purchased from Equitek-Bio Inc. (Kerrville, TX).

2.2.2 PLA removal from I/S nonwovens

The 50% PLA "sea" of the 108 I/S nonwovens had to be removed to liberate the PBT "islands" prior to grafting. PLA was decomposed using 10% w/w sodium hydroxide in DI water at 80-90°C. I/S nonwovens were submerged in caustic bath for 5 min with constant stirring until all of the PLA had been dissolved from the nonwovens. The PBT nonwovens were then washed extensively with DI water until a neutral pH was achieved. Samples were then allowed to air dry overnight. Fig. 2.2A and 2.2B display a 108 I/S PBT nonwoven before and after the removal of PLA, respectively.

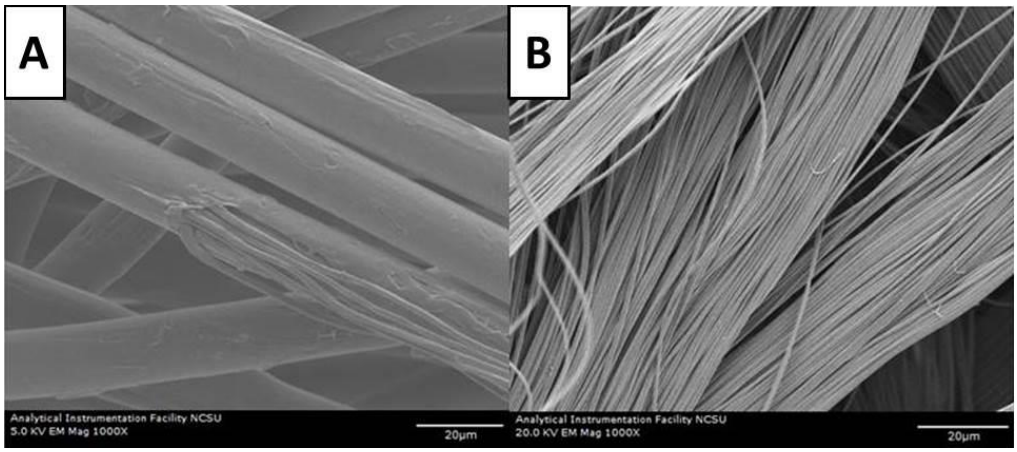

Fig. 2.2 (A) 108 I/S PBT nonwoven prior to PLA removal. (B) 108 I/S nonwoven post PLA removal. The PBT fibers released after PLA removal maintain the general direction of the original PLA fibers.

In Fig. 2.2A PLA is still present, encapsulating the PBT "islands", showing the initial larger fibers of about 15 μm in diameter prior to PLA removal. Fig. 2.2B shows the nonwoven post PLA removal to liberate 108 discreet PBT fibers that are approximately 1 μm in diameter.

2.2.3 UV-induced polyGMA grafting onto PBT nonwovens

The GMA grafting solution consisted of 20% v/v GMA monomer in 1-butanol as the solvent. The photoinitator benzophenone (BP) was added to the grafting solution in a BP:GMA ratio of 1:20 (mol:mol) [12]. Commercially available PBT nonwovens and 108 I/S PBT nonwovens after PLA removal were cut to 75 x 50 mm size samples and weighed prior to grafting, samples were approximately 200 mg and 180 mg for commercial PBT and 108 I/S PBT respectively. Nonwovens were saturated with grafting solution by spraying 1.5-2.0 ml of grafting solution via syringe, and placed between two borosilicate glass slides (75 x 50 mm). A UV lamp (model EN-180L, Spectronics Corporation, Westbury, NY) with a 365 nm wavelength and an intensity of 5 mW/cm^2 was used to induce free radical polymerization of the GMA onto the PBT surface [13]. The distance between the lamp and the sample was 3 mm. Samples were irradiated at various exposure times to achieve different degrees of polyGMA grafting with different % weight gains. After polyGMA grafting, the samples were placed in a flask containing 100 ml of THF, the flask with the THF and samples was sonicated with an ultrasonic bath (Bransonic 3510R-MT, Branson Ultrasonics Corporation, Danbury, CT) for 30 min to remove any unreacted grafting solution or untethered polyGMA. Following the THF wash the samples were removed from the flask and placed in a flask containing 100 ml of methanol, the flask containing the samples and methanol was sonicated with an ultrasonic bath for 10 min to remove THF from the nonwovens. Following the methanol wash the samples were removed from the flask and allowed to dry in air overnight.

The final weight of the nonwovens was measured and the degree of polyGMA grafting was determined using Eq. 1 in terms of a % weight gain due to grafting.

$$Degree\ of\ polyGMA\ grafting\ (\%\ weight\ gain) = \frac{W_f - W_i}{W_i} \times 100\% \quad (1)$$

In Eq. 1 W_i is the initial nonwoven weight prior to grafting and W_f is the final nonwoven weight after polyGMA grafting. The % weight gain defined in Eq. 1 is abbreviated as % Wt. Gain in the figures presented in this paper.

2.2.4 Functionalization of polyGMA grafted PBT nonwovens

PolyGMA grafted PBT nonwovens were functionalized to produce weak anion exchangers by immersion in 50% v/v aqueous diethyl amine (DEA) solution, thus creating a tertiary amine on the polyGMA brushes [19]. Grafted PBT nonwoven samples between 180 and 200 mg (75 x 50 mm) were immersed in 100 ml of the DEA solution. The reaction was kept at a constant 30°C with agitation at 100 rpm using an incubation shaker (Certomat® RM, B. Braun Biotech International, Melsungen, Germany) contained in an incubation hood (Certomat® HK, B. Braun Biotech International, Melsungen, Germany). Following amination, samples were placed in a flask containing 100 ml of DI water, the flask was placed in an ultrasonic bath (Bransonic 3510R-MT, Branson Ultrasonics Corporation, Danbury, CT) for 5 min, to remove excess DEA. Following sonication, the DI water wash was replaced with fresh DI water and the process was repeated until a neutral pH of 7.0 was verified with pH testing paper, 10 washes ensured that all DEA had been removed from the nonwoven. Any unreacted epoxy groups were hydrolyzed by immersion of the sample in 100 ml of 100 mM sulfuric acid overnight [19]. Following hydrolysis of the epoxy groups, samples were placed in a flask containing 100 ml of DI water, the flask was placed in an

ultrasonic bath (Bransonic 3510R-MT, Branson Ultrasonics Corporation, Danbury, CT) for 5 min, to remove excess sulfuric acid. Following sonication, the DI water wash was replaced with fresh DI water and the process was repeated until a neutral pH of 7.0 was verified with pH testing paper, 10 washes ensured that all the sulfuric acid had been removed from the nonwoven. The samples were then air dried overnight.

PolyGMA grafted PBT nonwovens were functionalized to create strong cation exchangers by attaching phosphoric acid groups to the polyGMA brushes. Approximately 20 mg (25 x 15 mm) of grafted PBT nonwoven samples were immersed in 10 ml of 85% w/w phosphoric acid and incubated at 80 °C overnight (Isotemp 115, Fisher Scientific, Fairlawn, NJ) [24]. Following functionalization the samples were placed in a flask containing 100 ml of DI water, the flask was placed in an ultrasonic bath (Bransonic 3510R-MT, Branson Ultrasonics Corporation, Danbury, CT) for 5 min, to remove excess phosphoric acid. Following sonication, the DI water wash was replaced with fresh DI water and the process was repeated until a neutral pH of 7.0 was verified with pH testing paper, 5 washes ensured that all phosphoric acid had been removed from the nonwoven. Any unreacted epoxy groups were hydrolyzed by immersion of the sample in 10 ml of 100 mM sulfuric acid overnight. Following hydrolysis of the epoxy groups, samples were placed in a flask containing 100 ml of DI water, the flask was placed in an ultrasonic bath (Bransonic 3510R-MT, Branson Ultrasonics Corporation, Danbury, CT) for 5 min, to remove excess sulfuric acid. Following sonication, the DI water wash was replaced with fresh DI water and the process was repeated until a neutral pH of 7.0 was verified with pH testing paper, 10 washes ensured that all the sulfuric acid had been removed from the nonwoven. The samples were then air dried overnight.

2.2.5 Material characterization

To determine the average fiber diameter and evaluate the effectiveness of UV grafting, scanning electron microscopy images were obtained using a Hitachi S-3200N variable pressure scanning electron microscope (VPSEM) (Hitachi High Technologies America, Inc., Schaumberg, IL). Nonwoven samples were sputter coated with Pd/Au in argon gas. Images were captured using the microscope with an accelerating voltage of 20 kV at a working distance of 33 mm. The distances across fiber diameters were measured on the SEM micrographs using the Revolution software from 4pi Analysis, Inc. (Hillsborough, NC). The average fiber diameter of the 108 I/S PBT and the commercially available PBT nonwovens were determined by measuring the distance across 150 random fibers of the SEM micrographs.

The specific surface areas of the 108 I/S PBT nonwoven after removal of the PLA sea and the commercially available meltblown nonwoven were determined using nitrogen adsorption by the Brunauer, Emmet and Teller (BET) multipoint analysis. One gram of nonwoven material was loaded into a 12 mm sample holder and analyzed on an Autosorb^{TM}-1C chemisorption-physisorption analyzer (Quantachrome Industries, Boynton Beach, FLA) measuring 39 nitrogen partial pressure points.

The average pore sizes of the commercially available PBT meltblown nonwoven and the 108 I/S PBT nonwoven after PLA removal were determined using capillary flow porometry. Nonwoven samples were tested on a CFP-1100-AX capillary flow porometer (Porous Materials Inc., Ithaca, NY). The wetting liquid was Galwick^{TM} (Porous Materials Inc., Ithaca, NY), with a surface tension of 15.9 dynes/cm.

2.2.6 Static (equilibrium) protein adsorption

2.2.6.1 Static equilibrium protein adsorption at various degrees of polyGMA grafting

Commercially available PBT nonwovens and 108 I/S PBT nonwovens were tested for their equilibrium static protein binding capacity at various degrees of polyGMA coverage in a weak anion exchange format, as well as a strong cation exchange format. Commercially available PBT nonwovens grafted at 2.5, 5.9, 7.2, 12 and 20 % weight gains and 108 I/S PBT nonwovens grafted at 5.6, 12, and 20 % weight gains were functionalized as weak anion exchangers with DEA. These membranes were challenged with pure BSA as a model protein to establish the static equilibrium binding capacity for these anion exchange membranes. BSA has a molecular weight of 66.5 kDa and an isoelectric point of 4.7 [Sigma Aldrich, St. Louis MO]. Approximately 20 mg (25 x 15 mm) of nonwoven sample was placed in a 3 ml solid phase extraction (SPE) tube and washed with 3 ml of low ionic strength binding buffer, 20 mM Tris HCl pH 7.0, 5 times. Samples were equilibrated for at least 30 min in binding buffer on a rotator (Tissue culture rotator, Glas-col, Terre Haute, IN) prior to BSA binding. Once equilibrated 3 ml of 10 mg/ml BSA in 20 mM Tris HCl pH 7.0 were added to each sample and allowed to bind overnight for 15 hours. The low ionic strength buffer at pH 7.0 ensures that the DEA functionalized grafted PBT is positively charged and that BSA is negatively charged to facilitate binding with a minimal amount of ions that would disrupt protein binding. After binding, samples were washed with 3 ml of 20 mM Tris HCl pH 7.0. Five washes with 20 mM Tris HCl pH 7.0 were required to remove all the unbound protein, verified by a negligible amount of protein in the fifth and final wash using UV-Vis spectroscopy at 280 nm. Bound BSA was eluted using a high ionic strength elution buffer, 3 ml of 20 mM Tris HCl pH 7.0 + 1 M NaCl as the elution buffer. The high concentration of ions in the elution buffer effectively disrupts the ionic interaction, removing the protein from

the nonwoven. Elution fractions were collected and protein concentrations were determined using UV-Vis spectroscopy at 280 nm. Static equilibrium binding capacity (M_{eq}, in mass of protein per mass of membrane) values were determined using Eq. 2.

$$M_{eq}\ \left(\frac{mg}{g}\right) = \frac{Protein\ Concentration\ \left(\frac{mg}{ml}\right) \times Volume\ of\ Elution\ Fraction}{Mass\ of\ membrane} \quad (2)$$

In a similar fashion, strong cation exchange membranes were synthesized by functionalizing grafted PBT nonwovens with phosphate groups. Commercially available PBT meltblown nonwovens grafted at 5.3, 10 and 18 % weight gains and 108 I/S PBT nonwovens grafted at 7, 12, and 18 % weight gains were functionalized to produce strong cation exchangers. These membranes were challenged with pure polyclonal hIgG as a model protein to establish the equilibrium binding capacity for these cation exchange membranes. Polyclonal hIgG has a molecular weight of 150 kDa and an isoelectric point between 7-9 [Equitek-Bio, Kerrville TX]. Approximately 20 mg (25 x 15 mm) of nonwoven sample were placed in a 3 ml SPE tube and washed with 3 ml low ionic strength binding buffer, 20 mM acetate pH 5.5, 5 times. Samples were equilibrated for at least 30 min in binding buffer on a rotator (Tissue culture rotator, Glas-col, Terre Haute, IN) prior to hIgG binding. Once equilibrated, 3 ml of 10 mg/ml hIgG in 20 mM acetate pH 5.5 were added to each sample and allowed to bind overnight for 15 hours. The low ionic strength buffer at pH 5.5 ensures that the phosphoric acid functionalized grafted PBT is negatively charged and that hIgG is positively charged to facilitate binding with a minimal amount of ions that would disrupt protein binding. After binding, samples were washed with 3 ml of 20 mM acetate pH 5.5. Five washes with 20 mM acetate pH 5.5 were required to remove all the unbound protein, verified by a negligible amount of protein in the fifth and final wash using UV-Vis

spectroscopy at 280 nm. Bound hIgG was eluted using 3 ml of a high ionic strength elution buffer, 20 mM acetate pH 5.5 + 1 M NaCl. The high concentration of ions in the elution buffer effectively disrupts the ionic interaction, removing the protein from the nonwoven. Elution fractions were collected and protein concentration was determined using UV-Vis spectroscopy at 280 nm. Eq. 2 was used to calculate the static equilibrium binding capacity.

2.2.6.2 Kinetics of protein adsorption

These experiments were aimed to determine the rate of protein adsorption on grafted ion exchange functionalized nonwoven PBT membranes. In this experiment, commercially available PBT nonwovens and 108 I/S PBT nonwovens were grafted at the same degree of polyGMA coverage (% weight gain), as well as, the same dry polyGMA graft thickness. The dry thickness of the polyGMA graft can be estimated from the % weight gain of polyGMA of the sample and the densities of polyGMA and PBT, assuming that the grafting is both uniform and conformal. These assumptions allow the volumes of the original PBT fiber and the polyGMA graft layer to be treated as concentric cylinders with a cylindrical outer grafted layer surrounding a cylindrical PBT inner core. Using the % weight gain as defined in Eq. 1 with expressions for the outer volume of the cylindrical polyGMA grafted layer and the inner volume of the PBT cylindrical core it is possible to derive an expression for the approximate dry grafted layer thickness (δ) as shown in Eq. 3. A complete derivation of Eq. 3 can be found in the Supplemental Information: Derivation of dry polyGMA graft thickness.

$$\delta = \sqrt{\left(\frac{\%\, weight\ gain}{100\%}\right)\frac{\rho_{PBT}}{\rho_{polyGMA}} r_1^2 + r_1^2} - r_1 \qquad (3)$$

In Eq. 3, δ is the dry polyGMA graft thickness, r_1 is the average fiber diameter of the specific PBT nonwoven that has been grafted, ρ_{PBT} is the density of PBT polymer (1.30 g/cm^3, [25]) and $\rho_{polyGMA}$ is the density of dry polyGMA polymer (0.80 g/cm^3,[26]). Table 2.1 contains the list of samples produced for the experiments analyzing the influence of contact time on protein binding with their respective % weight gains, dry polyGMA brush thicknesses and type of functionalization.

Table 2.1: PolyGMA grafted nonwovens used in protein adsorption rate studies with specific degrees of grafting, dry graft thickness (δ), and ion exchange functionality.

Material type	% weight gain	δ (nm)	Ion exchange function
Commercial PBT	20	227	Anion exchange
Commercial PBT	5.9	70	Anion exchange
108 I/S PBT	20	69	Anion exchange
Commercial PBT	18	205	Cation exchange
Commercial PBT	5.3	63	Cation exchange
108 I/S PBT	18	63	Cation exchange

Approximately 20 mg (25 x 15 mm) of nonwoven sample was placed in a 3 ml SPE tube and washed extensively with binding buffer, 20 mM Tris HCl pH 7.0 for anion exchange experiments with BSA, or 20 mM acetate pH 5.5 for cation exchange experiments with hIgG. Samples were equilibrated for at least 30 min in binding buffer on a rotator (Tissue culture rotator, Glas-col, Terre Haute, IN) prior to protein binding. Once samples were equilibrated they were challenged with either 3 ml of 10 mg/ml BSA or 3 ml of 10 mg/ml hIgG for anion exchange or cation exchange nonwovens respectively. Protein was allowed to bind at various exposure times between 30 seconds to 15 hours. After binding, anion exchange samples that had bound BSA were washed five times with 3 ml of 20 mM Tris HCl pH 7.0 and cation exchange samples that bound hIgG were washed five times with

3 ml of 20 mM acetate pH 5.5 to remove any unbound protein. The BSA was eluted using 3 ml of the high ionic strength elution buffer, 20 mM Tris HCl pH 7.0 + 1 M NaCl. The hIgG was eluted using 3 ml of the high ionic strength elution buffer, 20 mM acetate pH 5.5 + 1 M NaCl. The elution fractions were analyzed using UV-Vis spectroscopy at 280 nm and the amount of protein bound for each material was calculated using Eq. 2.

2.3 Results and discussion

2.3.1 Material characterization

Commercial PBT melt blown nonwovens and 108 I/S PBT nonwovens after PLA removal were evaluated with the variable pressure scanning electron microscope (VPSEM) to determine the average fiber diameter. The commercial PBT nonwovens had an average fiber diameter of 3000 nm ± 900 nm and the 108 I/S PBT nonwovens had an average fiber diameter of 916 nm ± 174 nm. The specific surface area of the nonwovens was determined using the BET method for nitrogen adsorption. The commercial PBT nonwovens were found to have a specific surface area of 0.86 m^2/g and 108 I/S PBT after PLA removal had a specific surface area of 2.45 m^2/g according to the BET analysis. The average flow pore size was determined using capillary flow porometry. Commercial PBT exhibited a mean flow pore size of 8.73 µm ± 3.10 µm and the 108 I/S PBT after PLA removal had a mean flow pore size of 8.09 µm ± 11.9 µm. Fig. 2.2 shows the 108 I/S PBT before (A) and after (B) removal of the PLA "sea". It can be noticed that the fibers after removal of PLA largely keep their original directional arrangement. This causes the material to have a wide pore size distribution, with the pore structure of the original material being maintained, and the addition of finer pores produced once the PLA is removed.

2.3.2 Grafting of PBT nonwovens

Commercial PBT and 108 I/S PBT nonwovens were successfully grafted with various degrees of polyGMA coverage. The results for the degree of grafting at increasing UV exposure times are presented in Fig. 2.3.

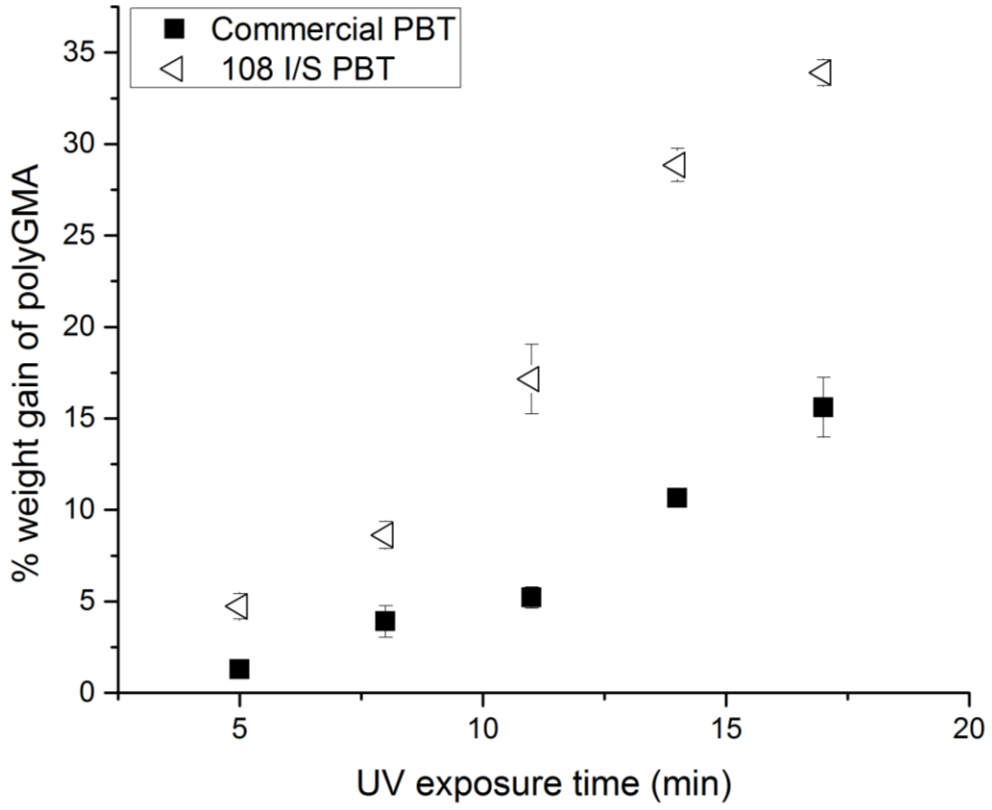

Fig. 2.3 Extent of polyGMA grafting at various UV exposure times for commercial PBT nonwoven and 108 I/S nonwovens after PLA removal.

From Fig. 2.3 it is apparent that the 108 I/S PBT nonwovens graft at a faster rate than the commercial PBT nonwovens. Compared to the commercial PBT nonwovens, the 108 I/S PBT nonwovens have 2.85 times more available area for initiation of GMA polymerization, resulting in approximately a 2.4 times higher rate of grafting. Both nonwovens exhibit complete conformal and uniform polyGMA graft coverage at different minimum degrees of

grafting: above 3% weight gain for the commercial PBT melt blown nonwoven and above 6% weight gain for 108 I/S PBT nonwoven. SEM images of the 108 I/S PBT nonwoven and the commercial PBT nonwoven before and after grafting at 20% weight gain are presented in Fig. 2.4.

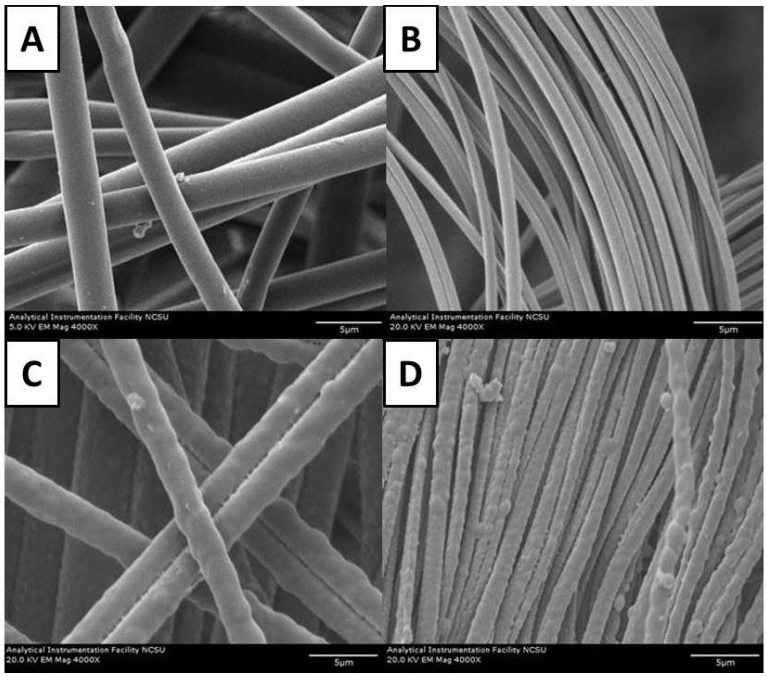

Fig. 2.4 (A) Commercial PBT nonwoven prior to grafting, (B) 108 I/S PBT nonwoven prior to grafting, (C) commercial PBT nonwoven grafted to 20% weight gain, (D) 108 I/S PBT nonwoven grafted to 20% weight gain.

Fig. 2.4C and 2.4D display a visible increased roughness on the surface of the PBT fibers attributed to polyGMA grafting that is not present in Fig. 2.4A and 2.4B for the un-grafted PBT nonwoves. In addition to increasing the rate of polyGMA grafting, the smaller diameters of the 108 I/S fibers have a significant impact on the thickness of the grafted layer. In Fig. 2.4C and 2.4D both the commercial PBT and the 108 I/S PBT have the same 20% weight gain of polyGMA grafting. However, there is more available surface area to graft in a

given sample of the 108 I/S nonwoven, resulting in a thinner grafted layer thickness than in a commercial PBT nonwoven. The actual dry graft thickness for various degrees of grafting on commercial PBT and 108 I/S PBT were calculated using Eq. 3 and presented in Table 2.1. A visual schematic comparing the dry polyGMA graft thickness for commercial PBT and 108 I/S PBT grafted at 20% weight gain and commercial PBT grafted at 5.9% weight gain are presented in Fig. 2.5.

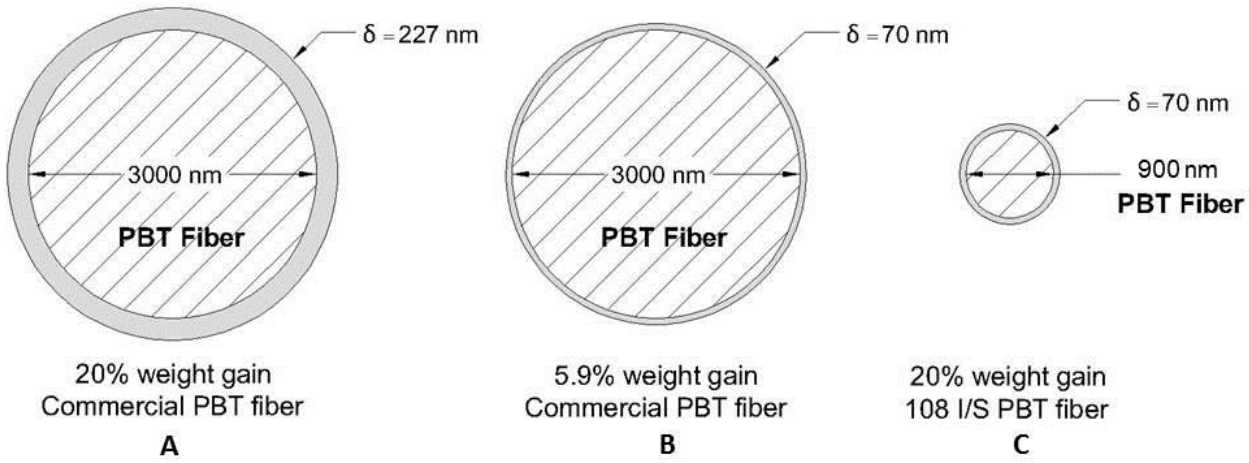

Fig. 2.5 Schematic comparing the fiber diameter and dry graft layer thicknesses of (A) commercial PBT grafted to 20% weight gain, (B) commercial PBT nonwoven grafted to 5.9% weight gain, and (C) 108 I/S PBT nonwoven grafted to 20% weight gain.

The visual representations in Fig. 2.5 illustrate how a thicker polyGMA graft layer is required to achieve 20% weight gain on commercial PBT nonwovens (Fig. 2.5A) compared to 108 I/S PBT nonwovens (Fig. 2.5C) for the same % weight gain of grafting. It can also be seen that in order for the grafted commercial PBT nonwoven to have the same grafted layer thickness as an I/S PBT nonwoven, the % weight gain of the commercial PBT needs to be over three times smaller than that of the I/S grafted nonwoven (compare Fig. 2.5B to Fig. 2.5C). As will be seen subsequently, the grafted layer thickness controls the rate of

adsorption of protein to the membrane. However, the equilibrium binding capacity is only a function of the % weight gain.

2.3.3 Equilibrium protein binding ion exchange capacity of derivatized PBT nonwovens

Commercial PBT nonwovens and 108 I/S nonwovens were grafted at various % weight gains and their equilibrium protein binding capacities for both anion exchange capture of BSA and cation exchange capture of hIgG were determined. The results of these experiments are shown in Fig. 2.6.

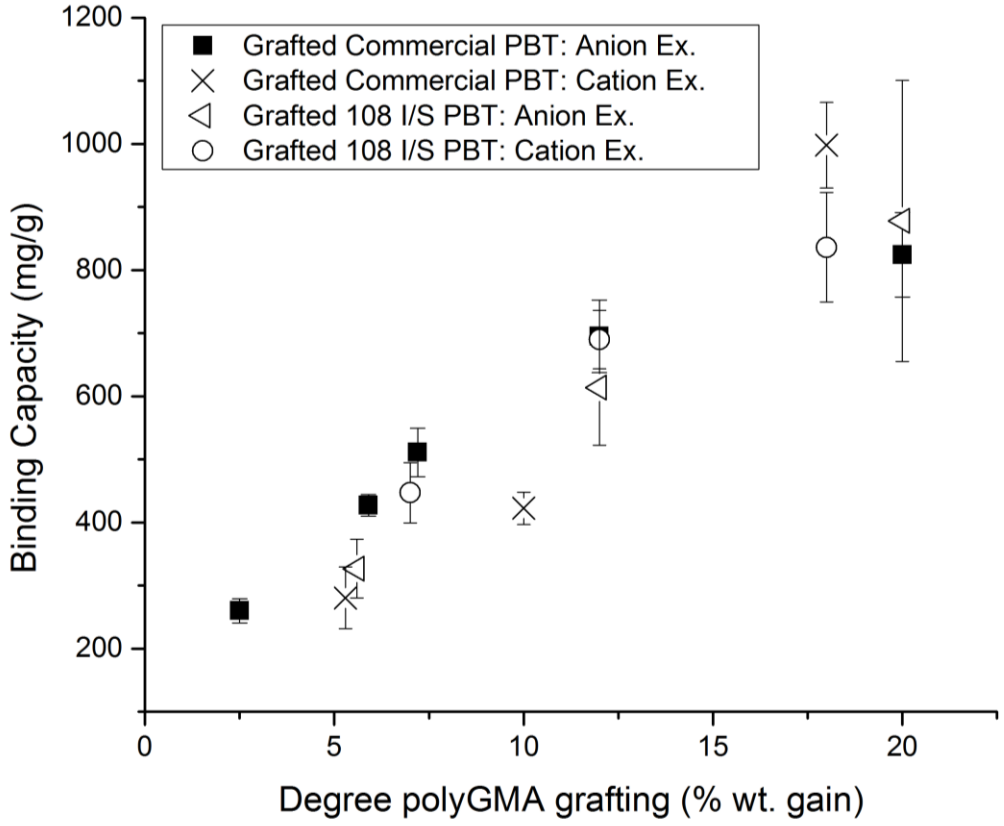

Fig. 2.6 Equilibrium binding capacity for 108 I/S PBT nonwoven and commercial PBT nonwoven grafted at various degrees and functionalized either to be a cation or anion exchanger to bind IgG and BSA respectively.

The results of Fig. 2.6 show that equilibrium protein binding capacity increases linearly with increased degree of polyGMA grafting (% weight gain), for both anion and cation exchange

membranes and for proteins of two very different molecular weights and sizes. The 108 I/S PBT nonwovens have 2.85 times more specific surface area than the commercial PBT nonwovens yet they both achieved very similar equilibrium binding capacities. These results indicate that, given enough time, both a medium sized protein like BSA (66.5 kDa) and a large protein like hIgG (150 kDa) are able to penetrate into the grafted layers of the sample until the entire grafted layer is saturated with protein [31, 32]. Even though these proteins have much different molecular weights, BSA and hIgG have similar specific volumes (0.733 cm^3/g and 0.739 cm^3/g respectively) [32, 33]. When both the commercial PBT nonwoven and the I/S PBT nonwoven samples have the same original mass and the same % weight gain they have the same mass of grafted layer, and therefore it is not hard to understand how the equilibrium protein binding capacity on a mass basis would be the same. These results also indicate that the grafted layers under the binding solution conditions used in this experiment must be either flexible or porous enough to allow penetration of even a large molecule like hIgG which has a radius of gyration of 100 nm. Since these grafted layers are highly charged, during binding conditions at low ionic strengths the grafted layers are likely in an extended configuration, allowing protein penetration.

It is also important to note that for the high % weight gain samples the equilibrium protein binding capacities are extremely large, reaching values of over 800 mg of bound protein per gram of nonwoven at 20% weight gain. If the BSA and hIgG were adsorbing to the outer surface of the fibers only, and not penetrating into the grafted layer, the binding capacities would be much lower. Monolayer adsorption of BSA and hIgG have been reported to be somewhere in the range of 2.5-6 mg/m^2 and 2-5.5 mg/m^2 respectively [27-30]. Given these monolayer coverage numbers and the measured specific surface area of the

commercial PBT nonwovens, the monolayer binding capacity for BSA and hIgG would be 5.2 and 4.7 mg/g respectively. Similarly, the maximum monolayer coverage of BSA and hIgG on the 108 I/S PBT nonwovens would be 14.7 and 13.5 mg/g respectively. All of the equilibrium binding capacities reported in Fig. 2.6 are between 50 and 200 times greater than monolayer protein adsorption. This is very strong evidence that the polyGMA brushes created a 3-dimensional binding environment, where equilibrium protein adsorption scales with the amount of polymer brush available for binding per mass of membrane. Fig. 2.6 shows that both nonwovens with the same extent of polyGMA grafting exhibit the same equilibrium protein binding capacity. For instance at 20% weight gain the commercial PBT nonwovens captured 823 ± 66 mg/g of BSA at equilibrium and the 108 I/S PBT nonwovens with 20% weight gain captured 817 ± 164 mg/g of BSA by anion exchange. Fig. 2.5 shows that the 20% weight gain polyGMA dry graft thickness is larger for the commercial PBT nonwovens (δ= 227 nm) than the 108 I/S PBT nonwovens (δ= 69 nm). The % weight gain determines the equilibrium binding capacity however the distribution of protein at equilibrium is very different between the commercial PBT nonwovens and the 108 I/S PBT nonwovens. At equilibrium, protein is distributed in a thinner layer over a larger surface area for the 108 I/S PBT nonwovens compared to the commercial PBT nonwovens that require a thicker polyGMA grafted layer to bind the same amount of protein due to the lower specific surface area of the material.

2.3.4 Rates of adsorption to polyGMA grafted anion and cation exchange nonwovens

In section 2.3.3 it was shown that ion exchange functionalized polyGMA grafted nonwovens exhibit very high equilibrium binding capacities. However, for some applications it is necessary to understand the effects of % weight gain and grafted layer thickness on the

kinetics of protein adsorption to the polyGMA brush layers. Fig. 2.7 displays the results for BSA capture by anion exchange at various protein exposure times for commercially grafted PBT at 20% and 5.9% wt. gain, as well as, 108 I/S grafted PBT at 20% wt. gain. These degrees of grafting were chosen because, at 20% weight gain both the commercial PBT and the 108 I/S PBT have the same amount of polyGMA grafting and equilibrium binding capacity displayed in Fig. 2.6 and commercial PBT grafted at 5.9% grafting has the same polyGMA graft thickness as the 108 I/S PBT as can be seen in Fig. 2.5, and should have similar rates of protein adsorption. The 108 I/S grafted at 5.9% weight gain was not investigated because it is at the lower limit of grafting necessary to give complete conformal grafting and would result in high variability in the material tested for protein binding.

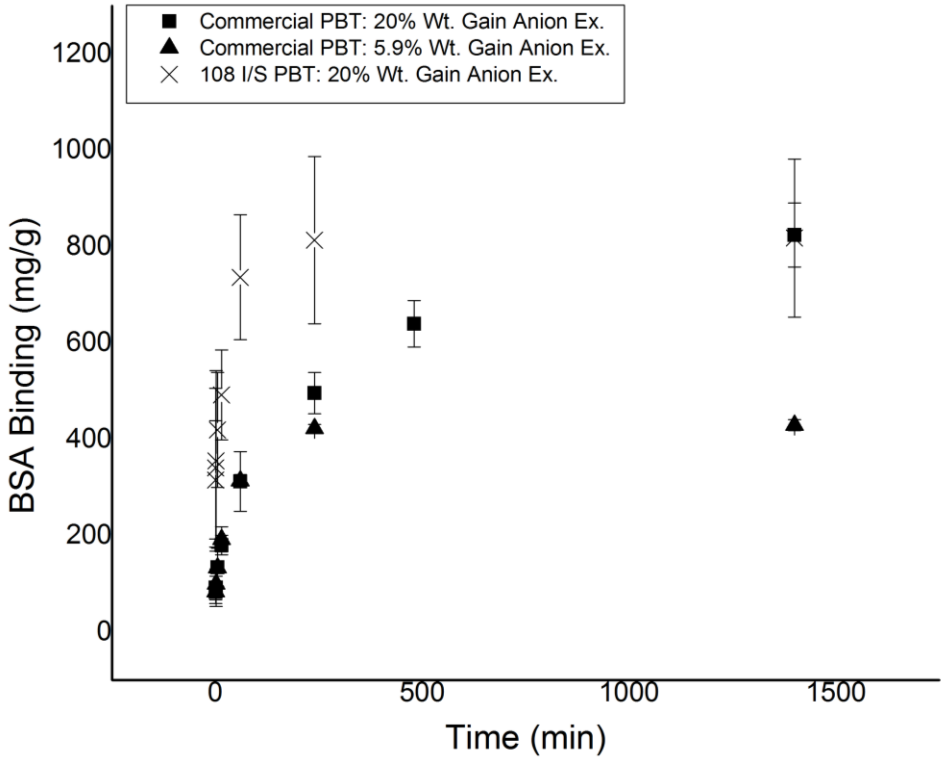

Fig. 2.7 BSA capture at various contact times for anion exchange functionalized grafted nonwovens: commercial PBT grafted at 20% and 5.9% weight gain, as well as, 108 I/S PBT grafted at 20% weight gain. Experiments done in batch systems.

These experiments were done in batch, under static or non-flow conditions. In Fig. 2.7 the rate of adsorption of BSA to commercially available PBT and 108 I/S PBT nonwovens grafted to the same extent of polyGMA grafting at 20% weight gain were compared for protein capture at various contact times. At 20% weight gain both the commercial PBT nonwovens and the 108 I/S PBT nonwovens converge to the same binding capacity (~800 mg/g) given sufficient contact time, consistent with the results shown previously. However, it can be seen that BSA adsorbs to the 20% weight gain grafted commercial PBT nonwovens at a much slower rate than to the 108 I/S PBT nonwovens. After 4 hours the 108 I/S PBT nonwovens grafted at 20% weight gain had already reached its equilibrium binding capacity, compared to the commercial PBT nonwovens grafted at 20% weight gain that had only reached 60% of the equilibrium binding capacity. Fig. 2.7 also shows that the commercial PBT nonwoven grafted at 5.9% weight gain had also achieved its equilibrium binding capacity after 4 hours of protein contact time. The 108 I/S PBT nonwovens grafted to 20% weight gain and the commercial PBT nonwovens grafted to 5.9% weight gain have the same dry polyGMA graft thickness of 70 nm according to Eq. 3 and as depicted in Fig. 2.5. This is good evidence that the rate of adsorption of proteins by ion exchange to these grafted nonwoven fabrics is largely determined by the diffusional limitations through the grafted layer, and thus dominated by the grafted layer thickness, which is in turn determined by the initial fiber diameter of the nonwoven and the % weight gain of grafted material.

The kinetics of hIgG adsorption by cation exchange to grafted commercial PBT nonwovens and 108 I/S PBT nonwovens were also investigated. Fig. 2.8 displays the results for hIgG capture at various contact times for commercially grafted PBT at 18% and 5.3% wt. gain, as well as 108 I/S grafted PBT at 18% wt. gain cation exchangers.

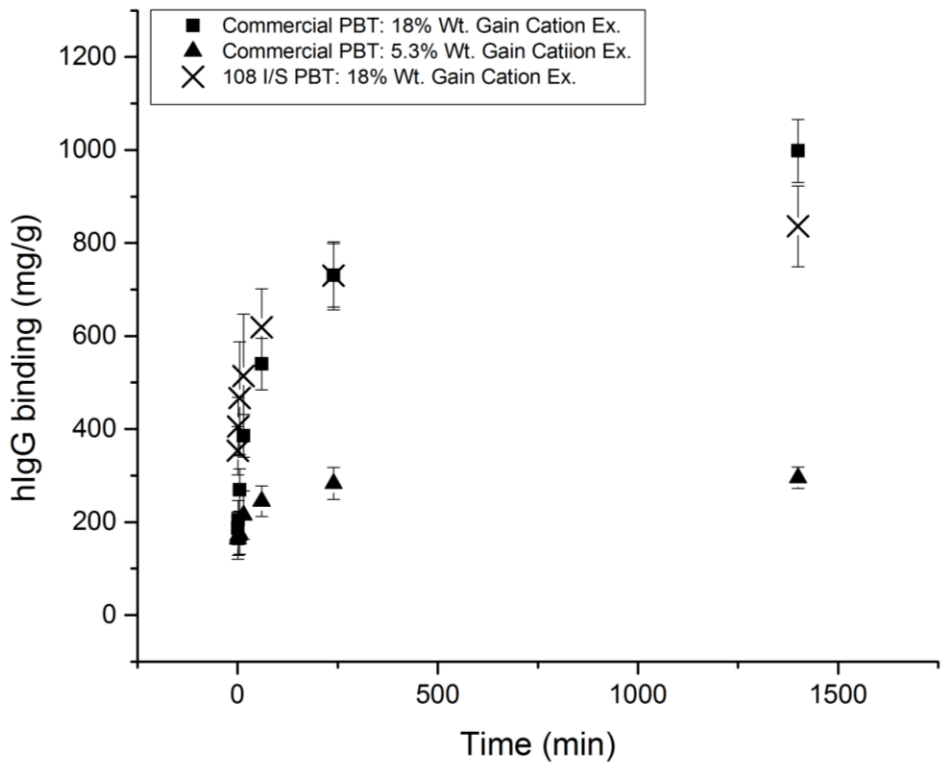

Fig. 2.8 hIgG adsorption at various contact times for cation exchange functionalized grafted nonwovens: commercial PBT grafted at 18% and 5.3% weight gain, as well as 108 I/S PBT grafted at 18% weight gain. Experiments done in batch systems.

Fig. 2.8 shows how commercial PBT nonwovens and 108 I/S PBT nonwovens grafted to the same extent of polyGMA grafting, 18% weight gain, converge to similar equilibrium hIgG binding capacities when functionalized as cation exchangers. This is the same behavior shown in Fig. 2.7 for anion exchange membranes. The 108 I/S PBT nonwoven sample grafted to 18% weight gain reached equilibrium binding after 4 hours compared to the commercial PBT nonwoven grafted at 18% weight gain that required a full day of protein contact. The commercial PBT nonwovens with 5.3% weight gain, grafted to the same graft thickness (δ = 63 nm) as the 108 I/S PBT nonwovens grafted with 18% weight gain also

reached equilibrium in approximately 4 hours. Again, these results are totally analogous to the results found for anion exchange nonwovens in Fig. 2.7, providing further proof that the kinetic phenomena being observed are not dependent on the grafted layer charge type, or the size of the protein being adsorbed.

For practical applications it is important to evaluate how protein binds at short residence times. For example, if these membranes are to be used for protein capture in downstream purification of biologics, it would be desirable for the residence time in the adsorption device to be 5 minutes or less. Fig. 2.9 shows the protein binding data in Figs. 2.7 and 2.8 for the anion and cation exchange grafted nonwovens discussed above for BSA and hIgG contact times under 15 min.

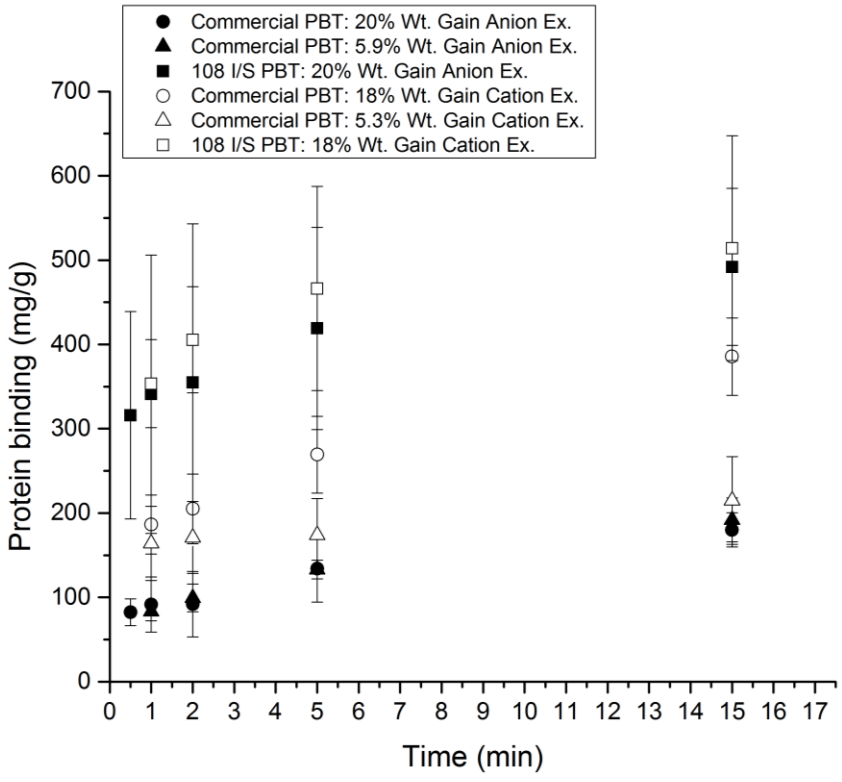

Fig. 2.9 Protein binding for contact times 15 min or less, for all of the ion exchange functionalized grafted nonwovens that were tested for BSA and hIgG binding rates.

In Fig. 2.9 it is apparent that the grafted 108 I/S PBT nonwovens are capable of binding more protein at very short contact times in both cation and anion exchange mode than any of the functionalized grafted commercial PBT nonwovens. The ability of the 108 I/S PBT nonwovens to bind more protein initially is due to the higher specific surface area of the fabric. Recall that the specific surface area of the I/S PBT nonwoven after PLA removal is 2.85 times larger than the specific surface area of the commercial meltblown PBT nonwoven. The data present in Fig. 2.9 was extrapolated to time t = 0 to estimate the initial amount of protein bound (M_i) that occurred instantaneously due adsorption of protein on the nonwovens surface area before any diffusion into the polyGMA layer has occurred. The initial amounts of protein adsorption are given in Table 2.2.

Table 2.2: Initial amount of protein adsorbed (M_i) due to surface area adsorption.

Sample	Initial amount of protein binding (M_i) (mg/g)
Commercial PBT: 20% Wt. Gain Anion Ex.	76
Commercial PBT: 5.9% Wt. Gain Anion Ex.	73
108 I/S PBT: 20% Wt. Gain Anion Ex.	311
Commercial PBT: 18% Wt. Gain Cation Ex.	165
Commercial PBT: 5.3% Wt. Gain Cation Ex.	163
108 I/S PBT: 18% Wt. Gain Cation Ex.	338

If the results presented in Table 2.2 are averaged for the functionalized commercial PBT nonwovens (120 mg/g average initial protein binding) and the 108 I/S PBT nonwovens (325 mg/g average initial protein binding) it is observed that the 108 I/S PBT nonwovens bind 2.7 times more protein initially than the commercial PBT nonwovens. This is in close agreement with the 2.85 times higher experimental surface area for the 108 I/S PBT nonwovens than the

commercial PBT nonwovens. For this reason it becomes advantageous to use the grafted 108 I/S PBT nonwovens when very short residence times are required because they can achieve fairly high binding capacities strictly due to higher specific surface area.

The results of the adsorption rate measurements for both cation and anion exchange grafted nonwovens indicate that the adsorption process is diffusion limited in these functionalized polyGMA brush matrices, requiring several hours to reach equilibrium. To minimize these diffusional challenges higher surface area (smaller fiber diameter) nonwoven fabrics result in thinner grafted layer thicknesses for the same % weight gain compared to lower surface area (larger fiber diameter) materials, as shown in Fig. 2.5. The thinner polyGMA layer reduces the diffusion distance and shortens the time to reach equilibrium while maintaining high equilibrium binding capacities as seen in Figs. 2.7 and 2.8. In addition to reducing the time to reach equilibrium for specific degrees of polyGMA grafting the higher specific surface area 108 I/S PBT nonwovens also contributes to a higher initial amount of protein adsorption as observed in Fig. 2.9. The overall equilibrium protein binding capacity will be determined by the degree of polyGMA grafting but the effective rates of protein capture are determined by the initial specific surface area of the nonwoven and the thickness of the polyGMA brush layer.

2.3.5 Model for the kinetics of protein adsorption to grafted polyGMA nonwovens

The insights provided by the results of both the equilibrium and rate measurements for protein adsorption to the anionic and cationic grafted layer nonwovens described above suggest that it may be possible to develop a mathematical model to describe the adsorption process, and that this mathematical model should be qualitatively and quantitatively consistent with the experimental results. The rate of adsorption of a charged protein to a

charged binding site is nearly instantaneous compared to the rate of mass transfer limitations in ion exchange media [34,35]. It has already been proposed that in the case of diffusion into functionalized polymer layers the rate-determining step for protein adsorption is the penetration into the polymer layer [36]. A cross sectional illustration of how protein adsorbs over time to the functionalized polyGMA brush layer grafted around a PBT fiber is presented in Fig. 2.10.

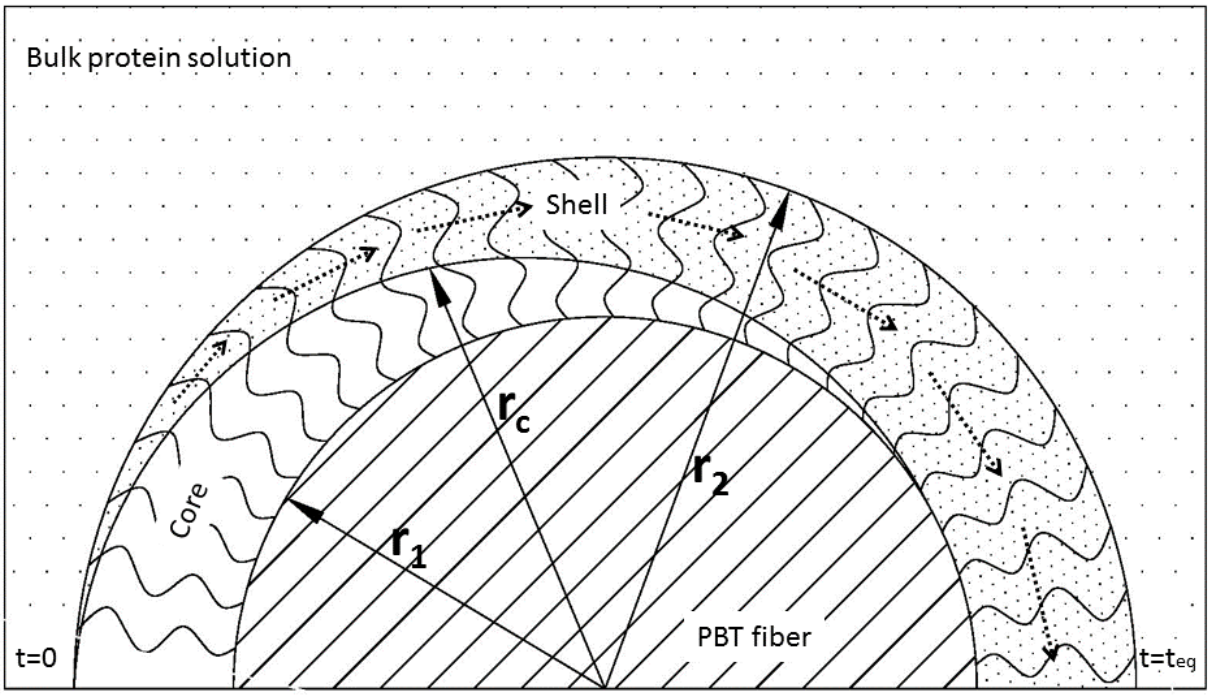

Fig. 2.10 Schematic cross section of a grafted PBT fiber filling with protein over time, converting an available polyGMA "core" into a saturated protein/polyGMA shell as time (t) progresses, r_1= PBT fiber radius, r_c= core radius, r_2= grafted fiber radius.

Because the rate of adsorption to the grafted layer is likely to be much faster than the rate of diffusion of protein through the layer, it is not unreasonable to theorize that once a protein molecule is bound to charged groups on the outer surface of the grafted layer, additional molecules entering the grafted layer will have to diffuse through the layer containing the

bound proteins. Once the unbound protein diffuses through the bound protein layer and encounters free charged groups on the polymer it will bind immediately and the bound protein layer will grow with time until it reaches the surface of the PBT fiber. The phenomenon just described is consistent with the traditional shrinking core model [34 – 37] that has been applied to the diffusion of proteins in chromatographic resins [38]. The bound protein on the polyGMA grafted layer can be viewed as forming a "shell" that creates a significant diffusional resistance for protein mass transport into the remaining layer of unbound polyGMA. Fig. 2.10 shows how the thickness of the shell increases over time until the entire polyGMA brush layer has bound protein. The unbound polyGMA brushes are the "core" in this model that shrinks as protein penetrates the "shell" and binds to the brushes. Initially the thickness of the "shell" with adsorbed protein will be zero and the rate of adsorption of protein to the outer surface will be very fast. As time progresses the "shell" thickness and the diffusional resistance to mass transfer increase until the adsorbed protein shell reaches the surface of the PBT and the "core" shrinks to zero. We also assume that, because the diffusion process is slow relative to the rate of adsorption, the diffusion process is in a quasi-steady state so that the rate of protein transport by diffusion into the polyGMA brush layer is constant with position, so that at any point in the shell the rate of adsorption of protein to the charged polymer is equal to the rate of diffusion through the shell. With these assumptions, at any radial position within the grafted layer, the rate of adsorption of protein is equal to the rate of radial diffusion of protein into the polyGMA brush layer, expressed by Eq. 4.

$$R_a = D_e \frac{\partial C_{\text{protein}}}{\partial r} (2\pi r L) \qquad (4)$$

In Eq. 4, R_a is the total rate of adsorption of protein to the shell at a given radial position, D_e is the effective diffusivity of protein in the polyGMA brush matrix with adsorbed protein, C_{protein} is the protein concentration that is diffusing through the polyGMA layer, L is the length of a given fiber, and r is the radial position. Since the rate of protein binding by the polyGMA brushes is nearly instantaneous then the concentration of protein at the interface between the "core" and the "shell" ($r = r_{c)}$ can be taken to be zero. Additionally, since diffusion through the shell is the rate-limiting step the concentration of protein at the exterior of the shell ($r = r_2$) is the equivalent to that of the bulk protein concentration in solution, denoted as C_{bulk}. Integrating Eq. 4 from the inner to the outer radius of the grafted layer leads to an expression for the radial variation in the rate of adsorption of protein,

$$R_a = \frac{D_e(2\pi L)C_{bulk}}{ln\left(\frac{r_2}{r_c}\right)} \qquad r_1 < r_c < r_2 \tag{5}$$

The rate of protein diffusing into the core and binding to the polyGMA is equal to the mass rate of consumption of polyGMA "core" material available for binding,

$$R_a = R_c \tag{6}$$

The rate of disappearance of mass of unoccupied polyGMA "core" can be expressed in terms of the density and the time rate of change of volume occupied by the polyGMA (Eq. 7),

$$R_c = -\rho_{core}(2\pi r_c L)\frac{dr_c}{dt} \tag{7}$$

Substitution of Eqs. 6 and 7 into Eq. 5 yields an equation for the time rate of change of the interface between the "core" of polyGMA and the "shell" with bound protein,

$$-\rho_{core}(2\pi r_c L)\frac{dr_c}{dt} = \frac{D_e(2\pi L)C_{bulk}}{ln\left(\frac{r_2}{r_c}\right)} \tag{8}$$

At time $t = 0$, the core radius is r_2. Integration of Eq. 8 with respect to time leads to an expression for the mass adsorbed into the grafted layer as a function of time,

$$\Psi = \frac{t}{\tau} = \frac{1}{2}\left(\frac{M-M_i}{M_{eq}-M_i}\right) + \left[\frac{1}{1-\phi^2} - \frac{M-M_i}{M_{eq}-M_i}\right] ln\sqrt{1-\left(\frac{M-M_i}{M_{eq}-M_i}\right)(1-\phi^2)} \quad (9)$$

A derivation of this equation can be found in the Supplemental Information: Derivation of the shrinking core model. In Eq. 9 M is the mass of protein bound at any given time, M_{eq} is the mass of protein bound at equilibrium and M_i is the initial mass of protein bound at time $t = 0$ due to adsorption on the external surface area of the nonwovens. The shrinking core model does not predict this initial protein adsorption (M_i) but it can be estimated from our experimental results (see Table 2.2). When using this model, the fraction of the equilibrium amount of protein adsorbed to the polyGMA brush layer as a function of time after this initial immersion step in solution is given by $[(M-M_i)/(M_{eq}-M_i)]$. The total amount of protein bound to the polyGMA brush layer as a function of time is dependent on two parameters: τ and ϕ which vary for each different nonwoven with different fiber diameter and grafted layer thickness,

$$\tau = \frac{(r_2^2-r_1^2)\rho_{core}}{2D_e C_{bulk}} \quad (10)$$

$$\phi = \frac{r_1}{r_2} \quad (11)$$

In Eq. 10 and 11, r_1 and r_2 are the radii of the PBT fiber and the fiber covered with the polyGMA brush layer respectively as can be seen in Fig. 2.10. Additionally in Eq. 10, D_e is the effective diffusivity for protein through the shell layer, and C_{bulk} is the concentration of protein solution in the liquid phase, which was 10 mg/ml for each experiment performed.

It is known that polyGMA brushes swell in aqueous solvents when functionalized with charged groups as a result of electrostatic repulsion between the charges [2]. Therefore, the dry polyGMA brush thickness calculated by Eq. 3 cannot be used to determine r_2 and a swollen polyGMA brush thickness must be calculated. If we assume that polyGMA brushes

are completely extended when the brush layer is completely filled with protein we can estimate the polyGMA brush thickness r_2. This is a reasonable assumption because proteins are known to achieve a high packing efficiency in polyelectrolyte brush matrices when given sufficient time [14]. The mass of protein adsorbed per mass of the membrane at equilibrium is M_{eq} (mass protein/ mass membrane) and is the equivalent to the binding capacity of the material. The mass of protein bound can be converted to the volume of protein bound using the partial specific volume of the protein. The volume occupied by protein is that of an annular cylinder around the PBT fiber. Using this geometry, r_2 can be calculated to give the swollen polyGMA brush thickness using Eq. 12. The derivation of Eq. 12 can be found in the Supplementary Information: Derivation of swollen polyGMA brush radius.

$$r_2 = \sqrt{M_{eq}\bar{v}\rho_{PBT}r_1^2 + r_1^2} \tag{12}$$

In Eq. 12, M_{eq} is the equilibrium binding capacity, $\bar{v}$ is the partial specific volume of protein ($\bar{v}_{BSA}$ = 0.733 cm^3/g and $\bar{v}_{IgG}$ = 0.739 cm^3/g), ρ_{PBT} is the density of PBT fibers (ρ_{PBT} =1.33 g/cm^3), and r_1 is the radius of the PBT fibers.

In addition to increasing the observed brush thickness, the swelling of the polyGMA brushes effectively increases the volume the brushes occupy resulting in a decreased observed density for the "core". The unbound swollen polyGMA brushes make up the "core" and the density of these brushes is the density of the core. We know the mass of the polyGMA brushes from the weight gain on the PBT nonwovens and we can calculate the volume of the swollen polyGMA brushes using the calculated values for r_2. The mass and the volume for the polyGMA brushes can be used to calculate an effective density of the "core"

that is expressed by Eq. 13, the derivation can be found in the Supplementary Information: Derivation of polyGMA core density.

$$\rho_{core} = \frac{\frac{\%\, weight\ gain}{100\%}\rho_{PBT} r_1^2}{r_2^2 - r_1^2} \tag{13}$$

In Eq. 13 ρ_{core} is the effective density of the "core" that protein adsorbs to, the % weight gain is the mass of polyGMA added to the nonwoven from grafting, ρ_{PBT} is the density of the PBT fibers, r_1 is the radius of the PBT fibers and r_2 is the swollen polyGMA radius. The calculated values for r_2 as well as the subsequent swollen polyGMA brush thicknesses, the effective core densities, and the values for ϕ are presented in Table 2.3.

Table 2.3: Radius of swollen polyGMA layer grafted to PBT, the swollen polyGMA thickness, the effective "core" density, and ϕ values for various grafted nonwoven samples.

Sample	r_2 (nm)	$\delta_{swollen\ polyGMA}$ (nm)	ρ_{core} (g/cm^3)	$\phi = \frac{r_1}{r_2}$
Commercial PBT: 20% Wt. Gain Anion Ex.	2004.0	504.0	0.331	0.748
Commercial PBT: 5.9% Wt. Gain Anion Ex.	1780.6	280.6	0.187	0.842
108 I/S PBT: 20% Wt. Gain Anion Ex.	610.9	152.9	0.333	0.750
Commercial PBT: 18% Wt. Gain Cation Ex.	2099.4	599.4	0.244	0.714
Commercial PBT: 5.3% Wt. Gain Cation Ex.	1699.3	199.3	0.243	0.883
108 I/S PBT: 18% Wt. Gain Cation Ex.	615.0	157.0	0.291	0.745

Using the ϕ values presented in Table 2.3, the experimental data for total mass adsorbed into the membrane as a function of time can be used to fit the only remaining parameter τ in Eq. 9. From these values of τ it is then possible to estimate values of the effective diffusivity of the proteins diffusing through the "shell" of protein adsorbed to the polyGMA grafted layer.

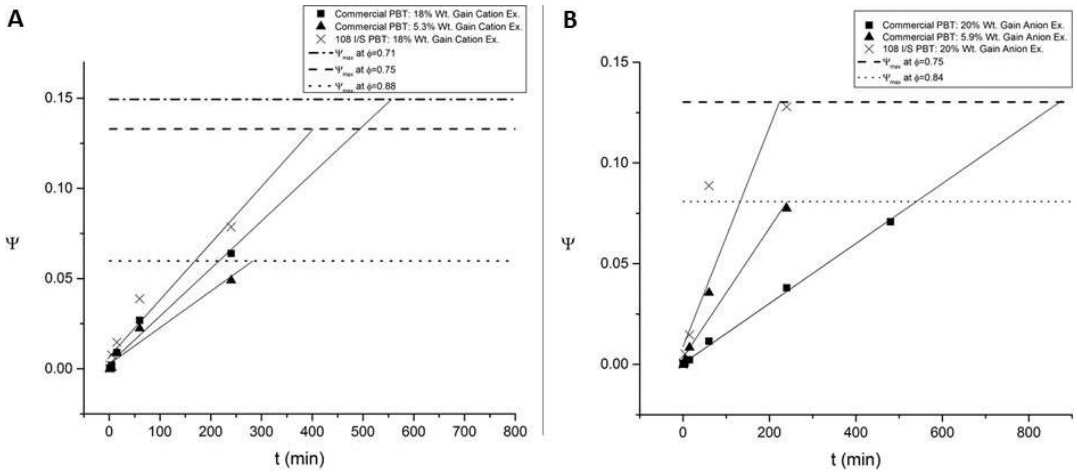

Fig. 2.11 (A) Ψ values calculated for experimental data for the conversion of the anion exchange functionalized polyGMA nonwovens plotted vs. time with lines of best fit. (B) Ψ values calculated for experimental data for the conversion of the cation exchange functionalized polyGMA nonwovens plotted vs. time with lines of best fit.

Fig. 2.11 A and B show the lines of best fit for the results of Ψ vs. protein contact time (t) for all the nonwovens tested in the kinetic binding experiments. The horizontal dotted and dashed lines found in Fig. 2.11 are the maximum values of Ψ (Ψ_{max}) for equilibrium adsorption of the functionalized polyGMA "core" with protein for the various values of ϕ obtained in Table 2.3. The times at which the lines of best fit found in Fig. 2.11 reach Ψ_{max} are the times required to reach equilibrium protein binding (t_{eq}). Additionally, the slopes of the lines of best fit found in Fig. 2.11 are equivalent to the inverse of τ as defined by Eq. 9.

Once τ is known, values for the effective diffusivity (D_e) of protein transport through the "shell" can be calculated using Eq. 10. The values of t_{eq}, τ, and D_e are presented in Table 2.4.

Table 2.4: Characteristic time of adsorption (τ), the time required to achieve complete conversion of the polyGMA "core" (t_{eq}), and the calculated effective diffusivity (D_e) for protein diffusion through the "shell" in the shrinking core model.

Sample	τ (min)	t_{eq} (min)	D_e x 10^{-13} (cm^2/s)
Commercial PBT: 20% Wt. Gain Anion Ex.	6716	876	7.25
Commercial PBT: 5.9% Wt. Gain Anion Ex.	3109	241	4.61
108 I/S PBT: 20% Wt. Gain Anion Ex.	1839	223	2.47
Commercial PBT: 18% Wt. Gain Cation Ex.	3798	556	11.6
Commercial PBT: 5.3% Wt. Gain Cation Ex.	4955	283	2.61
108 I/S PBT: 18% Wt. Gain Cation Ex.	3189	402	1.28

The experimental effective diffusivities obtained from the best fit values of τ for the anion exchange and cation exchange systems are shown in Table 2.4. For BSA diffusion through the protein filled anion exchange functionalized polyGMA layers, effective diffusivities were between 2.47×10^{-13} and 7.25×10^{-13} cm^2/s with an average effective diffusivity of 4.77×10^{-13} cm^2/s. For hIgG diffusion through the protein filled cation exchange functionalized polyGMA layers, effective diffusivities were between 1.28×10^{-13} and 11.6×10^{-13} cm^2/s with an average effective diffusivity of 5.16×10^{-13} cm^2/s. According to the Stokes-Einstein equation BSA and IgG have diffusion coefficients of 6.23×10^{-7} cm^2/s and 3.41×10^{-7} cm^2/s respectively, in water at room temperature. Typical pore diffusion coefficients for proteins in

chromatography resins are on the order of 10^{-9} to 10^{-12} cm^2/s [39, 40]. The effective diffusivities for protein capture on the ion exchange functionalized polyGMA grafted nonwovens are significantly lower than most pore diffusion coefficients in chromatography resins. It is clear that protein capture by the ion exchange functionalized polyGMA brushes suffer from a severe diffusion limitation in the polyGMA/protein "shell" depicted in Fig. 2.10, requiring several minutes if not hours to reach equilibrium as shown in Table 2.4.

The shrinking core model relies on ϕ and τ to predict how protein adsorbs in the polyGMA "core" over time. Using the values for ϕ and τ found in Table 2.3 and 2.4 respectively the shrinking core model results can be compared to the experimental data for protein adsorption to the functionalized polyGMA "core" as a function of time. The results for the mass adsorption of BSA to the anion exchange polyGMA "core" vs. t/τ using values of ϕ are shown in in Fig. 2.12.

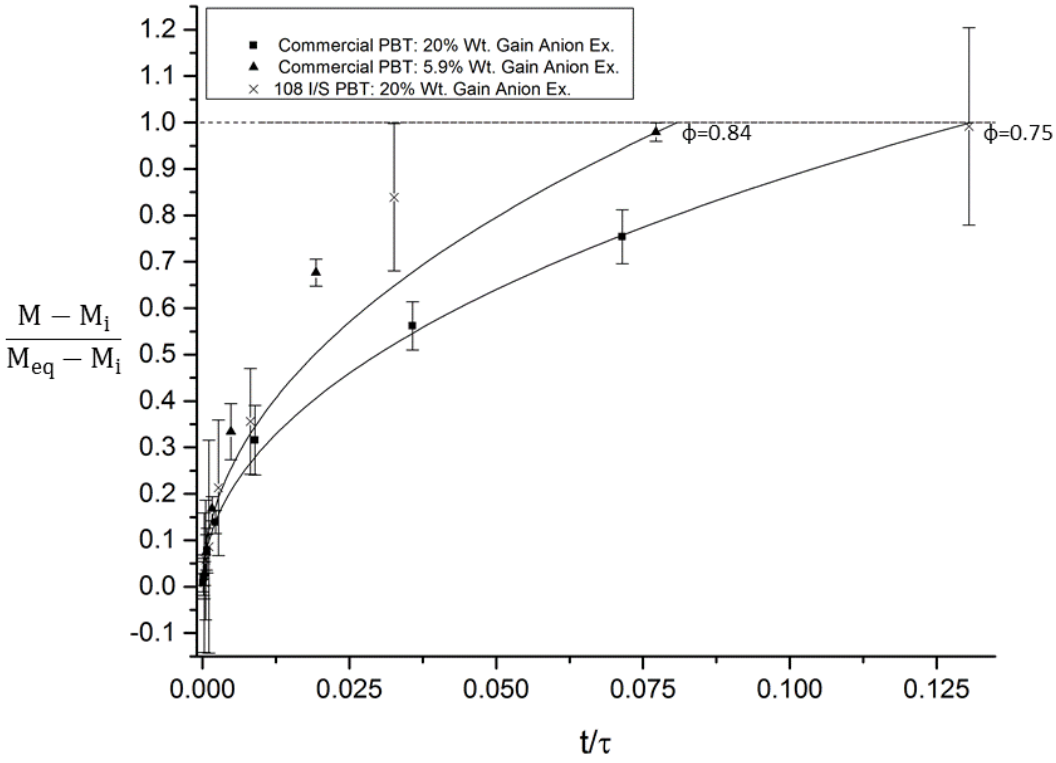

Fig. 2.12 Experimental and shrinking core model results for the adsorption of BSA to the anion exchange polyGMA as a function of time. Commercial PBT at 20% weight gain: ϕ = 0.75 and τ = 6716 min, commercial PBT at 5.9% weight gain: ϕ = 0.84 and τ = 3109 min, and 108 I/S PBT at 20% weight gain: ϕ = 0.75 and τ = 1839 min.

As Fig. 2.12 shows, the shrinking core model provides a good approximation of the experimental data. In the shrinking core model as the thickness of the polyGMA graft increases around a given PBT fiber diameter, values of ϕ decrease, values for Ψ_{max} increase as can be seen in Fig. 2.11, and the characteristic time scale of adsorption (τ) increases. Due to these reasons longer times are required to reach equilibrium for samples with thicker graft layers as can be seen in Table 2.4. This phenomenon can particularly be seen when comparing the commercial PBT grafted at 20% weight gain and 5.9% having swollen polyGMA brush thicknesses of 504 nm and 281 nm respectively. Both samples utilized the same starting material with different degrees of polyGMA coverage resulting in substantially

different values of ϕ, Ψ_{max}, and τ. Therefore, according to the shrinking core model the commercial PBT with the thinner grafted layer will exhibit a faster rate of conversion and achieve equilibrium sooner. This is observed with the commercial PBT grafted at 5.9% weight gain achieving equilibrium in 241 min compared to the commercial PBT grafted at 20% weight gain reaching equilibrium in 876 min.

The 108 I/S PBT nonwoven has a smaller PBT fiber diameter than the commercial PBT nonwoven and results in thinner grafted polyGMA brush layer as Fig. 2.5 displays. However, there was proportionality between the values of r_1 and r_2 for commercial PBT and the 108 I/S PBT nonwovens grafted to 20% weight gain resulting in similar values for ϕ and similar trends in the shrinking core model as Fig. 2.12 shows. Although the values of ϕ are the same for both the 108 I/S PBT nonwovens and the commercial PBT nonwovens grafted to 20% weight gain their characteristic time scales of adsorption are substantially different with τ being 1839 min for the 108 I/S nonwovens grafted at 20% weight gain and 6716 min for the commercial PBT nonwovens grafted at 20% weight gain. The smaller characteristic time scale of adsorption observed for the 108 I/S PBT nonwoven grafted at 20% weight gain results in equilibrium being reached after 223 min compared to the commercial PBT nonwovens grafted to 20%weight gain requiring 876 min to reach equilibrium. Both the commercial PBT grafted to 5.9% weight gain and the 108 I/S PBT grafted to 20% weight gain had shorter polyGMA brush thicknesses and substantially shorter times required to reach equilibrium binding, between 220 and 250 min, according to the shrinking core model compared to the commercial PBT nonwovens grafted at 20% weight gain that required almost 900 min. This is strong evidence that reducing the thickness of the polyGMA grafted

layer results in faster rates of conversion of the polyGMA core and shorter times to reach equilibrium in this diffusion limited adsorption process.

The results for the conversion of the cation exchange polyGMA "core" by hIgG binding plotted vs. t/τ with the shrinking core model fit to various values of ϕ are presented in Fig. 2.13.

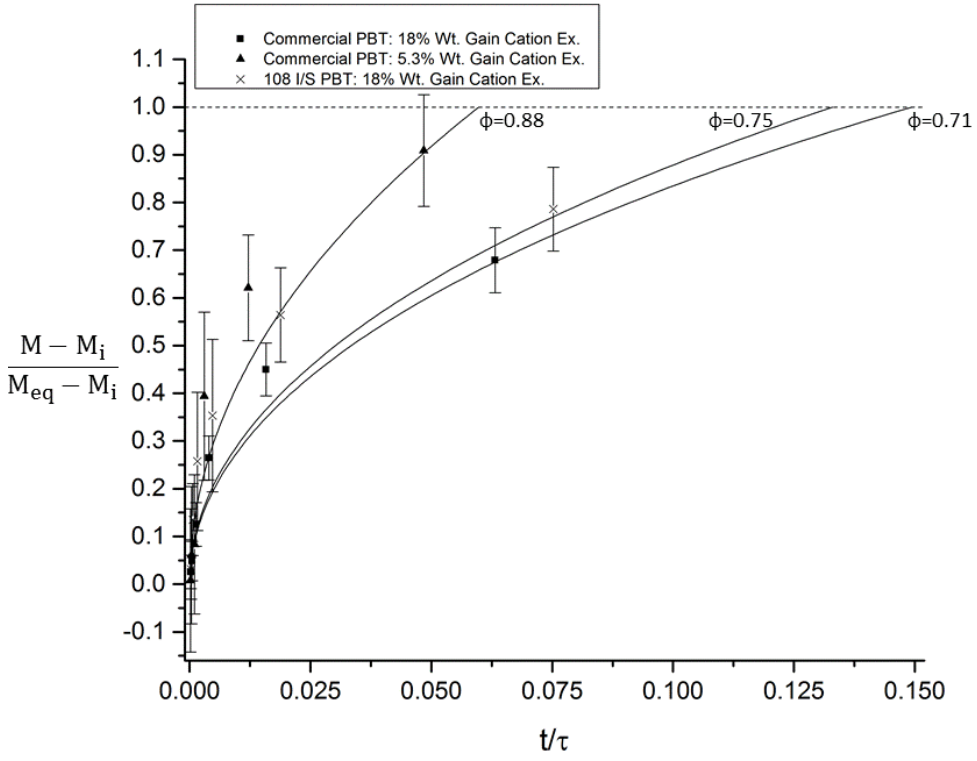

Fig. 2.13 Adsorption of hIgG to cation exchange polyGMA "core" as a function of time. Commercial PBT at 18% weight gain: ϕ = 0.71 and τ = 3789 min, commercial PBT at 5.3% weight gain: ϕ = 0.88 and τ = 4955 min, and 108 I/S PBT at 18% weight gain: ϕ = 0.74 and τ = 3189 min.

As Fig. 2.13 shows, the shrinking core model is a fair approximation of the experimental data for the different ϕ values. Similarly to the anion exchange nonwovens, shorter times to reach equilibrium are observed for thinner polyGMA layers for a given PBT fiber diameter. The commercial PBT grafted to 5.3% weight gain was able to achieve equilibrium in 283

min compared to polyGMA grafting of 18% weight gain that required 556 min to reach equilibrium. The 108 I/S PBT nonwoven grafted at 18% weight gain also achieved equilibrium binding in a shorter amount of time compared to the commercial PBT grafted at 18% weight gain. However, the differences in equilibrium binding time were not as large as for the anion exchange samples as Table 2.4 demonstrates.

The shrinking core models depicted in Fig. 2.12 and 2.13 demonstrate a very fast initial rate of protein binding that can be seen at the very short time scales of protein binding. As a significant amount of protein binds, a "shell" that imposes a diffusion limitation for protein adsorption is created as depicted in Fig. 2.10. The protein bound polyGMA "shell" gets thicker over time and the distance of diffusion in this dense layer gets larger requiring longer times for protein diffusion to reach the available core for binding. This is observed in Fig. 2.12 and 2.13 as a decreasing rate of protein adsorption both experimentally and in the shrinking core model as the material approaches equilibrium.

It is clear that protein capture by the ion exchange functionalized polyGMA brushes suffers from a severe diffusion limitation, requiring several minutes if not hours to reach equilibrium. Therefore it is advantageous to use thinner polyGMA brush layers reducing the distance of diffusion and decreasing the required time for complete conversion. Further by using a high surface area nonwoven such as the 108 I/S PBT the polyGMA binding volume can be distributed in thinner layers as Fig. 2.5 shows, reducing capture times while still maintaining high protein binding capacities.

2.4 Conclusions

Complete and conformal polyGMA brushes were successfully grafted to commercial PBT nonwoven and higher surface area 108 I/S PBT nonwoven. Rates of polyGMA grafting were dependent on the available surface area of the nonwoven surface as can be seen by the 2.4 times faster rate of grafting observed in the 108 I/S PBT nonwoven. Grafted commercial PBT nonwoven and 108 I/S PBT nonwoven were successfully derivatized to be weak anion and strong cation exchangers for capture of BSA and hIgG respectively. It was determined that the equilibrium static protein binding capacities were dependent on the degree of polyGMA grafting and not the specific surface area of the material. Equilibrium static protein binding capacities as high as 1000 mg/g for 18-20% polyGMA weight gain were achieved, indicating that polyGMA brushes were capable of increasing protein capture several times that of monolayer coverage. Although grafted PBT nonwovens were capable of achieving very high binding capacities, there was a significant diffusion limitation observed. The effective diffusivity of protein through a dense polyGMA/protein matrix was successfully determined using a shrinking core model. The average effective diffusion coefficients were six orders of magnitude slower than protein film diffusion. The shrinking core model demonstrated how thinner polymer grafts reached equilibrium at faster rates due to a shorter diffusion path. The comparatively higher surface area nonwovens successfully reduced polyGMA brush thicknesses for specific degrees of polyGMA coverage while still maintaining high equilibrium binding capacities. It was observed that the higher surface area 108 I/S PBT nonwoven with thinner polyGMA grafts was capable of reducing the significance of the diffusion limitation in the polyGMA/protein layer, resulting in shorter times to reach equilibrium compared to the commercial PBT nonwoven. Additionally, the

108 I/S nonwoven PBT demonstrated a higher amount of initial protein binding compared to the commercial PBT nonwoven, which is advantageous in applications requiring short residence times.

Acknowledgements

The authors are grateful for the financial support provided by the North Carolina Biotechnology Center (NCBC) and the Kenan Institute of Engineering, Technology and Science. Additionally, the authors are grateful for the nonwoven materials provided by The Nonwovens Institute (NWI) located at the North Carolina State University, as well as, facility use of the Golden LEAF Biomanufacturing Training and Education Center (BTEC) located at the North Carolina State University.

2.5 Appendix: Supplemental Information

2.5.A Derivation of dry polyGMA graft thickness

The dry thickness of the polyGMA graft, Eq. 3, can be derived from the % weight gain defined by Eq. A.1 (Eq. 1).

$$Degree\ of\ polyGMA\ grafting\ (\%\ weight\ gain) = \frac{W_f - W_i}{W_i} \times 100\% \quad \text{(A.1)}$$

In Eq. A.1, W_i is the initial nonwoven weight prior to grafting and W_f is the final nonwoven weight after polyGMA grafting. The final weight of the nonwoven post grafting is the sum of the initial weight and the weight introduced from polyGMA polymer, defined by Eq. A.2.

$$W_f = W_i + W_{polyGMA} \quad \text{(A.2)}$$

In Eq. A.2 $W_{polyGMA}$ is the weight of grafted polyGMA introduced to the exterior of the PBT fiber. Substituting Eq. A.2 for the final weight of grafted nonwoven, Eq. A.1 becomes Eq. A.3.

$$\frac{\%\, weight\ gain}{100\%} = \frac{W_{polyGMA}}{W_i} \tag{A.3}$$

$W_{polyGMA}$ and W_i in Eq. A.3 can be expressed using the density and volume of dry polyGMA polymer and PBT polymer with Eq. A.4 and A.5 respectively.

$$W_{polyGMA} = \rho_{polyGMA} V_{polyGMA} \tag{A.4}$$

$$W_i = \rho_{PBT} V_{PBT} \tag{A.5}$$

In Eq. A.4 $\rho_{polyGMA}$ and $V_{polyGMA}$ are the density and volume of dry polyGMA polymer similarly in Eq. A.5 ρ_{PBT} and V_{PBT} are the density and volume of the PBT fibers. Substituting Eq. A.4 and A.5 into Eq. A.3, results in Eq. A.6.

$$\frac{\%\, weight\ gain}{100\%} = \frac{\rho_{polyGMA} V_{polyGMA}}{\rho_{PBT} V_{PBT}} \tag{A.6}$$

Assuming the polyGMA grafting layer is conformal the volumes in Eq. A.6 can be expressed geometrically as concentric cylinders, depicted by Fig. 2.14.

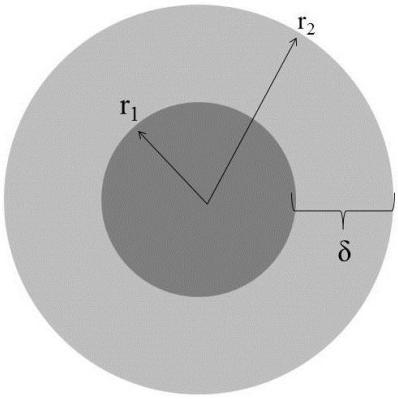

Fig. 2.14 Schematic of a grafted PBT fiber, r_1 is the radius of the PBT fiber, r_2 is the radius of PBT fiber with polyGMA grafting, δ is the thickness of the dry polyGMA layer.

The geometric formula for a cylinder consisting of PBT fiber and an annular cylinder consisting of dry polyGMA are expressed by Eq. A.7 and A.8 respectively.

$$V_{PBT} = \pi L r_1^2 \tag{A.7}$$

$$V_{polyGMA} = \pi L (r_2^2 - r_1^2) \tag{A.8}$$

In Eq. A.7 and A.8, L is the length of the PBT fiber, r_1 is the radius of the PBT fiber and r_2 is the radius of the PBT fiber with a dry polyGMA grafted layer. Defining the volumes this way results in Eq. A.9.

$$\frac{\%\, weight\ gain}{100\%} = \frac{\rho_{polyGMA}(r_2^2 - r_1^2)}{\rho_{PBT} r_1^2} \tag{A.9}$$

In Fig. 2.14, $r_2 = r_1 + \delta$, by substituting this expression into Eq. A.9 and solving for δ results in the Eq. A.10 (Eq. 3).

$$\delta = \sqrt{\left(\frac{\%\, weight\ gain}{100\%}\right)\frac{\rho_{PBT}}{\rho_{polyGMA}} r_1^2 + r_1^2} - r_1 \tag{A.10}$$

2.5.B Derivation of the shrinking core model

In the shrinking core model we assume that diffusion through the polyGMA/protein shell is rate limiting. We also assume that the diffusion of protein into the polyGMA brush layer is constant and is equivalent to the amount of protein being bound. Therefore, the amount of protein consumed per time, or the rate of adsorption is equal to the radial diffusion of protein into the polyGMA brush layer given by Eq. B.1.

$$R_a = D_e \frac{\partial C_{protein}}{\partial r} (Surface\ Area) \tag{B.1}$$

In Eq. B.1 R_a is the rate of protein adsorption, D_e is the effective diffusivity in the polyGMA brush matrix, $C_{protein}$ is the protein concentration in the polyGMA layer, r is the radius of a cylinder in which protein is transported in the radial direction and the surface area is that of

cylindrical geometry of the grafted PBT fibers for which protein is transported across. The surface area of a cylinder is defined by Eq. B.2.

$$Surface\ Area = 2\pi rL + 2\pi r^2 \quad \text{(B.2)}$$

In Eq. B.2 r is the radius of a cylinder and L is the length of a cylinder. For the PBT fibers grafted with polyGMA it can be assumed that $L>>r$, and that any diffusion into the ends of the cylinder is negligible. Substituting Eq. B.2 into Eq. B.1 we get Eq. B.3

$$R_a = D_e \frac{\partial C_{protein}}{\partial r} (2\pi rL) \quad \text{(B.3)}$$

Since we are assuming that binding of proteins by the polyGMA brushes is nearly instantaneous at the frontier of the "core" the concentration of protein in the "core" is 0 at $r=r_c$. Additionally since diffusion through the shell is the rate limiting step the concentration of protein at the end of the shell ($r=r_2$) is the equivalent to that of the bulk protein concentration. These conditions establish one set of boundary conditions for solving Eq. B.3. The boundary conditions are presented in Eq. B.4 and Eq. B.5 for the concentration of protein at the frontier of the core and for the end of the shell respectively.

$$r = r_c \qquad C_{protein} = 0 \quad \text{(B.4)}$$

$$r = r_2 \qquad C_{protein} = C_{bulk} \quad \text{(B.5)}$$

If these boundary conditions are used to solve Eq. B.3, Eq. B.6 can be obtained.

$$R_a = \frac{D_e(2\pi L)C_{bulk}}{ln\left(\frac{r_2}{r_c}\right)} \qquad r_1<r_c<r_2 \quad \text{(B.6)}$$

Since we are assuming adsorption of protein by the polyGMA brushes to be instantaneous, the rate of protein being captured (R_a) is the same as the rate of the empty polyGMA brushes ("core") being occupied (R_c) according to the quasi steady-state approximation. This is defined by Eq. B.7.

$$R_a = R_c \tag{B.7}$$

The rate of disappearance of mass of unoccupied polyGMA "core" can be expressed in terms of the density and the time rate of change of volume occupied by the polyGMA expressed by Eq. B.8,

$$R_c = -\rho_{core}(2\pi r_c L)\frac{dr_c}{dt} \tag{B.8}$$

By substituting Eq. B.8 into Eq. B.6, Eq. B.9 is obtained.

$$-\rho_{core}(2\pi r_c L)\frac{dr_c}{dt} = \frac{D_e(2\pi L)C_{bulk}}{ln\left(\frac{r_2}{r_c}\right)} \tag{B.9}$$

Before any protein has bound to the polyGMA brushes the radius of the "core" is the same as the radius of the entire polyGMA grafted layer. Once protein begins binding to the polyGMA brushes the radius of the core begins to shrink, therefore the radius of the core is dependent on the time that the material has been in contact with protein. These give the second set of boundary conditions necessary to solve Eq. B.9 and are defined by Eq. B.10 and Eq. B.11 for before adsorption starts and once adsorption is occurring respectively.

$$t = 0 \qquad r_c = r_2 \tag{B.10}$$

$$t = t \qquad r_c = r_c \tag{B.11}$$

If these boundary conditions are used to solve Eq. B.9 a solution for how the "core" shrinks over time can be obtain, and is expressed by equation B.12.

$$2r_c^2 ln\left(\frac{r_2}{r_c}\right) + r_c^2 - r_2^2 = -\frac{4D_e C_{bulk}}{\rho_{core}}t \tag{B.12}$$

It is possible to express Eq. B.12 in terms of fractional conversion by using the relationship presented in Eq. B.13.

$$1 - \frac{M - M_i}{M_{eq} - M_i} = \frac{Core\ volume}{Original\ core\ volume} \tag{B.13}$$

Assuming that protein completely and evenly fills the polyGMA brush layer the fractional conversion of the polyGMA brush layer by protein adsorption can be expressed in terms of the available core volume given by Eq. B.13. The fractional conversion of the polyGMA brush layer is defined by $[(M-M_i)/(M_{eq}-M_i)]$, where M is the mass of protein bound to the polyGMA layer at any time, t, M_{eq} is the mass of protein bound to the polyGMA brush layer at equilibrium, and M_i is the initial mass of protein bound due to adsorption on the surface area of the nonwovens. The shrinking core model does not account for this initial protein adsorption (M_i), only diffusion and adsorption in the depth of the polyGMA brush layer. The core volume during binding and original core volume are defined by Eq. B.14 and B.15 respectively.

$$Core\ volume = \pi L r_c^2 - \pi L r_1^2 \tag{B.14}$$

$$Original\ core\ volume = \pi L r_2^2 - \pi L r_1^2 \tag{B.15}$$

Using the definitions of Eq. B.14 and Eq. B.15, Eq. B.13 becomes Eq. B.16.

$$1 - \frac{M-M_i}{M_{eq}-M_i} = \frac{r_c^2-r_1^2}{r_2^2-r_1^2} \tag{B.16}$$

By substituting Eq. B.16 into Eq. B.12 the fractional conversion of the polyGMA brush core over time according to the shrinking core model can be obtained after some algebraic manipulation, and is expressed by Eq. B.17 (Eq. 9).

$$\Psi = \frac{t}{\tau} = \frac{1}{2}\left(\frac{M-M_i}{M_{eq}-M_i}\right) + \left[\frac{1}{1-\phi^2} - \frac{M-M_i}{M_{eq}-M_i}\right] ln\sqrt{1-\left(\frac{M-M_i}{M_{eq}-M_i}\right)(1-\phi^2)} \tag{B.17}$$

In Eq. B.17 τ is the rate of adsorption of the polyGMA brushes for protein binding and is dependent on the effective diffusivity, thickness of the polyGMA graft layer, the density of the polyGMA brush layer and the concentration of protein in the bulk solution, it is defined by Eq. B.18 (Eq. 10).

$$\tau = \frac{(r_2^2 - r_1^2)\rho_{core}}{2D_e C_{bulk}} \quad \text{(B.18)}$$

Additionally in Eq. B.17 ϕ is the ratio of the radius of the PBT fiber compared to the radius of the polyGMA graft layer, it is defined by Eq. B.19 (Eq. 11).

$$\phi = \frac{r_1}{r_2} \quad \text{(B.19)}$$

2.5.C Derivation of swollen polyGMA brush radius

It is known that polyGMA brushes swell in aqueous solvents when functionalized electrostatically. If we assume that polyGMA brushes are completely extended when the brush layer is completely filled with protein we can calculate the swollen polyGMA brush radius r_2. The mass of protein adsorbed per the mass of the membrane at equilibrium is M_{eq} (mass protein/ mass membrane) and is the equivalent to the binding capacity of the material. The mass of protein bound can be converted to the volume of protein bound by Eq. C.1.

$$M_{eq}\bar{v} = \frac{Volume\ protein}{Mass\ membrane} \quad \text{(C.1)}$$

In Eq. C.1 $\bar{v}$ is the specific volume of protein and can be used to calculate the volume of protein occupying the polyGMA brush layer as can be seen in Fig. 2.15.

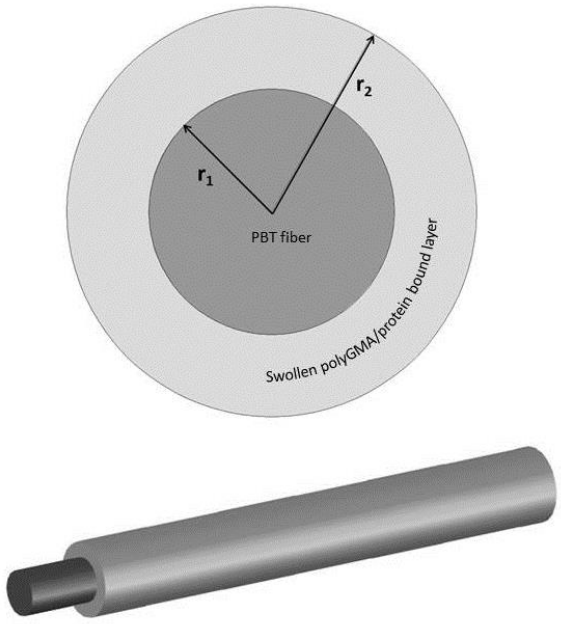

Fig. 2.15 Cross sectional view of PBT fiber grafted with polyGMA and 3-dimensional view of a PBT fiber grafted with polyGMA

In Fig. 2.15, r_2 is the radius of the swollen polyGMA brush layer completely filled with protein and r_1 is the radius of the PBT fiber. Each one of these occupies a cylindrical volume as defined by Eq. C.2 and Eq. C.3 for the volume of the PBT fiber and the volume of the PBT fiber that has been grafted with polyGMA respectively.

$$Volume\ PBT\ fiber = \pi L r_1^2 \quad \text{(C.2)}$$

$$Volume\ PBT\ fiber + Volume\ polyGMA\ brushes = \pi L r_2^2 \quad \text{(C.3)}$$

In Eq. C.2 and C.3 L is the length of PBT fiber and is assumed to be $L>>r$ for most cases. Using Eq. C.2 and C.3 the volume of the polyGMA brush layer can be solved for and is presented by Eq. C.4.

$$Volume\ polyGMA\ brushes = \pi L(r_2^2 - r_1^2) \quad \text{(C.4)}$$

Since we are assuming that the volume of the polyGMA brushes is equal to the volume of protein at equilibrium, Eq. C.4 can be substituted into Eq. C.1 resulting in Eq. C.5.

$$M_{eq}\bar{v} = \frac{\pi L(r_2^2 - r_1^2)}{Mass\ membrane} \tag{C.5}$$

The mass of the membrane is defined in terms of the volume and density of the PBT fiber (ρ_{PBT}) given by Eq. C.6.

$$Mass\ membrane = \rho_{PBT}\pi L r_1^2 \tag{C.6}$$

Eq. C.5 can be rewritten in terms of the volume and density of the PBT fiber given by Eq. C.6 to yield Eq. C.7.

$$M_{eq}\bar{v} = \frac{(r_2^2 - r_1^2)}{\rho_{PBT} r_1^2} \tag{C.7}$$

Eq. C.7 can be rearranged to explicitly state the radius of the swollen polyGMA brush layer r_2, given by Eq. C.8 (Eq. 12).

$$r_2 = \sqrt{M_{eq}\bar{v}\rho_{PBT} r_1^2 + r_1^2} \tag{C.8}$$

2.5.D Derivation of polyGMA core density

The density of the "core" in the shrinking core model is that of the density of the unbound functionalized polyGMA brushes. The swelling behavior of electrostatically charged polyGMA brushes in aqueous solvents requires the effective density of the core to be calculated from the mass of the polyGMA brushes and the volume that the swollen brushes occupy, this expression is given by Eq. D.1.

$$\rho_{core} = \frac{Mass\ polyGMA\ bruhses}{Volume\ polyGMA\ brushes} \tag{D.1}$$

The mass of the polyGMA brushes can be calculated from the amount of polyGMA added to the nonwovens, defined by Eq. D.2.

$$Mass\ polyGMA\ brushes = W_f - W_i \tag{D.2}$$

In Eq. D.2 W_f is the weight of the nonwoven membrane post grafting and W_i is the weight of the PBT nonwoven prior to grafting. The differences in the weights of nonwovens pre and post grafting can be related to the % weight gain given by Eq. D.3.

$$Mass\ polyGMA\ brushes = W_f - W_i = \frac{\%\ weight\ gain}{100\%} W_i \quad \text{(D.3)}$$

In Eq. D.3 the initial weight of the PBT nonwoven (W_i) can be calculated from the volume and density of the PBT fiber. A cylindrical geometry was used to calculate the volume of the PBT fiber and the density of PBT is known from literature to be (ρ_{PBT}= 1.33 g/cm^3) [25]. An expression for W_i in terms of the volume and density of the PBT fiber is presented in Eq. D.4.

$$W_i = \rho_{PBT} \pi L r_1^2 \quad \text{(D.4)}$$

In Eq. D.4, L is the length of the PBT fiber and r_1 is the radius of the PBT fiber. The volume of the polyGMA brush layer can be calculated by the difference in volume of the PBT fiber grafted with swollen polyGMA brushes and the PBT fiber. An expression for the mass of the polyGMA layer in terms of the % weight gain added by polyGMA and the volume and density of the PBT fiber can be obtained by substituting Eq. D.4 into Eq. D.3. This results in Eq. D.5.

$$Mass\ polyGMA\ brushes = \frac{\%\ weight\ gain}{100\%} \rho_{PBT} \pi L r_1^2 \quad \text{(D.5)}$$

The volumes of the PBT fiber and the grafted PBT fiber in the swollen state are given be Eq. D.6 and Eq. D.7 respectively.

$$Volume\ PBT\ fiber = \pi L r_1^2 \quad \text{(D.6)}$$

$$Volume\ PBT\ fiber + Volume\ polyGMA\ brushes = \pi L r_2^2 \quad \text{(D.7)}$$

Solving for the volume of the swollen polyGMA brushes using Eq. D.6 and Eq. D.7, results in Eq. D.8.

$$Volume\ polyGMA\ brushes = \pi L (r_2^2 - r_1^2) \quad \text{(D.8)}$$

The radius of the PBT fiber (r_1) and the radius of the swollen polyGMA brush layer (r_2) are visually depicted by Fig. C.1. Using the expression for the mass of the polyGMA brush layer given be Eq. D.5 and the volume of the swollen polyGMA brush layer given by Eq. D.8 the "core" density can be determined and is represented by Eq. D.9 (Eq. 13).

$$\rho_{core} = \frac{\frac{\%\, weight\ gain}{100\%}\rho_{PBT} r_1^2}{r_2^2 - r_1^2} \tag{D.9}$$

2.6 References

[1] D.K. Roper, E. Lightfoot, Separation of biomolecules using adsorptive membranes, J. Chromatogr. A 702 (1995) 357-367.

[2] E. Klein, Affinity membranes: a 10-year review, J. Membr. Sci. 179 (2000) 1-27.

[3] C. Charcosset, Purification of proteins by membrane chromatography, J. Chem. Technol. Biotechnol. 71 (1998) 95-110.

[4] A. Lyddiatt, Process chromatography: current strains and future options for the desorptive recovery of intracellular proteins, Curr. Opin. Biotechnol. 13 (2002) 95-103.

[5] J. Zhou, T. Tressel, Basic concepts in Q membrane chromatography for large scale antibody production, Biotechnol. Prog. 22 (2006) 341-349.

[6] I.M. Hutten, Handbook of Nonwoven Filter Media, Butterworth-Heinemann, Oxford, Burlington, MA 2007

[7] T. Przybycien, N. Pujar, L. Steele, Alternative bioseparation operations: life beyond packed-bed chromatography, Curr. Opin. Biotechnol. 15 (2004) 469-478.

[8] W. Muller, New ion exchangers for the chromatography of biopolymers, J. Chromatogr. 510 (1990) 133-140.

[9] S. Tsuneda, H. Kagawa, K. Saito, T. Sugo, Hydrodynamic evaluation of three-dimensional adsorption of protein to a polymer chain grafted onto a porous substrate, J. Colloid Interface Sci. 176 (1995) 95-100.

[10] K. Kobayashi, S. Tsuneda, K. Saito, H. Yamagishi, S. Furasaki, T. Sugo, Preparation of microfiltration membranes containing anion exchange groups, J. Membr. Sci. 76 (1993) 209-218.

[11] H. Shinano, S. Tsuneda, K. Saito, S. Furasaki, T. Sugo, Ion exchange of lysozyme during permeation across a microporous sulfopropyl-group-containing hollow fiber, Biotechnol. Prog. 9 (1993) 193-198.

[12] Y. Zheng, H. Liu, P. Gurgel, R. Carbonell, Polypropylene nonwoven fabrics with conformal grafting of poly(glycidyl methacrylate) for bioseparations, J. Membr. Sci. 364 (2010) 362-371.

[13] H. Liu, Y. Zheng, P. Gurgel, R. Carbonell, Affinity membrane development from PBT nonwoven by photo-induced graft polymerization, hydrophilization and ligand attachment, J. Membr. Sci. 428 (2013) 562-575.

[14] B. Bowes, A. Lenhoff, Protein adsorption and transport in dextran-modified ion-exchange media. II. Intraparticle uptake and column breakthrough, J. Chromatogr. A 1218 (2011) 4698-4708.

[15] K. Saito, T. Kaga, H. Yamagishi, S. Furasaki, T. Sugo, J. Okamoto, Phosphorylated hollow fibers synthesized by radiation grafting and crosslinking, J. Membr. Sci. 43 (1989) 131-141.

[16] K. Kato, E. Uchida, E. Kang, Y. Uyama, Y. Ikada, Polymer surface with graft chains, Prog. Polym. Sci. 28 (2003) 209-259.

[17] M. Benes, D. Horak, F. Svec, Methcylate-based chromatographic media, J. Sep. Sci. 28 (2005) 1855-1875.

[18] E.G. Vlakh, T.B. Tennikova, Preparation of methacrylate monoliths, J. Sep. Sci. 30 (2007) 2801-2813.

[19] H. Liu, Surface modified nonwoven membranes for bioseparations, Raleigh NC USA, North Carolina State Univ., PhD thesis, 2012.

[20] A. Durany, N. Anantharamaiah, B. Pourdeyhimi, High surface area nonwovens via fibrillating spunbonded nonwovens comprising Islands-in-the-Sea bicomponent filaments: structure-process-property relationships, J. Mater. Sci. 44 (2009) 4926-5934.

[21] D. Li, Y. Xia, Electrospinning of nanofibers: Reinventing the wheel?, Adv. Mater. 16 (2004) 1151-1170.

[22] D. Reneker, I. Chun, Nanometre diameter fibers of polymer, produced by electrospinning, Nanotechnology 7 (1996) 216-223.

[23] N. Fedorova, B. Pourdeyhimi, High strength nylon micro- and nanofiber based nonwovens via spundbonding, J. Appl. Polym. Sci. 104 (2007) 3434-3442.

[24] S. Choi, Y. Nho, Adsorption of Pb^{2+}, Cu^{2+}, and Co^{2+} by polypropylene fabric and polyethylene hollow fiber modified by radiation-induced graft copolymerization, Korean J. Chem. Eng. 16 (1999) 241-247.

[25] Dupont (2004) Product information: Dupont™ Crastin® 6130 NC010, Wilmington, DE.

[26] Sigma (2008) Product information: Poly(glycidyl methacrylate), St. Louis, Mo.

[27] J. Buijs, J. Lichtenbelt, W. Norde, J. Lyklema, Adsorption of monoclonal IgGs and their $F(ab')_2$ fragments onto polymeric surfaces, Colloids Surf., B 5 (1995) 11-23.

[28] S. Chen, L. Liu, J. Zhou, S. Jiang, Controlling antibody orientation on charged self-assembled monolayers, Langmuir 19 (2003) 2859-2864.

[29] M. Soderquist, A. Walton, Structural changes adsorbed on polymer surfaces, J. Colloid Interface Sci. 75 (1980) 386-397.

[30] N. Watanabe, T. Shirakawa, M. Iwahashil, K. Ohbu, T. Seimiya, Effect of surface charge on adsorption of bovine serum albumin as studied by ellipsometry 1. Adsorption on a cationic monolayer, Colloid Polym. Sci. (1986) 903-908.

[31] B. Fair, A. Jamieson, Studies of protein adsorption on polystyrene latex surfaces, J. Coll. Inter. Sci. 77 (1980) 525-534.

[32] Sigma (2000) Product information: Albumin from bovine serum, St. Louis, Mo.

[33] T.Jossang, J. Feder, E. Rosenqvist, Photon correlation spectroscopy of human IgG, J. Protein Chem. 7 (1988)165–171.

[34] G. Carta, A. Ubiera, T. Pabst, Protein mass transfer kinetics in ion exchange media: measurements and interpretations, Chem. Eng. Technol. 28 (2005) 1252-1264.

[35] F. Sarfert, M. Etzel, Mass transfer limitations in protein separations using ion-exchange membranes, J. Chromatogr. A 764 (1997) 3-20.

[36] F. Fang, J. Satulovsky, I. Szleifer, Kinetics of protein adsorption and desorption on surfaces with grafted polymers, Biophysical Journal 89 (2005) 1516-1533.

[37] O. Levenspiel, Chemical Reaction Engineering Chapter 25, Wiley and sons, Hoboken, NJ (1999)

[38] E. Schirmer, G. Carta, Protein adsorption kinetics in charged agarose gels: effect of agarose content and modeling, AIChE Journal 55 (2009) 331-341.

[39] G. Skidmore, B. Horstmann, H. Chase, Modelling single-component protein adsorption to the cation exchanger S Sepharose FF, J. Chromatogr. 498 (1990) 113-128

[40] F. Leinweber, U. Tallarek, Chromatographic performance of monolithic and particulate stationary phases hydrodynamics and adsorption capacity, J. Chromatogr. A 1006 (2003) 207-228.

Chapter 3

Heat Induced Grafting of Poly(glycidyl methacrylate) on Polybutylene Terephthalate Nonwovens for Bioseparations

Abstract

Polybutylene terephthalate (PBT) nonwovens were successfully grafted with poly(glycidyl methacrylate) (polyGMA) using a heat induced grafting approach with the thermal initiator benzoyl peroxide (Bz_2O_2) . This grafting method resulted in complete, uniform and conformal grafted layers around the PBT fibers that could be further functionalized as ion exchangers for protein capture. Protein binding capacities as high as 200 mg/g were achieved for ion exchange PBT nonwovens grafted to 20% weight gain using this thermal initiated grafting method. Compared to UV grafted polyGMA PBT nonwovens, the rates of protein adsorption are several times faster for the heat grafted PBT nonwoven, reaching equilibrium within minutes; UV grafted polyGMA ion exchange PBT nonwovens require hours to reach equilibrium. However, ion exchange polyGMA UV grafted PBT nonwovens are capable of binding between 5 and 7 times more protein at a given degree of polyGMA coverage compared to a heat grafted polyGMA PBT nonwovens. This is likely due to a structural difference between the polyGMA layers obtained with the two grafting methods. To investigate these differences, targets of various molecular weights (ATP, lysozyme, BSA, hIgG) were adsorbed by ion exchange to both UV and heat-induced grafted materials. The results of this experiment demonstrated that increased target sizes resulted in decreases in the number of target molecules bound on both materials. This decrease was significantly larger for heat grafted nonwovens indicating that this grafting method results in a polyGMA layer that either has a smaller volume, more rigid matrix or smaller pores available for binding

compared to the UV grafting method. Protein adsorption isotherms for the two grafting methods confirmed that both methods resulted similar strengths of protein binding, with dissociation constants on the order of $K_d \sim 10^{-6}$ M which is consistent with ion exchange binding on polymer brush networks.

Keywords: heat grafting, benzoyl peroxide, ion exchange, nonwovens, polybutylene terephthalate

3.1 Introduction

Surface initiated polymerization of nonwoven fabrics is a useful technique for introducing a thin polymer layer with substantially different surface properties than the material being grafted. In bioseparations polymer grafting has been used to functionalize polyolefin and polyester based nonwoven membranes to be high capacity protein capture devices [1-7]. Polyolefin and polyester are inexpensive thermoplastic polymers commonly used in high-rate nonwoven manufacturing technologies. These nonwoven membranes are particularly attractive as platforms for bioseparations since they are highly engineered to exhibit controllable porosities, fiber diameters, with sufficient mechanical integrity for filtration applications [8]. On the other hand these materials suffer from low specific surface areas, are chemically inert making functionalization difficult, and are hydrophobic in nature making them incompatible for protein capture in aqueous phases [9]. Grafting of polymer brushes to the surface of the nonwoven fibers has the potential to create a 3-dimensional environment that is hydrophilic and can be chemically modified for protein adsorption resulting in protein capture devices with high capacities [1-5]. Zhang *et al*. successfully grafted complete and conformal, poly-glycidyl methacrylate (GMA) polymer layers to a polypropylene (PP) nonwoven and functionalized the material to create a weak anion

exchanger. This resulted in bovine serum albumin (BSA) capture with a binding capacity of 120 mg/g of membrane [6]. Similarly Liu *et al*. grafted complete and conformal polyGMA layers to polybutylene terephthalate (PBT), and then functionalized it to be a completely hydrophilic membrane that significantly reduced nonspecific protein adsorption to negligible amounts [7]. Liu *et al*. also investigated polyGMA grafted PBT, functionalized as a weak anion exchanger, for the capture of BSA. In this study it was determined that the equilibrium binding capacity was dependent on the degree of GMA polymerization around the PBT fibers due to an increase in the size of the 3-dimensional binding polymer layer around the fibers [10].

Zheng *et al*. and Liu *et al*. both employed a UV-light induced radical polymerization to graft GMA monomer from the surface of the polyolefin and polyester respectively [6,7]. Irradiation based polymerizations have been extensively investigated for the grafting of vinyl monomers onto polymeric based membranes [1]. High-energy radiation such as x-rays, γ-ray and energy rich particle rays are all capable of inducing radical polymerization directly on a chemically inert surface without the necessity of an initiator [11]. However, these type of polymerizations are complicated and elaborate, requiring high cost experimental setups with excessively stringent reaction conditions which are possible at laboratory scales but are rarely seen industrially [11]. Additionally, often a pretreatment radiation step is required to activate the surface of the polymer substrate being grafted before the actual monomer polymerization from the surface [11]. UV-light radiation based polymerization is a more robust radical vinyl polymerization used heavily in commercial applications. This type of polymerization requires a photoinitiator that undergoes homolysis in the presence of UV-light creating a radical that can abstract a proton from a polymeric nonwoven surface, forming an initiation

site for vinyl polymerization [1,6,7,11]. The issue with UV-light polymerization is that it is limited to the penetration depth of the light source. Therefore, nonwoven samples that are sufficiently thick or have small pores or low porosity will absorb incident light and this will result in graft coverage gradients in the material due to a lack of UV-light penetration.

There is a need to develop a polymerization technique that can graft polymer layers onto nonwoven membranes regardless of the pore structure, thickness and shape of the material. Thermally driven surface polymerization has the potential to be a process that is robust and facile at creating a polymer grafted layer on a nonwoven surface that is independent of the morphology of the membrane being grafted. Thermally induced vinyl polymerization is commonly used industrially to create bulk polymerizations in solution but has found limited application for surface modification of membranes [11]. A few studies have been conducted investigating thermal grafting of vinyl monomers on polyethylene terephthalate (PET) and PP [12-15]. Arslan has successfully grafted polyGMA onto PET then further functionalized the material for removal of chromium from aqueous solutions [12]. Carroll *et al*. grafted acrylic acid, 2-(N,N-dimethyl amino)ethyl methacrylate, and poly(ethylene glycol) monomethyl ether monoacrylate to PP to reduce membrane fouling by organic waste [13]. However, almost no work has been done on the thermal grafting of polyGMA onto PBT nonwovens for applications in bioseparations.

This paper describes a methodology for creating highly conformal polyGMA grafts on PBT nonwovens using a thermally induced radical polymerization initiated by benzoyl peroxide (Bz_2O_2) at elevated temperatures. Bz_2O_2 is a thermal initiator very similar in structure and function to the photoinitiator benzophenone used for photo induced grafting of polyGMA onto PBT nonwovens. Additionally, Bz_2O_2 has been shown to initiate thermal

grafting on polyester fabrics [12,14,15] and the homolysis of Bz_2O_2 at elevated temperatures has the potential to create radical polymerization sites on the PBT surface for polyGMA propagation as well. The epoxy end groups in polyGMA introduce chemical functionality to the PBT surface that enables the covalent attachment of amines, thiols, and hydroxyl groups [16,17]. Liu *et al*. successfully converted PBT nonwovens photo grafted with polyGMA into weak anion and strong cation exchangers for bioseparations by covalently attaching diethylamine (DEA) and sulfonic acid via the epoxy groups of polyGMA respectively [7]. In this work polyGMA thermally grafted onto PBT nonwovens has been evaluated for its potential use in protein capture via anion and cation exchange. A direct comparison is drawn between the thermal induced and the UV induced polyGMA grafting of PBT nonwovens regarding graft morphology, chemical functionalization, protein capture ability, as well as the thermodynamics and binding kinetics of protein adsorption.

3.2 Experimental

3.2.1 Materials and reagents

Macopharma (Tourcoing, France) provided commercially available meltblown PBT nonwovens with a basis weight of 52 g/m^2. Glycidyl methacrylate (GMA) was purchased from Pflatz & Bauer (Waterbury, CT). Inhibitors in GMA were removed through a pre-packed inhibitor removal column to remove hydroquinone and monomethyl ether hydroquinone (Sigma Aldrich, St. Louis, MO). Benzophenone (BP) was purchased from Sigma Aldrich (St. Louis, MO). Benzoyl peroxide (70% wt.) (Bz_2O_2) , N,N-dimethylformamide (DMF), sodium hydroxide, 1-butanol, isopropyl alcohol, tris base, hydrochloric acid, sodium chloride and sodium acetate trihydrate were purchased from Fisher

Scientific (Fairlawn, NJ). Tetrahydrofuran (THF), methanol, sulfuric acid, and acetic acid were purchased from BDH (West Chester, PA). Diethylamine (DEA) was purchased from Alfa Aesar (Ward Hill, MA). Sodium sulfite was purchased from Acros Organics (Fairlawn, NJ). Solid phase extraction tubes were purchased from Supelco (Bellefonte, PA). Albumin from bovine serum (BSA), egg white lysozyme, and adenosine 5'-triphosphate (ATP) were purchased from Sigma Aldrich (St. Louis, MO). Human immunoglobulin G (hIgG) was purchased from Equitek-Bio Inc. (Kerrville, TX).

3.2.2 Heat induced polyGMA grafting onto PBT nonwovens

Nonwoven PBT was cut into 75 x 50 mm size samples and weighed prior to grafting. Sample weights were approximately 200 mg. These samples were immersed in 20 ml of a thermal initiator solution containing 75 mM Bz_2O_2 in DMF at room temperature for 1 hour to allow Bz_2O_2 to adsorb to the surface of PBT. Thermal initiator saturated samples were removed from the initiator solution and laid across a towel to wick excess initiator solution from the pores of the nonwoven. Samples were then placed in 20 ml of thermal grafting solution at a specific polymerization temperature and allowed to graft for a given amount of time. The grafting solution consisted of various GMA monomer concentrations of 5, 10, 20, 30 and 40 % (v/v) in DMF. The polymerization temperatures were kept constant at 70, 80 or 90 °C using a hot water bath (Isotemp 115, Fisher Scientific, Fairlawn, NJ). Grafting was allowed to proceed anywhere from 30 min to 6 hours. After polyGMA grafting, the samples were placed in a flask containing 100 ml of THF, and the flask with the THF and samples was sonicated in an ultrasonic bath (Bransonic 3510R-MT, Branson Ultrasonics Corporation, Danbury, CT) for a total of 30 min to remove any unreacted grafting solution or untethered polyGMA. The THF solvent was replaced after 15 minutes of the sonication process and

sonication continued for 15 minutes after replacement of the solvent. Following the THF wash the samples were removed from the flask and placed in a flask containing 100 ml of methanol. The flask containing the samples and methanol was sonicated in an ultrasonic bath for 10 min to remove THF from the nonwovens. Following the methanol wash the samples were removed from the flask and allowed to dry in air overnight. The final weights of the nonwovens were measured and the degree of polyGMA grafting was determined using Eq. 1 and expressed in terms of a % weight gain due to grafting.

$$Degree\ of\ polyGMA\ grafting\ (\%\ weight\ gain) = \frac{W_f - W_i}{W_i} \times 100\% \quad (1)$$

In Eq. 1 W_i is the initial nonwoven weight prior to grafting and W_f is the final nonwoven weight after polyGMA grafting.

3.2.3 UV induced polyGMA grafting onto PBT nonwovens

The GMA grafting solution consisted of 20% v/v GMA monomer in 1-butanol as the solvent. The photoinitator benzophenone (BP) was added to the grafting solution in a BP:GMA molar ratio of 1:20 (mol:mol). Nonwoven PBT was cut into 75 by 50 mm size samples and weighed prior to grafting, with each sample weighing approximately 200 mg. The nonwoven PBT samples were placed onto a borosilicate glass microscope slide, also 75 by 50 mm, to be prepared for grafting. Using a syringe, 1.5-2.0 ml of grafting solution was evenly distributed onto the membrane and a second borosilicate glass slide was placed on top of the nonwoven. A UV lamp (model EN-180L, Spectronics Corporation, Westbury, NY) was used to induce the free radical polymerization of polyGMA onto the nonwovens. The UV lamp had a wavelength of 395 nm, an intensity of 5 mW/cm^2 and nonwoven samples were placed 3 mm from the light source. Samples were irradiated at various exposure times to achieve different degrees of polyGMA grafting with different % weight gains. After

polyGMA grafting, the samples were placed in a flask containing 100 ml of THF, the flask was sonicated in an ultrasonic bath (Bransonic 3510R-MT, Branson Ultrasonics Corporation, Danbury, CT) for 30 min to remove any unreacted grafting solution or untethered polyGMA. Following the THF wash the samples were removed from the flask and placed in a flask containing 100 ml of methanol. The flask containing the samples and methanol was sonicated with an ultrasonic bath for 10 min to remove THF from the nonwovens. Following the methanol wash the samples were removed from the flask and allowed to dry in air overnight. The final weight of the nonwovens was measured and the degree of polyGMA grafting was determined using Eq. 1 in terms of a % weight gain.

3.2.4 Functionalization of polyGMA grafted PBT nonwovens

PolyGMA grafted PBT nonwovens grafted using both heat and UV-light were functionalized to produce weak anion exchangers by immersion in 50% v/v aqueous diethyl amine (DEA) solution, thus creating a tertiary amine on the polyGMA brushes [10]. Grafted PBT nonwoven samples weighing approximately 100 mg (35 x 50 mm) were immersed in 100 ml of the DEA solution. The reaction was kept constant at 30°C with agitation at 100 rpm using an incubation shaker (Certomat® RM, B. Braun Biotech International, Melsungen, Germany) contained in an incubation hood (Certomat® HK, B. Braun Biotech International, Melsungen, Germany). Following amination, samples were placed in a flask containing 100 ml of DI water; the flask was placed in an ultrasonic bath (Bransonic 3510R-MT, Branson Ultrasonics Corporation, Danbury, CT) for 5 min, to remove excess DEA. Following sonication, the DI water wash was replaced with fresh DI water and the process was repeated until a neutral pH of 7.0 was verified with pH testing paper. Using 10 washes ensured that all DEA had been removed from the nonwoven. Any unreacted epoxy groups were hydrolyzed

by immersion of the sample in 100 ml of 100 mM sulfuric acid overnight [10]. Following hydrolysis of the epoxy groups, samples were placed in a flask containing 100 ml of DI water, the flask was placed in an ultrasonic bath (Bransonic 3510R-MT, Branson Ultrasonics Corporation, Danbury, CT) for 5 min, to remove excess sulfuric acid. Following sonication, the DI water wash was replaced with fresh DI water and the process was repeated until a neutral pH of 7.0 was verified with pH testing paper. The use of 10 washes ensured that all the sulfuric acid had been removed from the nonwoven. The samples were then air dried overnight.

PolyGMA grafted PBT nonwovens were functionalized to create strong cation exchangers by attaching sulfonic acid groups to the polyGMA brushes. Approximately 100 mg (35 x 50 mm) samples of grafted PBT nonwoven samples were immersed in 20 ml of sodium sulfite solution containing sodium sulfite, isopropyl alcohol (IPA), and water (Na_2SO_3:IPA:Water=10:15:75 %wt.). The reaction was incubated at 80 °C for 8 hours (Isotemp 115, Fisher Scientific, Fairlawn, NJ) [5]. Following functionalization the samples were placed in a flask containing 100 ml of DI water, the flask was placed in an ultrasonic bath (Bransonic 3510R-MT, Branson Ultrasonics Corporation, Danbury, CT) for 5 min, to remove excess sodium sulfite solution. Following sonication, the DI water wash was replaced with fresh DI water and the process was repeated until a neutral pH of 7.0 was verified with pH testing paper. The use of 5 washes ensured that all sodium sulfite solution had been removed from the nonwoven. Any unreacted epoxy groups were hydrolyzed by immersion of the sample in 10 ml of 100 mM sulfuric acid overnight. Following hydrolysis of the epoxy groups, samples were placed in a flask containing 100 ml of DI water, the flask was placed in an ultrasonic bath (Bransonic 3510R-MT, Branson Ultrasonics Corporation,

Danbury, CT) for 5 min, to remove excess sulfuric acid. Following sonication, the DI water wash was replaced with fresh DI water and the process was repeated until a neutral pH of 7.0 was verified with pH testing paper. The use of 10 washes ensured that all the sulfuric acid had been removed from the nonwoven. The samples were then air dried overnight.

3.2.5 Material characterization

To evaluate the effectiveness, conformity, and uniformity of the heat grafting and UV grafting methods, scanning electron microscopy images were obtained using a Hitachi S-3200N variable pressure scanning electron microscope (VPSEM) (Hitachi High Technologies America, Inc., Schaumberg, IL). Grafted nonwoven samples were sputter coated with Pd/Au in argon gas. Images were captured using the microscope with an accelerating voltage of 5 kV at a working distance of 33 mm. The SEM micrographs were captured using the Revolution software from 4pi Analysis, Inc. (Hillsborough, NC).

The surface chemical composition of PBT nonwoven membranes after polyGMA grafting were characterized by ATR-FTIR using a Nicolet™ iS™10 FT-IR spectrometer with a diamond HATR crystal (Thermo Fisher Scientific, Waltham, MA). Each spectrum was collected with 64 scans at a resolution of 4 cm^{-1}. The beam radius was 5 mm with a range of inverse wavelengths of 4000-675cm^{-1}, and the analysis depth of penetration was ~ 0.67 μm at 2000 cm^{-1}.

The nitrogen content in samples before and after DEA modification were analyzed with a PE 2400 CHN elemental analyzer (PerkinElmer Inc, Waltham, MA) by combusting samples completely to elemental gases CO_2, H_2O and N_2 and detecting these. The

determination of total nitrogen content provided a direct measurement of DEA ligand density.

3.2.6 Static (equilibrium) binding

3.2.6.1 Model protein binding to heat grafted polyGMA nonwovens

It was of interest to investigate the equilibrium protein binding capacity for PBT nonwovens grafted using different heat induced grafting conditions to determine if the resulting grafted layer exhibits a variance for protein binding. Heat grafted polyGMA PBT nonwovens, grafted with various monomer concentrations and polymerization temperatures at varying degrees of polyGMA coverage were tested for their equilibrium static protein binding capacity when functionalized as weak anion exchange membranes. PBT nonwovens were grafted with GMA monomer concentrations of 10, 20 and 30 % GMA (v/v) and polymerization temperatures of 70, 80, 90 °C, at specific polymerization times to achieve degrees of polyGMA coverage of 5, 10, 15 and 20 % weight gain. These membranes were functionalized with DEA to become weak anion exchangers and challenged with pure BSA as a model protein to establish their static equilibrium binding capacity. BSA has a molecular weight of 66.5 kDa and an isoelectric point of 4.7 [Sigma Aldrich, St. Louis MO]. Approximately 20 mg (25 x 15 mm) samples of nonwoven were placed in a 3 ml solid phase extraction (SPE) tube and washed with 3 ml of low ionic strength binding buffer, 20 mM Tris HCl pH 7.0, 5 times. Samples were equilibrated for at least 30 min in binding buffer on a rotator (Tissue culture rotator, Glas-col, Terre Haute, IN) prior to BSA binding. Once equilibrated, 3 ml of 10 mg/ml BSA in 20 mM Tris HCl pH 7.0 were added to each sample and allowed to bind overnight for 15 hours. The low ionic strength buffer at pH 7.0 ensures that the DEA functionalized grafted PBT is positively charged and that BSA is negatively

charged to facilitate binding with a minimal amount of ions that would disrupt protein binding. After binding, samples were washed with 3 ml of 20 mM Tris HCl pH 7.0. Five washes with 20 mM Tris HCl pH 7.0 were required to remove all the unbound protein, verified by a negligible amount of protein in the fifth and final wash using UV-Vis spectroscopy at 280 nm. Bound BSA was eluted using a high ionic strength elution buffer (3 ml of 20 mM Tris HCl pH 7.0 + 1 M NaCl). The high ionic strength in the elution buffer effectively disrupts electrostatic interactions, removing the protein from the ion exchange nonwoven. Elution fractions were collected and protein concentrations were determined using UV-Vis spectroscopy at 280 nm. Static equilibrium binding capacity (q, in mass of protein per mass of membrane) values were determined using Eq. 2.

$$q\left(\frac{mg}{g}\right) = \frac{Protein\ Concentration\left(\frac{mg}{ml}\right) \times Volume\ of\ Elution\ Fraction}{Mass\ of\ membrane} \quad (2)$$

3.2.6.2 Model protein binding comparing heat grafted and UV grafted PBT nonwovens functionalized as anion and cation exchangers

PBT nonwovens grafted with polyGMA using heat and UV light were functionalized as weak anion and as strong cation exchangers for capture of model proteins to compare their differences in equilibrium binding capacity for the two grafting methods. The heat grafted PBT nonwovens were grafted with a monomer concentration of 30% (v/v) at a polymerization temperature of 80 °C for this binding investigation and all subsequent protein and biomolecule binding attempts. Heat grafted and UV grafted polyGMA PBT nonwovens grafted between 3 and 26% weight gain were functionalized with DEA creating weak anion exchangers for the capture of the model protein BSA. Approximately 20 mg (25 x 15 mm) nonwoven samples were placed in 3 ml solid phase extraction (SPE) tubes and washed with 3

ml of low ionic strength binding buffer, 20 mM Tris HCl pH 7.0, 5 times. Samples were equilibrated for at least 30 min in binding buffer on a rotator (Tissue culture rotator, Glas-col, Terre Haute, IN) prior to BSA binding. Once equilibrated 3 ml of 10 mg/ml BSA in 20 mM Tris HCl pH 7.0 were added to each sample and allowed to bind overnight for 15 hours. After binding, samples were washed with 3 ml of 20 mM Tris HCl pH 7.0. Five washes with 20 mM Tris HCl pH 7.0 were required to remove all the unbound protein, verified by a negligible amount of protein in the fifth and final wash using UV-Vis spectroscopy at 280 nm. Bound BSA was eluted using a high ionic strength elution buffer (3 ml of 20 mM Tris HCl pH 7.0 + 1 M NaCl). Elution fractions were collected and protein concentrations were determined using UV-Vis spectroscopy at 280 nm. Equilibrium binding capacities were calculated using Eq. 2.

In a similar fashion, heat grafted and UV grafted polyGMA PBT nonwovens grafted between 5 and 25% weight gain were functionalized with sulfonic acid creating strong cation exchangers for the capture of the model protein hIgG. These membranes were challenged with pure polyclonal hIgG as a model protein to establish the equilibrium binding capacity for these cation exchange membranes. Polyclonal hIgG has a molecular weight of 150 kDa and an isoelectric point between 7-9 [Equitek-Bio, Kerrville TX]. Approximately 20 mg (25 x 15 mm) samples of nonwovens were placed in 3 ml SPE tubes and washed with 3 ml low ionic strength binding buffer(20 mM acetate pH 5.5) 5 times. Samples were equilibrated for at least 30 min in binding buffer on a rotator (Tissue culture rotator, Glas-col, Terre Haute, IN) prior to hIgG binding. Once equilibrated, 3 ml of 10 mg/ml hIgG in 20 mM acetate pH 5.5 were added to each sample and allowed to bind overnight for 15 hours. The low ionic strength buffer at pH 5.5 ensures that the sulfonic acid functionalized grafted PBT is

negatively charged and that hIgG is positively charged to facilitate binding with a minimal amount of ions that would disrupt protein binding. After binding, samples were washed with 3 ml of 20 mM acetate pH 5.5. Five washes with 20 mM acetate pH 5.5 were required to remove all the unbound protein, verified by a negligible amount of protein in the fifth and final wash using UV-Vis spectroscopy at 280 nm. Bound hIgG was eluted using 3 ml of a high ionic strength elution buffer (20 mM acetate pH 5.5 + 1 M NaCl). The high concentration of ions in the elution buffer effectively disrupts the ionic interaction, removing the protein from the nonwoven. Elution fractions were collected and protein concentration was determined using UV-Vis spectroscopy at 280 nm. Eq. 2 was used to calculate the static equilibrium binding capacity.

3.2.6.3 Various target binding to heat grafted and UV grafted PBT nonwovens functionalized as ion exchangers

To investigate the effect of molecule size on binding, UV and heat grafted PBT nonwovens were challenged with various target proteins and biomolecules of different molecular weights. Heat grafted and UV grafted nonwovens grafted between 6 and 26% weight gain functionalized as anion exchangers with DEA were challenged with the small biomolecule ATP. ATP has a molecular weight of 507 Da and a pK_a of 6.5 [Sigma Aldrich, St. Louis MO]. It is known that ATP can readily adsorb to anion exchange chromatography media [18,19]. Approximately 20 mg (25 x 15 mm) nonwoven samples were placed in 3 ml solid phase extraction (SPE) tubes and washed with 3 ml of low ionic strength binding buffer, 20 mM Tris HCl pH 7.0, 5 times. Samples were equilibrated for at least 30 min in binding buffer on a rotator (Tissue culture rotator, Glas-col, Terre Haute, IN) prior to ATP binding. Once equilibrated 3 ml of 10 mg/ml ATP in 20 mM Tris HCl pH 7.0 were added to

each sample and allowed to bind overnight for 15 hours. After binding, samples were washed with 3 ml of 20 mM Tris HCl pH 7.0. Five washes with 20 mM Tris HCl pH 7.0 were required to remove all the unbound ATP, verified by a negligible amount of ATP in the fifth and final wash using UV-Vis spectroscopy at 256 nm. Bound ATP was eluted using a high ionic strength elution buffer (3 ml of 20 mM Tris HCl pH 7.0 + 1 M NaCl). Elution fractions were collected and ATP concentrations were determined using UV-Vis spectroscopy at 256 nm, equilibrium binding capacities were calculated using Eq. 2.

In a similar fashion, heat grafted and UV grafted polyGMA PBT nonwovens grafted between 6 and 26% weight gain were functionalized with sulfonic acid and challenged with lysozyme protein, a medium sized protein compared to the other biomolecules investigated. Lysozyme has a molecular weight of 14.3 kDa and an isoelectric point of 11.35 [Sigma Aldrich, St. Louis MO]. Approximately 20 mg (25 x 15 mm) nonwoven samples were placed in 3 ml SPE tubes and washed with 3 ml low ionic strength binding buffer, 20 mM acetate pH 5.5, 5 times. Samples were equilibrated for at least 30 min in binding buffer on a rotator (Tissue culture rotator, Glas-col, Terre Haute, IN) prior to lysozyme binding. Once equilibrated, 3 ml of 10 mg/ml lysozyme in 20 mM acetate pH 5.5 were added to each sample and allowed to bind overnight for 15 hours. After binding, samples were washed with 3 ml of 20 mM acetate pH 5.5. Five washes with 20 mM acetate pH 5.5 were required to remove all the unbound protein, verified by a negligible amount of protein in the fifth and final wash using UV-Vis spectroscopy at 280 nm. Bound lysozyme was eluted using 3 ml of a high ionic strength elution buffer (20 mM acetate pH 5.5 + 1 M NaCl). Elution fractions were collected and protein concentration was determined using UV-Vis spectroscopy at 280 nm. Eq. 2 was used to calculate the static equilibrium binding capacity.

3.2.7 Kinetics of protein adsorption

These experiments were aimed to determine the rate of protein adsorption on thermally grafted polyGMA PBT nonwovens functionalized as ion exchangers. Heat grafted polyGMA nonwoven PBT, grafted to 6, 15 and 24% weight gain, were functionalized with DEA for capture of BSA or with sulfonic acid for capture of hIgG. Approximately 20 mg (25 x 15 mm) of nonwoven samples were placed in 3 ml SPE tubes and washed extensively with binding buffer, 20 mM Tris HCl pH 7.0 for anion exchange experiments with BSA, or 20 mM acetate pH 5.5 for cation exchange experiments with hIgG. Samples were equilibrated for at least 30 min in binding buffer on a rotator (Tissue culture rotator, Glas-col, Terre Haute, IN) prior to protein binding. Once samples were equilibrated they were challenged with either 3 ml of 10 mg/ml BSA or 3 ml of 10 mg/ml hIgG for anion exchange or cation exchange nonwovens respectively. Protein was allowed to bind at various exposure times between 5 min and 24 hours. After binding, anion exchange samples that had bound BSA were washed five times with 3 ml of 20 mM Tris HCl pH 7.0 and cation exchange samples that bound hIgG were washed five times with 3 ml of 20 mM acetate pH 5.5 to remove any unbound protein. The BSA was eluted using 3 ml of the high ionic strength elution buffer, 20 mM Tris HCl pH 7.0 + 1 M NaCl. The hIgG was eluted using 3 ml of the high ionic strength elution buffer, 20 mM acetate pH 5.5 + 1 M NaCl. The elution fractions were analyzed using UV-Vis spectroscopy at 280 nm and the amount of protein bound for each material was calculated using Eq. 2.

3.2.8 Protein adsorption isotherm

The adsorption isotherms for BSA and ATP binding onto anion exchange PBT nonwovens, as well as, hIgG and lysozyme binding onto cation exchange PBT nonwovens

were investigated for nonwovens grafted using the heat grafting method and the UV-light grafting method. Approximately 20 mg (25 x 15 mm) nonwoven samples were placed in 3 ml SPE tubes and washed extensively with binding buffer, 20 mM Tris HCl pH 7.0 for anion exchange experiments, or 20 mM acetate pH 5.5 for cation exchange experiments. Samples were equilibrated for at least 30 min in binding buffer on a rotator (Tissue culture rotator, Glas-col, Terre Haute, IN) prior to protein binding. Once samples were equilibrated the anion exchange membranes were challenged with 3 ml of protein having concentrations ranging from 0.03 mg/ml to 10 mg/ml of either BSA or ATP. Similarly, the cation exchange membranes were challenged with 3 ml of protein having concentrations ranging from 0.03 mg/ml to 10 mg/ml of either hIgG or lysozyme. Protein was allowed to bind overnight for 15 hours at room temperature (23 °C). After binding, the 3 ml of unbound protein were collected for quantification to determine the unbound protein concentration. The protein bound anion exchange nonwoven samples were then washed five times with 3 ml of 20 mM Tris HCl pH 7.0 and cation exchange samples that bound hIgG were washed five times with 3 ml of 20 mM acetate pH 5.5 to remove any unbound protein. The BSA and ATP were eluted using 3 ml of the high ionic strength elution buffer (20 mM Tris HCl pH 7.0 + 1 M NaCl). The hIgG and lysozyme were eluted using 3 ml of the high ionic strength elution buffer (20 mM acetate pH 5.5 + 1 M NaCl). The concentrations of the unbound and elution fractions were analyzed using bicinchoninic acid method (BCA protein assay kit, Pierce, Rockford, IL) or UV-Vis spectroscopy at 280 nm (256 nm for ATP). Eq. 2 was used to determine the amount of protein bound to the nonwoven material. The data for the amount of protein bound at a specific free protein concentration was fit to the Langmuir adsorption model using the Origin 9 software package from OriginLab (Northampton, MA).

$$q = \frac{q_m C}{K_d + C} \quad (3)$$

In Eq. 3 q is the amount of protein bound to the nonwoven sample (mg/g), q_m is the maximum binding capacity (mg/g), C is the free protein concentration (mg/ml) and K_d is the dissociation constant (mg/ml).

3.3 Results and Discussion

3.3.1 Thermally induced grafting of polyGMA on PBT

In an effort to optimize the heat induced grafting of poly(GMA) onto commercial PBT using the thermal initiator Bz_2O_2, monomer concentrations ranging from 5 % to 40 % (v/v GMA in DMF) were investigated with polymerization temperatures between 70 °C and 90 °C. The results for the extent of grafting over various polymerization times for the conditions tested are presented in Fig. 3.1.

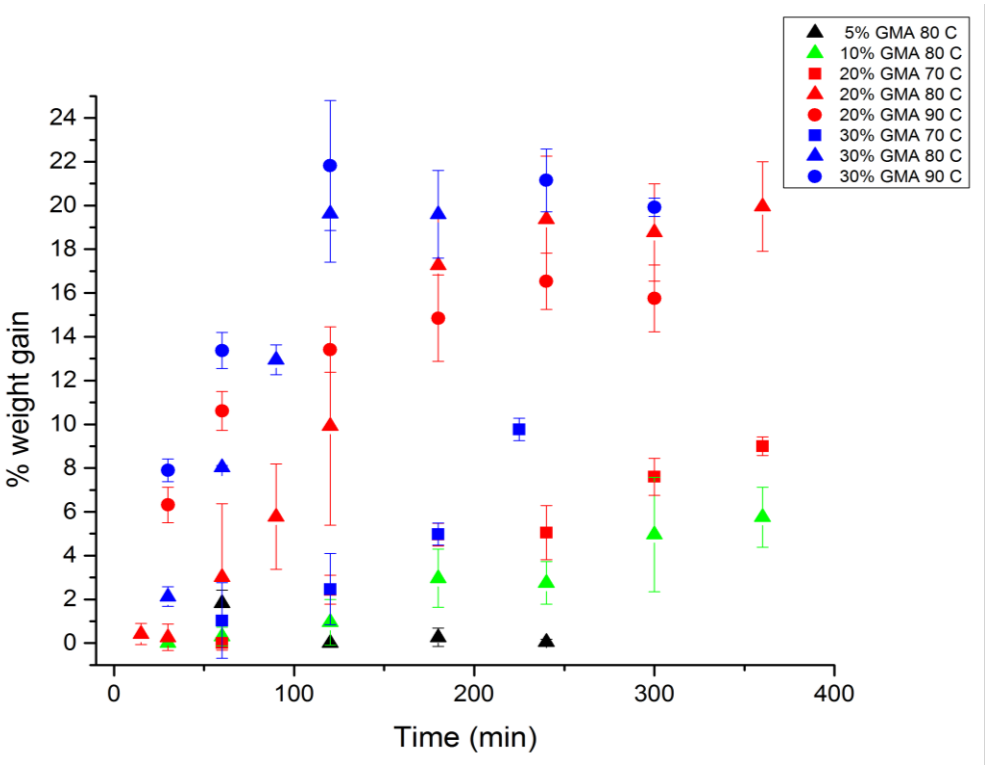

Fig. 3.1 Heat induced grafting evaluated by % weight gain for different GMA concentrations (% v/v) and different polymerization temperatures over a range of polymerization times.

From Fig. 3.1 it is apparent that increasing the monomer concentration results in an increase in the rate of grafting and the overall extent of grafting at given polymerization time. It was determined that there is a preferred range of monomer concentration to achieve efficient grafting. At a GMA monomer concentration of 5 % (v/v) effectively no grafting was observed. At a GMA monomer concentration of 10 % (v/v), poly(GMA) grafting was observed, however the overall extent of grafting even after 6 hours of polymerization was very low only reaching a 5 % weight gain of poly(GMA). Increasing the monomer concentration to 20% (v/v) or 30% (v/v) resulted in grafting as high as 20% weight gain after only 2 hours. At a GMA monomer concentration of 40 % (v/v) a rapid uncontrolled bulk polymerization occurred resulting in the complete solidification of the grafting solution; this

was not observed for monomer concentrations at or below 30 % (v/v). This effect has been observed in other investigations of vinyl polymer grafting onto polymeric substrates using thermally induced polymerization: past a threshold concentration polymerization in solution overcomes polymerization onto the polymeric surface [12,14,15]. For these reasons it is recommended that GMA monomer concentrations be kept between 20 % and 30 % (v/v) for this polymerization scheme. At a given temperature, a 30 % (v/v) GMA monomer concentration exhibited a faster rate of polymerization compared to a 20 % monomer concentration for polymerization times less than 2 hours, as can be seen in Fig. 3.1. The extent of grafting over time for polymerization with 20 % and 30 % GMA (v/v) at polymerization times less than 2 hours showed a linear time relationship as seen in Fig. 3.1, indicating a first order rate of grafting with respect to monomer concentration [11,15]. Therefore, it is reasonable that increasing the monomer concentration would result in an increase in the rate of grafting. For polymerization times longer than 2 hours a plateau in the extent of grafting is observed for 20 % and 30 % (v/v) GMA, at polymerization temperatures at or above 80 °C as can be seen in Fig. 3.1. This is a common phenomenon observed for the grafting of vinyl polymers onto polyester substrates using the thermal initiator Bz_2O_2 [12,14,15]. There are a number of potential reasons for this: depletion of available initiator, a reduction in the available active sites on the PBT fiber, the development of a diffusion barrier due to an increased viscosity of polyGMA in solution, or an increased termination rate of the polyGMA grafting compared to initiation.

From Fig. 3.1 it is apparent that temperature has a significant influence on the rate polymerization with higher temperatures resulting in higher observed weight gains at shorter polymerization times. The polymerization temperature affects the decomposition rate of

Bz_2O_2 into its radical form that enables polymerization at the PBT surface. Increasing the temperature results in an increased rate of decomposition of Bz_2O_2; the rates of decomposition of Bz_2O_2 in benzene at 60, 78, and 100 °C are $2x10^{-6}$, $2.3x10^{-5}$ and $5x10^{-4}$ s^{-1} respectively [20]. As a result, every 20 °C increase in polymerization temperature results in an order of magnitude increase in the rate of radical formation and therefore faster initiation is observed. It is observed in Fig. 3.1 that at 70 °C grafting proceeds very slowly with 8% weight gain being the highest achieved after 4 hours of polymerization for 30% (v/v) GMA. On the other hand at 80 °C and 90 °C polymerization proceeds substantially faster and is capable of achieving 20% weight gains of polyGMA coverage in approximately 3 hours at 80 °C and 2 hours at 90 °C. It should be noted that 80 °C is the recommended polymerization temperature for thermal initiation using Bz_2O_2 [11]. Thermal grafting conditions of 30 % (v/v) GMA at 80 °C gave the most consistent and reproducible polyGMA grafting onto the PBT nonwovens.

Heat induced grafting of polyGMA onto nonwoven PBT resulted in complete, conformal, highly uniform polyGMA coverage around the surface of the PBT fibers. This can be seen in the SEM images presented in Fig. 3.2.

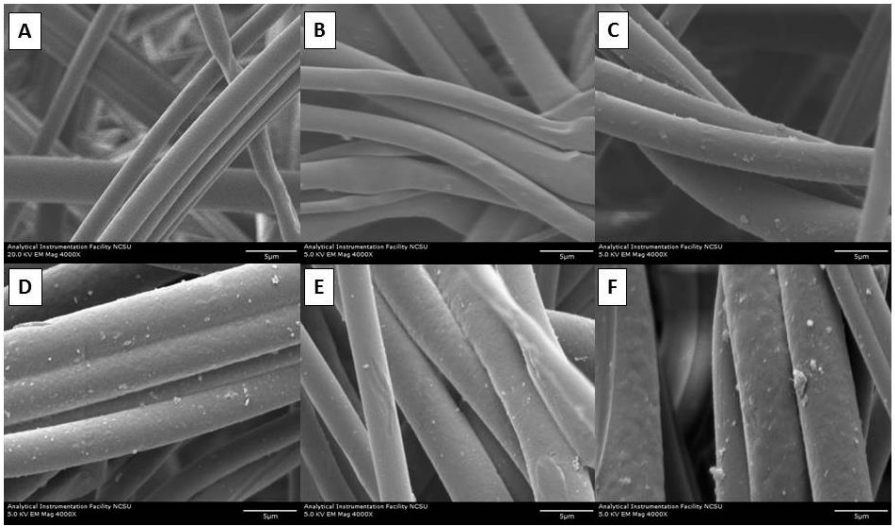

Fig. 3.2 SEM micrographs (4000x) of heat induced grafting onto PBT nonwovens for increasing % weight gain. (A) PBT nonwoven prior to grafting, (B) PBT nonwoven grafted to 1.5 % weight gain, (C) PBT nonwoven grafted to 7.5 % weight gain, (D) PBT nonwoven grafted to 11.5 % weight gain, (E) PBT nonwoven grafted to 16 % weight gain, (F) PBT nonwoven grafted to 19% weight gain.

Fig. 3.2B-3.2F display a visible surface roughness that is attributed to a polyGMA grafted layer that is not present on the native PBT nonwoven shown in Fig. 3.2A. Increased polyGMA graft coverage results in an increase in surface roughness of the fibers as can be seen comparing PBT nonwovens grafted at low weight gains (1.5 % weight gain, Fig. 3.2B) to PBT nonwovens grafted at high weight gains (19 % weight gain, Fig. 3.2F). It is also important to note that this method of heat grafting is capable of grafting to the entirety of the PBT surface without any pore blockage resulting in highly uniform, conformal, discreetly grafted fibers.

After polyGMA grafting, ATR-FTIR was used to analyze the surface chemistry of the grafted PBT nonwovens to ensure that the heat grafting method would maintain the integrity of the pendant epoxy groups inherent in polyGMA. Fig. 3.3 shows the ATR-FTIR spectra for

blank PBT nonwoven as well as for PBT nonwoven grafted with increasing extents of polyGMA grafting.

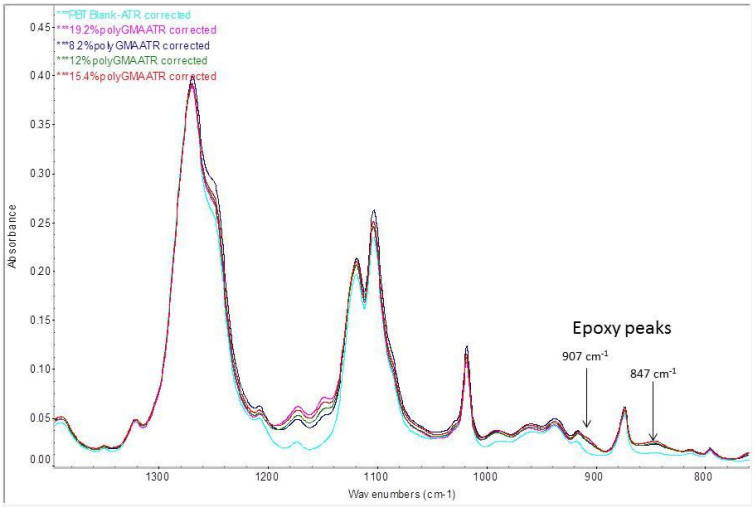

Fig. 3.3 FTIR spectra identification of signature epoxy peaks at 847 cm^{-1} and 907 cm^{-1} as well as an ester peak associated with poly(GMA) at 1150 cm^{-1} comparing blank PBT nonwoven with PBT nonwoven thermally grafted with increasing weight gains of poly(GMA).

Comparing the spectrum for blank PBT with PBT thermally grafted with polyGMA, it can be observed that a characteristic ester peak (at 1150 cm^{-1}) and epoxy peaks (at 847 cm^{-1} and 907 cm^{-1}) are present on the grafted PBT that is not present on the native PBT. Additionally, the intensity of these peaks increases with the amount of polyGMA in terms of % weight gain. These results indicate that thermal grafting successfully grafts polyGMA with viable epoxy pendant groups that are capable of further functionalization.

3.3.2 Comparison of ligand density after functionalization for PBT nonwovens grafted at various monomer concentrations and polymerization temperatures

Elemental analysis was performed on the heat grafted PBT nonwovens functionalized as weak anion exchangers with DEA to determine the ligand density of membranes grafted under various conditions. The results of the ligand density as a function of % weight gain for PBT nonwovens grafted at monomer concentrations of 20 % and 30 % (v/v) GMA at polymerization temperatures between 70 °C and 90 °C are presented in Fig. 3.4.

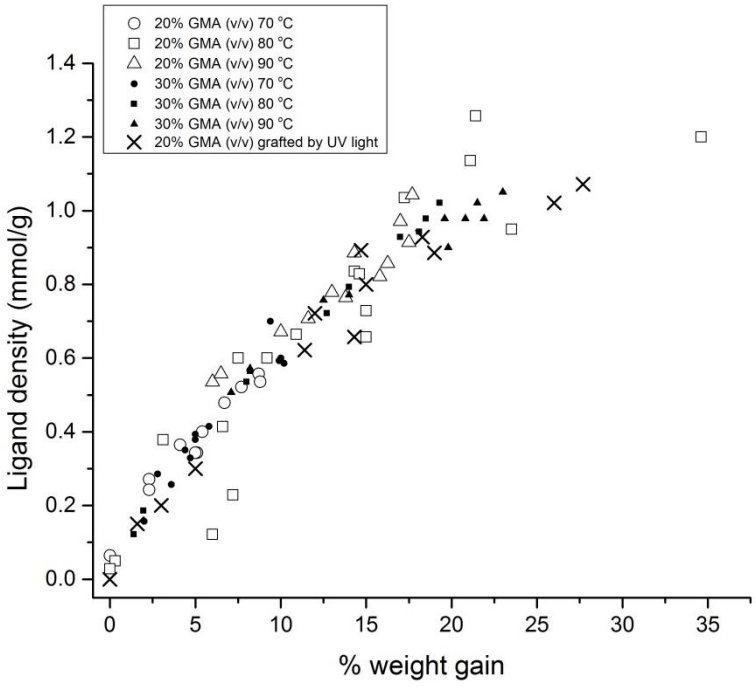

Fig. 3.4 DEA functionalized polyGMA grafted nonwovens; comparing heat induced polyGMA grafted nonwovens at various conditions to UV induced polyGMA grafted nonwovens. Densities determined via elemental analysis.

Also present in Fig. 3.4 is the DEA ligand density determined for PBT nonwovens grafted with UV-light for various % weight gains. UV grafting is the primary methodology for vinyl

grafting of polyester and polyolefin membranes and has been investigated extensively for the grafting of polyGMA onto PBT nonwovens [1,6,7,10]. For these reasons it is the benchmark for comparison of the thermally grafted PBT nonwovens in this investigation. From Fig. 3.4 it is apparent that the ligand density increases with the extent of polyGMA grafting for all of the grafted membranes. The linear nature of the data in Fig. 3.4 indicates that ligand density is directly proportional with the amount of polyGMA coverage. A comparison of the ligand density for nonwovens grafted at monomer concentrations of 20 % and 30 % (v/v) GMA for polymerization temperatures between 70 °C and 90 °C demonstrates that there is no observable difference in DEA ligand density for any of these conditions over the entire range of polyGMA graft coverage. Additionally, there is no difference in ligand density between the heat grafted nonwovens and the UV grafted nonwovens over the entire range of polyGMA graft coverage. This is a strong indication that for all of the conditions evaluated for the heat grafted polyGMA nonwovens and UV grafted nonwovens there are the same number of available epoxy groups that can be readily functionalized to become weak anion exchange binding sites.

3.3.3 Equilibrium protein binding ion exchange capacity of derivatized PBT nonwovens

BSA was chosen as the model protein to evaluate how the various thermally induced grafting conditions affect the overall equilibrium binding capacity when these materials are functionalized as ion exchangers. Fig. 3.5A and 3.5B display the equilibrium BSA binding capacities for PBT thermally grafted at various monomer concentrations and various polymerization temperatures respectively at specific degrees of polyGMA coverage when functionalized as anion exchangers.

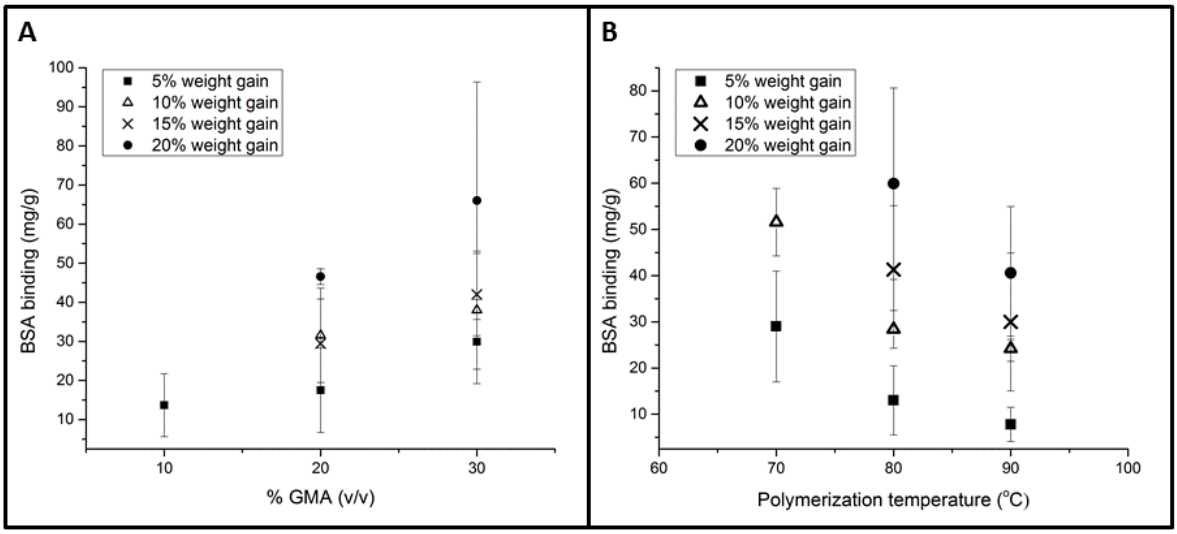

Fig. 3.5 Equilibrium BSA binding for anion exchange functionalized thermally grafted PBT nonwovens for various grafting conditions, (A) various % GMA (v/v) monomer concentrations tested for heat grafting and (B) various polymerization temperatures tested for heat grafting.

The results of Fig. 3.5A and 3.5B indicate that equilibrium protein binding capacity increases with initial monomer concentration in the grafting solution and decreases with increasing grafting polymerization temperature. This is an indication that the environment for protein binding changes depending on the grafting conditions even though similar % weight gains may be achieved. Fig. 3.4 demonstrates that DEA ligand density is almost solely dependent on the extent of polyGMA grafting and not on the grafting conditions; this includes the UV induced grafting. This contrasts with both Fig. 3.5A and 3.5B which demonstrate a strong dependence on the specific thermal grafting conditions for equilibrium protein binding. This is an indication that the structure and properties of the polyGMA grafted layers and consequently the accessibility of protein binding sites are strongly dependent on the grafting conditions [11,21-23]. Also apparent from both Fig. 3.5A and 3.5B is that the overall equilibrium binding capacity increases with the degree of polyGMA grafting (% weight gain). This observation is consistent with previous investigations that determined

equilibrium protein binding on ion exchange functionalized polyGMA grafted PBT nonwovens grafted using UV-light was dependent on the extent of grafting [7,10].

It is of interest to compare the equilibrium protein binding capacities for ion exchange functionalized PBT nonwovens grafted using a thermally induced grafting approach and a UV induced grafting approach. Fig. 3.6 compares equilibrium protein binding of UV and heat grafted PBT nonwovens functionalized as both anion and cation exchange membranes for capture of BSA and hIgG respectively. Heat grafted membranes grafted with a monomer concentration of 30 % (v/v) GMA at a temperature of 80 °C achieved the highest overall protein binding capacity according to Fig. 3.4 and were primarily used for all subsequent investigations unless otherwise state.

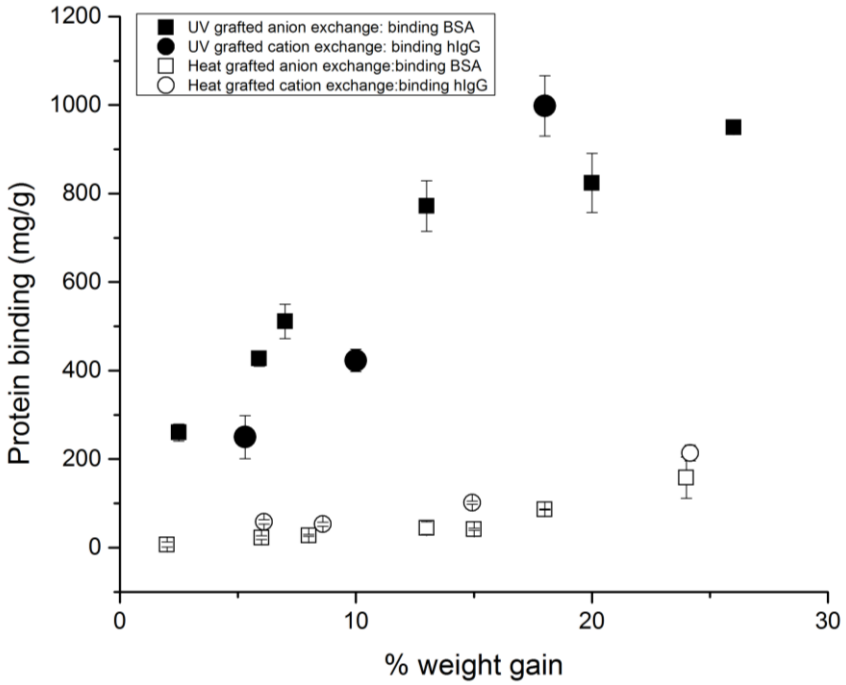

Fig. 3.6 Comparison of equilibrium protein binding capacity of PBT nonwovens grafted thermally and by UV-light functionalized as anion and cation exchanger for capture of BSA and hIgG respectively. Thermally grafted nonwovens grafted with 30% (v/v) GMA at 80 °C.

Fig. 3.6 shows how the equilibrium binding capacity is directly proportional to the extent of grafting for both the UV grafted PBT nonwovens and the heat grafted PBT nonwovens. However, the observed equilibrium protein binding capacities are on average 4.8 and 6.7 times higher for the UV grafted nonwovens functionalized as anion and cation exchangers respectively compared to their heat grafted counterparts. The results in Fig. 3.4 demonstrated that both the heat grafted nonwovens and the UV grafted nonwovens had very similar ligand densities when functionalized as anion exchangers. However, the equilibrium binding capacities presented in Fig. 3.6 are many times higher for the UV grafted nonwovens. This observation also indicates that the structures of polyGMA grafts are dependent on the grafting conditions and methodology. It is obvious from Fig. 3.6 that UV grafting creates a polyGMA structure that can accommodate more protein binding than the polyGMA structure obtained using a thermally induced grafting approach. Visual comparisons of PBT fiber cross sections grafted with UV-light and grafted thermally are presented in Fig. 3.7A and 3.7B respectively.

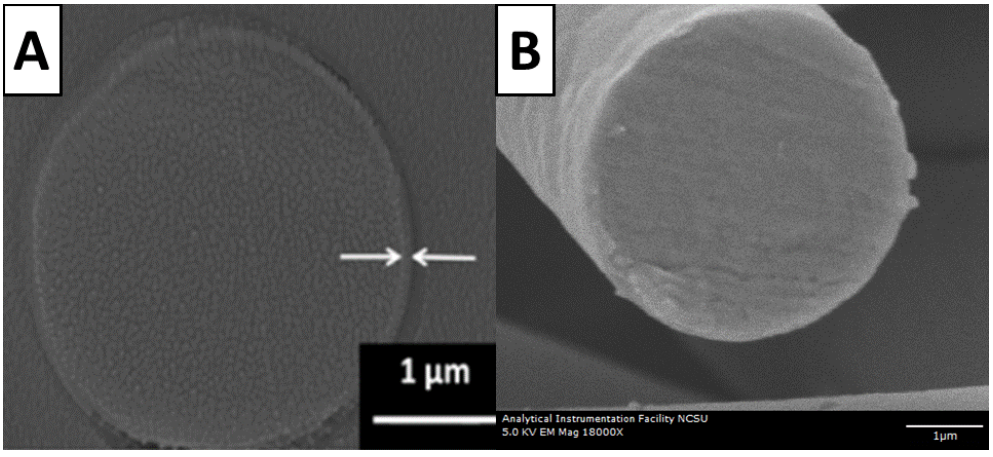

Fig. 3.7 SEM images for PBT fiber cross sections grafted with UV light (A) [7] and with thermally induced grafting (B).

In Fig. 3.7A there is a visible distinction between the polyGMA grafted layer and the PBT fiber for the UV grafted nonwoven, Fig. 3.7A is an adaptation from a investigation by Liu *et al.* [7]. This distinction is not present in Fig. 3.7B for the thermally grafted PBT nonwoven. This indicates that the density of the thermally grafted polyGMA layer is close to that of PBT and therefore unable to be resolved using SEM microscopy.

Vinyl grafting onto polymeric supports by radiation based free radical polymerization is known to create vinyl polymer brushes that are anchored to the polymeric surface [1-7]. These polymeric brushes tend to be tentacle-like in nature, highly linear and flexible [3,11,24]. Polymer brushes result in a 3-dimensional binding environment where protein can pack efficiently throughout the entire volume of the grafted layer due to the ability of the polymer brushes to expand, rearrange and accommodate more protein [25]. Vinyl grafting by heat induced free radical polymerization on the other hand results in far less flexible coated layers. Thermal based polymerizations result in higher rates of chain transfer compared to polymerizations by UV-light [11,21-23]. High rates of chain transfer result in highly branched polymer chains, as well as, highly cross-linked polymer networks, both of which would have significant effects on the density of the grafted polyGMA layer. A visual schematic representation of the proposed differences in the structures of the polyGMA matrix that result from UV light induced grafting and thermally induced grafting are presented in Fig. 3.8.

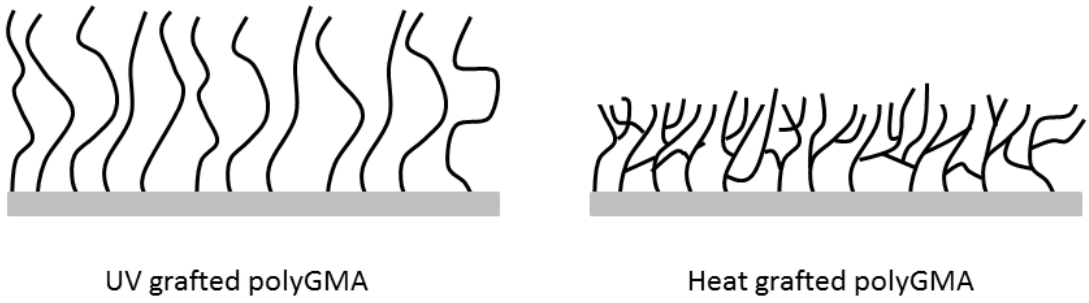

Fig. 3.8 Schematic representation of the proposed structure of polyGMA grafted layers resulting from UV light induced grafting and heat induced grafting.

This type of morphology would limit the grafted layer's ability to bind protein in two ways: (1) a grafted polyGMA layer with a higher density would have a smaller volume to accommodate proteins for a specific % weight gain and (2) a highly cross-linked polymer network would be substantially more rigid in nature resulting in protein diffusion issues into the depth of the grafted layer due to size exclusion and an inability of grafted polymer rearrangement to accommodate more protein. Since chain transfer rates are a function of temperature, this explains why there was an observed decrease in protein binding for increasing polymerization temperatures as Fig. 3.5B demonstrates; polyGMA grafts synthesized at 90 °C are more likely to be highly branched and cross-linked than polyGMA grafts synthesized at 70 °C. Additionally, the potentially higher density of the heat grafted nonwovens would allow for similar ligand densities as the UV-light grafted nonwovens due to a similar number of active epoxy groups for a given % weight gain. However, the volume of the polyGMA layer of the heat grafted nonwovens would be less than the UV-light grafted layer and would not be able to accommodate the same volume of protein in the grafted layer.

3.3.4 Equilibrium binding of various size targets

Target molecules with varying molecular weights were adsorbed to the heat grafted and UV grafted ion exchange nonwovens to investigate and compare the binding environment between the two grafting methods. ATP having the lowest molecular weight of 0.5 kDa was bound to anion exchange functionalized nonwovens, lysozyme having the second lowest molecular weight of 14.3 kDa was bound to cation exchange functionalized nonwovens, BSA having the second largest molecular weight of 66.5 kDa was bound to anion exchange functionalized nonwovens, and hIgG having the largest molecular weight of 150 kDa was bound to cation exchange functionalized nonwovens. The results for equilibrium binding (mg/g) of these molecules for various extents of polyGMA grafting are presented in Fig. 3.9A and 3.9B for heat grafted PBT nonwovens and UV grafted nonwovens respectively.

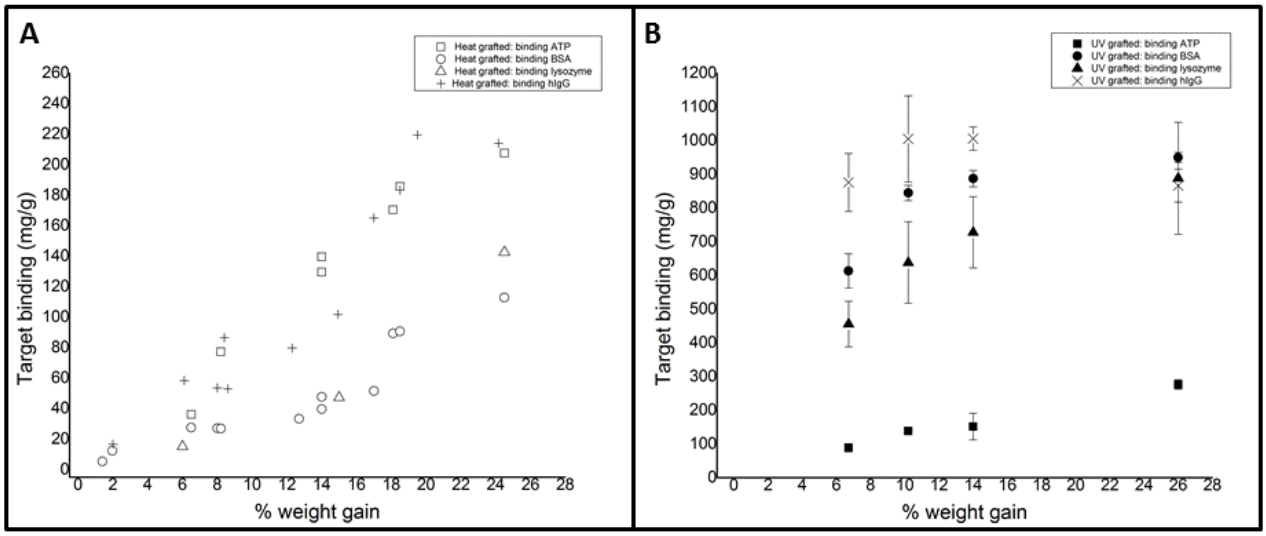

Fig. 3.9 Equilibrium binding capacity of various target molecules reported in terms of mass bound per mass of membrane bound to membranes with varying extents of polyGMA grafting for (A) heat grafted nonwovens and (B) UV grafted nonwovens.

From Fig. 3.9A it is evident that the heat-grafted nonwovens were capable of binding BSA and lysozyme with similar equilibrium mass binding capacities (100-120 mg/g at 25% weight gain) in terms of mass bound. The heat-grafted nonwovens bound hIgG and ATP with similar mass binding capacities, with both molecules binding significantly more mass than BSA and lysozyme. It is interesting to note that ATP is three orders of magnitude smaller than hIgG yet bound almost the same amount to the nonwoven on a per mass basis. BSA and lysozyme have molecular weights that are intermediate between those of ATP and hIgG but bound significantly less on a per mass basis. Fig. 3.9B on the other hand shows a strong dependence on the targets' molecular weight and the amount bound on a per mass basis. For the UV grafted nonwovens an increasing molecular weight results in an increase in the binding capacity on a per mass basis as shown in Fig. 3.9B.

To determine if the equilibrium binding capacities of polyGMA grafted nonwovens are limited by size exclusion and the volume of the polyGMA layer available for binding or are limited by the number of binding sites available, the binding capacities of Fig. 3.9 are reported on a molar basis in Fig. 3.10.

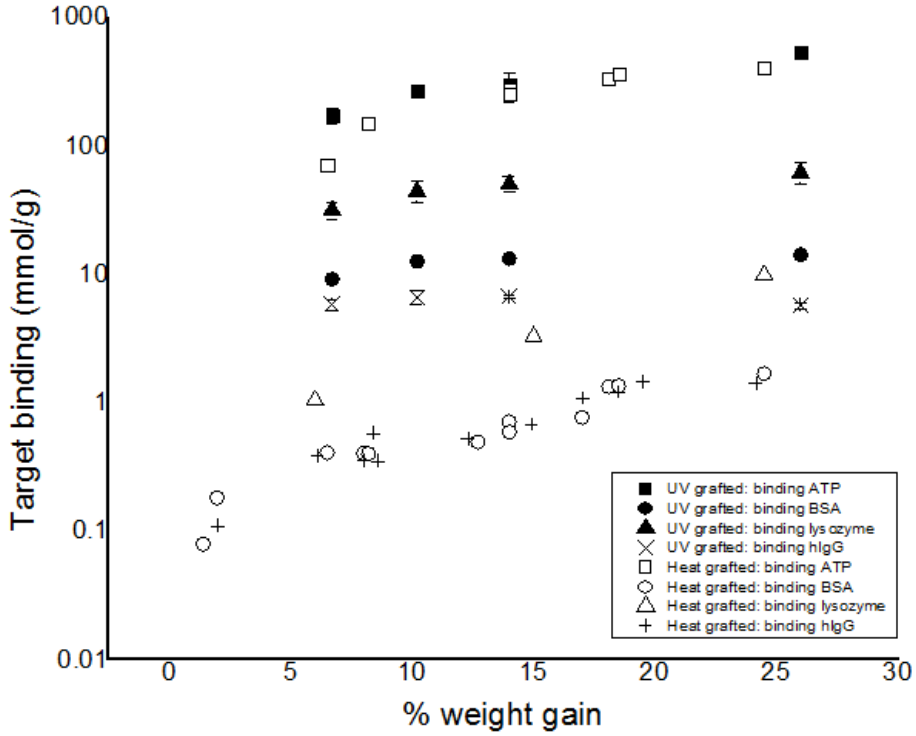

Fig. 3.10 Equilibrium binding capacity of various target molecules reported in terms of mmol bound per mass of membrane bound to membranes with varying extents of polyGMA grafting for heat grafted nonwovens and UV grafted nonwovens.

Due to the orders of magnitude differences in the targets' molecular weights, the molar binding capacities are presented on a lognormal scale in Fig. 3.10. In Fig. 3.10 the UV grafted nonwoven ion exchangers show a strong dependence of the molar binding capacity on the size of the target and the number of moles bound. hIgG, being the largest target, bound between 5 and 7 mmol/g, BSA the second largest target bound between 9 and 17 mmol/g, lysozyme the second smallest target bound between 30 and 60 mmol/g and ATP, the smallest target, bound between 170 and 600 mmol/g. The heat grafted nonwovens demonstrated a similar trend as Fig. 3.10 shows, the exception being the two largest targets tested bound

nearly the same number of molecules. The heat-treated nonwovens bound between 0.1 and 2 mmol/g for both BSA and hIgG, between 1 and 10 mmol/g for lysozyme and between 70 and 400 mmol/g for ATP. Also apparent from Fig. 3.10 is that both the UV grafted and the heat-grafted nonwovens bound similar amounts of ATP for the same specific % weight gains. The amount of protein bound (mmol/g) varies drastically between the UV grafted and the heat grafted nonwovens for the larger proteins tested. This is an indication that ATP is small enough that it can access the entire polyGMA layer for both materials. Therefore, the amount of ATP bound (mmol/g) is dependent on the ligand density of the nonwoven which is a determined by the overall extent of grafting as indicated in Fig. 3.4. This also demonstrates that there might be size exclusion effects occurring in the heat grafted nonwovens that are creating the large discrepancy in protein binding when compared to the UV grafted nonwovens. To evaluate this possibility target molar binding capacities are plotted as a function of target molecular weight for both the UV grafted and heat grafted nonwovens at various specific % weight gains in Fig. 3.11.

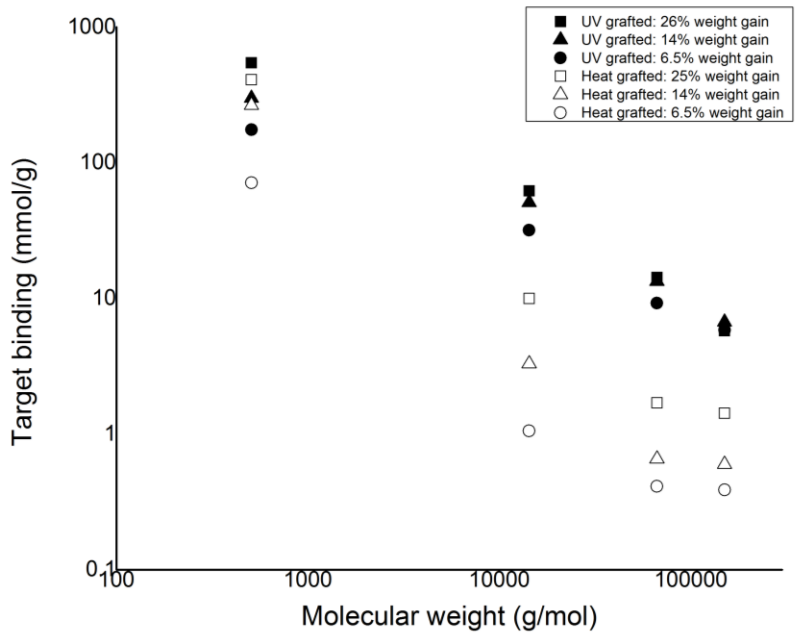

Fig. 3.11 Target binding as a function of the targets molecular weight for both the UV grafted PBT nonwovens and heat grafted PBT nonwovens grafted at 6.5%, 14%, and 25 % weight gain.

Fig. 3.11 is presented on a log-log scale to help visualize the trends between the UV grafted and the heat grafted nonwovens for binding of targets that have orders of magnitude different molecular weights and molar binding capacities. For both the UV grafted and the heat grafted nonwovens an increasing molecular weight results in drastic declines in the equilibrium molar binding capacity. Naturally, one can only fit so many molecules in a given polyGMA binding volume and therefore fewer molecules bind as molecular weight increases. However, the extent of this effect is different between the heat grafted nonwovens and the UV grafted nonwovens. For ATP binding, both the heat grafted and UV grafted nonwovens bound a very similar number of ATP molecules for a specific weight gain as shown in Fig. 3.11. However, as the molecular weight of the target molecule increases the number of

molecules bound (mmol/g) diverges between the two grafting methods as can be seen in Fig. 3.11. The resulting divergence in binding capacity for larger targets indicates that the heat grafted nonwovens have either less available binding volume or that the polymer network is more size exclusive than the UV grafted nonwovens. This result further validates that grafting using a thermally induced and heat driven polymerization is likely to result in a polyGMA network that is highly branched and cross-linked compared to a UV grafted polyGMA network. A highly branched/cross-linked polyGMA network is likely to have less volume to accommodate biomolecules and proteins due to its increased density. Additionally, a high degree of cross-linking is likely to make the matrix more rigid preventing polymer brush rearrangement to pack proteins efficiently and would also create pores that may be inaccessible to larger molecules.

3.3.5 Rates of adsorption to heat and UV polyGMA grafted nonwovens functionalizes as ion exchangers

Ion exchange functionalized polyGMA grafted PBT nonwovens grafted with UV-light exhibit very slow rates of protein adsorption that is a function of the polyGMA layer thickness [10]. To investigate if the rates of protein adsorption are different for BSA adsorption on anion exchange functionalized nonwovens grafted using a heat grafting method and a UV grafting method, both materials were exposed for BSA at varying contact times and evaluated for the amount of protein bound. The results for BSA binding over varying contact times for anion exchange heat grafted and UV grafted nonwovens are presented in Fig. 3.12.

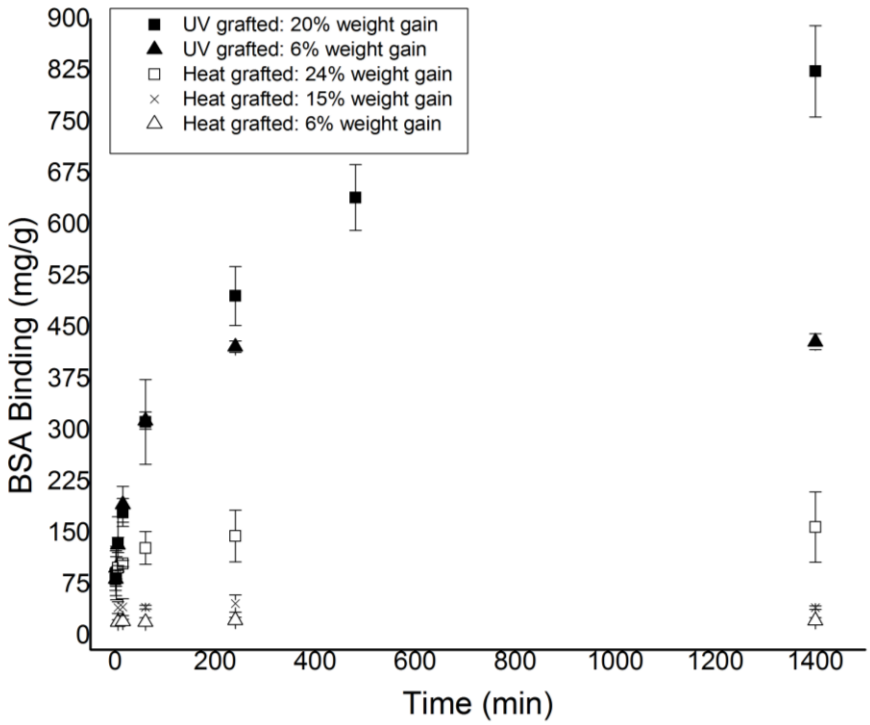

Fig. 3.12 BSA capture at various contact times for anion exchange functionalized grafted nonwovens: UV grafted at 20% and 5.9% weight gain (data adapted from Chapter 2 of this dissertation), as well as, heat grafted at 24%, 15% and 6% weight gain. All experiments done in batch systems.

From the results of Fig. 3.12 it is evident that the UV grafted polyGMA anion exchange nonwovens exhibit extremely slow rates of adsorption. The UV grafted polyGMA nonwoven grafted to 5.9% weight gain was able to reach equilibrium after about 4 hours of protein contact time and at 20% weight gain over 8 hours are required to reach equilibrium binding. The heat grafted nonwovens functionalized as anion exchangers exhibited much faster binding kinetics compared to the UV grafted anion exchangers. At the lower degrees of polyGMA grafting, 6 % and 15 % weight gain, equilibrium binding was achieved after 5 min of protein exposure for the anion exchange functionalized heat grafted nonwovens. At a high degree of polyGMA grafting, 24 % weight gain, equilibrium BSA binding is reached after 1

hour, with over 60% of the equilibrium binding capacity reached after 5 min of protein exposure.

The kinetics of hIgG adsorption by cation exchange to polyGMA grafted nonwovens grafted using the UV grafting method and the heat grafting method were also investigated. Fig. 3.13 displays the results for hIgG capture at various contact times for cation exchange nonwovens grafted with both methods.

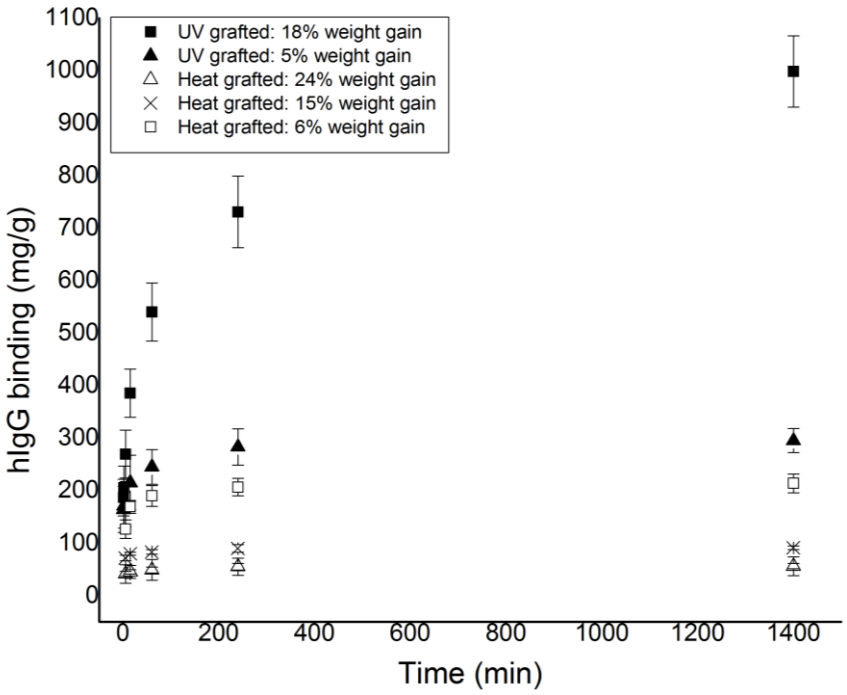

Fig. 3.13 hIgG capture at various contact times for cation exchange functionalized grafted nonwovens: UV grafted at 18% and 5% weight gain (data adapted from Chapter 2 of this dissertation), as well as, heat grafted at 24%, 15% and 6% weight gain. All experiments were done in batch systems.

As was the case in the anion exchange functionalized nonwovens, the cation exchange functionalized nonwovens grafted by the UV method exhibited slower rates of hIgG adsorption compared the cation exchange functionalized nonwovens grafted with heat. At

18% weight gain it takes nearly a full day to reach equilibrium for the cation exchange UV grafted polyGMA nonwovens. The PBT nonwovens UV grafted to a lower degree of coverage, 5% weight gain, reached hIgG binding equilibrium after 4 hours with over 80% of the equilibrium capacity reached after 1 hour, which is substantially faster than the UV grafted 20 % weight gain nonwoven as can be seen in Fig. 3.13. The heat grafted polyGMA nonwovens functionalized as cation exchangers demonstrated faster rates of hIgG capture compared to the UV grafted nonwovens as shown in Fig. 3.13. The heat grafted nonwovens grafted to 6 % and 15 % weight gain reached equilibrium after 5 min for hIgG binding. At a 24 % weight gain, the heat grafted nonwovens reaches equilibrium after 1 hour with over 60% of equilibrium binding reached after 5 min of protein exposure.

Heat grafting of polyGMA onto nonwoven PBT results in overall faster rates of protein adsorption compared to UV grafting of polyGMA onto nonwoven PBT when functionalized as ion exchangers as indicated in Fig. 3.12 and 3.13. However, equilibrium binding capacities are significantly lower for the ion exchange functionalized heat grafted nonwovens compared to the ion exchange functionalized UV grafted nonwovens as can be seen in Fig. 3.6, 3.12 and 3.13. The structural differences of the polyGMA layer created by heat grafting and UV grafting are likely to be the cause of the observed differences in the rates of protein adsorption. If the heat grafted polyGMA layers are denser, more rigid and contain inaccessible pores in the matrix compared to the UV grafted polyGMA layers there would be less capacity for protein adsorption and less ability and flexibility in the grafted polymer chains to rearrange and accommodate proteins as occurs in UV grafted layers. Protein diffusion and rearrangement are substantially slower phenomenon than convective

flow. Therefore, it is evident that the rate of protein binding on heat grafted nonwovens functionalized as ion exchangers are primarily dominated by convective mass transport where the UV grafted nonwovens exhibit a diffusion limitation that results in slow rates of protein binding [10]. Additionally, the heat grafted polyGMA layer has a smaller volume due to its higher density occurring from polymer branching. A smaller polyGMA volume available for binding would result in a lower overall binding capacity at a specific % weight gain and a shorter distance a protein would have to diffuse through that would also result in shorter times to reach equilibrium binding.

3.3.6 Adsorption isotherms

Adsorption isotherms for BSA binding on anion exchange nonwovens, as well as, hIgG binding on cation exchange nonwovens were performed for both grafting methods. The protein adsorption isotherms for the heat grafted and UV grated nonwovens, grafted at various weight gains, functionalized as anion exchangers for capture of BSA and as cation exchangers for capture of hIgG are presented in Fig. 3.14.

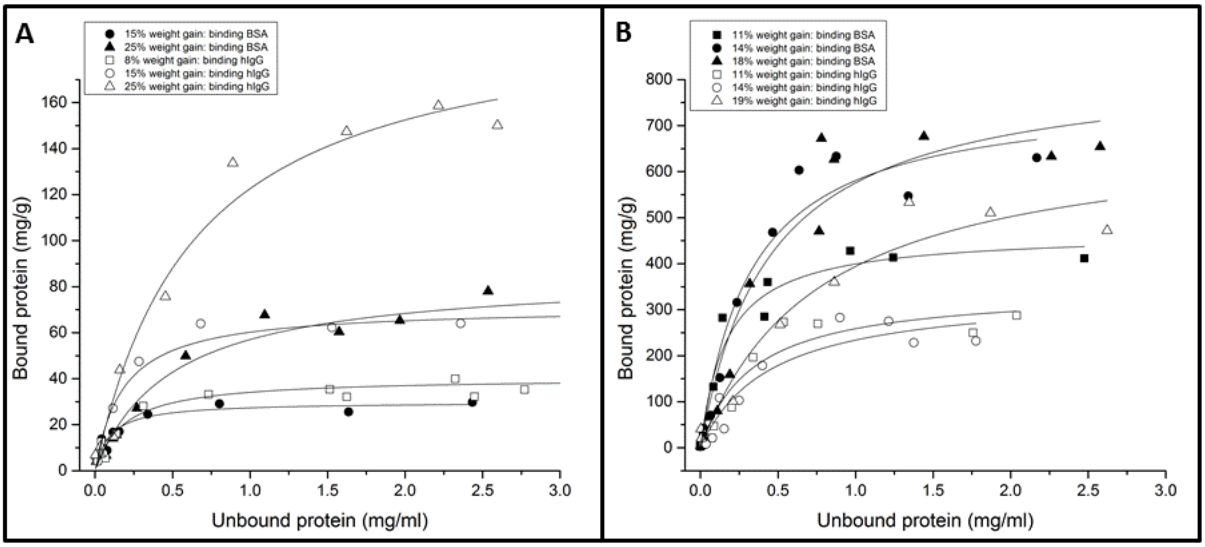

Fig. 3.14 Protein binding isotherms for various % weight gains. (A) Heat grafted nonwovens functionalized as anion exchangers for capture of BSA and as cation exchangers for capture of hIgG. (B) UV grafted nonwovens functionalized as anion exchangers for capture of BSA and as cation exchangers for capture of hIgG.

The protein adsorption isotherms for both grafting methods and both ion exchange functionalities exhibit Langmuir behavior as shown in Fig. 3.14A and 3.14B. The Langmuir adsorption model (Eq. 3) was fit to the data presented in Fig. 3.14. Although polymer grafted nonwovens functionalized as ion exchangers exhibit multilayer binding [3,10,24,27,28] with respect to the surface they are grafted, the polymer layer itself behaves as a single site adsorbent where the number of binding sites is determined by the charge density [27-29]. The apparent maximum binding capacity (q_m) and the dissociation constant (K_d) were calculated using Eq. 3. These values are presented in Table 3.1 for the samples grafted using the heat grafting method and Table 3.2 for the samples grafted using the UV grafting method.

Table 3.1: Apparent dissociation constant (K_d) and maximum binding capacity (q_m) obtained using a direct fit of the Langmuir model to the isotherm data shown in Fig. 3.14A for the heat grafted nonwovens functionalized as ion exchangers.

Degree polyGMA grafting (% weight gain)	Ion exchange functionality: protein bound	K_d (x10^{-6} M)	q_m (mg/g)	R^2
15	Anion exchange: BSA	1.4	30	0.88
25	Anion exchange: BSA	7.5	85	0.97
8	Cation exchange: hIgG	1.2	40	0.92
15	Cation exchange: hIgG	1.2	71	0.96
25	Cation exchange: hIgG	4.3	202	0.98

Table 3.2: Apparent dissociation constant (K_d) and maximum binding capacity (q_m) obtained using a direct fit of the Langmuir model to the isotherm data shown in Fig. 3.14B for the UV grafted nonwovens functionalized as ion exchangers.

Degree polyGMA grafting (% weight gain)	Ion exchange functionality: protein bound	K_d (x10^{-6} M)	q_m (mg/g)	R^2
11	Anion exchange: BSA	2.6	467	0.96
14	Anion exchange: BSA	4.9	771	0.96
18	Anion exchange: BSA	6.6	833	0.93
11	Cation exchange: hIgG	2.2	345	0.89
14	Cation exchange: hIgG	3.0	339	0.87
19	Cation exchange: hIgG	5.0	692	0.94

The calculated dissociation constants (K_d) are between 1.2 –7.5 x 10^{-6} M for all of the samples tested including both methods of grafting and both ion exchange functionalities used for capture of BSA and hIgG. These values are in agreement with reported values for protein binding on ion exchange functionalized polymer brushes and ion exchange functionalized polymer networks that have dissociation constants on the order of x 10^{-6} M [27-29]. These types of binding environments exhibit strong protein-matrix interactions as can be seen from their low K_d values. However, the addition of salt as an eluent effectively disrupts protein binding with the ion exchange matrix and causes ion exchange polymer brushes to collapse forcing displacement of protein [3]. The experimental results for the target molecule

adsorption isotherms of the heat grafted and UV grated nonwovens functionalized as anion exchangers for capture of ATP and as cation exchangers for capture of lysozyme are presented in the Appendix: Supplemental Information ATP and lysozyme adsorption isotherms.

3.4 Conclusions

PBT nonwovens were successfully grafted with polyGMA using a heat induced grafting method with the thermal initiator Bz_2O_2. The heat induced grafting results in a complete, uniform, conformal polyGMA layer around discreet PBT fibers. Grafted polyGMA nonwovens using this method were readily functionalized with DEA to become weak anion exchangers or with sulfonic acid to become strong cation exchangers. Equilibrium binding results for BSA bound to anion exchange heat grafted nonwovens indicated that the initial thermal grafting conditions had an impact on the overall binding capacity of the material. An increasing initial monomer concentration for grafting results in a polyGMA grafted layer that binds more protein and increasing polymerization temperature results in a polyGMA layer that binds less protein. Equilibrium binding capacities as high as 200 mg/g were observed for the heat grafted nonwovens grafted to 24% weight gain functionalized as a cation exchanger for binding of hIgG. The equilibrium binding capacities of the ion exchange heat grafted nonwovens was significantly lower than similar systems grafted using a UV induced radical polymerization for grafting. UV grafted polyGMA nonwovens functionalized as ion exchangers bound between 5 and 7 times more protein than the heat grafted polyGMA nonwovens, at a specific weight gain. However, kinetics of protein adsorption indicated that the heat grafted nonwovens were capable of achieving equilibrium binding on the order of

minutes compared to the UV grafted nonwovens that required several hours to reach equilibrium binding. Both materials have similar ligand densities at specific weight gains therefore it is likely that each grafting methodology results in a polyGMA grafted layer with significantly different structural properties. Ion exchange binding of biomolecules and proteins of varying molecular weights further reinforces the structural differences between the two grafting methods. For both grafting methodologies increasing molecular weight results in a decrease in the number of molecules bound at a given degree of polyGMA coverage. However this observation is more significant in the heat grafted polyGMA nonwoven samples indicating that the polymer matrix either has less available binding volume, a more rigid structure preventing efficient packing of proteins, or small pore structures that are inaccessible by larger proteins. These structural differences may be attributed to an increased degree of polymer branching and crosslinking that are not observed in the UV induced grafting method. Regardless of the proposed structural differences between the two grafting methods they exhibited similar strengths of binding with dissociation constants calculated to be on the order of 10^{-6}M which is consistent for protein binding on ion exchange polymer networks.

3.5 Appendix: Supplemental Information

3.5.A Lysozyme and ATP adsorption isotherms for heat grafted nonwovens

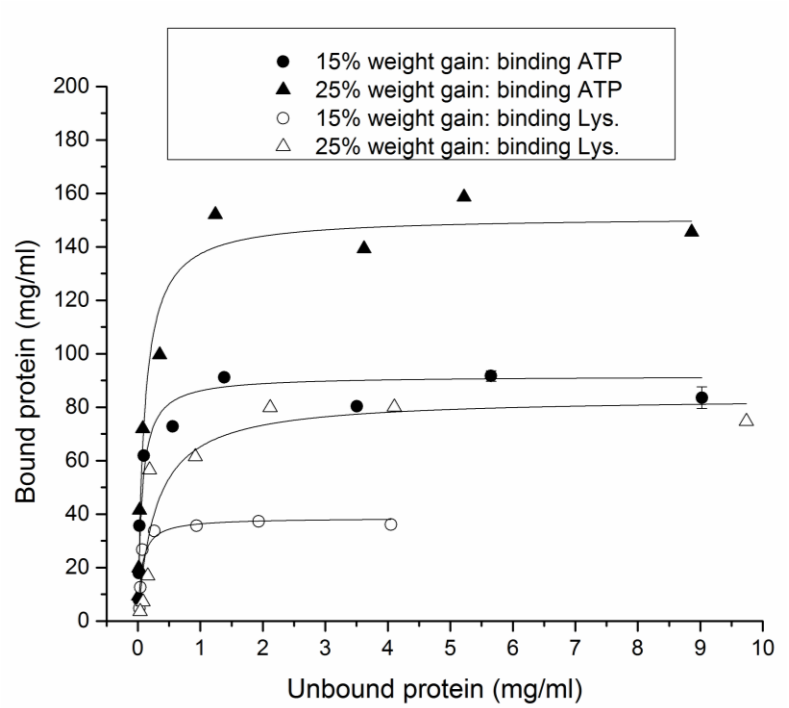

Fig. 3.5.A Adsorption isotherms for heat grafted nonwovens functionalized as anion exchangers for the capture of ATP and as cation exchangers for the capture of lysozyme.

Table 3.5.A: Apparent dissociation constant (K_d) and maximum binding capacity (q_m) obtained using a direct fit of the Langmuir model to the isotherm data shown in Fig. 3.5.A for the heat grafted nonwovens functionalized as ion exchangers.

Degree polyGMA grafting (% weight gain)	Ion exchange functionality: protein bound	K_d (x10^{-6} M)	q_m (mg/g)
15	Anion exchange: ATP	126	92
25	Anion exchange: ATP	200	151
15	Cation exchange: Lys.	4	39
25	Cation exchange: Lys.	19	84

3.5.B Lysozyme and ATP adsorption isotherms for UV grafted nonwovens

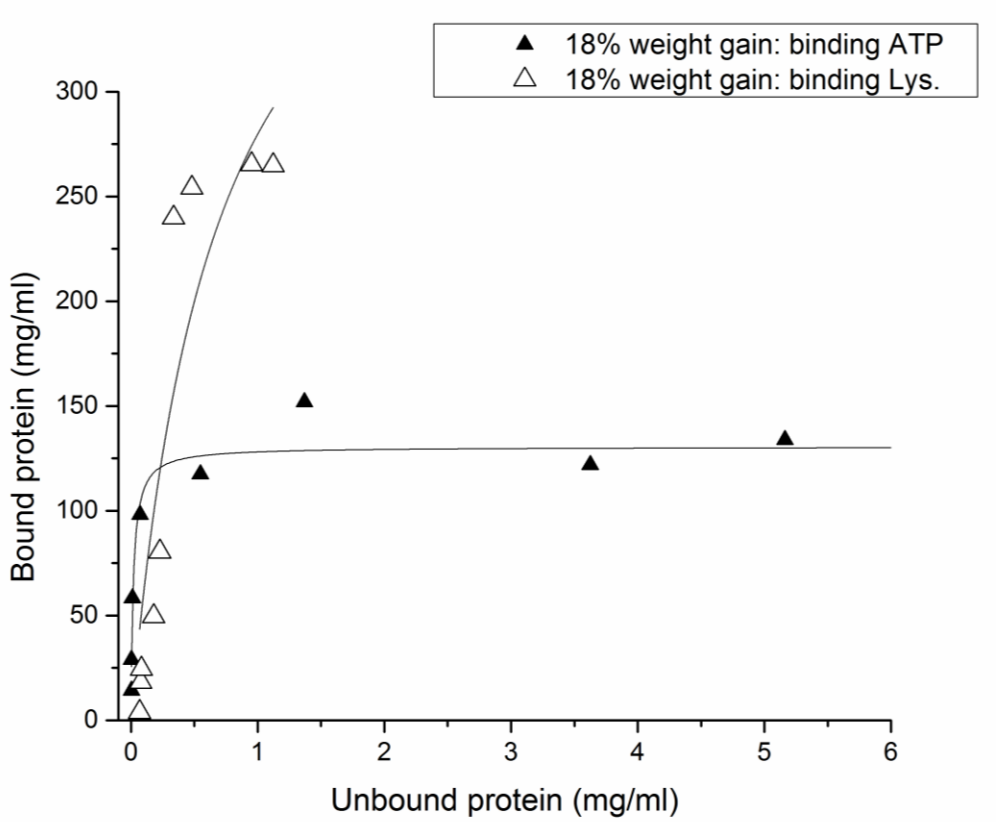

Fig. 3.5.B Adsorption isotherms for UV grafted nonwovens functionalized as anion exchangers for the capture of ATP and as cation exchangers for the capture of lysozyme.

Table 3.5.B: Apparent dissociation constant (K_d) and maximum binding capacity (q_m) obtained using a direct fit of the Langmuir model to the isotherm data shown in Fig. 3.5.B for the UV grafted nonwovens functionalized as ion exchangers.

Degree polyGMA grafting (% weight gain)	Ion exchange functionality: protein bound	K_d (x10^{-6} M)	q_m (mg/g)
18	Anion exchange: ATP	37	131
18	Cation exchange: Lys.	47	465

3.6 References

[1] E. Klein, Affinity membranes: a 10-year review, J. Membr. Sci. 179 (2000) 1-27.

[2] W. Muller, New ion exchangers for the chromatography of biopolymers, J. Chromatogr. 510 (1990) 133-140.

[3] S. Tsuneda, H. Kagawa, K. Saito, T. Sugo, Hydrodynamic evaluation of three-dimensional adsorption of protein to a polymer chain grafted onto a porous substrate, J. Colloid Interface Sci. 176 (1995) 95-100.

[4] K. Kobayashi, S. Tsuneda, K. Saito, H. Yamagishi, S. Furasaki, T. Sugo, Preparation of microfiltration membranes containing anion exchange groups, J. Membr. Sci. 76 (1993) 209-218.

[5] H. Shinano, S. Tsuneda, K. Saito, S. Furasaki, T. Sugo, Ion exchange of lysozyme during permeation across a microporous sulfopropyl-group-containing hollow fiber, Biotechnol. Prog. 9 (1993) 193-198.

[6] Y. Zheng, H. Liu, P. Gurgel, R. Carbonell, Polypropylene nonwoven fabrics with conformal grafting of poly(glycidyl methacrylate) for bioseparations, J. Membr. Sci. 364 (2010) 362-371.

[7] H. Liu, Y. Zheng, P. Gurgel, R. Carbonell, Affinity membrane development from PBT nonwoven by photo-induced graft polymerization, hydrophilization and ligand attachment, J. Membr. Sci. 428 (2013) 562-575.

[8] I.M. Hutten, Handbook of Nonwoven Filter Media, Butterworth-Heinemann, Oxford, Burlington, MA 2007

[9] T. Przybycien, N. Pujar, L. Steele, Alternative bioseparation operations: life beyond packed-bed chromatography, Curr. Opin. Biotechnol. 15 (2004) 469-478.

[10] H. Liu, Surface modified nonwoven membranes for bioseparations, Raleigh NC USA, North Carolina State Univ., PhD thesis, 2012.

[11] M. Mishra, Y. Yagci, Handbook of Vinyl Polymers: Radical Polymerization, Process, and Technology, CRC Press, Boca Raton, FL 2008

[12] M. Arslan, Preparation and Use of Amine-Functionalized Glycidyl Methacrylate-g-Poly(ethylene terephthalate) Fibers for Removal of Chromium(IV) from Aqueous Solution, Fibers and Polymer, 11 (2010) 325-330.

[13] T. Carroll, N. Booker, J. Meier-Haack, Polyelectrolyte-grafted microfiltration membranes to control fouling by natural organic matter in drinking water, J. Mem. Sci. 203 (2002) 3-13.

[14] S. Abdel-Fattah, S. Shalaby, E. Allam, A. Hebeish, Benzoyl peroxide induced graft polymerization of 2-methyl-5-vinylpyridine onto polyester/wool blend, J. Appl. Polym. Sci. 21 (1977) 3355-3365.

[15] M. Okoniewski, J. Sojka-Ledakowicz, Chemically induced graft copolymerization of acrylic acid on polyester frabrics. I. Kinetic investigation of grafting, J. Appl. Polym. Sci. 35 (1988) 1241-1249.

[16] M. Benes, D. Horak, F. Svec, Methcylate-based chromatographic media, J. Sep. Sci. 28 (2005) 1855-1875.

[17] E.G. Vlakh, T.B. Tennikova, Preparation of methacrylate monoliths, J. Sep. Sci. 30 (2007) 2801-2813.

[18] M. Bartolini, I. Wainer, C. Bertucci, V. Adrisan, The rapid and direct determination of ATPase activity by ion exchange chromatography and the application to the activity of heat shock protein-90, J. Pharm. Biomed. Anal. 73 (2013) 77-81.

[19] J. Yun, S. Shen, F. Chen, K. Yao, One-step isolation of adenosine triphosphate from crude fermentation broth of saccharomyces cerevisiae by anion-exchange chromatography using supermacroporous cryogel, J. Chromatogr. B. 860 (2007) 57-62.

[20] J. Brandrup, E.H. Immergut, E.A. Grulke, Polymer Handbook 4th Edition, John Wiley, NY, NY 1999

[21] H. Allcock, F. Lampe, Contemporary Polymer Chemistry 2nd Edition, Prentice Hall, Englewood, NJ 1990.

[22] G. Odian, Principles of Polymerization 4th Edition, Wiley and Sons, Hoboken, NJ 2004.

[23] C. Wolf, W. Burchard, Branching in free radical polymerization due to chain transfer. Application to poly(vinyl acetate), Macromol. Chem. 177 (1976) 2519-2538.

[24] K. Kato, E. Uchida, E. Kang, Y. Uyama, Y. Ikada, Polymer surface with graft chains, Prog. Polym. Sci. 28 (2003) 209-259.

[25] B. Bowes, A. Lenhoff, Protein adsorption and transport in dextran-modified ion-exchange media. II. Intraparticle uptake and column breakthrough, J. Chromatogr. A 1218 (2011) 4698-4708.

[26] D.K. Roper, E. Lightfoot, Separation of biomolecules using adsorptive membranes, J. Chromatogr. A 702 (1995) 357-367.

[27] S. Camperi, A. Navarro, F. Wolman, E. Smolko, O. Cascone, M. Gruselli, Protein adsorption onto tentacle cation-exchange hollow fiber membranes, Biotechnol. Prog. 15 (1999) 500-505.

[28] G. Brown, C. Muller, E. Theodosia, M. Franzreb, O. Thomas, Multi-cycle recovery of lactoferrin and lactoperoxidase from crude whey using fimbriated high-capacity magnetic cation. exchangers and a novel “rotor-stator” high-gradient magnetic separator, Biotechnol. Bioeng. 110 (2013) 1714-1725.

[29] G.Skidmore, B. Horstmann, H. Chase, Modelling single-component protein adsorption to the cation exchanger S Sepharose FF, J. Chromatogr. 498 (1990) 113-128

Chapter 4

Performance of ion exchange polyGMA grafted PBT nonwovens under flow conditions

Abstract

PolyGMA grafted PBT nonwovens functionalized as ion exchangers were evaluated for their performance under flow conditions. PBT nonwovens were grafted with polyGMA using a UV-light grafting technique and using a heat based grafting technique. It was determined that the UV-light based grafting method results in polyGMA brushes that extend from the surface of the nonwoven when functionalized with charged groups. The polyGMA brushes swell and shrink as the ionic strength of the solution changes. At low ionic strength the grafted layers swell significantly, reducing the membrane permeability and increasing the pressure drop. At high ionic strength the flow permeability increases and the pressure drop is greatly reduced. Ion exchange membranes synthesized using the heat based grafting method result in grafted layers with highly cross-linked polyGMA networks that do not exhibit this behavior and have much better flow properties than ion exchange membranes grafted with UV-light. The cation exchange polyGMA PBT nonwovens grafted using UV- light and heat exhibited dynamic binding capacities of 16 mg/ml and 20 mg/ml respectively at residence times from 1-5 minutes. The dynamic binding capacity is significantly lower than the equilibrium or static binding capacity of the membranes due to pore blockage occurring when the membranes are packed into the column for dynamic studies. The use of rigid PET nonwoven spacers increased the effective porosity of the columns, resulting in an increase in dynamic binding capacity for IgG of 24 mg/ml for the UV-light grafted materials and 35 mg/ml for the heat grafted materials.

Keywords: Polymer grafting, brush swelling, permeability, ion exchange, dynamic binding

4.1 Introduction

Packed bed chromatography is the predominant product capture and purification unit operation used in industry for the purification of therapeutic proteins. These materials have been engineered to recover target proteins at high binding capacities with very good resolution [1-2]. However, chromatography resins and agarose beads in particular suffer from diffusional limitations to protein diffusion into small pores or through a gel network resulting in long processing times [3-5] and dynamic binding capacities that decrease with increasing fluid superficial velocity in the column. Additionally, packed bed chromatography typically exhibits high pressure drops due to small hydraulic diameters and gel compaction at high flow rates [7-8]. This has led to the design of columns that can be several feet wide but only about a foot long to reduce pressure drops, and these are difficult to pack uniformly in order to obtain uniform flow distributions.

Membrane chromatography has the potential to overcome these limitations for packed bed chromatography. Microporous membranes are capable of processing large volumes at high throughputs with minimal pressure drops. In membranes, protein capture is dominated by convective flow requiring very short residence times to achieve complete saturation of the material [6]. However, protein binding capacity of membranes is usually low due to a limited available surface area for binding [9]. For this reason conventional membrane chromatography is best suited for large production volumes with target molecules at low concentrations, finding primary applications in impurity removal. For membranes to be used as a primary protein capture step, the binding capacity of the material needs to be increased. This can be done by increasing the surface area of the support or by introducing a three dimensional binding environment onto the surface of the membrane.

The grafting of polymers to the surfaces of the fibers in nonwoven membranes has been used to increase the binding capacities of these materials to levels adequate for the primary capture of proteins. Liu *et al.* successfully grafted complete and conformal, poly-glycidyl methacrylate (polyGMA) polymer layers to polybutylene terephthalate (PBT) nonwovens using UV-light and functionalized the material to be a weak anion exchanger [10]. It was determined that increasing the degree of polymer grafting resulted in an increase in the equilibrium protein binding capacity for the capture of bovine serum albumin (BSA) with static equilibrium capacities as high as 1000 mg/g achieved for a 12% degree of grafting. Heller *et al.* successfully grafted PBT nonwovens with layers of polyGMA using the thermal initiator benzoyl peroxide (Bz_2O_2) at elevated temperatures [11]. These membranes were functionalized as weak anion exchangers and strong cation exchangers for the capture of BSA and human immunoglobulin G (hIgG) respectively. Static equilibrium protein binding capacities were between 150 and 200 mg/g.

Ion exchange polymer grafting to surfaces is capable of increasing equilibrium protein binding by many times what the specific surface of the material can normally accommodate [10-12]. However, ion exchange polymer grafts exhibit complex properties that affect the kinetics of protein adsorption. For instance ion exchange polyGMA grafted layers grafted using UV-light are comprised of a network of polymer brushes that result in diffusion limited protein binding that require several hours to reach equilibrium [12]. Alternatively, ion exchange polyGMA grafted layers grafted using a thermal initiator and heat are believed to be highly branched and cross-linked networks that limit binding of large targets to a shallow layer of the polymer graft. This leads to faster protein binding kinetics compared to polymer brush networks reaching equilibrium binding on the order of minutes

[11] but also lower binding capacities. The behaviors of ion exchange grafted layers are also largely dependent on the ionic strength of their environment. Polyelectrolyte brushes are known to swell in a low ionic strength environment due to electrostatic repulsions between neighboring brushes. These same brushes collapse in high ionic strength environments because charged brushes associate with counter-ions and eliminate the electrostatic repulsions between brushes [13-15]. The swelling of weak ion exchange brushes can also be influenced by changes in the pH of the environment. In a study by Iwata *et al*. poly(acrylic acid) brushes were grafted to hollow fiber membranes. The grafting of the hollow fiber created molecular valves that would open and close with changes in the pH of the mobile phase to selectively allow or prevent liquid flow [16]. Cross-linking of a polyelectrolyte network has demonstrated to reduce any conformational changes of the grafted layer due to the ionic strength or pH of the environment [17]. The polymer chains of a highly cross-linked polymer network are physically constrained preventing dynamic mobility of the grafted polymer chains. In a study by Saito *et al*. hollow fiber membranes were grafted with cation exchange functionalized polyGMA brushes and covalently cross-linked to eliminate any swelling behavior due to changes in ionic strength [17].

This paper evaluates the performance of ion exchange functionalized PBT nonwovens grafted with polyGMA under flow conditions. Grafting of PBT nonwovens using UV-light and heat based grafting methods have demonstrated high static equilibrium protein binding capacities when functionalized as ion exchangers. Depending on the grafting technique used protein binding has shown to have adsorption kinetics ranging from minutes to hours. This could have significant implications on dynamic protein binding capacities and the overall productivity of the material. The ability of UV-light grafted PBT nonwoven ion exchangers

and heat grafted PBT nonwoven ion exchangers to dynamically capture the target protein hIgG was evaluated over a range of residence times. The ability of the ion exchange polyGMA grafted nonwovens to separate protein mixtures was also evaluated to determine if they could effectively purify hIgG from proteins with the same and opposite charges. The pressure drop and effective flow porosity of columns packed with ion exchange PBT nonwovens grafted using UV-light at various degrees of polymerization and grafted using the heat method were measured and the corresponding flow permeabilities were determined and compared to those of packed columns. The use of mechanically rigid nonwoven spacers to improve the column porosity, permeability and dynamic protein binding was also investigated.

4.2 Experimental

4.2.1 Materials and reagents

Macopharma (Tourcoing, France) provided commercially available melt blown PBT nonwovens with a basis weight of 52 g/m^2. PET nonwoven spacer fabric was provided by the Nonwovens Cooperative Research Center (NCRC, North Carolina State University, Raleigh, NC). Glycidyl methacrylate (GMA) was purchased from ReagentWorld (Ontario, Canada). Benzophenone (BP) was purchased from Sigma Aldrich (St. Louis, MO). Benzoyl peroxide (70% wt.) (Bz_2O_2) , N,N-dimethylformamide (DMF), sodium hydroxide, 1-butanol, isopropyl alcohol, tris base, hydrochloric acid, beta-mercaptoethanol sodium chloride and sodium acetate trihydrate, sodium carbonate and sodium bicarbonate were purchased from Fisher Scientific (Fairlawn, NJ). Tetrahydrofuran (THF), methanol, sulfuric acid, and acetic acid were purchased from BDH (West Chester, PA). Diethylamine (DEA) was purchased

from Alfa Aesar (Ward Hill, MA). Sodium sulfite was purchased from Acros Organics (Fairlawn, NJ). Solid phase extraction tubes were purchased from Supelco (Bellefonte, PA). Amicon Ultra centrifugal concentrator filters with a 3,000 NMWL were purchased from Fisher Scientific (Farilawn, NJ). Mini-PROTEAN TGX precast SDS-PAGE gels, 2x Laemmli sample buffer, 10x TGS running buffer, Brilliant Coomasie Blue stain and Precision Plus Protein Standard were purchased from BioRad (Hercules, CA)Albumin from bovine serum was purchased from Sigma Aldrich (St. Louis, MO). Human immunoglobulin G (hIgG) was purchased from Equitek-Bio Inc. (Kerrville, TX). A 10 mm inner diameter adjustable piston OmniFit column was purchased from Diba Industries (Danbury, CT).

4.2.2 PET nonwoven spacer characterization

To determine the average fiber diameter of the PET nonwoven spacer, scanning electron microscopy images were obtained using a Hitachi S-3200N variable pressure scanning electron microscope (VPSEM) (Hitachi High Technologies America, Inc., Schaumberg, IL). Nonwoven samples were sputter coated with Pd/Au in argon gas. Images were captured using the microscope with an accelerating voltage of 5 kV at a working distance of 33 mm. The thickness of the material, distances across fiber diameters and between neighboring fibers were measured on the SEM micrographs using the Revolution software from 4pi Analysis, Inc. (Hillsborough, NC). The average fiber diameter of the 108 I/S PBT and the commercially available PBT nonwovens were determined by measuring the distance across 100 random fibers of the SEM micrographs. The overall membrane thickness was determined using cross sectional SEM images, measuring the cross sectional distance of the spacer at 20 different locations.

To determine the extent of nonspecific hIgG adsorption to the PET nonwoven spacer a protein binding study was performed. PET nonwoven spacer was punched into 10 mm discs and approximately 20 mg of samples were placed in 3 ml solid phase extraction (SPE) tubes. The samples were washed 5 times with 3 ml of 20 mM Tris-HCl pH 6.5 and then equilibrated with 3 ml of binding buffer for 30 minutes prior to hIgG binding. After equilibration, 3 ml of 10 mg/ml IgG in 20 mM Tris-HCl pH 6.5 were added to each sample and allowed to bind overnight for 15 hours. After binding, unbound protein and a 3 ml wash of 20 mM Tris-HCl pH 6.5 were collected for protein quantification using UV-Vis spectroscopy at 280 nm. The amount of nonspecific protein binding was calculated using Eq. 1.

$$Nonspecific\ protein\ adsorption\ \left(\frac{mg}{g}\right) = \frac{V_{added} * C_o - V_{Collected} C_{unbound}}{mass\ of\ membrane} \quad (1)$$

In Eq. 1, V_{added} is the volume of protein added for binding (3 ml), C_o is the initial protein concentration (10 mg/ml), $V_{Collected}$ is the volume of collected after binding and $C_{unbound}$ is the concentration of protein of unbound protein determined by UV-Vis spectroscopy.

4.2.3 Heat induced polyGMA grafting onto PBT nonwovens

Nonwoven PBT was cut into 75 x 50 mm size samples and weighed prior to grafting; samples weights were approximately 200 mg. These samples were immersed in 20 ml of a thermal initiator solution containing 75 mM Bz_2O_2 in DMF at room temperature for 1 hour to allow Bz_2O_2 to adsorb to the surface of PBT. Thermal initiator saturated samples were removed from initiator solution and laid across a towel to wick excess initiator solution from the pores of the nonwoven. Samples were then placed in 20 ml thermal grafting solution that consisted of 30% (v/v) GMA monomer in DMF. The samples in the thermal grafting solution

were then placed in a hot water bath (Isotemp 115, Fisher Scientific, Fairlawn, NJ) at 80 °C and allowed to polymerize for 2 hours. After polyGMA grafting, the samples were placed in a flask containing 100 ml of THF, and sonicated in an ultrasonic bath (Bransonic 3510R-MT, Branson Ultrasonics Corporation, Danbury, CT) for 30 min to remove any unreacted grafting solution or untethered polyGMA. The THF was replaced after 15 min of sonication, and sonication continued for an additional 15 minutes. Following the THF wash the samples were removed from the flask and placed in a flask containing 100 ml of methanol. The flask containing the samples and methanol was sonicated with an ultrasonic bath for 10 min to remove THF from the nonwovens. Following the methanol wash the samples were removed from the flask and allowed to dry in air overnight. The final weight of the nonwovens was measured and the degree of polyGMA grafting was determined using Eq. 2 in terms of a % weight gain due to grafting.

$$Degree\ of\ polyGMA\ grafting\ (\%\ weight\ gain) = \frac{W_f - W_i}{W_i} \times 100\% \qquad (2)$$

In Eq. 2 W_i is the initial nonwoven weight prior to grafting and W_f is the final nonwoven weight after polyGMA grafting. In subsequent figures nonwovens grafted by this method are denoted HT.

4.2.4 UV induced polyGMA grafting onto PBT nonwovens

The GMA grafting solution consisted of 20% v/v GMA monomer in 1-butanol as the solvent. The photoinitator benzophenone (BP) was added to the grafting solution in a BP:GMA ratio of 1:20 (mol:mol). Nonwoven PBT was cut into a 75 by 50 mm size samples and weighed prior to grafting, weighing approximately 200 mg. The nonwoven PBT samples were placed onto a borosilicate glass microscope slide, also 75 by 50 mm, to be

prepared for grafting. Using a syringe, 1.5-2.0 ml of grafting solution was evenly distributed onto the membrane and a second borosilicate glass slide was placed on top of the nonwoven. A UV lamp (model EN-180L, Spectronics Corporation, Westbury, NY) is used to induce the free radical polymerization of polyGMA onto the nonwovens. The UV lamp had a wavelength of 365 nm, an intensity of 5 mW/cm^2 and nonwoven samples were placed 3 mm from the light source. Samples were irradiated at various exposure times to achieve different degrees of polyGMA grafting with different % weight gains. After polyGMA grafting, the samples were placed in a flask containing 100 ml of THF, the flask was sonicated in an ultrasonic bath (Bransonic 3510R-MT, Branson Ultrasonics Corporation, Danbury, CT) for 30 min to remove any unreacted grafting solution or untethered polyGMA. Following the THF wash the samples were removed from the flask and placed in a flask containing 100 ml of methanol, the flask containing the samples and methanol was sonicated in an ultrasonic bath for 10 min to remove THF from the nonwovens. Following the methanol wash the samples were removed from the flask and allowed to dry in air overnight. The final weight of the nonwovens was measured and the degree of polyGMA grafting was determined using Eq. 2 in terms of a % weight gain. In subsequent figures nonwovens grafted by this method are denoted UV.

4.2.5 Functionalization of polyGMA grafted PBT nonwovens

PolyGMA grafted PBT nonwovens grafted using both heat and UV-light were functionalized to produce weak anion exchangers by immersion in 50% v/v aqueous diethyl amine (DEA) solution, thus creating a tertiary amine on the polyGMA brushes. Grafted PBT nonwoven samples weighing approximately 100 mg (35 x 50 mm) were immersed in 100 ml of the DEA solution. The reaction was kept at a constant temperature of 30°C with agitation

at 100 rpm using an incubation shaker (Certomat® RM, B. Braun Biotech International, Melsungen, Germany) contained in an incubation hood (Certomat® HK, B. Braun Biotech International, Melsungen, Germany). Following amination, samples were placed in a flask containing 100 ml of DI water and sonicated in an ultrasonic bath (Bransonic 3510R-MT, Branson Ultrasonics Corporation, Danbury, CT) for 5 min to remove excess DEA. Following sonication, the DI water wash was replaced with fresh DI water and the process was repeated until a neutral pH of 7.0 was verified with pH testing paper; 10 washes ensured that all DEA had been removed from the nonwoven. Any unreacted epoxy groups were hydrolyzed by immersion of the sample in 100 ml of 100 mM sulfuric acid overnight. Following hydrolysis of the epoxy groups, samples were placed in a flask containing 100 ml of DI water, the flask was placed in an ultrasonic bath (Bransonic 3510R-MT, Branson Ultrasonics Corporation, Danbury, CT) for 5 min, to remove excess sulfuric acid. Following sonication, the DI water wash was replaced with fresh DI water and the process was repeated until a neutral pH of 7.0 was verified with pH testing paper; 10 washes ensured that all the sulfuric acid had been removed from the nonwoven. The samples were then air dried overnight.

PolyGMA grafted PBT nonwovens were functionalized to create strong cation exchangers by attaching sulfonic acid groups to the polyGMA brushes. Approximately 100 mg (35 x 50 mm) grafted PBT nonwoven samples were immersed in 20 ml of sodium sulfite solution containing sodium sulfite, isopropyl alcohol (IPA), and water (Na_2SO_3:IPA:Water=10:15:75 % by wt.). The reaction was incubated at 80 °C for 8 hours (Isotemp 115, Fisher Scientific, Fairlawn, NJ). Following functionalization the samples were placed in a flask containing 100 ml of DI water. The flask was placed in an ultrasonic bath (Bransonic 3510R-MT, Branson Ultrasonics Corporation, Danbury, CT) for 5 min, to remove

excess sodium sulfite solution. Following sonication, the DI water wash was replaced with fresh DI water and the process was repeated until a neutral pH of 7.0 was verified with pH testing paper; 5 washes ensured that all sodium sulfite solution had been removed from the nonwoven. Any unreacted epoxy groups were hydrolyzed by immersion of the sample in 10 ml of 100 mM sulfuric acid overnight. Following hydrolysis of the epoxy groups, samples were placed in a flask containing 100 ml of DI water, the flask was placed in an ultrasonic bath (Bransonic 3510R-MT, Branson Ultrasonics Corporation, Danbury, CT) for 5 min, to remove excess sulfuric acid. Following sonication, the DI water wash was replaced with fresh DI water and the process was repeated until a neutral pH of 7.0 was verified with pH testing paper; 10 washes ensured that all the sulfuric acid had been removed from the nonwoven. The samples were then air dried overnight.

4.2.6 Pulse experiments

A 10 mm I.D. OmniFit adjustable volume chromatography column was packed with 40 layers of 10 mm nonwoven discs. PBT nonwoven without any modification (column height = 0.3 cm), PBT nonwoven grafted to 5% weight gain (column height = 0.38 cm) using UV light functionalized with DEA to be an anion exchanger and PBT nonwoven grafted to 25% weight gain (column height = 0.40 cm) using heat functionalized with DEA to be an anion exchanger were evaluated for pulse experiments. The packed columns were tested on a Waters 616 HPLC system with a 20 μl sample loop and a Waters 2487 UV detector measuring absorbance at 280 nm (Waters Corporation, Milford, MA). Pulses of aqueous acetone (5% v/v) were injected into the columns at 5 superficial velocities between 0.04 cm/min and 1.27 cm/min. Pulse experiments were done under nonbinding conditions. The mobile phase for the PBT nonwoven without any modification was aqueous ethanol 20% v/v

and the mobile phase for the anion exchange polyGMA grafted PBT nonwovens was 20 mM Tris-HCl + 1 M NaCl pH 6.5. Any extra system volume was accounted for by performing the pulse experiments on an empty column.

The porosities of the grafted nonwovens were also evaluated when spacers were used to separate individual layers. The OmniFit column was packed with 20 layers of anion exchange PBT nonwovens grafted to 5% weight gain using UV-light that were alternated with 20 layers of PET nonwoven spacer (column height = 0.6 cm). Similarly a column was packed with 20 layers of anion exchange PBT nonwovens grafted to 25% weight gain using heat that were alternated with 20 layers of PET nonwoven spacer (column height = 0.6 cm). A column was also packed with 40 layers of just PET nonwoven spacer (column height = 1.0 cm). Pulses of aqueous acetone (5% v/v) were injected into the columns at various superficial velocities between 0.06 cm/min and 1.27 cm/min using a mobile phase of 20 mM Tris-HCl + 1 M NaCl pH 6.5 buffer.

4.2.7 Flow permeability

To evaluate the flow permeability of the modified nonwovens, pressure drops were measured across membrane packed columns. Nonwoven PBT grafted with polyGMA at weight gains of 5%, 10% and 20% using the UV-light grafting method functionalized with DEA to be anion exchangers and nonwoven PBT grafted with polyGMA at a 25% weight gain using the heat grafting method functionalized with DEA to be an anion exchanger were evaluated for their permeability under flow conditions. Nonwoven discs of 10 mm diameter were packed in an OmniFit column (10 mm I.D.) using between 2 and 10 layers of nonwoven sample. The packed columns were tested on a Waters 616 HPLC system with pressure

gauges (Ashcroft 600 ± 5 psi pressure gauge) installed at the inlet and outlet of the column to measure the pressure drops across the column. The pressure drops were measured at superficial velocities between 0.06 cm/min and 5 cm/min, using a mobile phase with a low salt concentration (20 mM Tris-HCl pH 7.0) and one with a high salt concentration (20 mM Tris-HCl +1 M NaCl pH 7.0). Additionally, to evaluate how salt concentration affects the pressure drop across the column, salt concentrations between 0 mM and 1000 mM NaCl were tested at a superficial velocity of 1.3 cm/min (1 ml/min).

The effect of PET nonwoven spacers used to separate individual layers of the grafted PBT nonwovens was also investigated. The OmniFit column was packed with 20 layers of anion exchange PBT nonwovens grafted to 5% weight gain using UV-light that were alternated with 20 layers of PET nonwoven spacer (column height = 0.6 cm). Similarly a column was packed with 20 layers of anion exchange PBT nonwovens grafted to 25% weight gain using heat that were alternated with 20 layers of PET nonwoven spacer (column height = 0.6 cm). A column was also packed with 40 layers of just PET nonwoven spacer (column height = 1.0 cm). The pressure drops were measured at superficial velocities between 0.06 cm/min and 5 cm/min, using a mobile phase with a low salt concentration (20 mM Tris-HCl pH 7.0) and one with a high salt concentration (20 mM Tris-HCl +1 M NaCl pH 7.0).

4.2.8 Dynamic binding capacity measurements

The dynamic binding capacities of cation exchange functionalized polyGMA grafted PBT nonwovens were determined for capture of hIgG. Grafted PBT nonwovens with the best flow properties were chosen for this investigation. PBT nonwovens grafted with polyGMA at 5% and 25% weight gain using the UV method and heat method respectively were

functionalized with sulfonic acid to create strong cation exchange membranes. These nonwovens were punched into 10 mm discs and 20 layers of membrane were packed into an OmniFit column (10 mm I.D.). The packed columns were tested on a Waters 616 HPLC system with a 1000 µl sample loop and a Waters 2487 UV detector measuring absorbance at 280 nm. The columns were equilibrated with 100 column volumes (equivalent to 30 min at a flow rate of 1 ml/min) of 20 mM Tris-HCl pH 6.5 prior to binding. Once equilibrated, 1 ml of 10 mg/ml hIgG in 20 mM Tris-HCl pH 6.5 was injected into the columns at superficial velocities of 0.04, 0.13 and 0.26 cm/min. After binding, the columns were washed with approximately 50-100 column volumes of 20 mM Tris-HCl pH 6.5. Bound protein was eluted with 20 mM Tris-HCl + 1 M NaCl pH 6.5 at the superficial velocities used for binding except for the slowest flow rate tested (0.04 cm/min); a superficial velocity of 1.3 cm/min was used for these experiments. To regenerate the columns 100 column volumes of 20 mM Tris-HCl +1 M NaCl pH 6.5 were passed through them at superficial velocity of 1.3 cm/min. Chromatograms, measured at 280 nm, were recorded using Waters Empower Pro Software (Waters Corporation, Milford, MA) ; the breakthrough curves were used to determine the dynamic binding capacities of the columns. The columns were evaluated for their dynamic binding capacity at 10% breakthrough of the initial protein concentration using Eq. 3.

$$10\%DBC = \frac{(V_{10\%BT} - V_{void}) \cdot C_o}{volume\ of\ functional\ membane} \quad (3)$$

In Eq. 3, $V_{10\%BT}$ is the volume that has passed through the column at 10% breakthrough, V_{void} is the void volume of the column and C_o is the initial hIgG concentration (10 mg/ml). The void volume of the column was measured at 10% breakthrough of protein (hIgG, 10 mg/ml) under nonbinding conditions.

To evaluate if an increased porosity would influence dynamic binding capacity PET nonwoven spacers were used to separate individual cation exchange polyGMA grafted PBT nonwoven layers. The 20 layer columns of the cation exchange PBT nonwovens grafted to 5% and 25% weight gain using the UV method and heat method were repacked alternating each cation exchange grafted layer with a PET nonwoven spacer layer, resulting in 40 total layers (20 cation exchange grafted nonwoven layers and 20 PET nonwoven spacer layers). The columns were equilibrated with 100 column volumes (equivalent to 30 min at a flow rate of 1 ml/min) of 20 mM Tris-HCl pH 6.5 prior to binding. Once equilibrated, 1 ml of 10 mg/ml hIgG in 20 mM Tris-HCl pH 6.5 was injected into the columns at superficial velocities of 0.04, 0.13 and 0.26 cm/min. After binding, the columns were washed with approximately 50-100 column volumes of 20 mM Tris-HCl pH 6.5. Bound protein was eluted with 20 mM Tris-HCl + 1 M NaCl pH 6.5 at the superficial velocities used for binding except for the slowest flow rate tested (0.04 cm/min); a superficial velocity of 1.3 cm/min was used for these experiments. To regenerate the columns 100 column volumes of 20 mM Tris-HCl +1 M NaCl pH 6.5 were passed through them at superficial velocity of 1.3 cm/min. The chromatograms of these experiments were used to calculate the dynamic binding capacities of these columns at 10% breakthrough using Eq. 3.

4.2.9 Protein recovery over multiple binding cycles

Columns packed with cation exchange PBT nonwovens grafted to 5% weight gain using UV-light and 25% weight gain using heat were evaluated for protein recovery over multiple binding attempts. These nonwovens were punched into 10 mm discs and 20 layers of membrane were packed into an OmniFit column (10 mm I.D.). The packed columns were tested on a Waters 616 HPLC system with a 1000 µl sample loop and a Waters 2487 UV

detector measuring absorbance at 280 nm. The columns were equilibrated with 100 column volumes (equivalent to 30 min at a flow rate of 1 ml/min) of 20 mM Tris-HCl pH 6.5 prior to binding. Once equilibrated, 1 ml of 10 mg/ml hIgG in 20 mM Tris-HCl pH 6.5 was injected into the columns at a superficial velocity 0.25 cm/min. After binding, the columns were washed with approximately 50-100 column volumes of 20 mM Tris-HCl pH 6.5. Bound protein was eluted with 20 mM Tris-HCl + 1 M NaCl pH 6.5 at a superficial velocity of 0.25 cm/min. Elution fractions were collected and quantified using UV-Vis spectroscopy at 280 nm to determine the amount protein bound to the column using Eq. 4.

$$Protein\ bound\left(\frac{mg}{g}\right) = \frac{Protein\ Concentration\left(\frac{mg}{ml}\right) \times Volume\ of\ Elution\ Fraction}{Mass\ of\ membrane} \quad (4)$$

4.2.10 Dynamic separation of protein mixtures

The separation ability of hIgG from protein mixtures was evaluated for cation exchange polyGMA grafted PBT nonwovens. PBT nonwovens grafted to 5% and 25% weight gain using the UV-light and the heat induced grafting methods respectively were functionalized with sulfonic acid creating strong cation exchange membranes. These nonwovens were punched into 10 mm discs and 20 layers (~100 mg) of membrane were packed into an OmniFit column (10 mm I.D.) for testing. The packed columns were tested on a Waters 616 HPLC system with a 1000 µl sample loop and a Waters 2487 UV detector measuring absorbance at 280 nm. The columns were equilibrated with 100 column volumes (equivalent to 30 min at a flow rate of 1 ml/min) of 20 mM Tris-HCl pH 6.5 prior to each binding attempt. The columns were challenged with a 1 ml mixture of proteins that consisted of 1 mg/ml hIgG + 1 mg/ml lysozyme in 20 mM Tris-HCl pH 6.5 and a mixture of 1 mg/ml hIgG + 1 mg/ml lysozyme + 1 mg/ml BSA in 20 mM Tris-HCl pH 6.5. The isoelectric point

of polyclonal hIgG is between 7 and 9, the isoelectric points for lysozyme and BSA are 11.34 and 4.7 respectively. For the hIgG and lysozyme mixture experiment the intent was to capture hIgG and Lysozyme in bind and elute mode, with separation achieved by the selective elution of hIgG using a pH change followed by the elution of lysozyme using an increased salt concentration. The columns were challenged with the mixture of hIgG and lysozyme at a superficial velocity of 0.25 cm/min (0.2 ml/min). After protein binding, the columns were washed with 20 column volumes of binding buffer, 20 mM Tris-HCl pH 6.5, to remove any unbound protein. The columns were then eluted with the first elution buffer; 20 mM carbonate buffer pH 10 for 60 column volumes. Following elution with pH 10 buffer a second high salt elution was used to elute any protein bound by electrostatic interaction using 20 mM Tris-HCl + 1 M NaCl pH 6.5 for 60 column volumes. The flow through, pH 10 elution and 1 M NaCl elution fractions were collected to be analyzed for purity using SDS-PAGE. Additionally, the pH 10 elution fractions were analyzed using UV 280 nm absorbance to determine the overall yield of this specific elution step using Eq. 4.

For the hIgG, lysozyme and BSA mixture experiment the intent was to capture hIgG and lysozyme in bind and elute mode and have the impurity, BSA, flow through the column. Separation of hIgG and lysozyme was achieved by the selective elution of hIgG using a pH change followed by the elution of lysozyme with an increased salt concentration. The columns were challenged with the mixture of hIgG, lysozyme and BSA at a superficial velocity of 0.25 cm/min (0.2 ml/min). After protein binding, the columns were washed with 20 column volumes of binding buffer, 20 mM Tris-HCl pH 6.5, to remove any unbound protein. The columns were then eluted with the first elution buffer; 20 mM carbonate buffer pH 10 for 60 column volumes. Following elution with pH 10 buffer a second high salt

elution was used to elute any protein bound by electrostatic interaction using 20 mM Tris-HCl + 1 M NaCl pH 6.5 for 60 column volumes. The flow through, pH 10 elution and 1 M NaCl elution fractions were collected to be analyzed for purity using SDS-PAGE. The separation of hIgG, lysozyme and BSA was repeated with the order of the elution buffers reversed to evaluate the mechanism of protein adsorption to the columns. The columns were challenged with the mixture of hIgG, lysozyme and BSA at a superficial velocity of 0.25 cm/min (0.2 ml/min). After protein binding, the columns were washed with 20 column volumes of binding buffer, 20 mM Tris-HCl pH 6.5, to remove any unbound protein. The columns were then eluted with the first elution buffer; 20 mM Tris-HCl + 1 M NaCl pH 6.5 for 60 column volumes. Following elution with 1 M NaCl buffer a second elution was performed using 20 mM carbonate buffer pH 10 for 60 column volumes. The flow through, pH 10 elution and 1 M NaCl elution fractions were collected to be analyzed for purity using SDS-PAGE.

All collected fractions had a final volume of 6 ml and were concentrated by a factor of 10 using centrifugal filter concentrators with a 3,000 NMWL (Millipore Amicon centrifugal filters, 3,000 NMWL) following the manufacturer's instructions using a micro centrifuge (Centrifuge 5417 R, Eppendorf, Hauppauge, NY). Prior to running the SDS-PAGE, samples were prepared under reducing conditions, 10 µl of the concentrated fractions, the protein load mixtures diluted to 0.5 mg/ml, pure hIgG (0.5 mg/ml), pure lysozyme (0.5 mg/ml) and pure BSA (0.5 mg/ml) were mixed with 9.5 µl of BioRad 2x Laemmli sample buffer + 5 µl of β-mercaptoethanol and heated to 90 °C for five minutes in a hot water bath (Isotemp 115, Fisher Scientific, Fairlawn, NJ). SDS-PAGE was performed with Mini-PROTEAN TGX precast gels, 10 µL of the reduced samples and 10 µl of molecular marker

(Biorad precision plus protein dual color standard) were loaded onto the gels. The gels were run at 200 V for approximately 35 minutes according to the manufacturer's instructions. The gels were then stained with Brilliant Coomassie Blue. Images of the gels were captured using a BioRad Gel Doc XR+ system (BioRad, Hercules, CA) with ImageLab software (BioRad, Hercules, CA). Densitometric analysis was performed using ImageLab software to calculate the relative purities of the samples.

4.3 Results and discussion

4.3.1 PET nonwoven spacer characterization

The structure of the PET nonwoven spacer material was analyzed with a variable pressure scanning electron microscope (VPSEM) to determine the average fiber diameter. The SEM micrographs of the PET nonwoven spacer are shown in Fig 4.1.

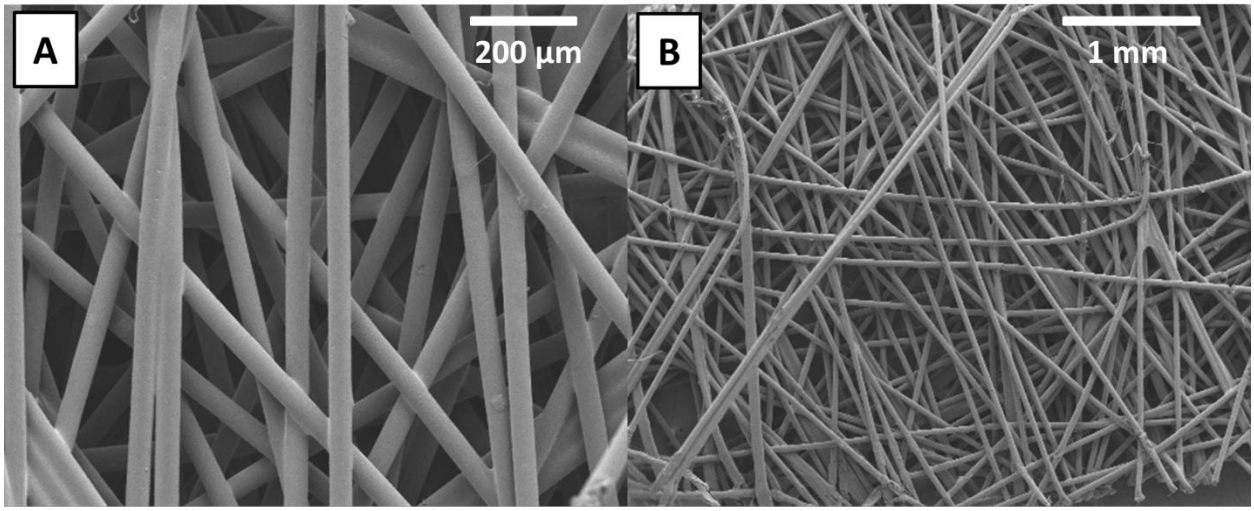

Fig. 4.1 SEM micrographs of PET nonwoven spacer at (A) 100x magnification and (B) 25x magnification.

It was determined from the SEM images that the material had an average fiber diameter of 45 ± 4 μm. The average thickness of the spacer material was approximately 550 ± 70 μm. From Fig. 4.1 it is apparent that the pore sizes of the PET nonwoven spacer are very large. After measuring the average distance between neighboring PET fibers it was estimated that the pore sizes of the nonwoven are larger than 100 μm.

The nonspecific adsorption of hIgG was determined by challenging the material with pure IgG in a low ionic strength buffer (20 mM Tris-HCl pH 6.5). The binding was allowed to proceed overnight, after binding the unbound protein was washed off of the spacers and collected for quantification using UV-Vis spectroscopy (280 nm). After quantification the amount of nonspecific protein adsorption was determined to be negligible using Eq. 1.

4.3.2 Porosity analysis of polyGMA grafted nonwoven PBT

The total porosity of packed chromatography columns can be calculated from measurements of the first absolute time moments of pulse injections of nonbinding tracers at varying superficial velocities [18]. Acetone is a common tracer for measuring the total porosity of chromatography columns since it shows no electrostatic interaction with ion exchange functionalized media [18]. The porosity was first evaluated for columns packed with blank PBT nonwovens and PBT nonwovens grafted with polyGMA to 5% and 25% weight gain using the UV-light and heat method respectively functionalized as anion exchangers. In addition, the porosity of columns packed with these same grafted nonwovens when a PET nonwoven spacer was used to separate individual layers, as well as, for the PET nonwoven spacer alone. Small volumes (20 μl) of dilute acetone (5% v/v) were injected into 40 layer columns of nonwoven PBT grafted to 5% weight gain using UV-light (column

height of 0.4 cm), nonwoven PBT grafted to 25% weight gain using the heat method (column height of 0.4 cm) and nonwoven PBT without grafting (column height of 0.4 cm). Similarly, acetone was injected into 40 layer columns made from 20 layers of the same grafted nonwovens with each layer separated by a PET nonwoven spacer (20 layers grafted PBT nonwoven and 20 layers PET nonwoven spacer layers, column height of 0.6 cm for both columns), as well as, into a 40 layer column of only PET nonwoven spacer (column height of 1.0 cm). The first absolute moments (μ_1) were measured for superficial velocities between 0.04 cm/min and 2.54 cm/min under nonbinding conditions. For the grafted anion exchange PBT nonwovens and the PET spacer nonbinding conditions are achieved using a high ionic strength mobile phase (20 mM Tris-HCl + 1 M NaCl pH 6.5). Plots of the measured first absolute moments for different average residence times (L/u_o) for these systems are shown in Fig. 4.2. The actual pulse responses of the columns from injections with acetone are shown in the Appendix: A. Pulse responses of acetone.

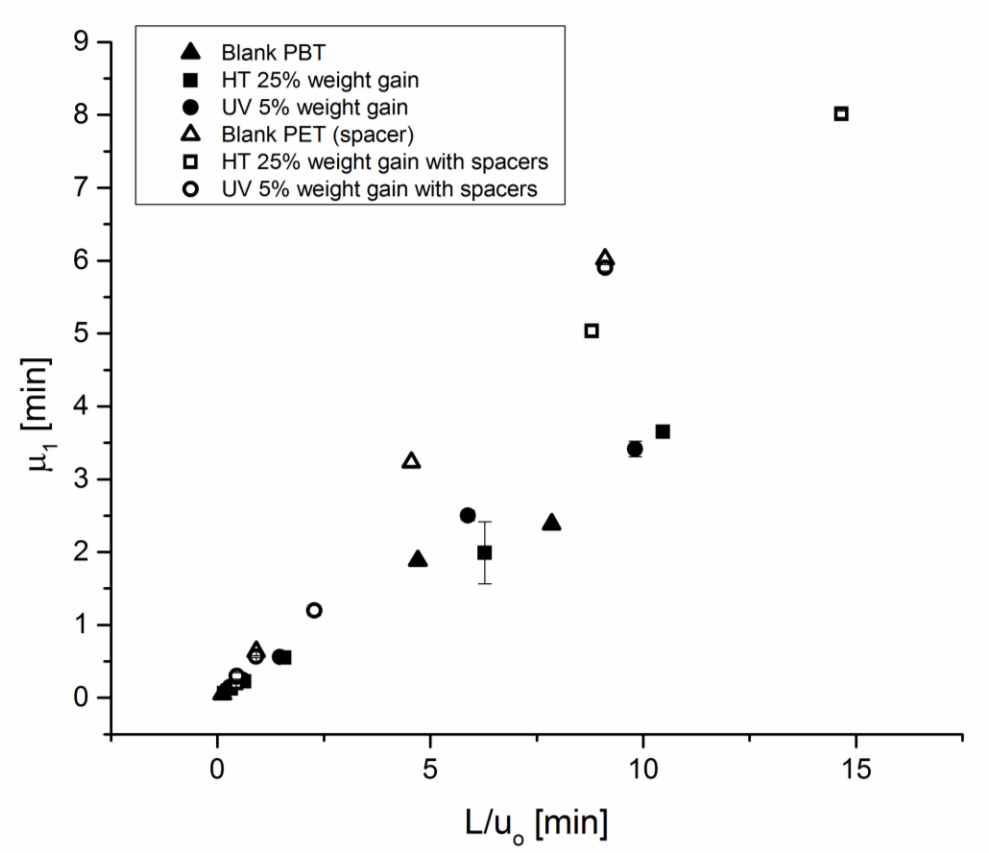

Fig. 4.2 First moments from pulse injections of acetone to columns packed with 40 layers of PBT nonwoven, 40 layers of PBT nonwoven grafted to 5% weight gain using UV-light, 40 layers of PBT nonwoven grafted to 25% weight gain using heat, 40 layers of PET spacer, 40 layers of grafted PBT nonwoven grafted to 5% weight gain with UV-light (20 layers)/PET spacer (20 layers) and 40 layers of grafted PBT nonwoven grafted to 25% weight gain with heat (20 layers)/PET spacer (20 layers).

In Fig. 4.2 the polyGMA PBT nonwovens grafted using UV-light are denoted as UV and the polyGMA PBT nonwovens grafted using heat are denoted HT and this is how they are represented on all proceeding figures and tables. The first absolute moment of the measured pulse injections exiting the columns are related to the porosities of the columns, the superficial velocities and the column heights by Eq. 5.

$$\mu_1 = \frac{\int_0^\infty C(L,t)tdt}{\int_0^\infty C(L,t)dt} = \frac{L}{u_o}\varepsilon_t \quad (5)$$

In Eq. 5 μ_1 is the first absolute moment (min), C is the concentration of tracer in the column (mg/ml), t is time (min), L is the column height (cm), u_o is the superficial velocity (cm/min) and ε_t is the effective flow porosity of the column. The flow porosity (ε_t) is the slope of the first moment versus residence time for data presented in Fig. 4.2. Using Eq. 5 and the slopes from Fig. 4.2 the column flow porosities of the tested samples were calculated and are shown in Table 4.1.

Table 4.1: Total column porosities (ε_t) determined by first moment analysis.

Sample	ε_t (%)
Blank PBT	31
HT 25% weight gain	34
UV 5% weight gain	36
Blank PET (spacer)	65
HT 25% weight gain with spacers	55
UV 5% weight gain with spacers	65

The flow porosities for the columns packed with grafted PBT nonwovens presented in Table 4.1 are the same for grafted and un-grafted materials at these extents of polymer grafting. All of the PBT nonwovens with and without grafting had porosities between 31% and 36%. It is important to recognize that these porosities were measured using a high ionic strength mobile phase. UV-light grafted ion exchange polyelectrolyte brushes have demonstrated significant

swelling under low ionic strength conditions [17]. A high ionic strength mobile phase ensures that no swelling of the charged polyGMA brush layers is occurring and that these are the largest porosities possible for these systems. The calculated porosities of the PBT nonwovens with and without grafting are similar to flow porosities encountered in packed bed chromatography using spherical particles, ε = 30-40% [19,20].

The measured flow porosity values in Table 4.1 for the PBT nonwovens without spacers are also significantly lower than the average porosity calculated for the PBT nonwoven packed in the column and estimated by measuring the apparent density of the columns and knowing the density of the PBT polymer, according to Eq. 6.

$$Porosity = \left(1 - \frac{\rho}{\rho_P}\right) x100\% \quad (6)$$

In Eq. 6, ρ is the apparent density of the column (mass/volume) which was estimated to be 0.6 g/cm^3 for a 40-layer PBT nonwoven packed column. The quantity ρ_P is the density of the PBT polymer (1.3 g/cm^3 [22]). The average porosity for a 40-layer PBT nonwoven packed column is 54% when calculated using Eq. 6. Similarly, the porosity of PBT nonwoven when not packed into the column can also be calculated using Eq. 6. The apparent density of the PBT nonwoven not packed into a column is approximately 0.18 g/cm^3 and the estimated porosity in this case is 86% according to Eq. 6, in agreement with other porosity values for nonwovens in the literature [20,21]. It is apparent that the porosity of the PBT nonwoven decreases from 86% to 54% when it is packed into the column due to a compression of the material. Additionally, the compression and layering of the PBT nonwoven in a column format also results in pore blockage that prevents flow and leads to flow porosity values of 30% when evaluated by the first moment analysis.

The addition of spacers significantly increases the porosity of the columns as the values in Table 4.1 indicate. The total porosity of just the PET spacer is 65% when calculated using a first moment analysis and is in close agreement with the average column porosity of 70% when calculated using Eq. 6 (ρ_{column} = 0.4 g/cm^3 and $\rho_{PE\ T}$= 1.38 g/cm^3 [Dupont]). The separation of individual layers of grafted PBT with PET nonwoven spacers resulted in an increase of porosity from 34% to 55% for the heat grafted nonwoven and an increase of porosity from 35% to 65% for the UV-light grafted nonwoven. The PBT nonwovens have a smaller average fiber diameter (3 μm) and a lower average pore size (8 μm) compared to the PET nonwoven (fiber diameter of 45 μm; pore size estimated to be greater than 100 μm). These results indicate that introducing PET nonwoven spacers are capable of reducing the compression and pore blockage of the PBT nonwovens that occur when consecutive PBT membranes are stacked in a column.

The acetone pulses can also give some insight into the packing and flow distribution of the column. The asymmetry of the column is a good indicator of whether a column is well packed with a good flow distribution throughout the column. The asymmetry factor for the pulse response in a packed column is calculated using Eq. 7.

$$A_s = \frac{t_{10\%Tail} - \mu_1}{\mu_1 - t_{10\%Front}} \quad (7)$$

In Eq. 7 A_s is the asymmetry factor, $t_{10\%Front}$ is the time at which the pulse front exiting the column reaches 10% of the initial acetone pulse concentration, $t_{10\%Tail}$ is the time at which the tail exiting the column reaches 10% of the initial acetone pulse concentration and μ_1 is the first moment. The asymmetry factors of the pulses coming from columns packed with 40 layers of the anion exchange PBT nonwovens grafted to 5% weight gain using UV-light and

to 25% weight gain using heat, as well as, when these columns are separated by PET nonwoven spacers (20 layer PBT and 20 layer spacer) are shown in Table 4.2. All of the asymmetry factors in Table 4.2 were calculated using the actual pulse responses of the columns injected with acetone at a superficial velocity of 1.3 cm/min. The actual pulse responses of the columns from injections with acetone are shown in the Appendix: A. Pulse responses of acetone. To determine the significance of column tailing contributing to any asymmetry observed in the pulse responses of the columns, the tailing factors (T_f) were calculated using Eq. 8.

$$T_f = \frac{(t_{5\%Tail} - t_{5\%Front})}{2 \cdot (\mu_1 - t_{5\%Front})} \quad (8)$$

In Eq. 8 T_f is the tailing factor, $t_{5\%Front}$ is the time at which the pulse front exiting the column reaches 5% of the initial acetone pulse concentration, $t_{5\%Tail}$ is the time at which the tail exiting the column reaches 5% of the initial acetone pulse concentration and μ_1 is the first moment. The tailing factors of the columns tested are shown in Table 4.2.

Table 4.2: Asymmetry factors and tailing factors of the pulses coming from columns packed with 40 layers of the PBT nonwovens grafted to 5% weight gain using UV-light and to 25% weight gain using heat as well as when these columns are separated by PET nonwoven spacers (20 layer PBT and 20 layer spacer).

Sample	A_s	T_f
UV 5% weight gain (40 layers)	3.8	2.7
HT 25% weight gain (40 layers)	4.3	3.0
UV 5% weight gain with spacers (40 layers)	2.5	1.9
HT 25% weight gain with spacers (40 layers)	4.3	2.9

These asymmetry factor values are much higher than normally encountered in a well-packed chromatography column, and are indicative of flow mal-distributions in the column that can reduce performance. To achieve good separation resolution in packed bed separations, it is important that the asymmetry factor of pulses remain in the range of 0.8 to 1.2 [23]. Looking at the shape of the pulse response, the asymmetry is being caused by significant tailing at the back end of the pulse response. The tailing factors reported in Table 4.2 are significantly higher than the industry standard ($T_f < 1.2$) for a well packed column with proper flow distribution [24]. Significant peak tailing, as observed in this investigation, is usually a sign of over compression of the column resulting in blocked pores where diffusion of the tracer increases the residence time in the column [23-25].

4.3.3 Flow characterization

The flow permeability of the ion exchange nonwovens grafted using the UV-light and heat induced grafting methods were evaluated by performing pressure drop measurements at various superficial velocities. Columns were packed with 2 or 10 layers of PBT nonwoven (2 layer column height = 0.02 cm, 10 layer column height = 0.1 cm) grafted using UV-light, with degrees of polyGMA coverage of 5%, 10% and 20% weight gain that were functionalized as weak anion exchangers. The pressure drops across the membranes were measured at superficial velocities between 0.3 cm/min and 5.0 cm/min. Similarly a column was packed with 10 layers of PBT nonwoven (10 layer column height = 0.1 cm) grafted using heat with a 25% weight gain and functionalized as a weak anion exchanger. Pressure drop measurements were made for superficial velocities between 0.3 cm/min and 5.0 cm/min. The pressure drops of these materials were investigated using a mobile phase with a low ionic strength (20 mM Tris pH 7.0) and with a high ionic strength (20 mM Tris + 1 M

NaCl pH 7.0) to determine how the swelling of a charged polyGMA grafted layer effects permeability. In addition to this, the pressure drop in anion exchange polyGMA grafted membranes was measured after protein adsorption. This was done by binding BSA electrostatically until equilibrium binding was reached using a low ionic strength buffer (20 mM Tris pH 7.0) as the mobile phase, to determine if protein binding had any influence on the permeability of the material. The measured pressure drops across these materials were normalized by dividing the pressure drop (ΔP) by the column height of the column (L = 0.04 cm) and the viscosity of the mobile phase (μ = 0.001 Pa•s, assumed to be that of water) to determine flow permeabilities.

The normalized pressure drop ($\Delta P/L\mu$) data was plotted as a function of the superficial velocity of the mobile phase and the results are shown in Fig. 4.3.

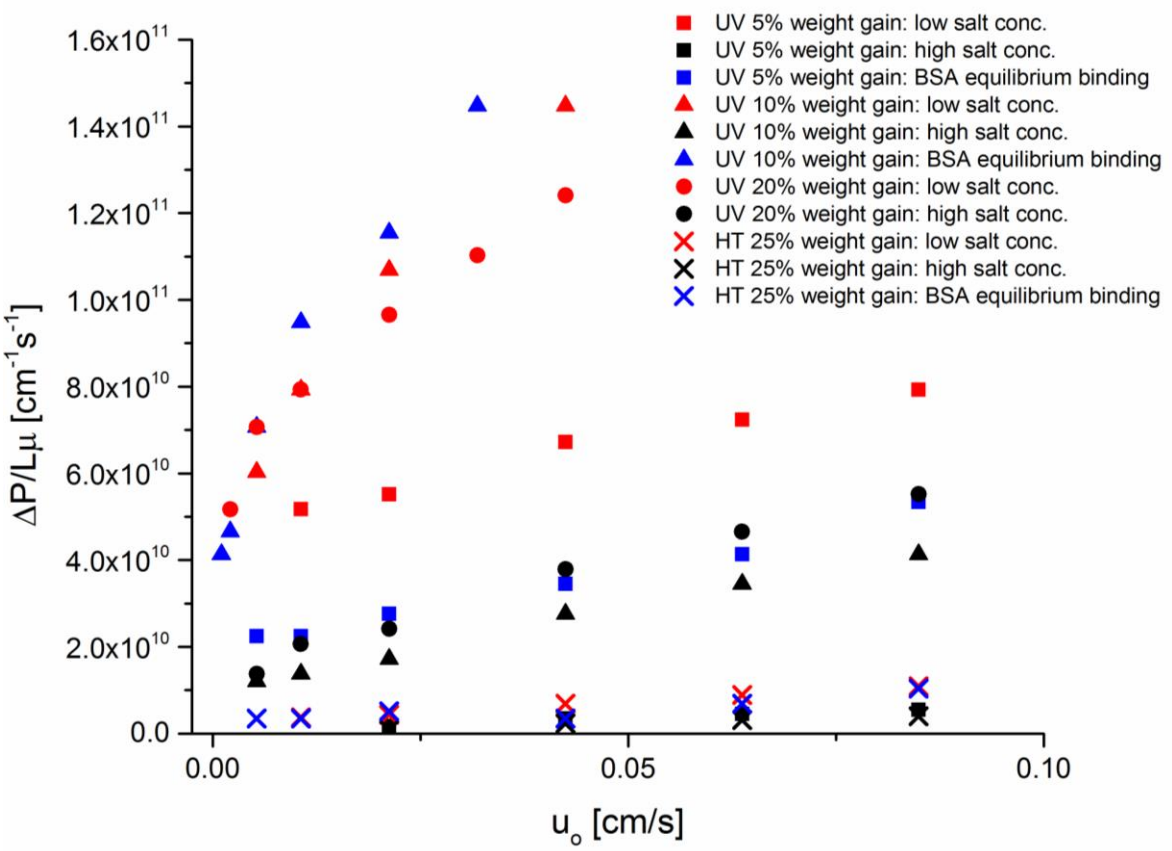

Fig. 4.3 Pressure drop versus superficial velocity columns packed with 2 layers of PBT nonwoven grafted using UV light with weight gains of 5%, 10% and 20% weight gain and using heat with a weight gain of 25% weight gain. Evaluated with a mobile phase of low ionic strength (20 mM Tris pH 7.0) and a mobile phase of high ionic strength (20 mM Tris+ 1M NaCl pH 7.0), also evaluated after equilibrium protein binding with a low ionic strength mobile phase.

From Fig. 4.3 it is apparent that very large pressure drops are observed for anion exchange PBT nonwovens grafted with UV-light when passing a low ionic strength mobile phase through them. The pressure drop is significantly larger for the UV-light grafted PBT nonwovens grafted to 10% and 20% weight gain compared to a degree of grafting of 5% weight gain as Fig. 4.3 shows. This indicates that the higher degrees of polyGMA grafting (10% and 20%) result in a significant amount of pore blockage for the nonwoven PBT when

the polymer layer is functionalized with charges and in a low ionic strength environment. The introduction of a mobile phase with high ionic strength resulted in a significant reduction in pressure drop for all of the ion exchange UV-light grafted PBT nonwovens. This is an indication that the polyGMA layer shrinks in the presence of counter-ions effectively increasing the pore size. Equilibrium protein binding had very little effect on pressure drop for the UV-light grafted nonwovens at 5% and 10% weight gain compared to when a low ionic strength mobile phase was passed through them. However, the anion exchange PBT nonwoven grafted to 20% weight gain using UV-light was unable to pass a low ionic strength mobile phase through it after it had reached equilibrium binding, result not shown in Fig. 4.3.

The heat grafted PBT nonwovens grafted to 25% weight gain and functionalized as anion exchangers demonstrated lower pressure drops compared to the UV grafted PBT nonwovens for the superficial velocities tested as Fig. 4.3 shows. Additionally, the difference in pressure drops between the high and low ionic strength mobile phases were significantly lower than for the UV-light grafted nonwovens. These are strong indications that less swelling occurs for the charged polyGMA layer of the heat grafted nonwovens compared to the UV-light grafted nonwovens. This believed to be due to significant structural differences between the ion exchange grafted polyGMA layers of the two techniques.

The permeability of the grafted nonwovens can be calculated using Darcy's law for low Reynolds numbers. Nonwoven filter media generally have sufficiently small pore sizes and therefore laminar flow can be assumed in almost all cases [26]. The expression for Darcy's law is presented in Eq. 9.

$$u_o = k\frac{\Delta P}{L\mu} \tag{9}$$

In Eq. 9, u_o is the superficial velocity (cm/s), k is the permeability coefficient (cm^2), ΔP is the pressure drop (Pa), L is the column height (0.04 cm) and μ is the viscosity of the mobile phase assumed to be that of water (0.001 Pa•s). The calculated permeability coefficients (k) are presented in Table 4.3.

Table 4.3: Calculated permeability coefficients for anion exchange PBT nonwovens grafted using UV-light at weight gains of 5%, 10% and 20% as well as grafted using heat at a weight gain of 25%. Evaluated with a low ionic strength mobile phase a high ionic strength mobile phase and after BSA protein had been bound in equilibrium.

Sample	$k_{\text{low ionic strength}}$ (cm^2)	$k_{\text{high ionic strength}}$ (cm^2)	$k_{\text{after BSA equilibrium binding}}$ (cm^2)
UV 5% DEA	2.6×10^{-12}	1.7×10^{-11}	2.6×10^{-12}
UV 10% DEA	4.4×10^{-13}	2.6×10^{-12}	2.9×10^{-13}
UV 20% DEA	5.8×10^{-13}	1.9×10^{-12}	No Flow
HT 25% DEA	1.0×10^{-11}	2.0×10^{-11}	1.0×10^{-11}

The calculated permeability coefficients in Table 4.3 are several orders of magnitude lower than what has previously been reported for nonwoven membranes. Permeability coefficients on the order of 10^{-7} cm^2 have been reported for nonwoven polypropylene. However, these nonwovens had very large fiber diameters (20 μm) that minimize column compression in addition to being loosely packed in a column resulting in large column flow porosities (75%) and low observed permeability [20].

For comparison the Blake-Kozeny equation was used to compare the calculated permeability's of Table 4.3 with the predicted permeability of a bed packed with resin of a similar particle diameter (3 μm, equivalent to PBT fiber diameter) and porosity (ε= 30%, equivalent to the porosity of blank PBT). The Blake-Kozeny equation is presented in Eq. 10.

$$k = \frac{d_p^2}{150} \frac{\varepsilon^3}{(1-\varepsilon)^2} \quad (10)$$

In Eq. 10, k is the permeability coefficient (cm), d_p is the particle diameter (cm), and ε is the porosity. Using Eq. 10 a particle with a 3 μm diameter and a porosity of ε=30% would have a predicted permeability of k=3x10^{-11} cm^2. This calculated value is very similar to the permeability coefficients for the heat grafted anion exchange PBT nonwovens under all conditions, as well as, the anion exchange PBT nonwovens grafted to 5% weight gain using UV-light when in a high ionic strength environment. The very low permeability of the PBT nonwovens of this investigation would seem to indicate a very tight packing of the PBT fibers. This may be attributed to a compressibility or pore blockage of the PBT nonwovens when operated in a stacked sheet column format under pressure, which only becomes exaggerated for nonwovens with ion exchange polymer grafting. The permeability of the UV grafted nonwovens was approximately 1 to 2 orders of magnitude lower than the heat grafted nonwovens. In addition, the permeability of the UV grafted nonwovens with a higher degree of polyGMA coverage (10% and 20%) were an order of magnitude lower than when the PBT nonwoven was grafted at 5% weight gain. PBT nonwovens grafted to 10% and 20% weight gain had permeability's on the same order of magnitude as agarose and dextran gels (1x10^{-13} – 2x10^{-12} cm^2) [27]. This indicates that at these degrees of polyGMA coverage all of the available pores of the native PBT nonwoven are filled with a swollen polyGMA network that has flow properties similar to a gel network.

It is also evident from Fig. 4.3 and Table 4.3 that there are significant changes in the permeability of charged polyGMA layers grafted to PBT nonwovens when a mobile phase of high ionic strength is used compared to a mobile phase of low ionic strength. This is a clear indication that a great deal of swelling of the anion exchange polyGMA layer is occurring in solutions of low ionic strength. This results in a reduction of the effective pore volume of the

nonwoven and a reduction in the permeability. To investigate how ionic strength influences the flow properties of the grafted nonwovens the pressure drop was measured at a flow rate of 1.3 cm/min (1 ml/min) at varying concentrations of NaCl. PBT nonwovens grafted with polyGMA using UV-light (5% = 10 layers, 10% = 2 layers, 20% = 2 layers) and using heat (25% = 10 layers) all functionalized to be weak anion exchangers were evaluated for their behavior with mobile phases of varying ionic strengths. The normalized pressure-drops ($\Delta P/L\mu$) measured at various salt concentrations are presented in Fig. 4.4.

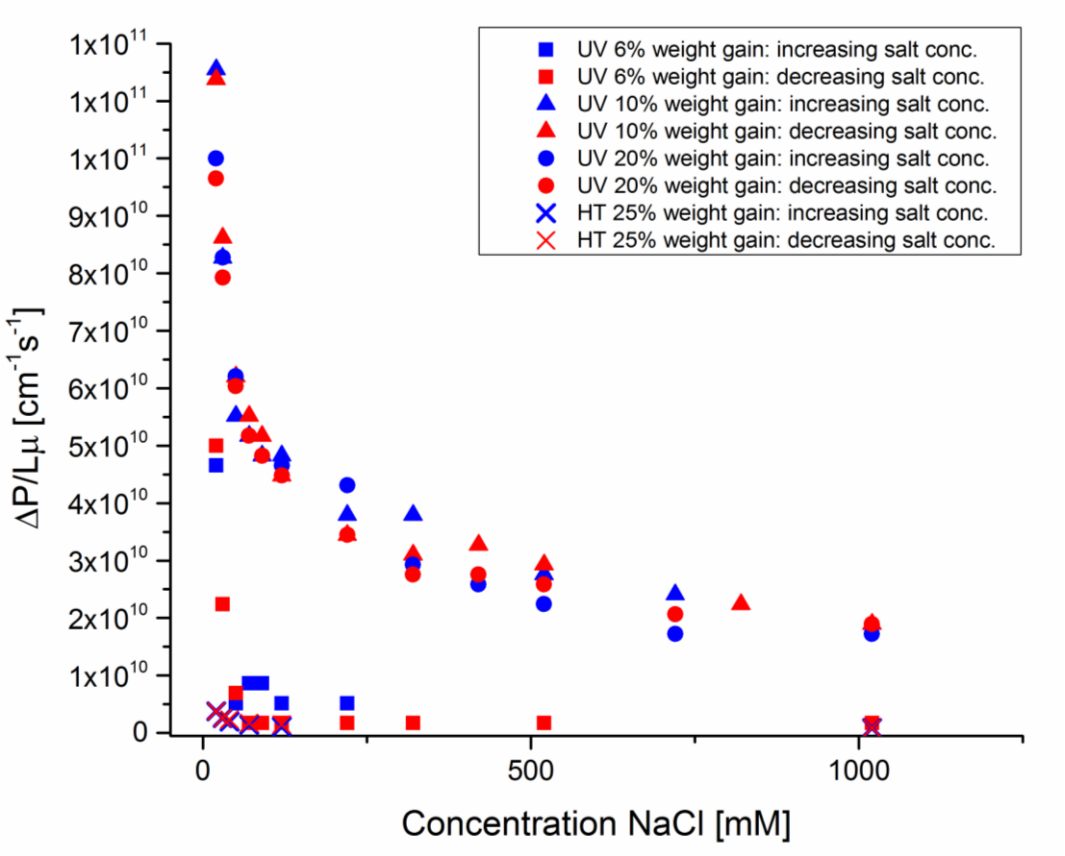

Fig. 4.4 Pressure drop versus increasing/decreasing NaCl concentration measured at 1.3 cm/min (1 ml/min) for nonwoven PBT grafted using UV light at weight gains of 5%, 10% and 20% and using heat at a weight gain of 25% all functionalized to be weak anion exchangers.

It is apparent from Fig. 4.4 that as the salt concentration (ionic strength) increases, the flow properties of the grafted materials improve, due to conformational changes in the grafted layer that are completely reversible. This is a common phenomenon in ion responsive polymer grafted surfaces. It has been shown that anionic polyacrylic acid (PAA) brushes grafted to surfaces display drastic conformational changes by increases in the ionic strength of their environment [28,29]. It has been determined that electrostatic repulsion of the PAA brushes in a low ionic strength environment results in a brush extension normal to the grafted surface that is observed by a swelling of the grafted layer. However, as ion concentration increases, Debye screening occurs reducing the electrostatic repulsion of the grafted layer and the brushes begin to collapse. At sufficiently high ion concentrations the PAA brushes become completely saturated with counter-ions and completely collapse; this is known as the salted brush regime. For these systems conformational changes are completely reversible by changing the ion concentration of the environment.

PolyGMA grafting by UV-light is believed to create polymer brushes that extend from the grafted surface [30-32]. In the case of polyGMA UV-light grafted PBT nonwovens functionalized as ion exchangers, the polyGMA brush layer has the potential to swell into the pores of the nonwoven due to electrostatic repulsion between brushes in low ionic strength environments creating large pressure drops across the membrane. As the ionic strength of the environment increases, the charged polyGMA brushes become saturated with counter-ions and the brush layer collapses. This occurs around a salt concentration of 100 mM as Fig. 4.4 demonstrates for the UV grafted nonwovens. PolyGMA grafting using heat is believed to create a highly branched and cross-linked polymer network [33-35]. This has the potential to

affect the swelling of the polyGMA layer when functionalized with a charge in two ways. First the polyGMA layer grafted using heat is denser than when grafted with UV-light resulting in a thinner observed grafted layer. Second cross-linking in the polyGMA layer creates a physical constraint on how far a polyGMA polymer chain can extend from a surface due to electrostatic repulsions, reducing the extent of swelling. In Fig. 4.3 and Fig. 4.4 the anion exchange polyGMA nonwovens grafted using heat demonstrated significantly lower pressure drops compared to the UV grafted nonwovens even though they had a higher overall degree of polyGMA grafting. Therefore, the polyGMA layer grafted using heat does not reduce the effective pore size of the PBT nonwoven the same way that UV grafting does. In addition, an increase in the ionic strength of the solution passing through the anion exchange heat grafted nonwoven does not reduce the pressure drop to the same extent that it does for the anion exchange UV grafted nonwovens as Fig. 4.4 shows. As a result, conformational changes in a charge functionalized polyGMA heat grafted layer due to ionic strength are less significant compared to ion exchange brushes grafted by UV-light. This is consistent with a study performed by Saito *et al*. that investigated the flow properties of phosphorylated polyGMA grafted to polyethylene hollow fibers (ε= 75%) [17]. In this work the flux of water was measured for the native hollow fiber (flux = 1.9 m^3/m^2hr), grafted with polyGMA (90-130% weight gain; flux = 1.5 m^3/m^2hr), grafted with polyGMA functionalized as a cation exchanger (90-130% weight gain; flux = 0.02 m^3/m^2hr) and grafted with cross-linked polyGMA functionalized as a cation exchanger (90-130% weight gain; flux = 0.18 m^3/m^2hr). Increasing the salt concentration to 1 M NaCl increased the flux of the hollow fiber grafted with polyGMA functionalized as a cation exchanger an order of magnitude (flux = 0.2 m^3/m^2hr) and had no effect on the flux of the cation exchange polyGMA grafted hollow fiber

with cross-linking. It was determined by Saito *et al*. that the polyGMA grafting without cross-linking resulted in significant swelling and pore blockage when functionalized to be cation exchangers that could be reduced with the introduction of salt. Additionally, cross-linking the polyGMA grafted layer prevented the swelling of polymer layer reducing the pore blockage of the hollow fiber. A visual representation of how charged polyGMA brushes grafted using UV-light and how a charged polyGMA cross-linked layer grafted using heat behave in low and high ionic strength environments are depicted in Fig. 4.5.

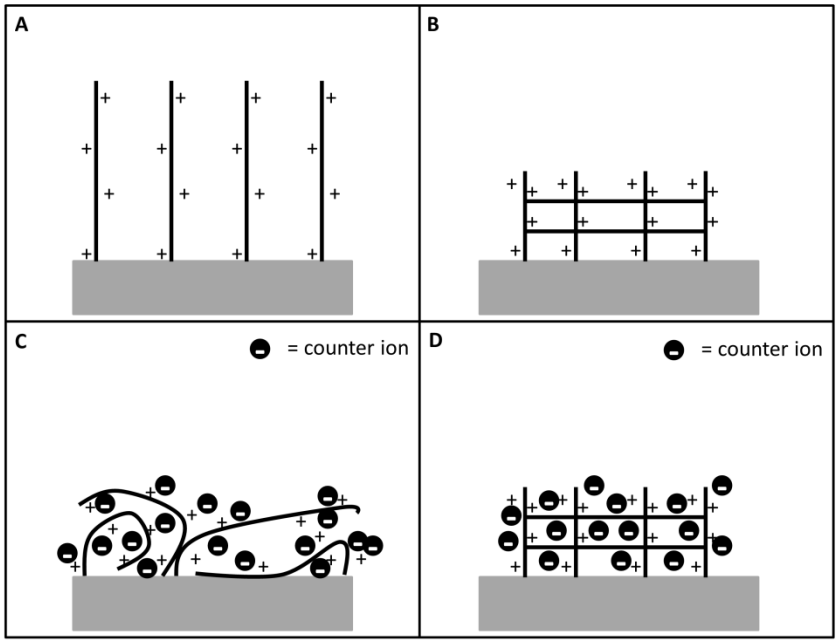

Fig. 4.5 Schematic representation of: (A) UV light grafted anion exchange polyGMA brushes in low ionic strength solution, (B) heat grafted anion exchange polyGMA cross-linked layer in low ionic strength solution, (C) UV light grafted anion exchange polyGMA brushes in high ionic strength solution, (D) heat grafted anion exchange polyGMA cross-linked layer in high ionic strength solution.

In Fig. 4.5A, the polyGMA brushes electrostatically repel one another resulting in an extension from the grafted surface, as counter-ions saturate the charges on the brushes the

polyGMA brushes collapse into the salted brushes regime depicted in Fig. 4.5C. The heat grafted nonwovens on the other hand are highly cross-linked as Fig. 4.5B depicts and do not have significant conformational changes when counter-ions are introduced as Fig. 4.5D depicts.

4.3.4 Effect of PET spacers on flow properties

The pressure drops of PBT nonwoven layers grafted with polyGMA separated by PET nonwoven spacers were also investigated. Columns were made by packing alternating layers of the anion exchange PBT nonwovens grafted to 5% weight gain using UV-light or 25% weight gain using heat with PET nonwoven spacers. In total the columns consisted of 20 layers of grafted PBT nonwoven and 20 layers of spacer (column height = 0.6 cm). In addition, the pressure drop of a 40 layer PET nonwoven spacer column (column height = 1.0 cm) was also tested. These columns were exposed to high and low ionic strength mobile phases for a range of superficial velocities. The results of this experiment are presented in Fig 4.6.

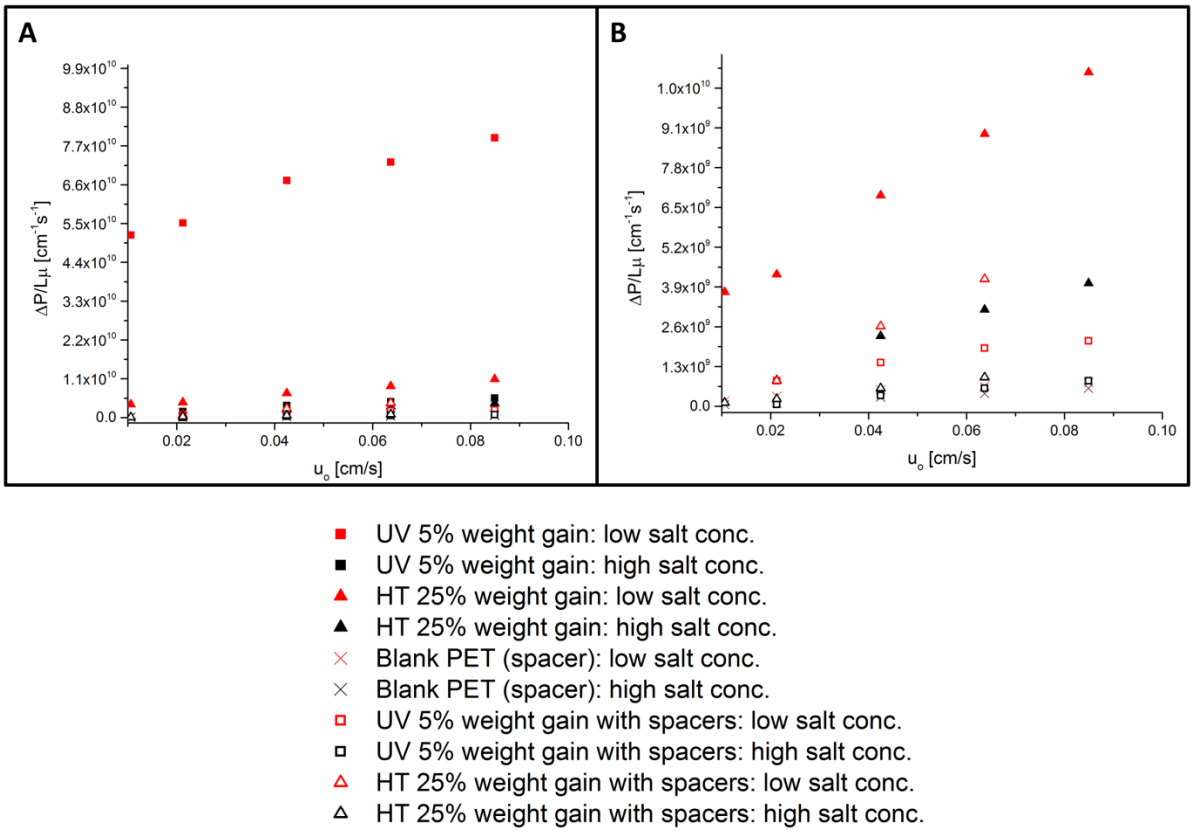

Fig. 4.6 (A)Pressure drop versus superficial velocity (high/low ionic strength): columns packed with anion exchange PBT nonwovens grafted at 5% weight using UV-light with and without PET nonwoven spacers, anion exchange PBT nonwovens grafted at 25% weight using heat with and without PET nonwoven spacers and for just the PET nonwoven spacers. (B) Expanded view of pressure drops ($\Delta P/L\mu$ between 0 and $1x10^{10}$ $cm^{-1}s^{-1}$).

The PET spacers had a significant impact in reducing the pressure drops across the column for the ion exchange grafted PBT nonwovens as Fig. 4.6 shows. The permeability coefficients (*k*) were calculated using Eq. 9 and are presented in Table 4.4.

Table 4.4: Calculated permeability coefficients for anion exchange PBT nonwovens grafted using UV-light at weight gains of 5% and grafted using heat at a weight gain of 25%, with individual layers separated by PET nonwoven spacers and for the PET spacer alone; Evaluated with a high and low ionic strength mobile phase.

Sample	$k_{\text{low ionic strength}}$ (cm^2)	$k_{\text{high ionic strength}}$ (cm^2)
UV 5%	2.6×10^{-12}	1.7×10^{-11}
HT 25%	1.0×10^{-11}	2.0×10^{-11}
UV 5% with spacers	4.7×10^{-11}	8.3×10^{-11}
HT 25% with spacers	1.3×10^{-11}	5.7×10^{-11}
PET Spacers	1.2×10^{-10}	1.4×10^{-10}

The use of spacers resulted in an increase of permeability for all of the columns packed with anion exchange polyGMA grafted PBT nonwovens as indicated in Table 4.4. The most significant change was observed for the anion exchange PBT nonwovens grafted to 5% weight gain using UV-light. The addition of spacers increased the permeability of the anion exchange UV-light grafted nonwovens an order of magnitude for a low ionic strength mobile phase and approximately 5 times for a high ionic strength mobile phase. The impact of spacers on permeability was less significant for the anion exchange PBT nonwovens grafted using heat. However, these membranes did not exhibit the same high pressure drops compared to the UV-light grafted PBT nonwovens as Fig. 4.3 shows and any permeability improvement with spacers is marginal for these membranes.

4.3.5 Dynamic binding capacity

The dynamic binding capacities of the polyGMA grafted nonwovens grafted using UV-light and heat, functionalized as cation exchangers were evaluated using hIgG as the target molecule. In this study 20 layers (column height = 0.2 cm) of PBT nonwoven grafted to 5% weight gain using UV-light and functionalized with sulfonic acid were packed into a column and challenged with a 1 ml injection of 10 mg/ml pure hIgG at superficial velocities

of 0.04 cm/min, 0.13 cm/min and 0.25 cm/min. A weight gain of 5% grafted using UV-light was chosen for this study due to its better flow properties compared to higher degrees of grafting that had shown to block the pores of the PBT membrane. Heat grafted PBT nonwovens grafted to 25% weight gain functionalized with sulfonic acid were tested in the exact same fashion. The use of PET spacers to separate individual layers of these grafted nonwovens were investigated to determine if increased column porosity had any influence on the dynamic binding capacity. These columns were packed with 20 layers of each cation exchange polyGMA grafted PBT nonwovens that were separated by 20 layers of PET nonwoven spacers (column height = 0.6 cm).

An example of a chromatogram from this experiment is presented in Fig. 4.7; this specific chromatogram is for a column packed with 20 layers of cation exchange PBT nonwovens grafted to 5% weight gain using UV-light (column volume = 0.16 ml, column mass = 0.1 g) tested at a superficial velocity of 0.25 cm/min.

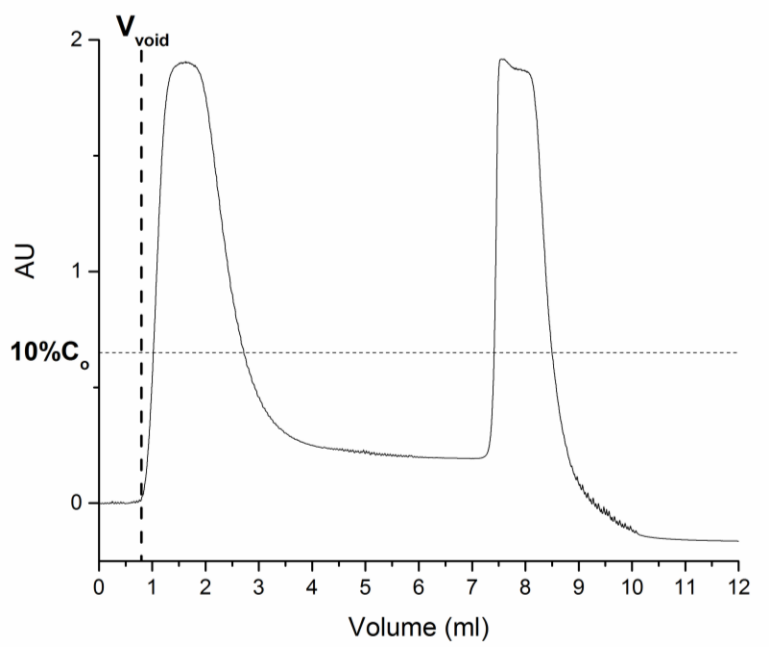

Fig. 4.7. Chromatogram obtained from the dynamic binding of hIgG (1ml; 10 mg/ml) of a column with 20 layers of cation exchange PBT nonwovens grafted to 5% weight gain using UV-light.

The chromatograms for the other columns tested can be found in the Appendix: B. Chromatograms from dynamic binding capacity experiments. The chromatograms from this experiment were used to calculate the dynamic binding capacity (10% DBC), evaluated at 10% breakthrough of the initial protein concentration (10 mg/ml) using Eq. 3. The results of the 10% DBC at different residence times for hIgG capture using cation exchange polyGMA grafted nonwovens with and without spacers are presented in Fig. 4.8. It is important to note that the calculated 10% DBC values reported in Fig. 4.8 only account for the volume of the modified PBT nonwovens and do not include the volume of the PET nonwoven spacers because spacers do not contribute to any protein binding and are solely there to increase the porosities of the columns for enhanced flow properties.

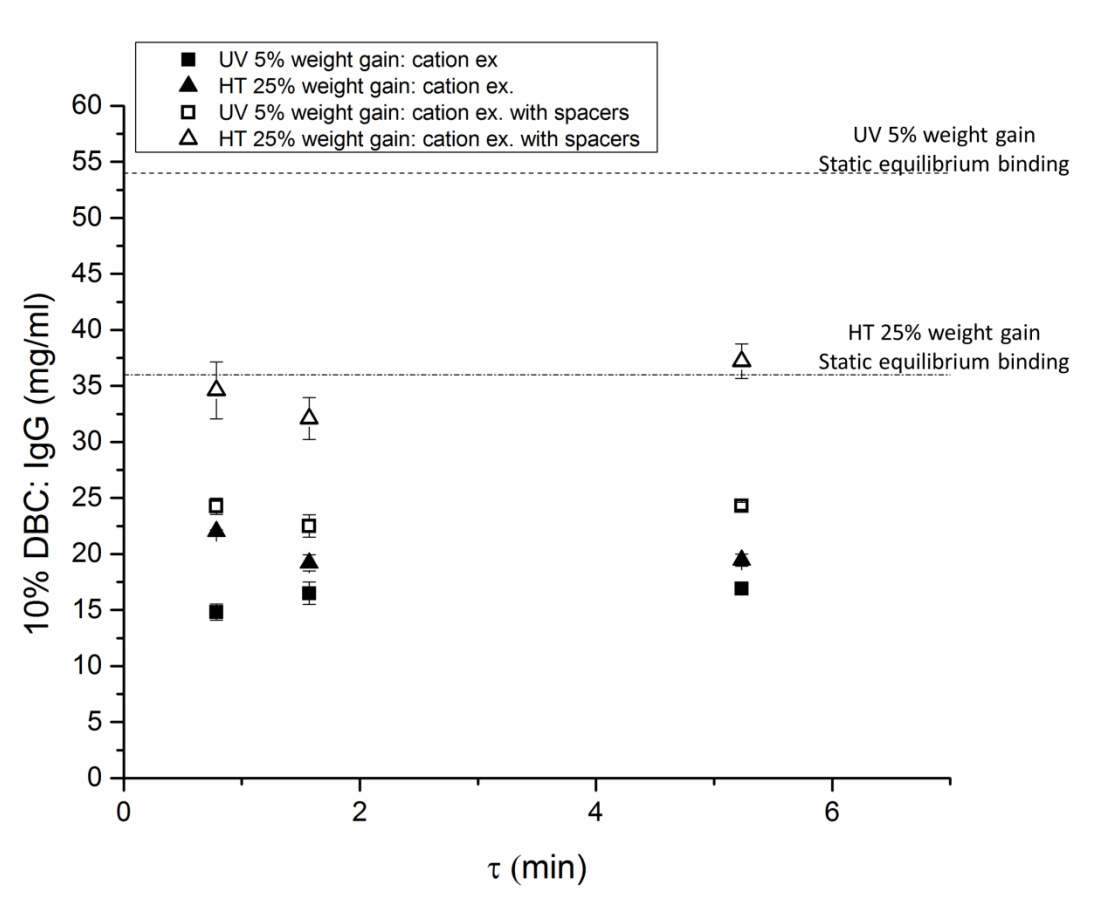

Fig. 4.8 Dynamic binding capacity at 10% breakthrough versus residence time using cation exchange PBT nonwovens grafted with UV light at 5% weight gain with and without spacers, as well as, grafted with heat at 25% weight gain with and without spacers for capture of hIgG. Dynamic binding was calculated only accounting for the volume of the functionalized polyGMA grafted PBT nonwovens.

From Fig. 4.8 it is shown that the UV grafted PBT nonwovens grafted to 5% weight gain and functionalized as cation exchangers bound approximately 16 mg/ml at all tested residence times. Introducing a PET nonwoven spacer to separate the individual PBT nonwoven layers increased the dynamic binding capacities to approximately 24 mg/ml (8.2 mg/ml if the 10% DBC is reported for the total column volume including inactive PET spacer) for all tested flow rates. In a previous study these membranes were tested statically in a loosely packed

configuration at various hIgG contact times [12]. At contact times of 5 min, 15 min and at equilibrium binding the cation exchange UV grafted PBT nonwovens at 5% weight gain bound hIgG at approximately 27 mg/ml (150 mg/g) , 36 mg/ml (200 mg/g) and 54 mg/ml (300 mg/g) respectively. When tested statically these nonwovens had high binding capacities on a per mass basis. However, the unpacked membranes used for static protein binding had very high porosities (86%) and very low densities (0.18 g/ml) that resulted in substantially lower binding capacities on a per volume basis. A protein contact time of 5 min is equivalent to a residence time of 5 min. At this residence time, the cation exchange UV-light PBT nonwovens that were packed straight into a column without spacers bound significantly less compared to when a spacer was used or when the membranes were tested statically. When spacers were used, the dynamic binding capacity at a residence time of 5 minutes was comparable to when the membranes were exposed statically to protein with a 5 minute contact time. When the PBT nonwovens were packed into a column as consecutive layers they had a calculated porosity of approximately 54% however the flow porosity calculated from the first moment analysis was approximately 35%. This difference in porosity is a strong indication that some of the pores of the material are being blocked from neighboring layers of PBT nonwoven when stacked in a column format under pressure. When the PBT nonwovens are tested statically the material is not confined and fibers are permitted to change position, the porosity of the PBT nonwovens when tested statically is approximately 86%. Introducing PET nonwoven spacers is capable of increasing the porosity of the column to 65%. It is also believed that separating individual layers of PBT nonwovens reduces any pore blockage that was previously occurring making a larger portion of the nonwoven available for protein capture. Therefore, increasing the porosity of the column was capable of

increasing the volume accessible for protein binding and resulted in very similar protein capture to when the material was tested statically at the same residence times. It is also apparent from Fig. 4.8 that dynamic binding capacities for the cation exchange polyGMA grafted PBT nonwovens using UV-light are substantially lower than the static equilibrium binding capacity of this material. It is important to note that this material is known to have diffusion limited mass transport through the grafted layer [12]. Therefore it is capable of achieving high equilibrium protein binding capacities, however, very long time scales (time scale of hours) are required to reach this capacity. In this investigation, 5 min was the longest residence time evaluated due to limitations of the HPLC systems and for practical reason. Practically speaking, membranes are appealing because of their high throughput capabilities; as a result testing excessively long residence times is not relevant.

The cation exchange polyGMA PBT nonwovens grafted to 25% weight gain using heat had dynamic binding capacities of 20 mg/ml for all tested residence times when spacers were not used. Introducing a PET nonwoven spacer to separate the individual PBT nonwoven layers increased the dynamic binding capacities to approximately 35 mg/ml (12 mg/ml if the 10% DBC is reported for the total column volume including inactive PET spacer) for all tested flow rates. In a previous study when these materials were tested statically with hIgG they had an equilibrium binding capacity of 36 mg/ml. The heat grafted materials observed similar porosities as UV-light grafted membranes when packed into a column. Additionally, very similar increases in porosity were observed when spacers were used to separate the individual layers of the PBT nonwoven. For the same reasons as with the UV-light grafted PBT nonwovens, using PET nonwoven spacers were capable of increasing

the dynamic binding capacities by increasing the accessible volume for protein capture in the membrane. At all residence times tested, the dynamic binding capacities of the heat grafted cation exchange PBT nonwovens when separated by spacers were similar to the static equilibrium binding capacity of the material. Heat grafted nonwovens are believed to have a highly cross-linked polyGMA grafted layer that creates size exclusion limitations for protein accessing the interior of the grafted layer. Although this reduces the amount of protein the material is capable of binding, it does not demonstrate the same diffusion limited mass transport that the UV-light grafted layers do [12]. It has previously been shown that the heat grafted ion exchange nonwovens reach static equilibrium protein binding within minutes compared to the UV-light ion exchange nonwovens that require hours to reach equilibrium binding.

4.3.6 Protein recovery over multiple binding attempts

Elution fractions from multiple dynamic binding attempts were collected and quantified to determine the amount of protein recovered from the columns for multiple binding cycles. Columns were packed with 20 layers of cation exchange nonwovens grafted to either 5% weight gain using UV-light or 25% weight gain using heat. The columns were challenged with 1 ml of 10 mg/ml pure hIgG at a superficial velocity of 0.25 cm/min (0.2 ml/min). After all of the unbound protein was washed from the column, bound hIgG was eluted using an increase in salt concentration (1 M NaCl) at a superficial velocity of 0.25 cm/min (0.2 ml/min). This was repeated over 5 binding and elution cycles to ensure that performance did not deteriorate over multiple binding attempts. The results of the collected hIgG elution fractions from the cation exchange PBT nonwovens grafted using UV-light (5% weight gain) and using heat (25% weight gain) are presented in Fig. 4.9.

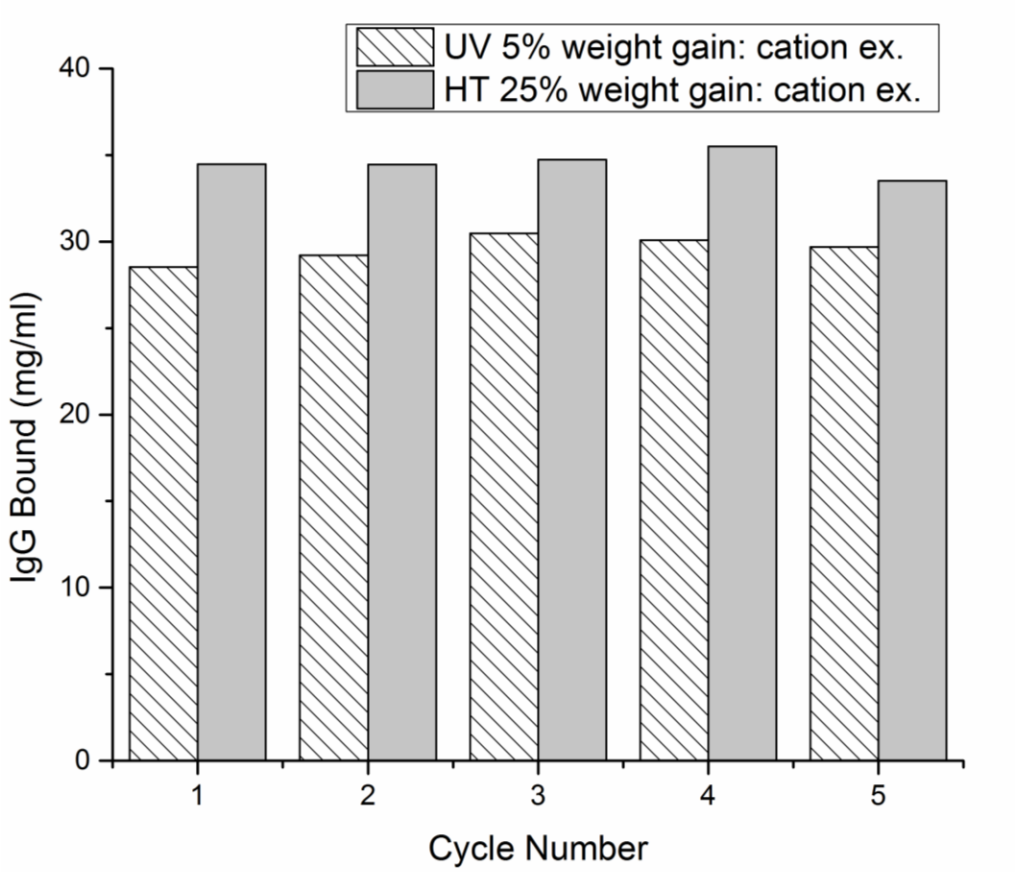

Fig. 4.9 hIgG recovered from elution fractions over 5 binding and elution attempts. Cation exchange UV-light grafted (5% weight gain, 20 layers) and heat grafted (25% weight gain, 20 layers) PBT nonwovens challenged with 1 ml of 10 mg/ml of pure hIgG at a superficial velocity of 0.25 cm/min (0.2 ml/min).

The cation exchange PBT nonwovens grafted to 5% weight gain using UV-light consistently recovered approximately 30 mg/ml and the cation exchange nonwovens grafted to 25% weight gain using heat consistently recovered approximately 35 mg/ml as Fig. 4.9 shows. Additionally, the amount of hIgG recovered does not decrease over multiple binding cycles for both materials tested indicating that the columns are capable of being completely regenerated and used for many binding attempts.

4.3.7 Separation of protein mixtures using cation exchange grafted PBT nonwovens

The cation exchange functionalized PBT nonwovens were evaluated for their ability to separate hIgG from a mixture of two similarly charged proteins, hIgG and lysozyme. One milliliter of protein mixture containing hIgG (1 mg/ml) and lysozyme (1 mg/ml) was injected into columns packed with 20 layers of cation exchange PBT nonwoven grafted to 5% weight gain using UV-light or grafted to 25% weight gain using heat. The columns were operated in a bind and elute mode of operation for both proteins. The binding buffer was 20 mM Tris-HCl pH 6.5 ensuring that both hIgG (pI=7-9) and lysozyme (pI=11.35) had a net positive charge and would bind to the cation exchange columns. After protein binding, hIgG was selectively eluted using 20 mM carbonate buffer pH 10. Once hIgG had been selectively eluted from the column any remaining protein bound to the column was eluted using a high salt buffer (20 mM Tris-HCl + 1 M NaCl pH 6.5). The flow rate was kept constant for all binding and elution conditions at a superficial velocity of 0.25 cm/min (0.2 ml/min). The chromatogram of these separations is presented in Fig 4.10.

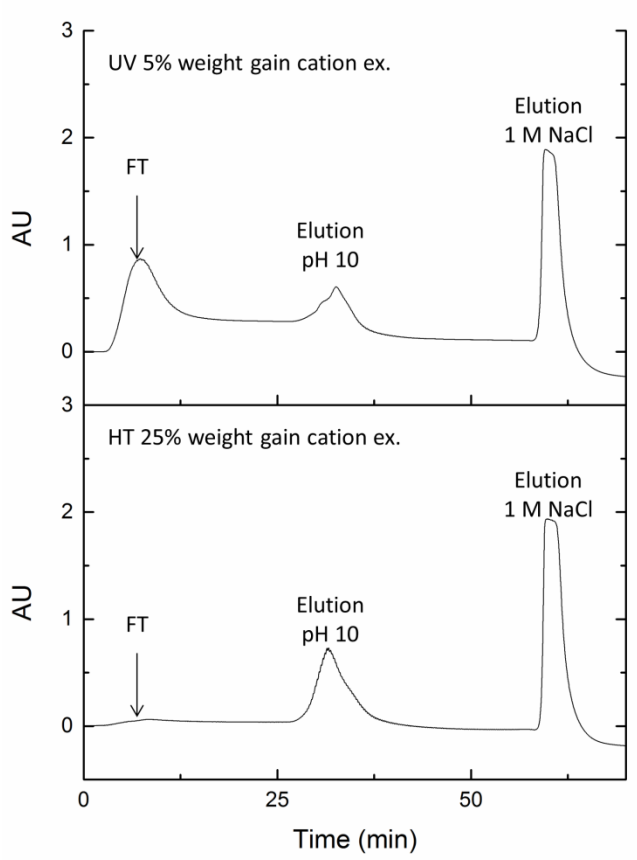

Fig. 4.10 Chromatogram of hIgG and lysozyme mixture separation using cation exchange nonwovens grafted to 5% weight gain using UV-light and 25% weight gain using heat. The injection is a 1 ml protein solution containing 1 mg/ml of hIgG and 1 mg/ml of lysozyme (binding buffer= 20 mM Tris-HCl pH 6.5, pH 10 elution buffer= 20 mM carbonate buffer pH 10, high salt elution buffer= 20 mM Tris-HCl + 1 M NaCl pH 6.5). The superficial velocity was 0.25 cm/min for binding and elution

The chromatogram in Fig 4.10 shows good separation resolution between the flow through peak, the elution peak using a pH 10 buffer and the elution peak using a 1 M NaCl buffer for both the UV-light grafted cation exchange PBT nonwovens and the heat grafted cation exchange PBT nonwovens. The flow through, pH 10 elution and the 1 M NaCl elution fractions in addition to the load mixture, pure hIgG and pure lysozyme were analyzed by SDS-PAGE. An image of the resulting gel is presented in Fig. 4.11.

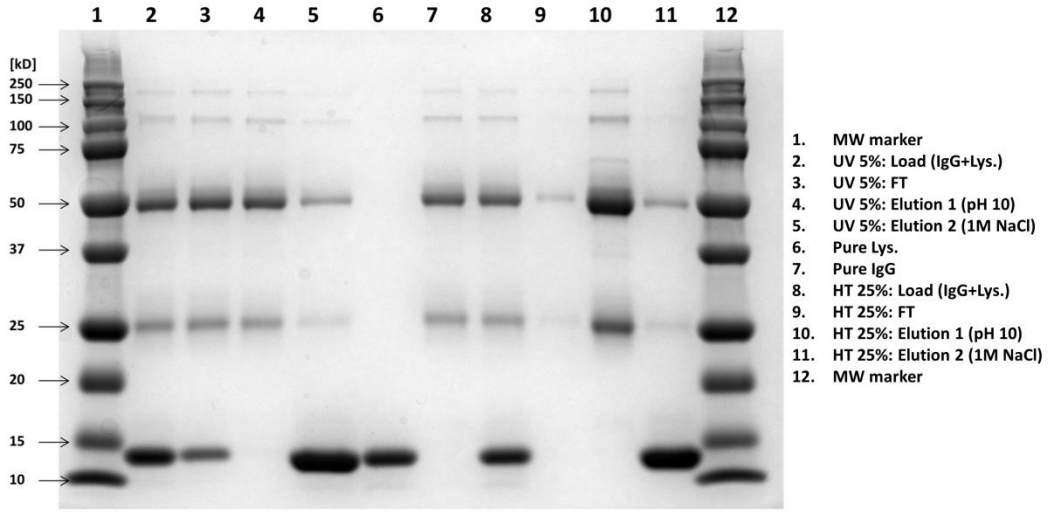

Fig. 4.11 SDS-PAGE results for the separation of hIgG and lysozyme using cation exchange polyGMA grafted nonwovens grafted to 5% weight gain using UV-light and 25% weight gain using heat. Bound proteins eluted first with a pH 10 buffer followed by elution with a high salt buffer.

Under reducing conditions lysozyme has a band around ~13 kD and hIgG has bands around ~50 kD and ~25kD corresponding to the heavy and light chains of hIgG respectively. Lanes 4 and 10 in Fig. 4.11 represent the pH 10 elution fractions for the cation exchange polyGMA grafted PBT nonwovens grafted to 5% weight gain using UV-light and 25% weight gain using heat respectively. These elution fractions were determined to be pure hIgG using the densitometric analysis of the ImageLab software. Lanes 5 and 11 in Fig. 10 represent the 1 M NaCl elution fractions for the cation exchange polyGMA grafted PBT nonwovens grafted to 5% weight gain using UV-light and 25% weight gain using heat respectively. Densitometric analysis was used to determine the relative band intensities of the high salt elution fractions. It was determined that the high salt elution fraction for the cation exchange PBT nonwovens grafted using UV-light (5% weight gain) contained approximately 20%

hIgG and 80% lysozyme. Similarly, the high salt elution fractions for the cation exchange PBT nonwovens grafted using heat (25% weight gain) contained approximately 20% hIgG and 80% lysozyme. The pH 10 elution fractions were analyzed using UV-Vis spectroscopy at 280 nm to quantify the recovery of hIgG. It was determined that for a 1 ml mixture containing hIgG at 1 mg/ml and lysozyme at 1 mg/ml, 20 layers (~0.1 g, ~0.16 ml) of the cation exchange PBT nonwovens were capable of recovering 0.65 mg (65%) and 0.30 mg (30%) of pure hIgG for the heat grafted nonwovens (25% weight gain) and the UV-light grafted nonwovens (5% weight gain) respectively. Overall these results indicate that the pH 10 buffer was capable of selectively eluting hIgG from the column by converting a significant portion hIgG to a net negative charge. The hIgG that was recovered in the high salt elution is likely due to local positively charged pockets on the protein that were not affected by an increased pH but were disrupted by an increase in ionic strength.

The cation exchange functionalized PBT nonwovens were evaluated for their ability to separate a mixture of positively charged hIgG and lysozyme and negatively charged BSA. One milliliter of protein mixture containing hIgG (1 mg/ml), lysozyme (1 mg/ml) and BSA (1 mg/ml) was injected into columns packed with 20 layers of cation exchange PBT nonwoven grafted to 5% weight gain using UV-light or grafted to 25% weight gain using heat. The binding buffer was 20 mM Tris-HCl pH 6.5 ensuring that both hIgG (pI=7-9) and lysozyme (pI=11.35) had a net positive charge and would bind to the columns and that BSA (pI=4.7) would have a net negative charge and in theory flow through the columns. After protein binding, an elution was performed using 20 mM carbonated buffer pH 10 followed by an elution with 20 mM Tris-HCl + 1 M NaCl pH 6.5. The flow rate was kept constant for

all binding and elution conditions at a superficial velocity of 0.25 cm/min (0.2 ml/min). The chromatogram of these separations is presented in Fig 4.12.

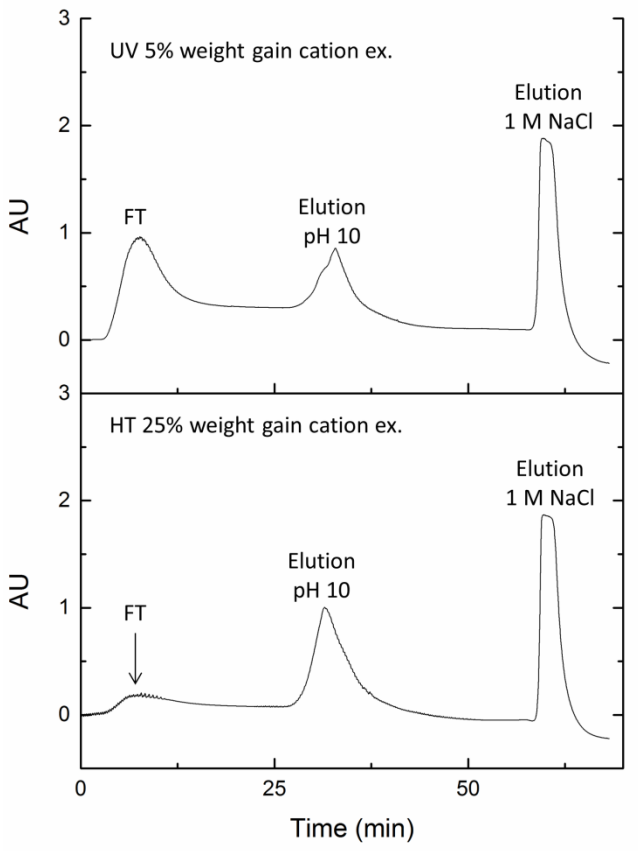

Fig. 4.12 Chromatogram of hIgG, BSA and lysozyme mixture separation using cation exchange nonwovens grafted to 5% weight gain using UV-light and 25% weight gain using heat. The injection is a 1 ml protein solution containing 1 mg/ml of hIgG, 1 mg/ml of BSA and 1 mg/ml of lysozyme (binding buffer= 20 mM Tris-HCl pH 6.5, pH 10 elution buffer= 20 mM carbonate buffer pH 10, high salt elution buffer= 20 mM Tris-HCl + 1 M NaCl pH 6.5). The superficial velocity was 0.25 cm/min for binding and elution.

The chromatogram in Fig. 4.12 shows good separation resolution between the flow through peaks, the elution peaks using pH 10 buffer and the elution peaks using 1 M NaCl buffer for both the UV-light grafted cation exchange PBT nonwovens and the heat grafted cation exchange PBT nonwovens. The flow through, pH 10 elution and the 1 M NaCl elution

fractions in addition to the load mixture, pure hIgG, pure lysozyme and pure BSA were analyzed by SDS-PAGE. An image of the resulting gel is presented in Fig. 4.13.

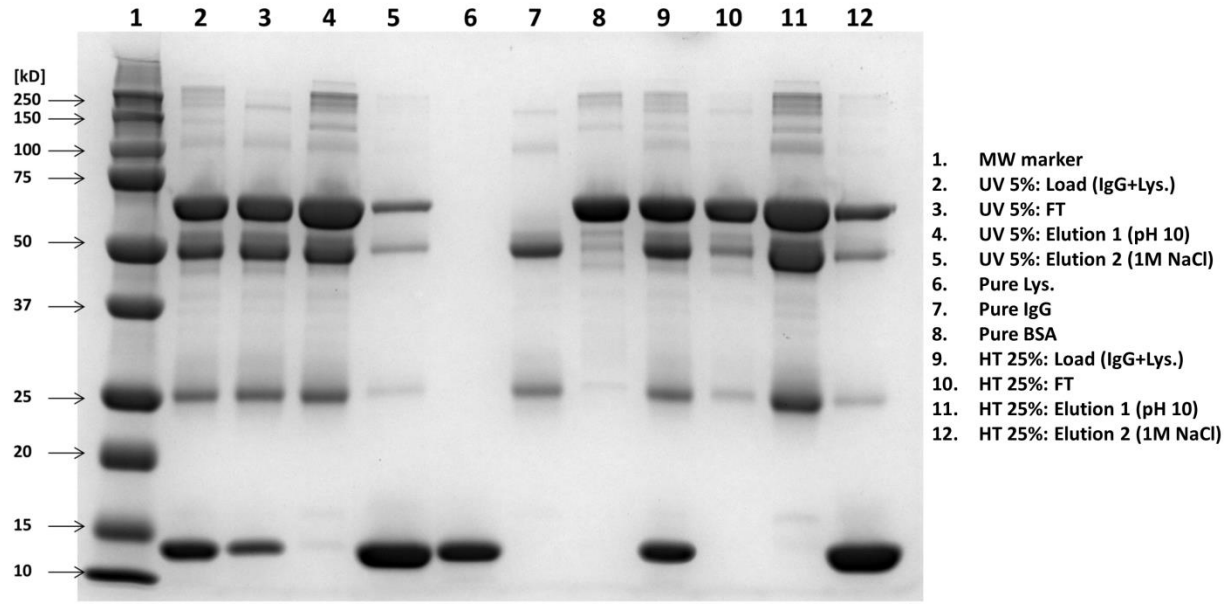

Fig. 4.13 SDS-PAGE results for the separation of hIgG, BSA and lysozyme using cation exchange polyGMA grafted nonwovens grafted to 5% weight gain using UV-light and 25% weight gain using heat. Bound proteins eluted first with a pH 10 buffer followed by elution with a high salt buffer.

Under reducing conditions BSA has a band around ~65kD. What is apparent from Fig. 4.13 is that BSA is present in the flow through, pH 10 elution and 1 M NaCl elution fractions for cation exchange PBT nonwovens grafted with both techniques. Under these binding conditions BSA has a net negative charge and should not bind to column. However, Fig. 4.13 indicates that BSA binds to the cation exchange nonwovens and can be eluted using an increase in pH or an increase in salt concentration. This phenomenon has been observed for binding of net negatively charged BSA to negatively charged surfaces grafted with poly

acrylic acid [36,37]. Vos *et al*. determined that the adsorption of BSA to the grafted surface under what should be electrostatically repulsive conditions is due to positively charged patches on BSA that bind to the negatively charge grafted layer that has a substantial charge density [37]. Increasing the pH or salt concentration is capable of disrupting these localized positively charged binding pockets on BSA as Fig. 4.13 shows.

To evaluate the mechanism of protein adsorption onto the cation exchange PBT nonwovens the columns were again challenged with a mixture hIgG (1 mg/ml), lysozyme (1 mg/ml) and BSA (1 mg/ml). These proteins were bound to cation exchange nonwovens using the same binding conditions and flow rate. However, the order of the elution was reversed using a high salt elution first to remove any electrostatically bound protein followed by an elution with a high pH buffer. The chromatogram of these separations is presented in Fig 4.14.

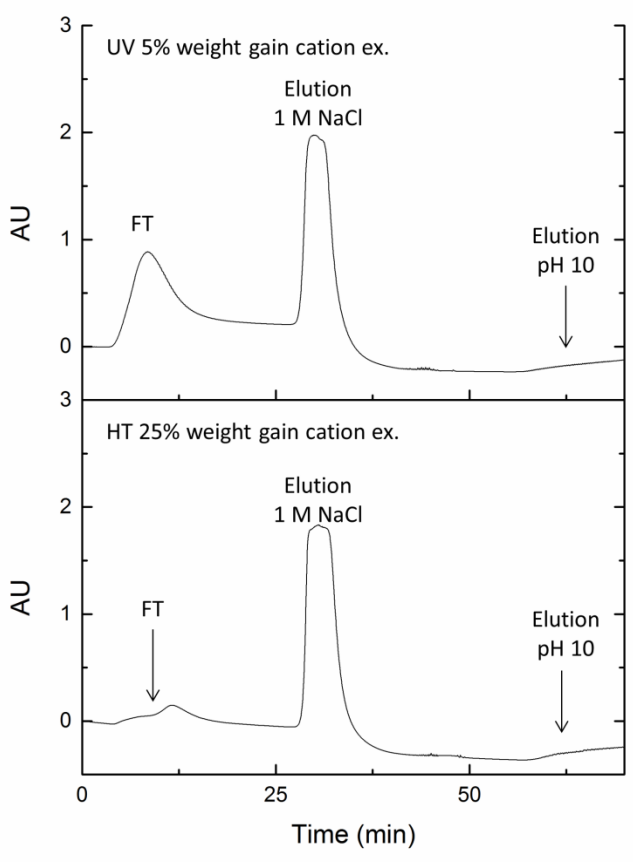

Fig. 4.14 Chromatogram of hIgG, BSA and lysozyme mixture separation using cation exchange nonwovens grafted to 5% weight gain using UV-light and 25% weight gain using heat. The injection is a 1 ml protein solution containing 1 mg/ml of hIgG, 1 mg/ml of BSA and 1 mg/ml of lysozyme (binding buffer= 20 mM Tris-HCl pH 6.5, high salt elution buffer= 20 mM Tris-HCl + 1 M NaCl pH 6.5, pH 10 elution buffer= 20 mM carbonate buffer pH 10). The superficial velocity was 0.25 cm/min for binding and elution.

It is apparent from Fig. 4.14 that nearly all of the bound protein is eluted by an increase in ionic strength observed by the very large peak for the elution with 1 M NaCl. The flow through, pH 10 elution and the 1 M NaCl elution fractions in addition to the load mixture, pure hIgG, pure lysozyme and pure BSA were analyzed by SDS-PAGE. An image of the resulting gel is presented in Fig. 4.15.

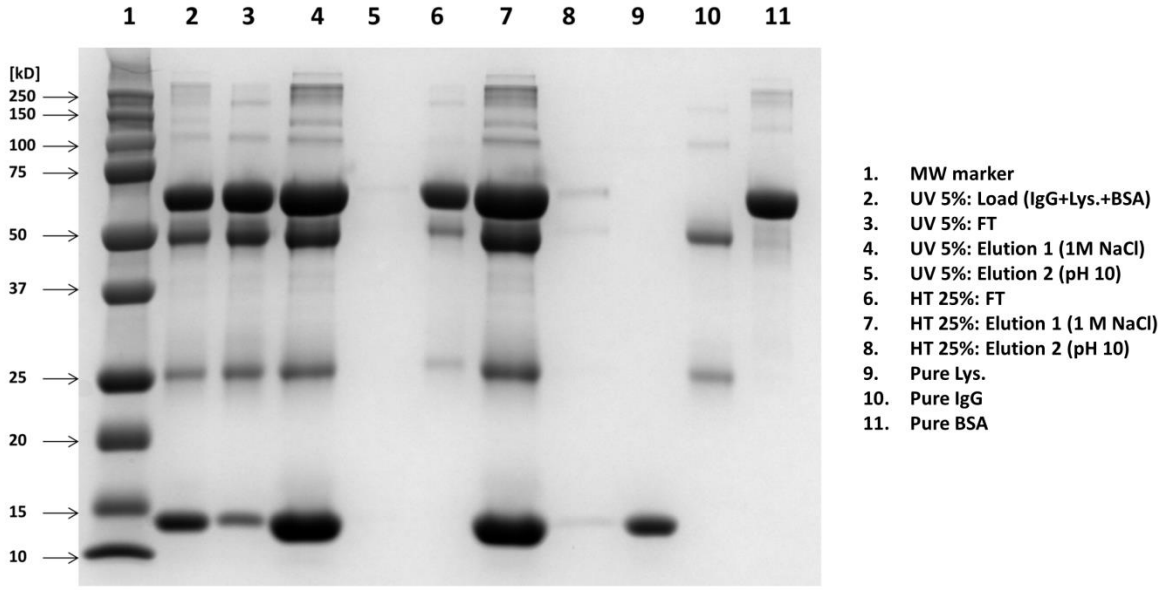

Fig. 4.15 SDS-PAGE results for the separation of hIgG, BSA and lysozyme using cation exchange polyGMA grafted nonwovens grafted to 5% weight gain using UV-light and 25% weight gain using heat. Bound proteins eluted first with a high salt buffer followed by elution with a pH 10 buffer.

In Fig. 4.15, lanes 4 and 7 correspond to the high salt elution fractions for the cation exchange polyGMA grafted PBT nonwovens grafted to 5% weight gain using UV-light and 25% weight gain using heat respectively. Lanes 5 and 8 correspond to the pH 10 elution fractions for the cation exchange polyGMA grafted PBT nonwovens grafted to 5% weight gain using UV-light and 25% weight gain using heat respectively. No quantifiable amount of protein was observed in lane 5 and less than 2.5% of the total protein bound to the column was observed in lane 8 according to densitometric analysis. The ability to remove 97.5%+ of the all of the proteins bound to the cation exchange functionalized polyGMA grafted PBT nonwovens by an increase in salt concentration indicates that electrostatic interaction is the dominating adsorption mechanism.

4.4 Conclusions

The performance of ion exchange PBT nonwovens grafted with polyGMA using a UV-light grafting method and a heat grafting method were evaluated under flow conditions. The total flow porosities of grafted PBT nonwovens packed as stacked flat sheets in a column format were determined to be between 30% and 36%. These low porosities are a strong indication that a majority of the PBT nonwovens pores are inaccessible to liquid penetration resulting in underutilization of the columns. The use of rigid PET nonwoven spacers to separate individual grafted PBT nonwoven layers was shown to increase the total column flow porosity to 55-65%. The pressure drops of the UV-light grafted PBT nonwoven ion exchangers demonstrated to be dependent on the ionic strength of the mobile phase. These results indicate that in a low ionic strength environment the ion exchange polyGMA brushes grafted using UV-light swell significantly, reducing the pore size of the material. It was determined that an increase in polyGMA grafting resulted in an increase in pressure drop due to the polyGMA layer swelling and blocking the pores at weight gains above 10%. For ion exchange membranes grafted with UV-light, introducing a high salt concentration mobile phase was capable of reducing the pressure drops due to a collapse of the brush layer. The pressure drops of the heat grafted ion exchange polyGMA PBT nonwovens did not demonstrate the same dependence on ionic strength as the UV-light grafted PBT nonwovens and had overall lower pressure drops. This observation further reinforces the idea that the UV-light polyGMA grafted layer is made of flexible polymer brushes and the heat grafted polyGMA layer is highly cross-linked and resistant to swelling. The introduction of PET spacers was shown to significantly increase the overall permeability of the columns and reduced the observed pressure drops for the ion exchange polyGMA grafted PBT

nonwovens. The dynamic binding capacities for hIgG capture using the cation exchange UV-light PBT nonwovens grafted to 5% weight gain was approximately 16 mg/ml for each residence time tested. Using PET spacers to increase the porosity of the column increased the dynamic binding capacity to 24 mg/ml which was similar to the static binding capacities achieved at 5 minute residence time. The static equilibrium capacity of this material is approximately 54 mg/ml; however, residence times too long for practical use of this material are required to reach this due to protein diffusion limitations in the polyGMA grafted layer. The dynamic binding capacities for hIgG capture using the cation exchange PBT nonwovens grafted using heat to 25% weight gain were approximately 20 mg/ml for each residence time tested. Using a PET spacer to increase the porosity of the column increased the dynamic binding capacity to 35 mg/ml which was similar to the static equilibrium binding capacity of the material. Heat grafted nonwovens do not exhibit the same diffusion limitations that UV-light grafted polyGMA nonwovens do and were able to achieve equilibrium at all residence times tested for dynamic binding. The cation exchange polyGMA grafted PBT nonwovens, grafted by both heat and UV-light, were also evaluated for their ability to selectively adsorb and selectively elute hIgG from a mixture of proteins. It was determined that the cation exchange polyGMA grafted PBT nonwovens were capable of capturing both hIgG and lysozyme and could selectively elute hIgG using an increase in pH. Columns could then be regenerated using a high salt concentration elution. It was also determined that BSA bound electrostatically to the cation exchange polyGMA grafted PBT nonwovens under electrostatically repulsive conditions. This is likely due to local positive charges on BSA that bind to the cation exchange polyGMA layers with large charge densities. It is believed that the dynamic binding capacities of ion exchange polyGMA grafted PBT nonwovens could be

improved by making membranes that are composites of large and rigid fibers dispersed amongst smaller fibers. This way the material would have a high specific surface area for protein capture while still maintain good flow properties. Additionally, more work needs to be done to understand the interactions of the charged polyGMA layers with protein binding including investigating how the charge density affects binding, as well as, investigating ligands and binding conditions that minimize the nonspecific electrostatic absorption of proteins like BSA.

4.5 Appendix

4.5.A. Pulse responses of acetone injections

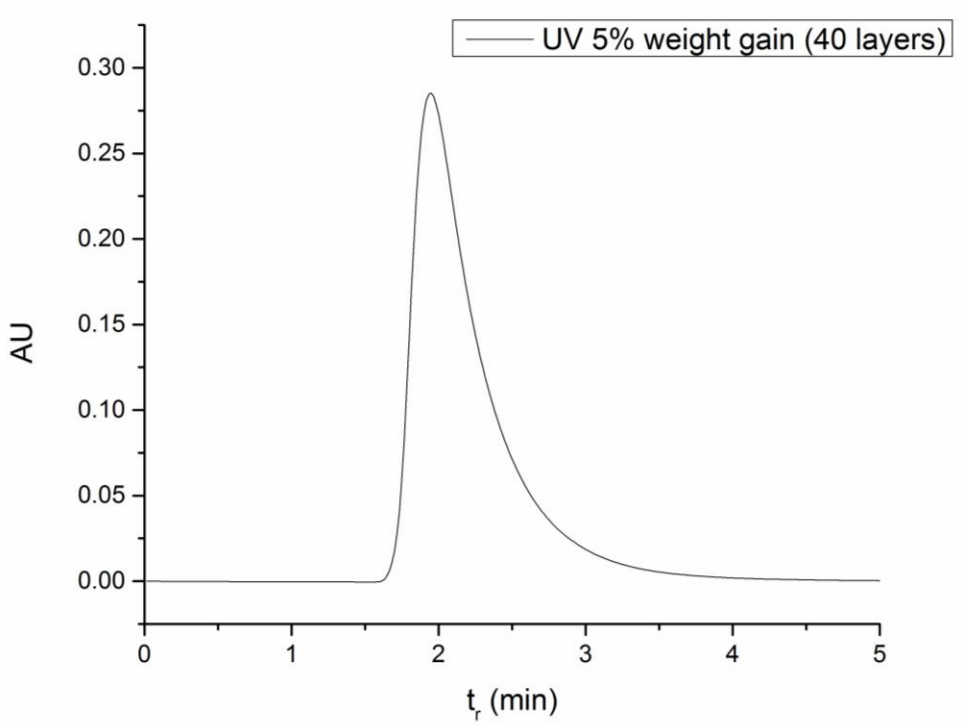

Fig. 4.A.1 Acetone (5% v/v) pulse injections (20 µl loop) at 1.3 cm/min using nonbinding conditions. Column packed with 40 layers of PBT nonwovens grafted to 5% weight gain using UV-light (column height= 0.4 cm).

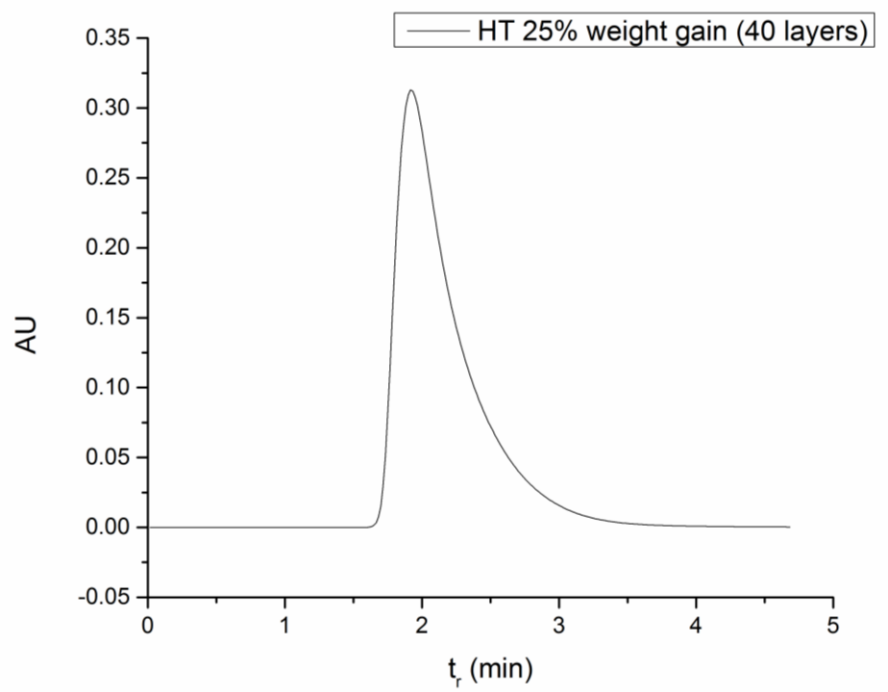

Fig. 4.A.2 Acetone (5% v/v) pulse injections (20 µl loop) at 1.3 cm/min using nonbinding conditions. Column packed with 40 layers of PBT nonwovens grafted to 25% weight gain using heat (column height = 0.4 cm).

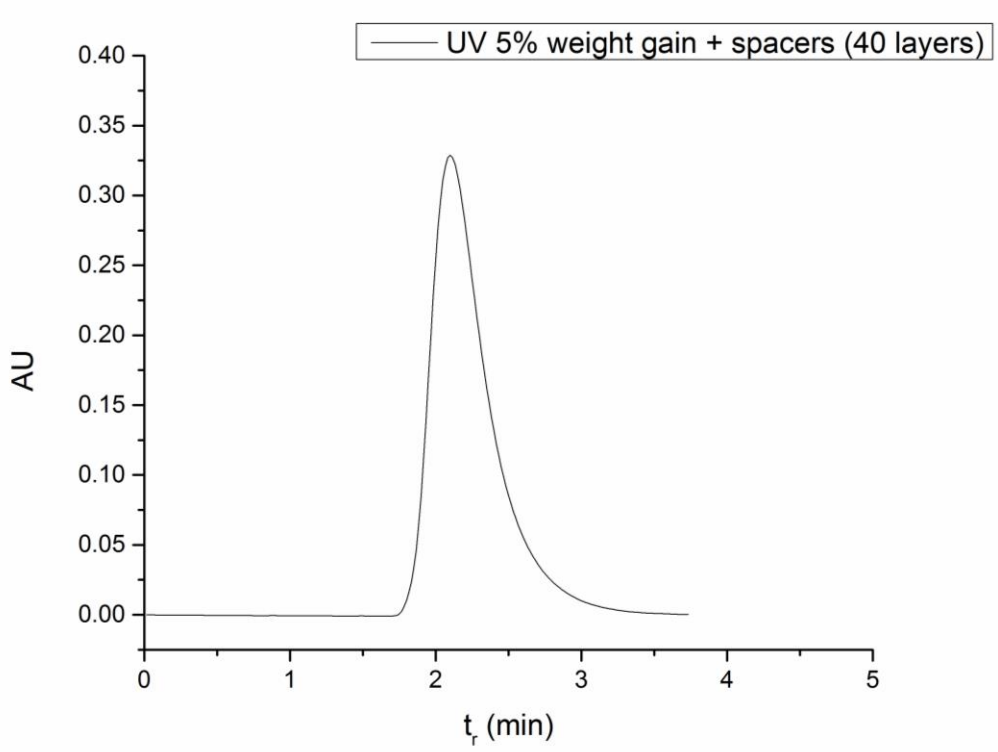

Fig. 4.A.3 Acetone (5% v/v) pulse injections (20 µl loop) at 1.3 cm/min using nonbinding conditions. Column packed with 20 layers of PBT nonwovens grafted to 5% weight gain using UV-light separated by 20 layers of PET nonwoven spacer(column height = 0.6 cm).

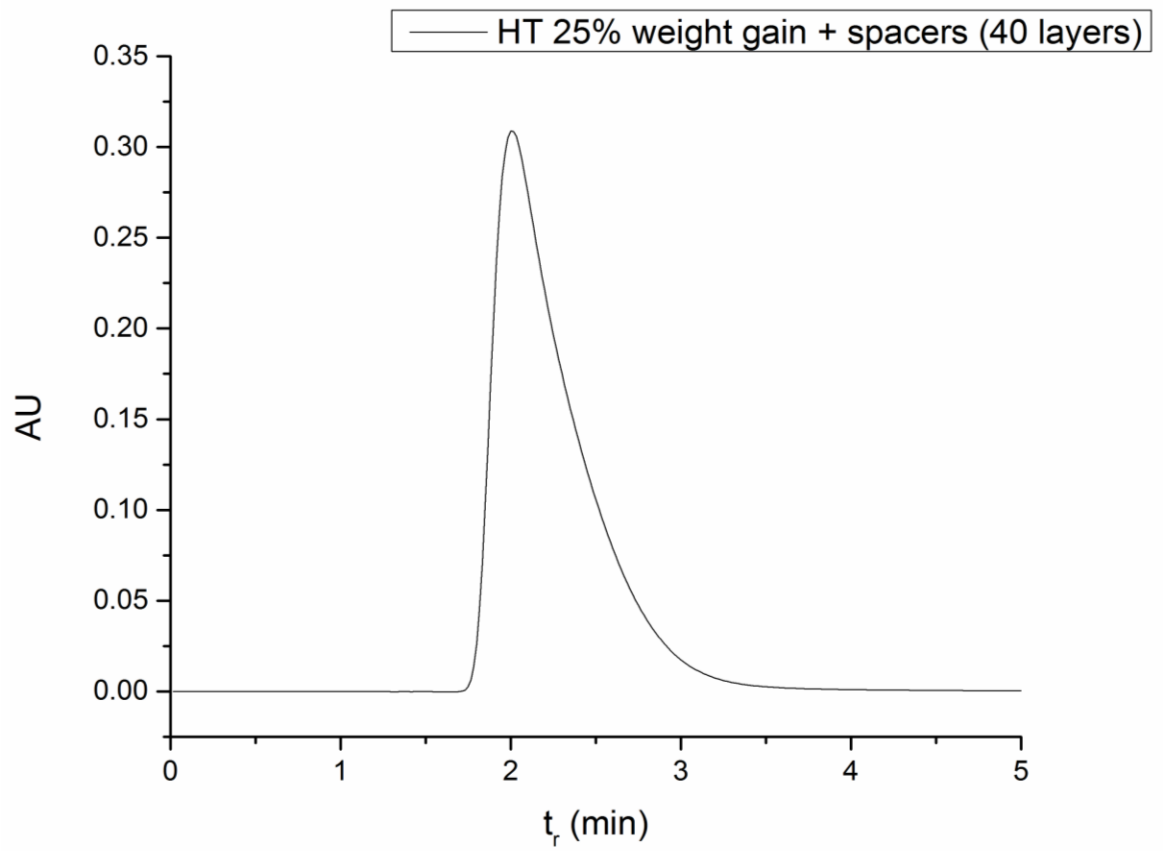

Fig. 4.A.4 Acetone (5% v/v) pulse injections (20 µl loop) at 1.3 cm/min using nonbinding conditions. Column packed with 20 layers of PBT nonwovens grafted to 25% weight gain using heat separated by 20 layers of PET nonwoven spacer(column height = 0.6 cm).

4.5.B Chromatograms from dynamic binding capacity experiments

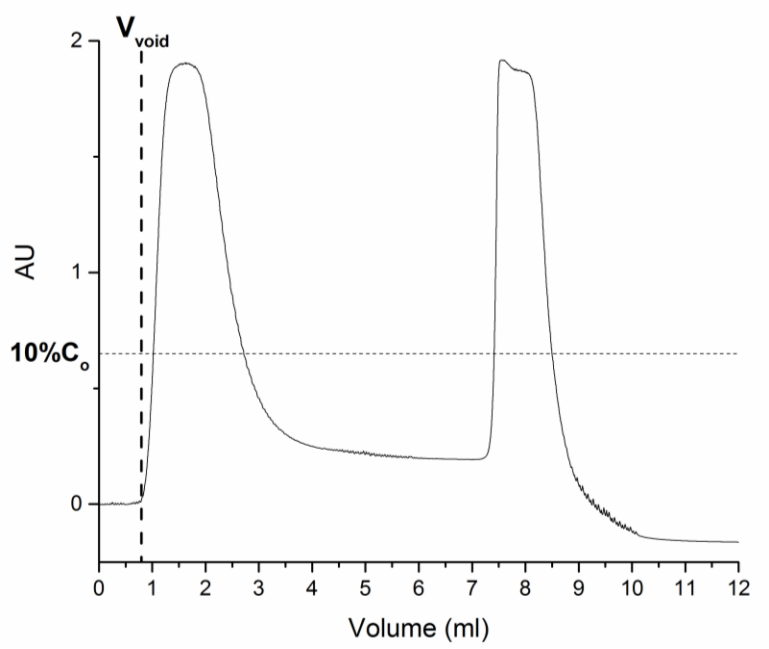

Fig. 4.B.1 (Fig. 7) Chromatogram obtained from the dynamic binding of hIgG (1ml; 10 mg/ml) to a column with 20 layers of cation exchange PBT nonwovens grafted to 5% weight gain using UV-light. Superficial velocity = 0.25 cm/min.

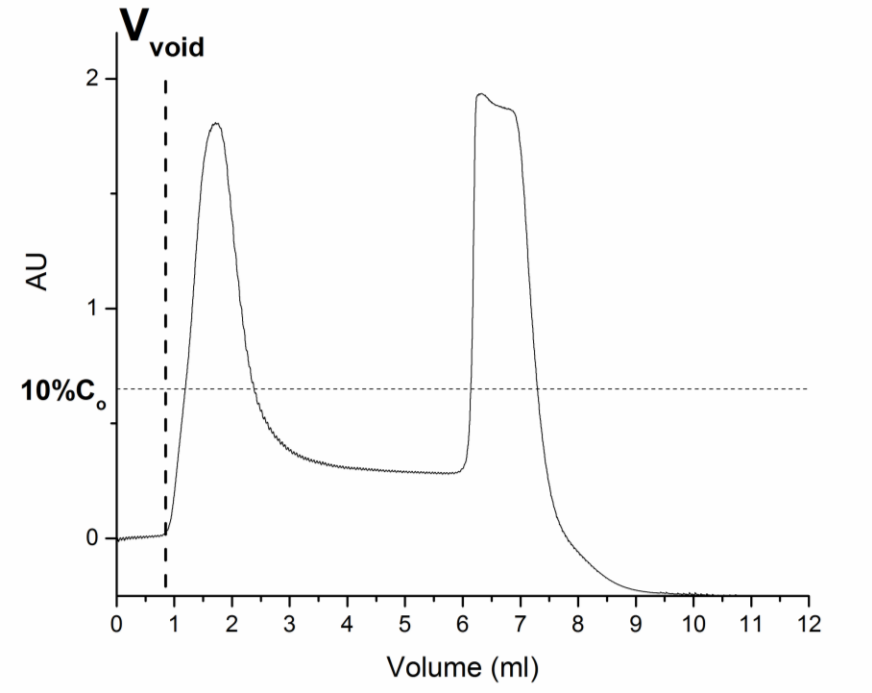

Fig. 4.B.2 Chromatogram obtained from the dynamic binding of hIgG (1ml; 10 mg/ml) to a column with 20 layers of cation exchange PBT nonwovens grafted to 25% weight gain using heat. Superficial velocity = 0.25 cm/min.

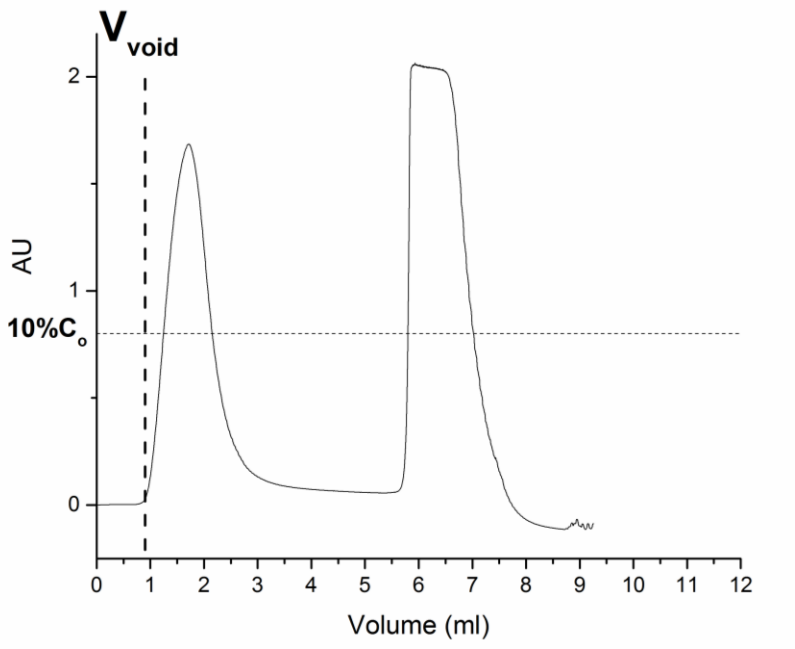

Fig. 4.B.3 Chromatogram obtained from the dynamic binding of hIgG (1ml; 10 mg/ml) to a column with 20 layers of cation exchange PBT nonwovens grafted to 5% weight gain using UV-light separated by 20 layers of PET nonwoven spacer. Superficial velocity = 0.13 cm/min.

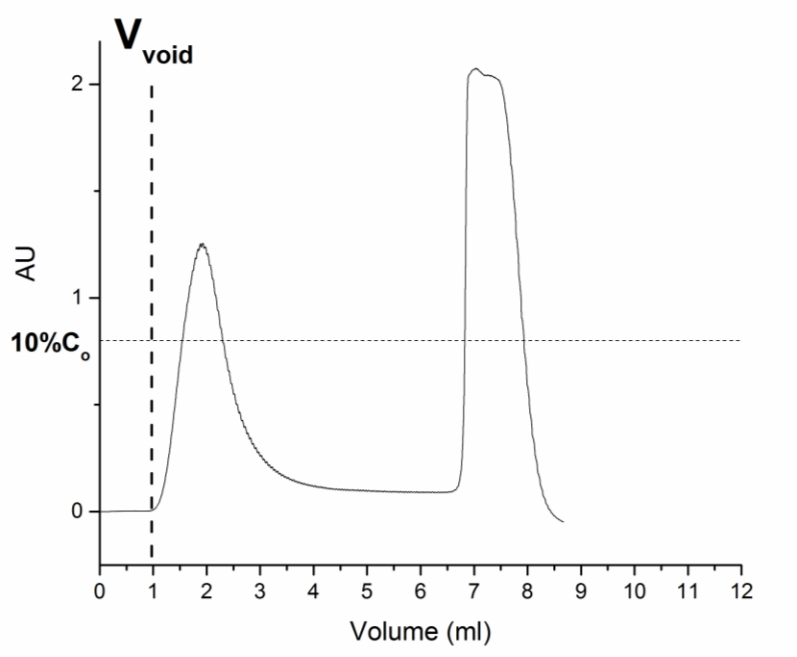

Fig. 4.B.4 Chromatogram obtained from the dynamic binding of hIgG (1ml; 10 mg/ml) to a column with 20 layers of cation exchange PBT nonwovens grafted to 25% weight gain using Heat separated by 20 layers of PET nonwoven spacer. Superficial velocity = 0.25 cm/min.

4.6 References

[1] K. Huse, H.J. Bohme, G.H. Scholz, J. Biochem. Biophys. Methods 51 ¨ (2002) 217.

[2] C.R. Lowe, A.R. Lowe, G. Gupta, J. Biochem. Biophys. Methods 49 (2001) 561.

[3] E. Klein, Affinity Membranes, Wiley, 1991.

[4] R. Ghosh, Protein separation using membrane chromatography: opportunities and challenges, Journal of Chromatography A, 952 (2002) 13-27.

[5] D.K. Roper, E.N. Lightfoot, J. Chromatogr. A 702 (1995) 3.

[6] S. Brandt, R.A. Goffe, S.B. Kessler, J.L. O'Connor, S. Zale, Bio/Technology 6 (1988) 779.

[7] X. Zeng, E. Ruckenstein, Biotechnol. Prog. (1999) 1003.

[8] H. Chenette, J. Robinson, E. Hobley, S. Husson, Development of high productivity, strong cation-exchange adosrbers for protein capture by graft polymerization from membranes with different pore sizes, Journal of Membrane Science (2012) 43-52.

[9] C. Charcosset, Purification of proteins by membrane chromatography, J. Chem. Technol. Biotechnol. 71 (1998) 95-110.

[10] H. Liu, P.V. Gurgel, R.G. Carbonell, Preparation and characterization of anion exchange adsorptive nonwoven membranes with high protein binding capacity, Journal of Membrane Science, 493 (2015) 349-359.

[11] M. Heller, K. Esinhart, B. Pourdeyhimi, R.G. Carbonell, Heat induced grafting of poly(glycidyl methacrylate) on polybutylene terephthalate, 2015, (*in preparation*).

[12] M. Heller, R. Wimbish, P. Gurgel, B. Pourdeyhimi, R.G. Carbonell, Reducing diffusion limitation in ion exchange grafted membranes using high surface area nonwovens, Journal of Membrane Science, 2015, (*submitted*).

[13] B. Bowes, A. Lenhoff, Protein adsorption and transport in dextran-modified ion-exchange media. II. Intraparticle uptake and column breakthrough, J. Chromatogr. A 1218 (2011) 4698-4708.

[14] H. Shinano, S. Tsuneda, K. Saito, S. Furasaki, T. Sugo, Ion exchange of lysozyme during permeation across a microporous sulfopropyl-group-containing hollow fiber, Biotechnol. Prog. 9 (1993) 193-198.

[15] H. Iwata, I. Hirata, Y. Ikada, Atomic force microscopic analysis of a porous membrane with pH sensitive molecular valves. Macromolecules 31 (1998) 3671-3678.

[16] H. Iwata, I. Hirata, Y. Ikada, Atomic force microscopic analysis of a porous membrane with pH sensitive molecular valves. Macromolecules 31 (1998) 3671-3678.

[17] K. Saito, T. Kaga, H. Yamagishi, S. Furasaki, T. Sugo, J. Okamoto, Phosphorylated hollow fibers synthesized by radiation grafting and crosslinking, J. Membr. Sci. 43 (1989) 131-141.

[18] F. Arnold, H. Blanch, C. Wilke, Analysis of affinity separation 2. The characterization of affinity columns by pulse techniques, Chem. Eng. J. Biochem. Eng. 30 (1985) B25-B36.

[19] V. Natarajan, S. Cramer, A methodology for the characterization of ion exchange resins, Separation Science and Technology 35 (2000) 1719-1742.

[20] O. Herigstad, P. Gurgel, R. Carbonell, Transport and binding characterization of novel hybrid particle impregnated membrane material for bioseparations, Biotechnology Progress 27 (2011) 129-139.

[21] Y. Zheng, H. Liu, P. Gurgel, R. Carbonell, Polypropylene nonwoven fabrics with conformal grafting of poly(glycidyl methacrylate) for bioseparations, J. Membr. Sci. 364 (2010) 362-371.

[22] Dupont (2004) Product information: Dupont™ Crastin® 6130 NC010, Wilmington, DE.

[23] GE Healthcare (2010), Application Note 28-9372-07 AA, Uppsala, Sweden.

[24] J. Dolan, Peaktailing and resolution, LC Resources, Walnut Creek, CA (2002).

[25] A. Rathore, R. Kennedy, K. O'Donnell, I. Bernberis, O. Kaltenbrunner, Qualification of chromatrography columns why and how we do it, Elements of Biopharmaceutical Production, 2003, 30-40.

[26] I.M. Hutten, Handbook of Nonwoven Filter Media, Butterworth-Heinemann, Oxford, Burlington, MA 2007

[27] J. White, W. Deen, Agarose-dextran gels as synthetic analogs of glomerular basement membrane: water permeation, Biophysical Journal 82 (2002) 2081-2089.

[28] B. Lego, W. Skene, S. Giasson, Swelling study of responsive polyelectrolyte brushes grafted from mica substrates: Effect of pH, salt, grafting density, Macromolecules 58 (2010) 4384-4393.

[29] E. Bittrich, K. Rodenhausen, K. Eichhorn, T. Hofmann, M. Shubert, M. Stamm, P. Uhlmann, Protein adsorption on and swelling of polyelectrolyte brushes: A

simultaneous ellipsometry-quartz microbalance study, Biointerphases 5 (2010) 159-167.

[30] S. Tsuneda, H. Kagawa, K. Saito, T. Sugo, Hydrodynamic evaluation of three-dimensional adsorption of protein to a polymer chain grafted onto a porous substrate, J. Colloid Interface Sci. 176 (1995) 95-100.

[31] M. Mishra, Y. Yagci, Handbook of Vinyl Polymers: Radical Polymerization, Process, and Technology, CRC Press, Boca Raton, FL 2008

[32] K. Kato, E. Uchida, E. Kang, Y. Uyama, Y. Ikada, Polymer surface with graft chains, Prog. Polym. Sci. 28 (2003) 209-259.

[33] J. Brandrup, E.H. Immergut, E.A. Grulke, Polymer Handbook 4th Edition, John Wiley, NY, NY 1999

[34] H. Allcock, F. Lampe, Contemporary Polymer Chemistry 2nd Edition, Prentice Hall, Englewood, NJ 1990.

[35] G. Odian, Principles of Polymerization 4th Edition, Wiley and Sons, Hoboken, NJ 2004.

[36] K. Henzler, B. Haupt, K. Lauterbach, A. Wittemann, O. Borisov, M. Ballauff, Adsorption of beta-lactoglobulin on spherical polyelectrolyte brushes: direct proof of counterion release by isothermal titration calorimetry, J. Am. Chem. Soc. 132 (2010) 3159-3163.

[37] W.M. Vos, P.M. Biesheavel, A. Kiezer, J.M. Kleijn, M.A. Stuart, Adsorption of the protein bovine serum albumin in a planar poly(acrylic acid) brush layer as measured by optical reflectometry, Langmuir, 24 (2008) 6575-6584.

Chapter 5

Conclusions and future work

5.1 Grafting of high surface area nonwovens for ion exchange capture of proteins

The specific surface area of a nonwoven membrane (area/mass) is inversely proportional to the average fiber diameter [1]. Commercially available PBT nonwovens manufactured by Macopharma had an average fiber diameter and specific surface area of approximately 3 μm and 0.9 m^2/g. In previous works this material has been successfully grafted with polyGMA using UV-light [2]. These membranes have been functionalized to be ion exchangers that have high equilibrium protein binding capacities. However, several hours are required to achieve their equilibrium binding capacities. The use of the novel high specific surface area islands-in-the-sea nonwovens was investigated to determine how an increased surface area affects the kinetics of protein adsorption.

Islands-in-the-sea (108 I/S) PBT nonwovens have a 108 island count with an average fiber diameter and specific surface area of approximately 900 nm and 2.5 m^2/g respectively. These nonwovens were successfully grafted with polyGMA using UV-light. Compared to the commercial PBT nonwovens the 108 I/S PBT nonwovens had a 2.4 times faster rate of grafting that was directly related to the 2.7 times more available surface area capable of initiating polymerization. The differences in surface area between the commercial PBT nonwovens and the 108 I/S PBT nonwovens also results in differences in the volume distribution of the polyGMA grafted layer. At a specific degree of polyGMA coverage (% weight gain) the grafting layer is thinner for the 108 I/S nonwoven because it is spread over a

higher surface area. For instance at 20% weight gain the commercial PBT nonwovens have a calculated dry polyGMA thickness of approximately 230 nm compared to the 108 I/S PBT nonwovens that have an approximate dry polyGMA thickness of 70 nm.

Grafted commercial PBT nonwovens and 108 I/S PBT nonwovens were successfully derivatized to be weak anion and strong cation exchangers for capture of BSA and hIgG respectively. All of the equilibrium binding capacities were between 50 and 200 times greater than monolayer protein adsorption. This is very strong evidence that the polyGMA brushes created a 3-dimensional binding environment, where equilibrium protein adsorption scales with the amount of polymer brush available for binding per mass of membrane. In this regard, the equilibrium static protein binding capacities are dependent on the degree of polyGMA grafting and not the specific surface area of the material. In this investigation equilibrium static protein binding capacities as high as 1000 mg/g (18-20% polyGMA weight gain) were achieved. Although grafted PBT nonwovens were capable of achieving very high binding capacities, there was a significant diffusion limitation observed by the slow rates of protein adsorption. It was experimentally determined that the higher specific surface area 108 I/S PBT nonwovens achieved the same amount of equilibrium protein binding in a fraction of the time compared to the commercial PBT nonwovens when grafted with polyGMA and functionalized to be ion exchangers. Additionally, due to the differences in surface area, the 108 I/S PBT nonwovens were capable of binding approximately 325 mg/g of protein instantaneously compared to the commercial PBT nonwovens that bound approximately 120 mg/g of protein instantaneously.

A shrinking core model was successfully used to characterize the rates of protein adsorption in the polyGMA grafted layer around the PBT fibers. Using this model the

effective diffusivities in the grafted layer could be determined. The average effective diffusion coefficients were six orders of magnitude slower than protein film diffusion. This slow rate of diffusion is believed to be due to protein having to diffuse through a dense polyGMA + bound protein "shell" before it can reach available binding sites on the polyGMA "core" layer. The shrinking core model demonstrated how thinner polymer grafts reached equilibrium at faster rates due to a shorter diffusion path. The comparatively higher surface area nonwovens successfully reduced polyGMA brush thicknesses for specific degrees of polyGMA coverage while still maintaining high equilibrium binding capacities. It was observed that the higher surface area 108 I/S PBT nonwovens with thinner polyGMA grafts were capable of reducing the significance of the diffusion limitation in the polyGMA/protein layer, resulting in shorter times to reach equilibrium compared to the commercial PBT nonwoven. Additionally, the 108 I/S nonwoven PBT demonstrated a higher amount of initial protein binding compared to the commercial PBT nonwoven, which is advantageous in applications requiring short residence times.

5.2 PolyGMA grafting of PBT using heat

The grafting of PBT using UV-light is capable of creating conformal and uniform polymer grafts around discreet fibers [2,3]. The issue with UV-light polymerization is that it is limited to the penetration depth of the light source. Therefore, nonwoven samples that are sufficiently thick or have minimal pore structure for incident light penetration will result in graft coverage gradients through the depth of the material. Thermally driven surface polymerization has the potential to be a process that is robust and facile at creating a polymer

grafted layer on a nonwoven surface that is independent of the morphology of the membrane being grafted.

PBT nonwovens were successfully grafted with polyGMA using a heat induced grafting method with the thermal initiator Bz_2O_2. The heat induced grafting results in a complete, uniform, conformal polyGMA layer around discreet PBT fibers with degrees of polyGMA grafting between 2% and 25% weight gain. The monomer concentration, temperature, polymerization time and polymerization solvent were evaluated to determine the optimal grafting conditions. It was determined that N,N-dimethylformamide (DMF) was the most suitable solvent that facilitated polyGMA grafting under the conditions tested. It was observed that increasing GMA monomer concentration resulted in an increase in the degree of polyGMA grafting; between 20 - 30% GMA (v/v in DMF) was the optimal monomer concentration for reproducible grafting. The limits of monomer concentration were 5 - 40% GMA (v/v) below this little grafting was observed and above this uncontrolled bulk polymerization of the solution occurred. The degree of polyGMA grafting increased with polymerization time until 2 hours had elapsed and further grafting could no longer be observed. There are a number of potential reasons for this, a depletion of available initiator, a reduction in the available active sites on the PBT fiber, the development of a diffusion barrier due to an increased viscosity of polyGMA in solution, or an increased termination rate of the polyGMA grafting compared to initiation. Increasing the polymerization temperature effectively increased the rate of polymerization. However, increased polymerization temperature might have some adverse effects on the structure of the grafting layer and for this reason a polymerization temperature of 80 °C is recommended for Bz_2O_2 according to the manufacturer's instructions. The chemical functionality of the PBT nonwoven surface

grafted with polyGMA using heat was determined using ATR-FTIR. It was determined that polyGMA grafting using the heat method was capable of introducing active epoxy groups onto the surface of the PBT nonwoven where the relative epoxy density increases with increasing degree of polyGMA coverage. The epoxy groups are capable of covalently attaching ion exchange ligands such as diethylamine or sulfonic acid [4,5]. The covalent attachment of diethylamine was evaluated using elemental analysis and it was determined that the ligand density of the grafted nonwoven increased with the degree of polyGMA grafting. Additionally, the DEA ligand densities were comparable with nonwoven samples polyGMA grafted using UV-light that had been functionalized to anion exchangers.

5.3 Structural differences of polyGMA layers grafted using UV-light and heat

Complete and conformal grafting of PBT nonwovens with polyGMA has been accomplished using UV-light and heat based grafting techniques. However, it is believed that there are structural differences between these two methods of grafting that can affect the performance of the nonwoven. Vinyl grafting onto polymeric supports using radiation based free radical polymerization, such as the UV-light grafting of polyGMA onto PBT nonwovens, is known to create vinyl polymer brushes that are anchored to the polymeric surface [6-8]. These polymeric brushes are tentacle-like in nature being highly linear and flexible [8-10]. Vinyl grafting by heat induced free radical polymerization on the other hand is far less controlled. Thermal based polymerizations result in higher rates of chain transfer compared to polymerizations by UV-light [11,11-13]. High rates of chain transfer result in highly branched polymer chains, as well as, highly cross-linked polymer networks, both of

which would have significant effects on the density and structure of the grafted polyGMA layer.

The PBT nonwovens with polyGMA grafted using UV-light and heat were functionalized to be ion exchangers and evaluated for their ability to capture biomolecules of various sizes. ATP (0.5 kDa), lysozyme (14.3 kDa), BSA (66.5 kDa) and hIgG (150 kDa) were used to challenge ion exchange PBT nonwovens grafted using both methods. It was observed that ion exchange polyGMA grafted PBT nonwovens grafted using both methods bound the same number of ATP molecules, the smallest target investigated. However, as the molecular weight of the target increased the UV-light grafted nonwovens were capable of binding a substantially larger number of target molecules compared to the heat grafted nonwovens. This indicates that there is either a smaller binding volume available for protein binding in the heat grafted nonwovens and/or size exclusion effects are occurring in the grafted layer of the heat grafted nonwovens. Any branching or cross-linking that is present in the heat grafted layer would result in a substantially denser polyGMA layer and smaller binding volume compared to the UV-light grafted polyGMA brushes. Additionally, crosslinking in the heat grafted layer creates a porous structure and these small pores may be responsible for any observed size exclusion effects observed by the material. Conversely, the UV-light grafted layer is believed to be flexible polymer brushes capable of accommodating biomolecules in the entirety of the grafted layer.

The potential structural differences between the UV-light and heat based grafting methods have also been observed in the swelling nature of the polyGMA grafted layer. Polyelectrolyte brushes are known to significantly swell in low ionic strength environments due to electrostatic repulsions of neighboring brushes that force them to extend normal to the

grafted surface [14,15]. In flow operations, PBT nonwovens grafted using UV-light and functionalized to be ion exchangers experienced large pressure drops due to a significant pore blockage of the nonwoven. However, when a high ionic strength mobile phase was introduced the observed pressure drops were significantly reduced due to an increase in the pore sizes of the material. It is believed that the changes in the pore size occur from a swelling or collapsing of the ion exchange UV-light polyGMA grafted layer when exposed to an environment of low or high ionic strength respectively. As the ionic strength of the environment increases, the charged polyGMA brushes become saturated with counter-ions and the brush layer collapses, increasing the pore volume of the nonwoven. The heat grafted ion exchange polyGMA PBT nonwovens did not experience the same high pressure drops as the UV-light grafted ion exchange nonwovens. Additionally, the pressure drops observed by the ion exchange heat grafted PBT nonwovens were not dependent on ionic strength like the UV-light grafted nonwovens were. This is consistent with the work of Saito *et al*. that investigated the flux through membranes that had been grafted with polyelectrolyte brushes with and without cross linking [16]. In this work polyelectrolyte brushes without cross linking experienced ionic strength dependent swelling that reduced the flux of the material when brushes were swollen in a low ionic strength environment. It was also determined that cross-linking of the brush layer prevented any swelling of the grafted layer from changes in ionic strength, due to physical constraints imparted by the cross-linked network.

For these reasons it is believed that polyGMA layers created by heat induced polymerization are highly cross-linked. The cross-linking creates physical constraints that limit the swelling behavior of the heat induced grafted layer when functionalized as ion exchangers. The UV-light grafted polyGMA layer on the other hand is believed to be a

network of independent free moving brushes. Therefore, a polyGMA layer grafted using UV-light and functionalized to be an ion exchanger is capable of accommodating protein throughout the entire layer resulting in comparatively higher equilibrium binding capacities. Additionally, the UV-light polyGMA grafted layer exhibits swelling that is strongly dependent on the ionic strength of the environment.

5.4 Protein capture performance of heat and UV-light grafted PBT nonwovens

PolyGMA grafting of PBT nonwovens is capable of creating a 3 dimensional environment for the ion exchange capture of BSA and hIgG. However, structural differences in the polyGMA grafted layer that arise between the UV-light and heat based grafting methods have a dramatic impact on the performance of the material for protein capture. When functionalized as ion exchangers both grafting methods demonstrate an increase in static equilibrium protein binding capacity with an increase in the degree of polyGMA coverage. However, the UV-light polyGMA grafted nonwovens on average bind between 5 to 7 times more mass of protein at a given degree of grafting compared to when they are grafted using heat to the same degree of grafting. This is largely believed to be due to the UV-light grafted polyGMA layer being a flexible brush structure compared to the heavily cross-linked structure of the polyGMA layer grafted using heat. The brush structure is capable of accommodating protein throughout the entirety of the grafted layer. Conversely it is believed that the cross-linking and branching of the heat grafted polyGMA layer creates many internal pores that are too small to accommodate protein diffusion into the interior of the layer, with an overall shallower observed binding volume. Regardless of the proposed structural differences between the two grafting methods they exhibited similar strengths of

binding with dissociation constants calculated to be on the order of 10^{-6}M which is consistent for protein binding on ion exchange polymer networks.

The differences in the grafted layer between the two methods also results in differences in the kinetics of protein adsorption. It has been shown for the UV-light grafted nonwovens that protein adsorption in the ion exchange polyGMA grafted layer suffers from very slow protein diffusion into the polyGMA layer. When tested statically, several hours are required for the UV-light polyGMA grafted PBT nonwovens to reach equilibrium binding. A shrinking core model was used to accurately characterize the rates of protein adsorption into a dense polyGMA brush layer that became filled with protein. Using this model average effective diffusion coefficients were calculated and found to be six orders of magnitude slower than protein film diffusion. Heat grafted PBT nonwovens did not demonstrate the same diffusion limitation that the UV-light grafted nonwovens did. When tested statically the ion exchange polyGMA grafted PBT nonwovens achieved equilibrium binding within minutes and in many cases instantaneous equilibrium binding was observed. This behavior is what you typically expect for adsorptive membranes where protein binding occurs on the surface of the material and convective flow is the dominating form of mass transfer for protein adsorption [17,18].

In the current investigation, to test the dynamic binding capacity of the grafted nonwovens, multiple layers of polyGMA grafted PBT nonwoven were punched into discs and stacked in a column to simulate a chromatography bed. Both grafting methods were evaluated for their dynamic binding capacity when they are functionalized as cation exchangers for the capture of hIgG. The UV grafted PBT nonwovens grafted to 5% weight gain and functionalized as cation exchangers bound approximately 16 mg/ml at all tested

residence times. The observed dynamic binding capacities were substantially lower than when the same materials were tested statically at similar residence times. When the membranes are packed into a column as stacked layers the porosity is substantially lower than when the membranes are tested statically. It is believed that the low observed porosity of the membranes when stacked in a column format is related to a significant amount of pore blockage in the membrane that makes a significant amount of the column volume inaccessible to protein binding. Introducing a PET nonwoven spacer to separate the individual PBT nonwoven layers was capable of significantly increasing the porosity of the column. The introduction of spacers also resulted in an increase of the dynamic binding capacity to 24 mg/ml for all tested residence times. Therefore, increasing the porosity of the column was capable of increasing the volume accessible for protein binding and resulted in very similar protein capture to when the material was tested statically at similar residence times. The dynamic binding capacities for the ion exchange UV-light grafted PBT nonwovens were substantially lower than the static equilibrium binding capacities for these materials. However, the longest residence time evaluated for dynamic binding was 5 min and it was determined that the diffusion limited mass transport of this material required several hours to reach equilibrium which is not practical for dynamic protein capture.

The cation exchange polyGMA PBT nonwovens grafted to 25% weight gain using heat had dynamic binding capacities of 20 mg/ml for all tested residence times when spacers were not used. Introducing a PET nonwoven spacer to separate the individual PBT nonwoven layers increased the dynamic binding capacity to approximately 35 mg/ml for all tested flow rates. Similar to the UV-light grafted PBT nonwovens, using PET nonwoven spacers was capable of increasing the porosity of the column while concomitantly increasing

the dynamic binding capacity. The dynamic binding capacity of the heat grafted PBT nonwovens when spacers are used is equivalent to the static equilibrium binding capacity for this material. The heat grafted polyGMA layers do not demonstrate a diffusion limited form of mass transport like the UV-light grafted polyGMA layers do. For this reason the heat grafted PBT nonwovens achieve equilibrium binding at very short residence times when evaluated dynamically.

The cation exchange polyGMA grafted PBT nonwovens grafted using both heat and UV-light, were also evaluated for their ability to separate protein mixtures. When challenged with a mixture of hIgG and lysozyme these membranes were capable of binding both proteins in bind and elute mode. Using a change in pH, hIgG was capable of being selectively eluted from the columns with high purity. The remaining bound protein was capable of being removed with an increase in salt concentration. The same columns were also challenged with a mixture of hIgG, lysozyme and BSA. These columns bound a significant amount of BSA in what should be electrostatically repulsive conditions. All of the bound proteins were effectively eluted using an increase in ionic strength indicating an electrostatic mechanism of adsorption. The nonspecific electrostatic adsorption of proteins is a common phenomenon for proteins that have localized charges capable of binding to surfaces that have very large charge densities [19,20].

A stacked column configuration was chosen for its ease of comparison to traditional packed bed chromatography. However, asymmetry values greater than 3 were observed for the columns indicating poor packing and flow mal-distribution. Compaction of the nonwovens in column format, observed by low flow porosities, in addition to any channeling that occurs due packing a column with potentially irregular nonwoven discs are believed to

be the cause of these large asymmetry values. Therefore, it might prove beneficial to test grafted PBT nonwovens in alternate configurations such as radial flow.

5.5 Composite PBT nonwovens for use as protein capture devices

As a protein capture device polyGMA grafting of PBT nonwovens have demonstrated high protein binding capacities when functionalized as ion exchangers. However, when packed into a column to be used for chromatographic separations commercial PBT nonwovens demonstrate a low porosity and low permeability creating flow issues. UV-light grafting only exaggerates the permeability of the material due to swelling of the polymer layer. Conversely, heat based grafting does not exhibit swelling of the polymer layer and contributes little to the permeability of the membrane. Additionally, ion exchange polyGMA layers grafted using heat do not exhibit diffusion limited protein adsorption the way UV grafted layers do and are capable of very fast binding kinetics.

Introducing a rigid spacer has shown to improve the flow properties of a column packed with ion exchange polyGMA grafted PBT nonwovens by increasing the porosity and permeability of the column. The improved flow properties of columns packed using spacers has resulted in better utilization of the grafted PBT nonwovens for the dynamic capture of protein. In the previous work it has also been determined that higher surface area nonwovens (smaller fiber diameters) are capable of binding more protein instantaneously.

The work of this investigation is the foundation for designing a novel PBT nonwoven membrane that is capable of binding large amounts of protein at very short residence times with ideal flow properties. It is believed that a composite material can be designed that maximizes the specific surface area of the nonwoven while maintaining good flow properties. Small PBT fibers (1-3 μm) can be interspersed with large PBT fibers (20-50 μm)

to create a nonwoven that has pore sizes between 10 and 100 μm and porosity above 60%. The idea is that large PBT fibers will support the smaller fibers and give the nonwoven a rigid structure where porosity will not be compromised from a compression of the material. The small fibers will provide the majority of the surface area for the capture of protein. Both grafting methods can be investigated for this novel material. However, the heat based grafting method has demonstrated higher dynamic binding capacities compared to the UV-light grafting method that is diffusion limited. The heat based grafting method is also capable of grafting surfaces of any size or shape and might be advantageous in this regard.

5.6 Membrane configuration and flow distribution

Flow distribution is a long documented issue for membrane chromatography [17,18]. It results in early breakthrough, band broadening and an underutilization of the membrane. The stacked disc column format of this investigation has proven to create flow mal-distribution issues observed as large asymmetry factors. It may be useful to design a membrane holder capable of reducing membrane compression and potentially sealing the membrane area to prevent any channeling. Great care must be taken in designing the membrane holder used for testing. It needs to be designed in a way that creates an evenly distributed mobile phase and prevents channeling or bypassing. It may be appropriate to test other flow configurations such as tangential or radial flow. In particular radial flow configurations are best suited for large scale applications and have been used in bind and elute chromatography capture steps [17]. However, flow distribution and module design for this type of filtration can also be challenging and care must be taken in designing these units.

5.7 Modifications of the polyGMA graft layer

The cation exchange functionalized polyGMA grafted nonwovens have demonstrated nonspecific electrostatic binding of proteins such as BSA. One possible explanation of this is the large charge density in the grafted layer capable of binding localized charge pockets on the BSA. It is believed that reducing the charge density in the polymer grafted layer may reduce any nonspecific protein adsorption due to electrostatic interaction. One potential way of accomplishing this is creating a copolymer grafted layer that has a reduced charge density compared to an ion exchange functionalized polyGMA layer. Hydroxyethylmethacrylate (HEMA) is a polymer capable of being grafted to surfaces through vinyl free radical polymerizations similar to the grafting mechanism of GMA. It also has a pendent hydroxyl group that is capable of reducing nonspecific protein adsorption. Establishing a grafting approach capable of grafting a copolymer such as polyGMA-co-polyHEMA may be capable of creating an ion exchange grafted layer that does not demonstrate electrostatic protein adsorption under repulsive conditions. Another potential way of reducing the charge density of the ion exchange polyGMA grafted layer would be to use a competing reaction to reduce the number of available epoxy groups. Diethylene glycol is known to react with the epoxy groups of polyGMA to create a grafted surface that rejects nonspecific protein adsorption [21,22]. It may be possible to functionalize PBT nonwovens grafted with polyGMA to be ion exchangers in the presence of DEG to compete with the functionalization reaction, reducing the charge density while introducing hydroxyl groups that would reduce nonspecific adsorption.

5.8 References

[1] A. Durany, N. Anantharamaiah, B. Pourdeyhimi, High surface area nonwovens via fibrillating spunbonded nonwovens comprising Islands-in-the-Sea bicomponent filaments: structure-process-property relationships, J. Mater. Sci. 44 (2009) 4926-5934.

[2] H. Liu, P.V. Gurgel, R.G. Carbonell, Preparation and characterization of anion exchange adsorptive nonwoven membranes with high protein binding capacity, Journal of Membrane Science, 493 (2015) 349-359.

[3] H. Liu, Y. Zheng, P. Gurgel, R. Carbonell, Affinity membrane development from PBT nonwoven by photo-induced graft polymerization, hydrophilization and ligand attachment, J. Membr. Sci. 428 (2013) 562-575.

[4] M. Benes, D. Horak, F. Svec, Methcylate-based chromatographic media, J. Sep. Sci. 28 (2005) 1855-1875.

[5] E.G. Vlakh, T.B. Tennikova, Preparation of methacrylate monoliths, J. Sep. Sci. 30 (2007) 2801-2813.

[6] S. Tsuneda, H. Kagawa, K. Saito, T. Sugo, Hydrodynamic evaluation of three-dimensional adsorption of protein to a polymer chain grafted onto a porous substrate, J. Colloid Interface Sci. 176 (1995) 95-100.

[7] K. Kobayashi, S. Tsuneda, K. Saito, H. Yamagishi, S. Furasaki, T. Sugo, Preparation of microfiltration membranes containing anion exchange groups, J. Membr. Sci. 76 (1993) 209-218.

[8] H. Shinano, S. Tsuneda, K. Saito, S. Furasaki, T. Sugo, Ion exchange of lysozyme during permeation across a microporous sulfopropyl-group-containing hollow fiber, Biotechnol. Prog. 9 (1993) 193-198.

[9] M. Mishra, Y. Yagci, Handbook of Vinyl Polymers: Radical Polymerization, Process, and Technology, CRC Press, Boca Raton, FL 2008

[10] K. Kato, E. Uchida, E. Kang, Y. Uyama, Y. Ikada, Polymer surface with graft chains, Prog. Polym. Sci. 28 (2003) 209-259.

[11] H. Allcock, F. Lampe, Contemporary Polymer Chemistry 2nd Edition, Prentice Hall, Englewood, NJ 1990.

[12] G. Odian, Principles of Polymerization 4th Edition, Wiley and Sons, Hoboken, NJ 2004.

[13] C. Wolf, W. Burchard, Branching in free radical polymerization due to chain transfer. Application to poly(vinyl acetate), Macromol. Chem. 177 (1976) 2519-2538.

[14] B. Lego, W. Skene, S. Giasson, Swelling study of responsive polyelectrolyte brushes grafted from mica substrates: Effect of pH, salt, grafting density, Macromolecules 58 (2010) 4384-4393.

[15] E. Bittrich, K. Rodenhausen, K. Eichhorn, T. Hofmann, M. Shubert, M. Stamm, P. Uhlmann, Protein adsorption on and swelling of polyelectrolyte brushes: A simultaneous ellipsometry-quartz microbalance study, Biointerphases 5 (2010) 159-167.

[16] K. Saito, T. Kaga, H. Yamagishi, S. Furasaki, T. Sugo, J. Okamoto, Phosphorylated hollow fibers synthesized by radiation grafting and crosslinking, J. Membr. Sci. 43 (1989) 131-141.

[17] R. Ghosh, Protein separation using membrane chromatography: opportunities and challenges, Journal of Chromatography A, 952 (2002) 13-27.

[18] C. Charcosset, Purification of proteins by membrane chromatography, J. Chem. Technol. Biotechnol. 71 (1998) 95-110.

[19] K. Henzler, B. Haupt, K. Lauterbach, A. Wittemann, O. Borisov, M. Ballauff, Adsorption of beta-lactoglobulin on spherical polyelectrolyte brushes: direct proof of counterion release by isothermal titration calorimetry, J. Am. Chem. Soc. 132 (2010) 3159-3163.

[20] W.M. Vos, P.M. Biesheavel, A. Kiezer, J.M. Kleijn, M.A. Stuart, Adsorption of the protein bovine serum albumin in a planar poly(acrylic acid) brush layer as measured by optical reflectometry, Langmuir, 24 (2008) 6575-6584.

[21] Y. Zheng, H. Liu, P. Gurgel, R. Carbonell, Polypropylene nonwoven fabrics with conformal grafting of poly(glycidyl methacrylate) for bioseparations, J. Membr. Sci. 364 (2010) 362-371.

[22] H. Liu, Y. Zheng, P. Gurgel, R. Carbonell, Affinity membrane development from PBT nonwoven by photo-induced graft polymerization, hydrophilization and ligand attachment, J. Membr. Sci. 428 (2013) 562-575.